Design, construction and testing of a Tesla Turbine.

by

Kris Holland

A thesis submitted in partial fulfillment

Of the requirements for the degree of

Master of Applied Science (MaSc) in Natural Resources Engineering

The Faculty of Graduate Studies

Laurentian University

Sudbury, Ontario, Canada

THESIS DEFENCE COMMITTEE/COMITÉ DE SOUTENANCE DE THÈSE
Laurentian Université/Université Laurentienne
Faculty of Graduate Studies/Faculté des études supérieures

Title of Thesis Titre de la thèse	Design, construction and testing of a Tesla Turbine
Name of Candidate Nom du candidat	Holland, Kristian
Degree Diplôme	Master or Science
Department/Program Département/Programme	Natural Resources Engineering
Date of Defence Date de la soutenance	Feb 26, 2016

APPROVED/APPROUVÉ

Thesis Examiners/Examinateurs de thèse:

Dr. Brahim Chebbi
(Supervisor/Directeur(trice) de thèse)

Dr. Dean Millar
(Committee member/Membre du comité)

Dr. Meysar Zeinali
(Committee member/Membre du comité)

Dr. Francois Godard
(External Examiner/Examinateur externe)

Approved for the Faculty of Graduate Studies
Approuvé pour la Faculté des études supérieures
Dr. David Lesbarrères
Monsieur David Lesbarrères
Acting Dean, Faculty of Graduate Studies
Doyen intérimaire, Faculté des études supérieures

ACCESSIBILITY CLAUSE AND PERMISSION TO USE

Abstract

This thesis presents the design, construction and testing of a boundary layer turbine, also known as a Tesla Turbine. A turbine, with discs of 92mm in diameter, central exhaust, plenum chamber, and swappable nozzles was constructed. The setup included instrumentation and a simple torque sensor with which to sense the relatively low torques given the low testing pressures. After construction, the setup was tested with various angles of nozzles ranging from 2.5° to 45° from tangential. The testing resulted in an estimated maximum efficiency of 8.5%, while running the rig at 3 bar, which is comparable to the literature. Unexpectedly, this maximum was achieved with a nozzle pointed at 45° from tangential, which may have been caused by the disc pack variant used in the tests.

Keywords:

Tesla Turbine boundary layer shear-torque bladeless test rig

Acknowledgements

I would like to provide thanks, first of all, to the immense patience of my supervisor, Dr. Brahim Chebbi.

Further thanks to the Center for Mining Excellence and Innovation, and specifically Allan Akerman, for funding and encouragement. Thanks to MITACS for their financial support.

The software was coded by Karim Omri, another Laurentian Student. This student is grateful to his timely help to get the software working.

Thanks to Steve Nixon, whose regular checks and balances, and questions, kept me on the right track. Steve is responsible for the original idea behind the torque sensor.

Thanks to Dr. Dean Millar who provided guidance, perspective, and a few laughs along the way.

Lastly, to my family, most notably my wife, Lori-Ann, without whom I could not have remained sane.

Table of Contents

List of Figures

Symbols

b	gap distance
d	diameter
FS	factor of safety
g	gravity
H	height
h	enthalpy
ID	inside diameter
L	load, as measured by a load cell
l	characteristic length
M_{at}	Mach number at throat
M	moment
$\dot{m}$	mass flow rate
n	moles of gas
P	pressure
P'	non dimensional pressure

P_m	modified pressure
p	power
OD	outside diameter
R	universal gas constant
R_e	Reynold's Number
r	radius
r_c	radial coordinate
r_n	non-dimensional radius
s	entropy
T	temperature
t	time
V	volume
$\dot{V}$	volume flow rate
v	velocity
W	work
z	axial coordinate
α	acceleration

β angle

γ specific heat

δ ½ distance between dics

ζ non-dimensional average relative tangential velocity

η efficiency

θ tangential direction

μ dynamic viscosity

ξ non-dimensional average relative radial velocity

ρ density

σ stress

τ torque

φ $= {}^{\bar{v}_{r_2}}/_{\omega r_2}$

ω angular velocity

1. Introduction

1.1. The Tesla Turbine.

The Tesla Turbine is a relatively simple device, given the fact that it is capable of achieving very high speeds, upwards of 35,000 RPM (Burton, 1955). The turbine, as patented by Nikola Tesla (1913), is made of a set of parallel discs on a shaft. A working fluid is injected from the outer circumference and passes over the discs, forming a complex boundary layer. The working fluid is then exhausted near or at the axis of rotation. Powered from the shaft, the turbine can function as centrifugal pump. The turbine can be run on any kind of fluid, including air, steam, water, or even oil. The turbine is also very tolerant of impurities, such as particulates or wet steam.

The Tesla Turbine is also known as a shear torque turbine, boundary layer turbine, and friction turbine. While it has some distinct advantages, and while Tesla himself made some impressive claims, it was almost forgotten for half a century. A flurry of interest happened in the 1960s, but then it was left unexplored again until the 1980s. Warren Rice (1991) promoted extended interest over the years, including many Masters and PhD theses.

There has been significant renewed interest in the last decade, but mostly outside of the academic arena. Consequently, much of the information available is limited, and focuses on designs and/or results without any significant analysis. Many of the turbines have been built with relatively little precision, accuracy or safety (Mrfixitrick, 2007). In addition, many of these systems do little to evaluate the conditions in the turbine; instead, they rely primarily on the rotational speed to infer the efficiency of the system.

In the various testing campaigns of the 1950s and 60s, the most notable the papers were produced by Leaman (1950), Beans (1966), Armstrong (1952) and Rice (1965). During this time, researchers tried to replicate claims made by Tesla regarding the turbine's efficiency. Tesla had claimed, as reported by Stearns (1911), that it was possible to achieve an efficiency of 80-90%, presumably of the 2nd law efficiency. The most efficiency that Leaman (1950) was able to get in reproducing Tesla's patent design was 31%. This makes the turbine significantly less efficient than other kinds of turbomachinery (McCloskey, 2003). As a consequence, the Tesla Turbine has been generally discounted for use in power generation. That being said, there have been mentions in the literature that this extreme efficiency was achieved through a staged turbine, though this seems not to be generally reported (Cairns, 2003).

Even so, the device has distinct advantages. Because it is very tolerant of poor working fluids, it can run fluids such as wet steam, which is harmful for high precision turbines (Rice, 1991). The system is also quite simple, in comparison to most turbomachinery, and is much less expensive to build and maintain. This means that there are possibilities of using the device for power generation and/or recovery where a traditional turbine might be impractical.

While there is currently no significant practical application of the Tesla Turbine in power generation, the pump version of this turbo machine, known as the Tesla pump, has been used effectively in some industries, notably pumping crude oil in deep sea wells (Crawford & Rice, 1974).

1.2. Nikola Tesla

Tesla was a prolific inventor. He is often credited for making modern society possible, given that he is the inventor of A/C Power. He was born in 1856 in Smijan, Austrian Empire, which is now Croatia, and immigrated to the United States in 1884. He worked for various people, including Thomas Edison and George Westinghouse. In spite of his inventive genius, Tesla died penniless in 1943 (O'Neill, 1944).

Tesla was notoriously distrustful of the patent system, and was known to leave off details of his inventions as trade secrets (Tesla Universe, 2015). Tesla (1911) wrote that he believed that the turbine was one of his "greatest inventions".

1.3. Motivations

While the Tesla Turbine has been described in the literature as an inefficient system, there is no question that it is overall a very robust design, and very cost effective given its simplicity. To that end, an optimized turbine would be useful in many situations. These include;

- Energy recovery, such as on water lines coming from the surface in a mine context,
- Primary power generation, in small contexts such as wood stoves,
- Secondary power generation, on (relatively) low pressure gasses from power plants

Given these things, it is possible that a turbine could make a difference to individuals, and the overall carbon footprint caused by energy on the planet.

Until recently, the literature focuses on claims made by Tesla, and there are relatively few that seek to purely assess the function of the device, how it might be improved, and the testing of those improvements. Recently, there have been several papers written that seek to go into greater detail, including Hoya & Guha (2009), Guha & Smiley (2009), and Guha & Sengupta (2013); but these have, like many of the predecessors, focused on the details of the specifics that Tesla (1913) had reported in his patent.

The author did not expect to be able to produce any finding that differed from previous works. Rather, the desire was to construct a platform on which these various tradeoffs could be assessed qualitatively, eventually leading to novel changes to the device overall. The reason for this would be to find niche applications for heat engine power generation that are not otherwise served, that would ultimately benefit individuals and sectors through small scale power generation and recovery.

1.4. Objectives

Given the aforementioned focus on the Tesla's basic design, the primary objective of this thesis was to create a test bed that would allow the variation of many variables. A platform was desired that one could easily test a multiplicity of components, while keeping the balance of variables constant. The features that could be varied included, but were not limited to, nozzle shape and angle, disc profile and surface finish, disc spacing and number, and many others.

The test bed would then carry sufficient instrumentation to be able to easily asses the results of the changes, to allow immediate evaluation of the effects on the turbine could be immediately made. Early on, the intention was to not only create the test bed, but also implement several changes to the turbine, and measure their effect. Unfortunately, it was necessary to scale this back to one series of changes, with nozzle angles.

1.5. Thesis outline

Chapter 2 covers a review of the literature, starting with Tesla's original design, the various designs and modifications that have come since, as well as theoretical considerations. At the end of the section, the expected results will also be covered. Chapter 3 reviews the detailed design of the turbine. Each component has considerations, such as size and/or safety, which need to be addressed prior to the final design. Once complete, the parts themselves would be designed as part of the whole system. Chapter 4 explores the experimental techniques and measurement system. These include the specific choices in instrumentation, through to the calibration and data acquisition methodology. The setup of the experiment and some discussion about the built device is covered. Chapter 5 analyses the data, as collected, as well as analysis, and comparison to the literature. Chapter 6 puts forward conclusions and recommendations.

2. Literature Review and Background Theory

In this section, an examination of Tesla's design, subsequent works, and the theory behind it will be presented.

2.1. Turbine Overview

The Tesla Turbine is generally described in the literature as an "almost pure impulse Turbine" (Hoya & Guha, 2009). It works by the interaction of a fluid that enters at the outside edge of a set of closely spaced disc platters, travelling circumferentially through gaps between the discs, transferring momentum via boundary layer interactions. The fluid then exhausts via holes in the platters along the centerline of the platters.

Its design is one of simplicity. The aforementioned discs are mounted to a shaft, and the fluid enters the chamber via a nozzle or nozzles that are placed at the outside edge, generally aimed in a tangential direction. Labyrinth seals are placed on the outside of the disc pack in order to prevent flow from bypassing the discs, while being non-contact. Power is then taken off from the shaft, and the fluid exits the turbine to either atmosphere, secondary stages, or through a power cycle.

To better describe the function of the device, one should begin with Tesla's reference patent design, which is noted in Figure 1.

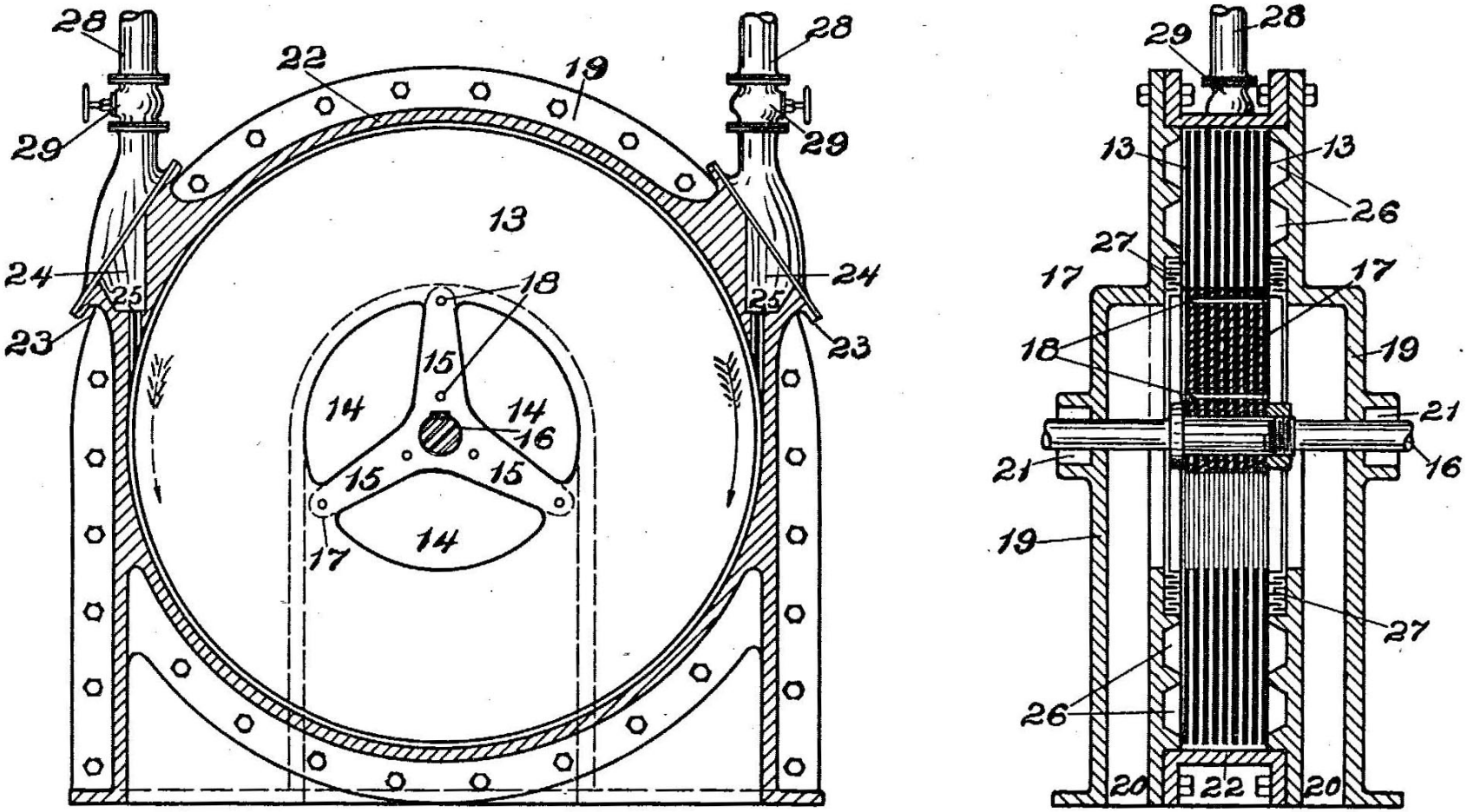

Figure 1- Tesla's original design, from his patent. (Tesla, 1913)

The components of the Tesla Turbine are:

13. Disc Platter Set
14. Exhaust Holes
15. Support Spokes
16. Shaft
17. Housing
18. Washer Spacers
19. End Castings
20. Bearings
21. Stuffing Boxes
22. Central Ring Gap
23. Flanged Extensions
24. Inlet
25. Nozzles
26. Circular Grooves
27. Labyrinth Seals
28. Supply Pipes
29. Valves

Tesla's published design is a reversible design, such that one could open one or the other of the valves (29), in order to affect a reversal of the turbine. The fluid follows a spiral path across the discs, and transfers momentum to the platters via boundary layer forces. Once the fluid has reached the inner radius of the platters, it is able to escape through exhaust holes, and ultimately out the turbine exhaust. The fluid path is illustrated in Figure 2. The disc pack is tightly confined, with the labyrinth seals ensuring that the discs can spin freely, while also ensuring that the fluid enters the gaps between the discs. Power is transferred via the shaft, which sits on a pair of bearings.

In principle, the maximum speed of the turbine is the velocity of the fluid applied tangentially to

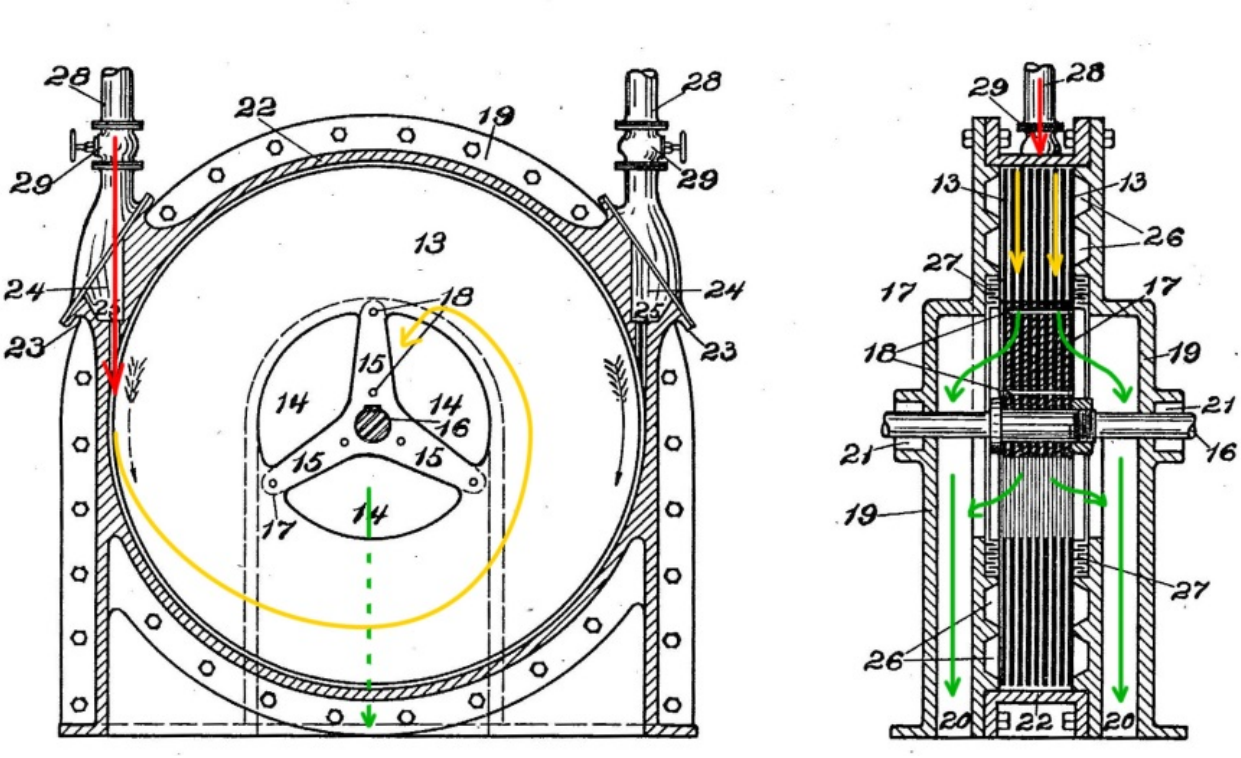

Figure 2 - Flow Path in Tesla's (1913) design

the disks, but there are obvious limitations, given system losses in the bearings, interactions between the discs and the seals, nozzle losses, and the efficiency of the momentum transfer.

Tesla, himself, built several versions of this design, with varying numbers of discs, and variability in the overall diameter of the system. Disc diameter varied from six to ten inches, where the discs themselves were made from steel (Stearns, 1911). It must be appreciated that at the time of its invention, metallurgy was still quite young, and the quality of the materials available to Tesla were limited.

2.2. Tesla's Patent

Tesla (1913) filed the patent on the turbine in 1909, and it was awarded in May 1913. Tesla was generally known to be distrustful of the patent system, and it is very likely that many salient details were left out. Also, given the very nature of patents, where it is desirable to be more general than specific, details such as the sizes of the discs, disc spacing, operating pressures, working fluid, temperature, and other details were left out completely.

2.3. Coordinate system for the turbine

To better understand the Tesla Turbine, one should begin with details around specific aspects of its function. To that end, one should define the geometrical space to be considered. A cylindrical coordinate system (r, θ, z) is defined in Figure 3, where the velocity vectors are v_r,

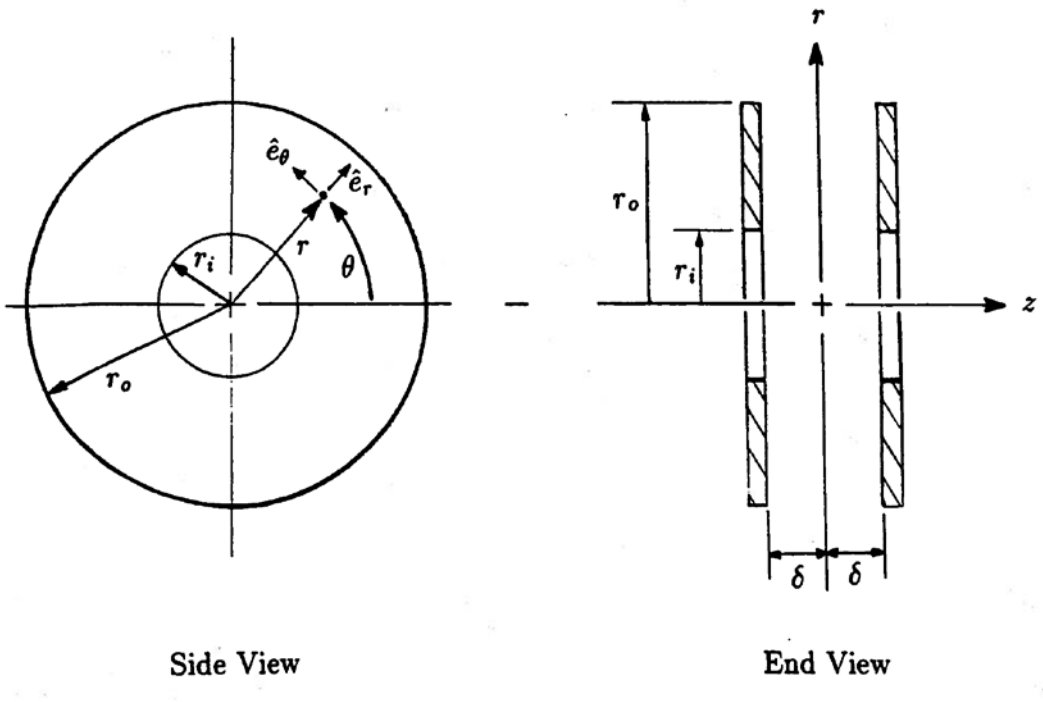

Figure 3 – System coordinates (Allen, 1990)

v_θ, v_z for the radial, tangential and axial directions, respectively. Similarly, parameters for the rotor are defined as the outer radius r_o, inner radius r_i, half disc spacing δ and number of disks N (Allen, 1990).

In addition, a fluid element between the dicscs should be considered, to illustrate the shear stresses, as illustrated in Figure 4. Shear stresses are τ_r and τ_t, for the radial and tangential directions, respectively. The stresses result from the differential velocity between the fluid and the discs via the boundary layer, which results in energy transfer (Allen, 1990).

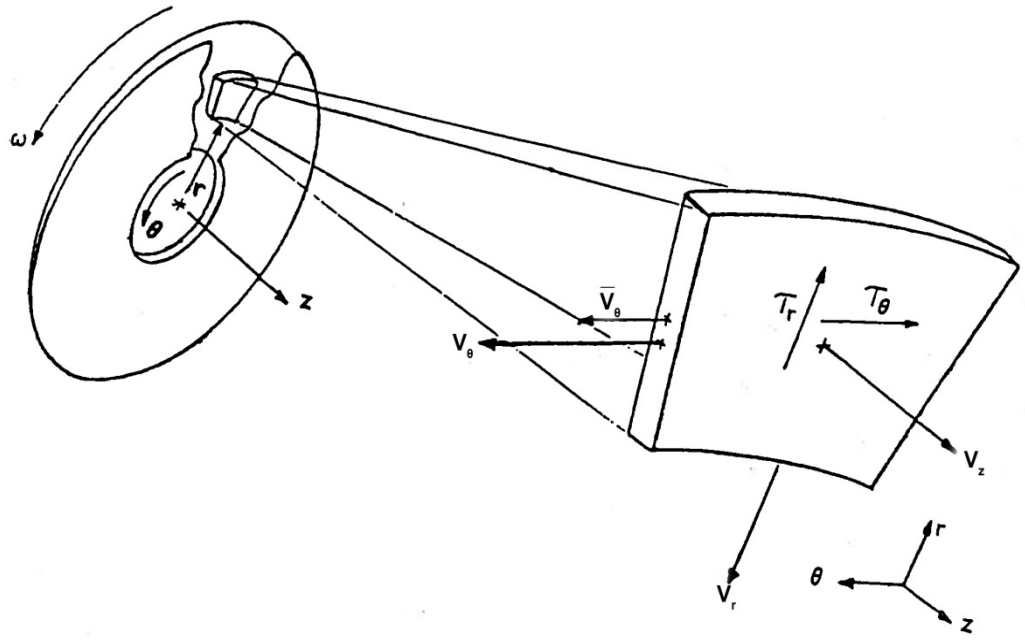

Figure 4 – Fluid element (Allen, 1990)

2.4. Reynolds Number

The Tesla Turbine can operate at a wide range of flow rates, and to understand the subsequent conditions, one must first determine the Reynold's number for the flow, under a given condition. The Reynold's number is calculated via equation 1;

$$Re = \frac{v * \rho * l}{\mu} \tag{1}$$

Where in this case, l, or characteristic length, is the gap between the discs, known as 2δ.

In the case of the Tesla Turbine, the calculation is complicated by the speed of the rotor at the time of consideration; at a low rotor speed, the velocity of the flow relative to the velocity of the disc surfaces is greatest, while at a steady state, they would be much closer to equal, since the relative velocity would be approaching a steady state value.

2.5. The Boundary Layer

The boundary layer is an important consideration for the Tesla Turbine; there is some debate as to the exact conditions that are found in the gap between the discs (Guha & Sengupta, 2013). The exact state of turbine affects these conditions; that is if it is accelerating, high or low speed or in a steady state. It would reasonably expected that the flow would be turbulent at start up, when the flow is much greater than the rotor speed, but it would likely become laminar as a steady no-

load state is achieved when the fluid absolute velocity is approximately equal to the rotor speed. The transition from laminar to turbulent is illustrated in Figure 5, for a flat plate.

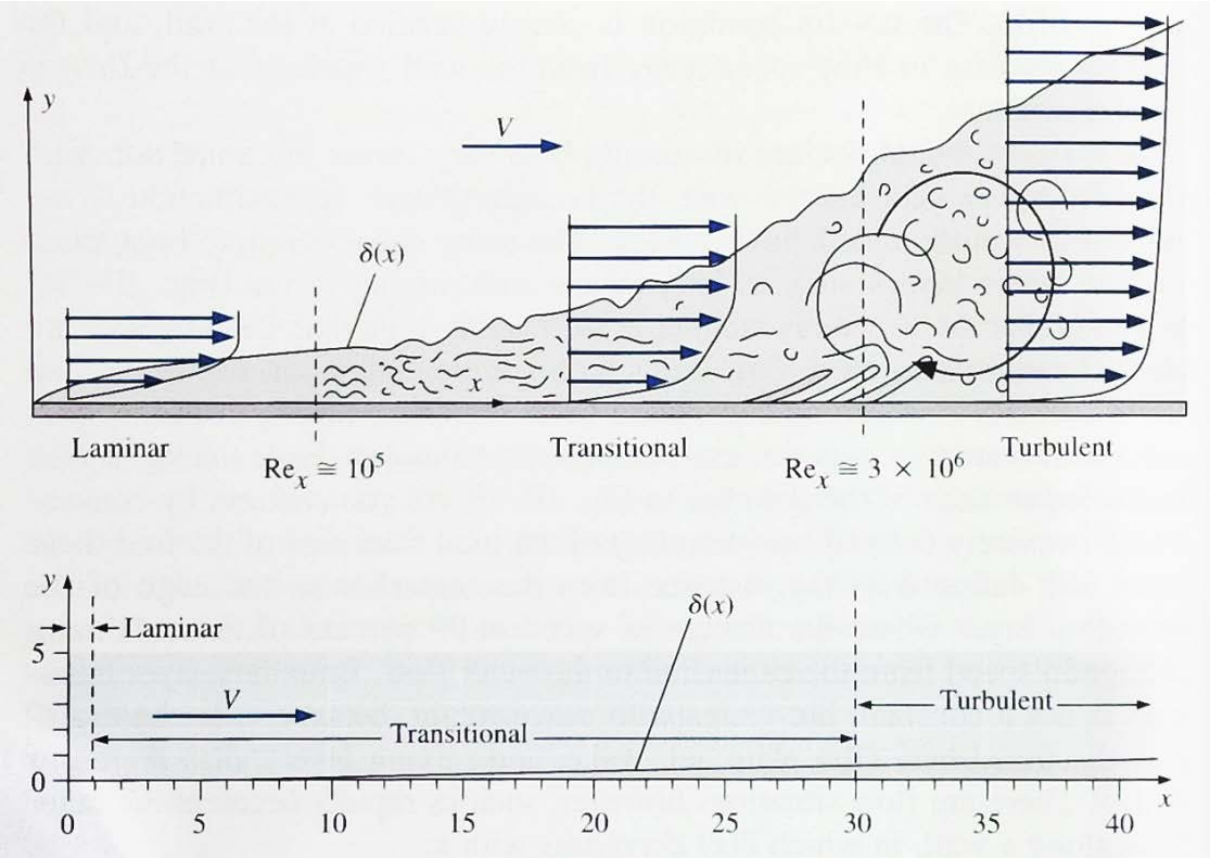

Figure 5 – Boundary layer; top has the vertical scale exaggerated, while the bottom is to scale. (Cengel & Cimbala, 2010)

However, the conditions in between the discs would be a closer approximation to that of Figure 6, with a variable length in x, depending on the flow path, and y would be equivalent to 2δ.

By changing δ, the core flow will be increased or decreased, and, at some point, the boundary layers will interact, causing turbulence and flow restriction. This would result in a significantly more difficult problem to analyze, given that the boundary layer calculations are approximations (Cengel & Cimbala, 2010).

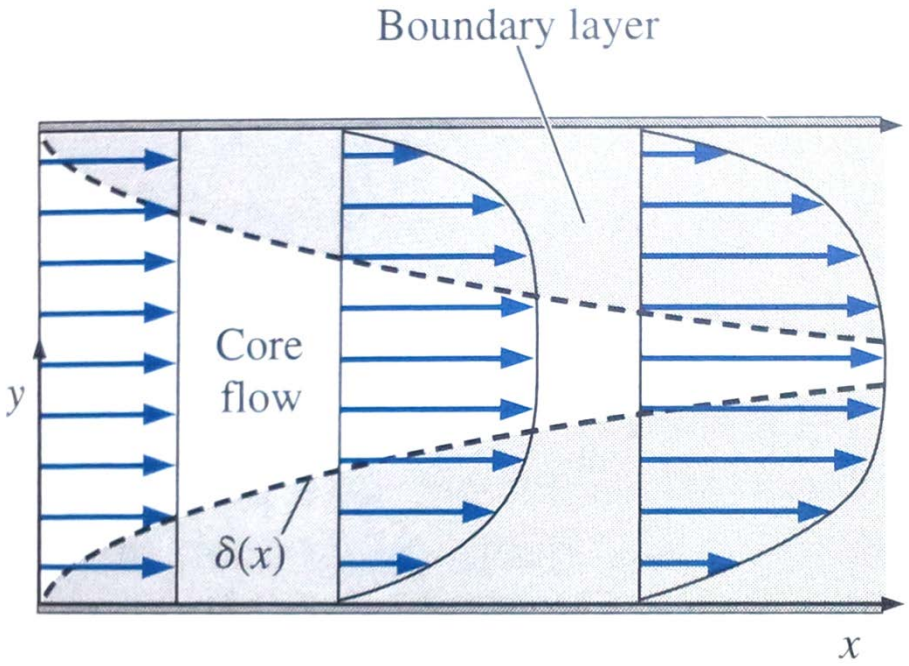

Figure 6 – Boundary layer flow between a two-dimensional channel. (Cengel & Cimbala, 2010)

The general approach should, therefore, start with computational fluid dynamics (CFD) analysis, which allows for the complete solution to the problem (Cengel & Cimbala, 2010). As written by Ladino (2004);

> *"It is interesting that for the flow between disks exist several different phenomena for the field flow. These conditions are turbulent inlet, laminarization from turbulent to laminar due to thickness of boundary layer, inflection of the profile, forward transition, acceleration of the flow due to continuity and conservation of angular momentum, creating a free vortex flow near the inner radius of the disk with high local Reynolds number and reverse transition or relaminarization."*

Such conditions are further complicated by variable speeds and loading of the rotor.

2.6. Theoretical Considerations for Flow in the Turbine.

After reviewing the literature, it was decided that the bulk of the design requirements for the current design would be taken from the most modern papers, that of Hoya and Guha (2009), and Guha and Smiley (2009), as described earlier. These two papers describe a rig that is of a reasonable size, and uses features that were deemed by the author as desirable, including the cantilevered disc pack, and bolt-on hub with exhaust.

The theory of Tesla Turbines is usually developed in terms of the Navier Stokes equations between two circular plates of inner radius (r_i) and outer radius (r_o) separated by a gap 2δ, as defined in section 2.3. These equations are conveniently written in a cylindrical coordinate system (r,θ,z) and in terms of the relative velocities with respect to rotating plates, v_r, v_θ and v_z:

Continuity equation 2;

$$\frac{\partial v_r}{\partial r_c} + \frac{v_r}{r_c} = 0 \tag{2}$$

θ - Momentum Equation 3;

$$v_r \frac{\partial v_\theta}{\partial r_c} + \frac{v_r v_\theta}{r_c} + 2\omega v_r = \nu \frac{\partial^2 v_\theta}{\partial z^2} \tag{3}$$

r - Momentum Equation 4;

$$v_r \frac{\partial v_r}{\partial r_c} - \omega^2 r_c - 2\omega v_\theta - \frac{{v_\theta}^2}{r_c} = -\frac{1}{\rho}\frac{dp}{dr_c} + \nu \frac{\partial^2 v_r}{\partial z^2} \tag{4}$$

z - Momentum Equation 5;

$$\frac{\partial \mathrm{P}_m}{\partial \mathrm{z}} = 0 \tag{5}$$

Where $\mathrm{P}_m = P - \rho g z$

Different approaches have been followed in solving these equations. We present here those adopted by Sengupta & Guha (2012), with the variables adjusted for internal consistency.

The boundary conditions 6-9 are applied to these equations

$$\text{at } r = \mathrm{r}_2 \qquad \overline{v_r} = \overline{v_{r_2}} \qquad \overline{v_\theta} = \overline{v_{\theta_2}} \tag{6}$$

$$\text{at } z = 0 \qquad v_r = 0 \qquad v_\theta = 0 \tag{7}$$

$$\text{at } z = \mathrm{b} \qquad v_r = 0 \qquad v_\theta = 0 \tag{8}$$

$$\text{at } z = \frac{2\delta}{2} \qquad \frac{\partial v_r}{\partial \mathrm{z}} = \frac{\partial v_\theta}{\partial \mathrm{z}} = 0 \tag{9}$$

where averaging, denoted by the symbol $\overline{(\,)}$, is performed in the z-direction

The velocities in the boundary layers are expressed as equations 10 and 11.

$$v_\theta(r_c, z) = \overline{v_{\theta_2}}\zeta(r_n)G(z) \tag{10}$$

$$v_r(r_c, z) = \overline{v_{r_2}}\xi(r_n)H(z) \tag{11}$$

where $r_n = {}^{r_i}/_{r_o}$, and where a parabolic velocity profile is assumed, in equations 12 and 13;

$$G = 6 * \frac{z}{2\delta}\left(1 - \frac{z}{2\delta}\right) \tag{12}$$

$$H = 6 * \frac{z}{2\delta}\left(1 - \frac{z}{2\delta}\right) \tag{13}$$

In order to develop a solution, the conservation equations are integrated in the z direction, giving two differential equations, 14 and 15:

$$\frac{d\zeta_m}{dr_n} = -\left\{\frac{1}{r_n} + 10\left(\frac{\upsilon}{\omega(2\delta)^2}\right)\frac{r_n}{\phi_2}\right\}\zeta_m - \frac{10}{6} \tag{14}$$

$$\frac{dP'}{dR} = r_n + 2\zeta_m + \frac{6}{5}\frac{\zeta_m^2}{r_n} + \frac{6}{5}\frac{\phi_m^2}{{r_n}^3} - 12\left(\frac{\upsilon}{\omega(2\delta)^2}\right)\frac{\phi_2}{r_n} \tag{15}$$

where $\Phi_2 \equiv {\bar{v}_{r_2}}/{\omega r_2}$, $\zeta_m = modified\ \zeta = {\bar{v}_\theta(r_c)}/{\bar{v}_{\theta 2}}$ and $P' = \frac{P - P_i}{\rho\omega^2 {r_o}^2}$

The above two equations can be solved analytically by Sengupta & Guha (2012) or numerically by Sengupta & Guha (2013) to yield a solution of the velocity profiles between the two disks. The obtained profile can be used to evaluate the wall shear stress per equation 16;

$$\tau_w = \left[\mu\frac{\partial v_\theta}{\partial z}\right]_{z=0} \tag{16}$$

which when integrated over the plate area and multiplied by the relevant number of disks gives the total torque exerted by the fluid on the turbine.

The torque can also be written in terms of the moment of inertia and angular acceleration of the disks as equation 17;

$$\tau = I\alpha \tag{17}$$

The power can be obtained by multiplying the torque by the angular velocity of the turbine, as shown in equation 18;

$$p = \tau\omega = [\tau_{accel} + \sum(\tau_{loss})]\omega \tag{18}$$

Figure 7 shows the result of above models as computed by Sengupta & Guha (2013), in both an absolute and relative frame.

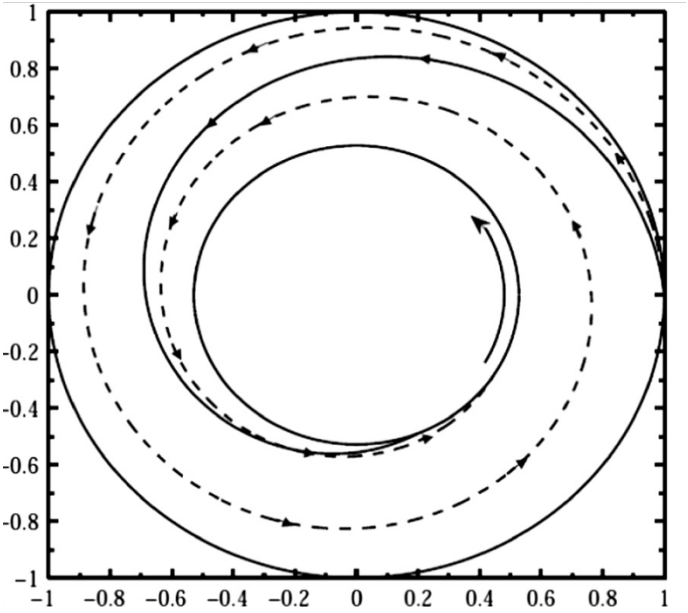

Figure 7 – Absolute (solid) and relative (dashed) path lines in a Tesla Turbine. (Sengupta & Guha, 2013)

2.7. CFD Approaches

The literature provides several examples of CFD analysis of a Tesla Turbine, which provides some insight to the overall conditions found therein. This problem has been considered by Sengupta & Guha (2013), Ladino (2004), Lapart & Jedrzejewski (2011). The results can be seen in Figures 8-11 below. These demonstrate that the flow is clearly a spiral flow, which had been suggested in other much earlier papers by Armstrong (1952) ,Rice (1965), North (1969), and others, which use a numerical approach. Unfortunately, these analyses do not readily consider the momentum transfer involved, and to do so was beyond the scope of this thesis.

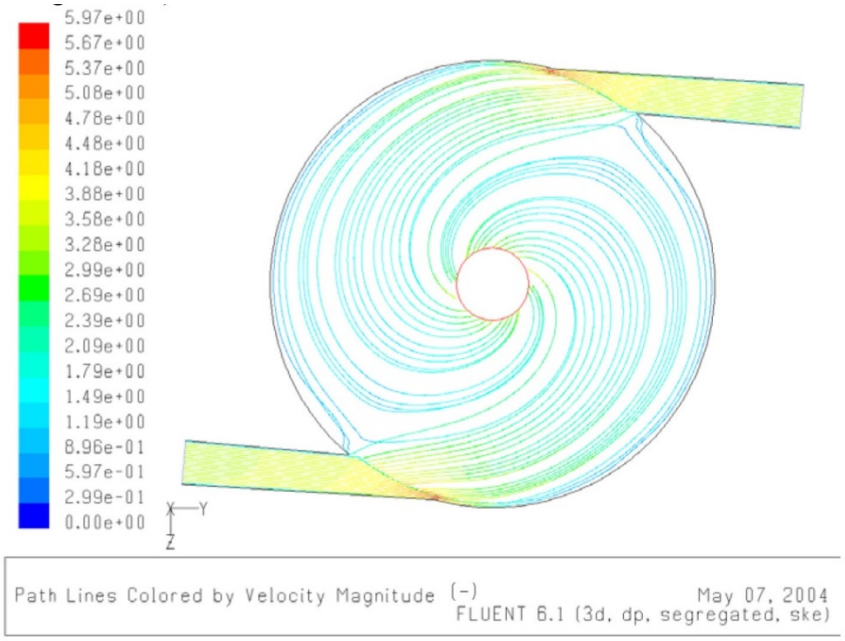

Figure 8 – Pathlines of flow in a two entry Tesla Turbine. (Ladino, 2004)

In Figure 8, the spiral path is clearly evident, but it is affected by the second inlet, shortening the spiral. It is also worthwhile to consider an axial cross section, per Figure 9, of the entry of the

flow over the discs, where a parting occurs. This suggests that there would certainly be advantages to a non rectilinear profile of the discs.

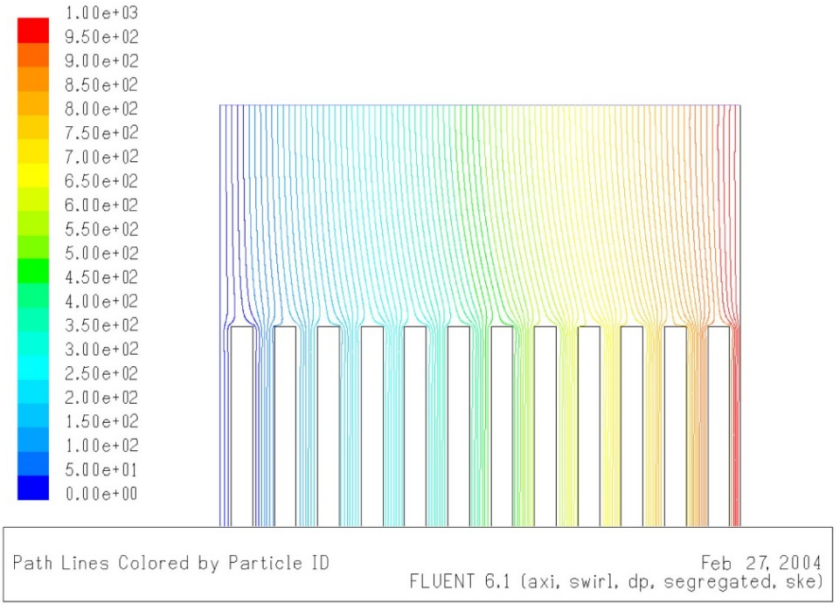

Figure 9 – Flow across the disc edges of a Tesla Turbine. (Ladino, 2004)

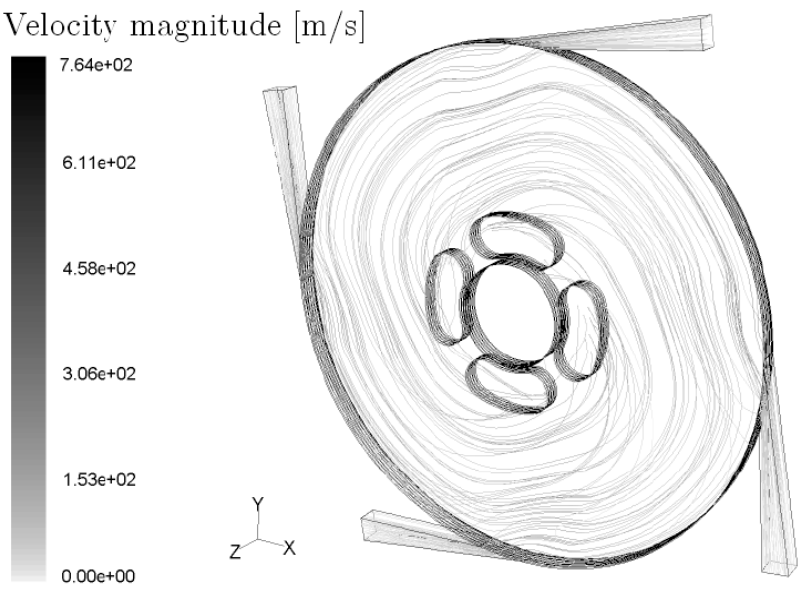

Figure 10 – Flow of a Tesla Turbine with four nozzle inlets. (Lapart & Jedrzejewsky, 2011)

Other considerations of the flow can be seen in Figure 10, which highlights the added complexity that the flow adds, while also providing insight to consequences of having a shaft and satellite orifices for exhaust.

In an effort to prove the model Sengupta & Guha (2012) developed, they created a CFD model that serves to provide additional enlightenment to the multi-axial conditions that exist in between the individual discs of the rotor. Figure 11 demonstrates the change in pressure across the discs, as well as the variation in radial and tangential velocities that exist between the discs.

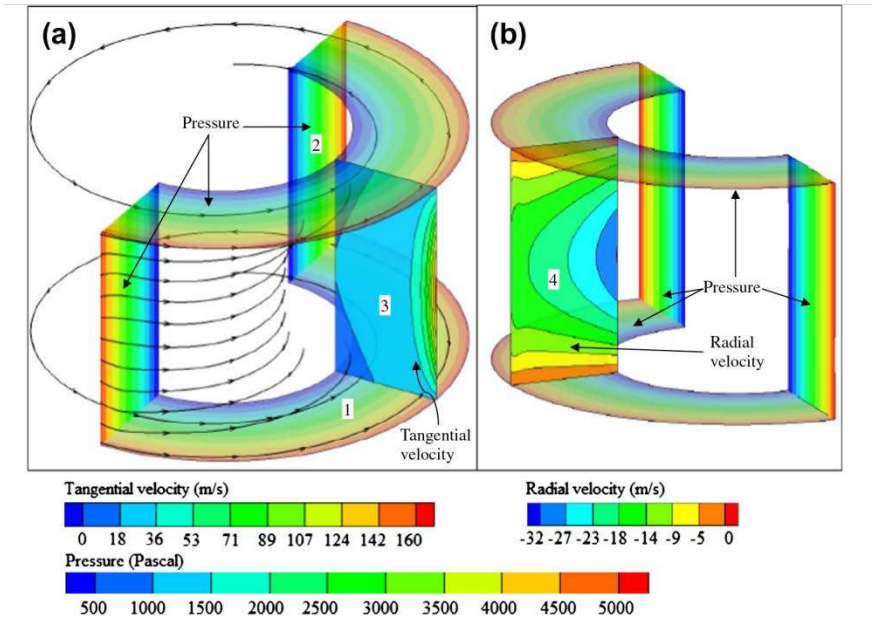

Figure 11 – Absolute pathlines, pressure and velocity fields between two discs in a Tesla Turbine. (Sengupta & Guha, 2013)

2.8. Various Designs from the Literature

As previously mentioned, the first set of inspections into the turbine occurred in the 1950s and 1960s. The first of which was a master's thesis by A. Leaman (1950), followed by a master's thesis by J. Armstrong (1952). There were several others, including theses by Warner, Iversen, Blaje and Rice, but the author was not able to secure copies for review in this document. Later, E.W. Beans (1961), and another PhD thesis, authored by R.C. North (1969). These should be considered the primary set of designs, as later designs are very similar to these.

2.8.1. Leaman's Design

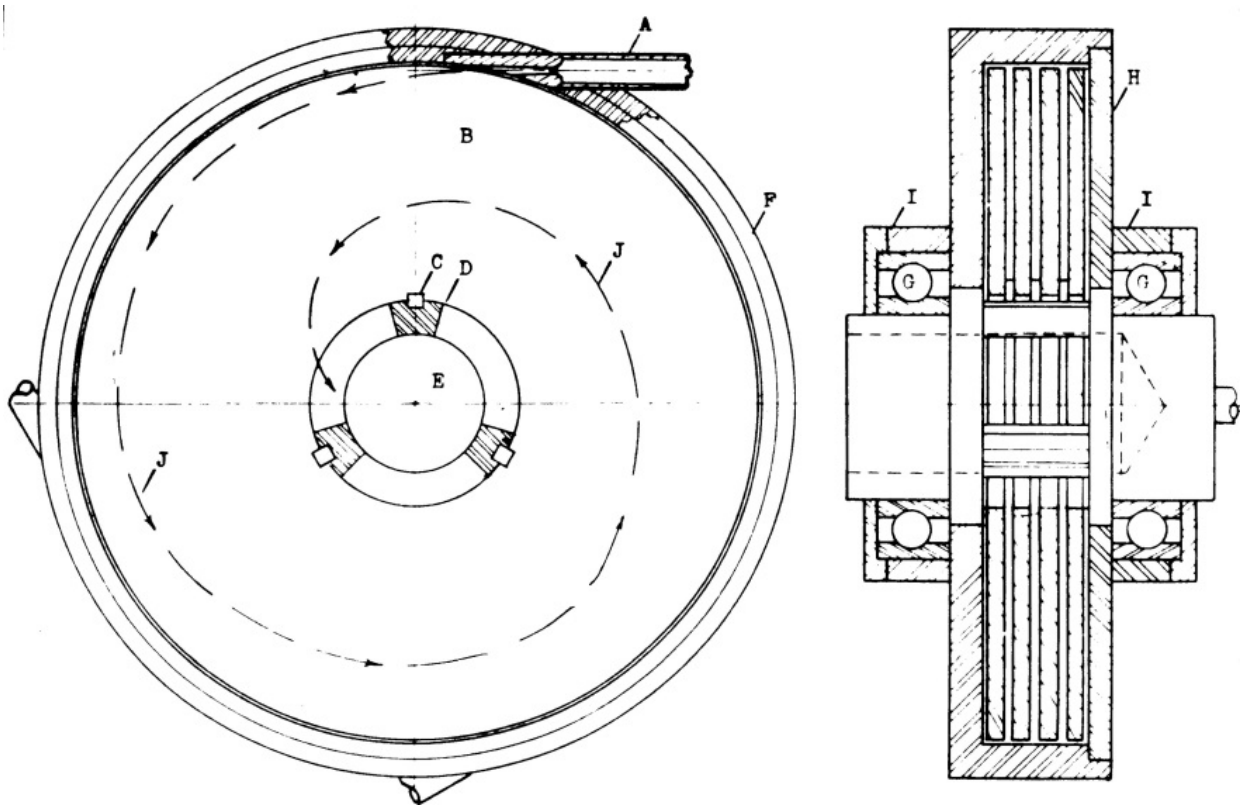

Figure 12 - Turbine Design by Leaman (1950)

Leaman (1950) built a turbine with a central exhaust, which is the first appearance of this feature. This turbine, shown in Figure 12, uses 4.6" (.126 m) discs, with a maximum inlet pressure of 85 psig (5.8 bar). The maximum speed reached exceeded 9,000 RPM, with an efficiency of 8.24%. In his design, Leaman had a slightly different approach for the affixing of the discs from Tesla's original concept, where the exhaust was delivered to a central cavity, and the shaft was slotted to allow for the exhaust flow to pass.

In his design, he used various surface textures of discs, to see the effects. He found that the smooth discs performed slightly better than rough discs.

2.8.2. Armstrong's Design

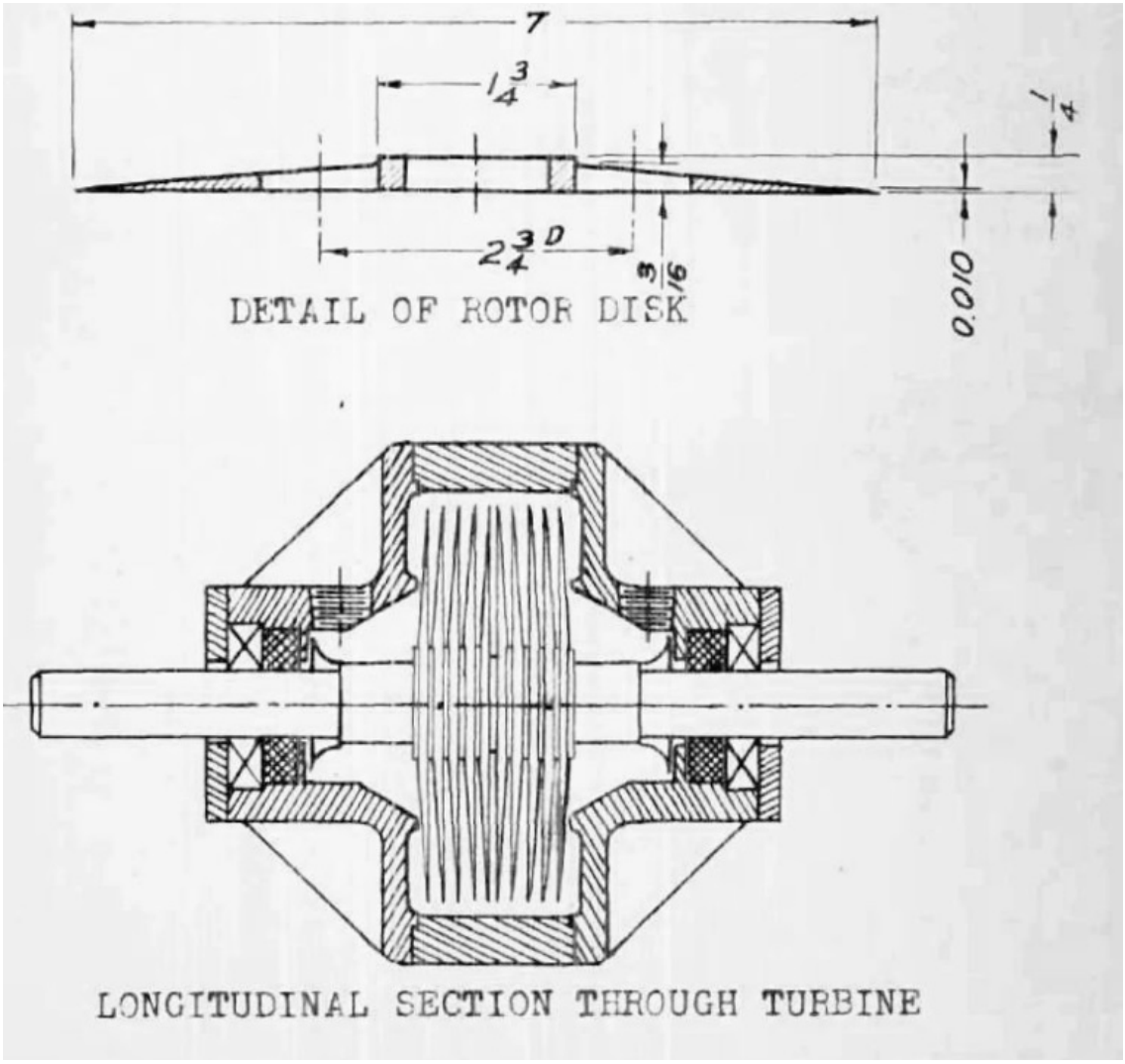

Figure 13 - Turbine design by Armstrong (1952)

Armstrong built a steam turbine, shown in Figure 13, which made several modifications to Tesla's design, most notably in the profile of the discs. He created a disc with very tapered edges, in an effort to decrease the turbulence caused as the fluid entered the turbine. He used 7" (.178 m) diameter discs, with steam at a pressure of 125 psi (8.6 bar). The maximum speed reached with the design was 9,000 RPM, with an efficiency of only ~4% (Armstrong, 1952).

2.8.3. Beans' Design

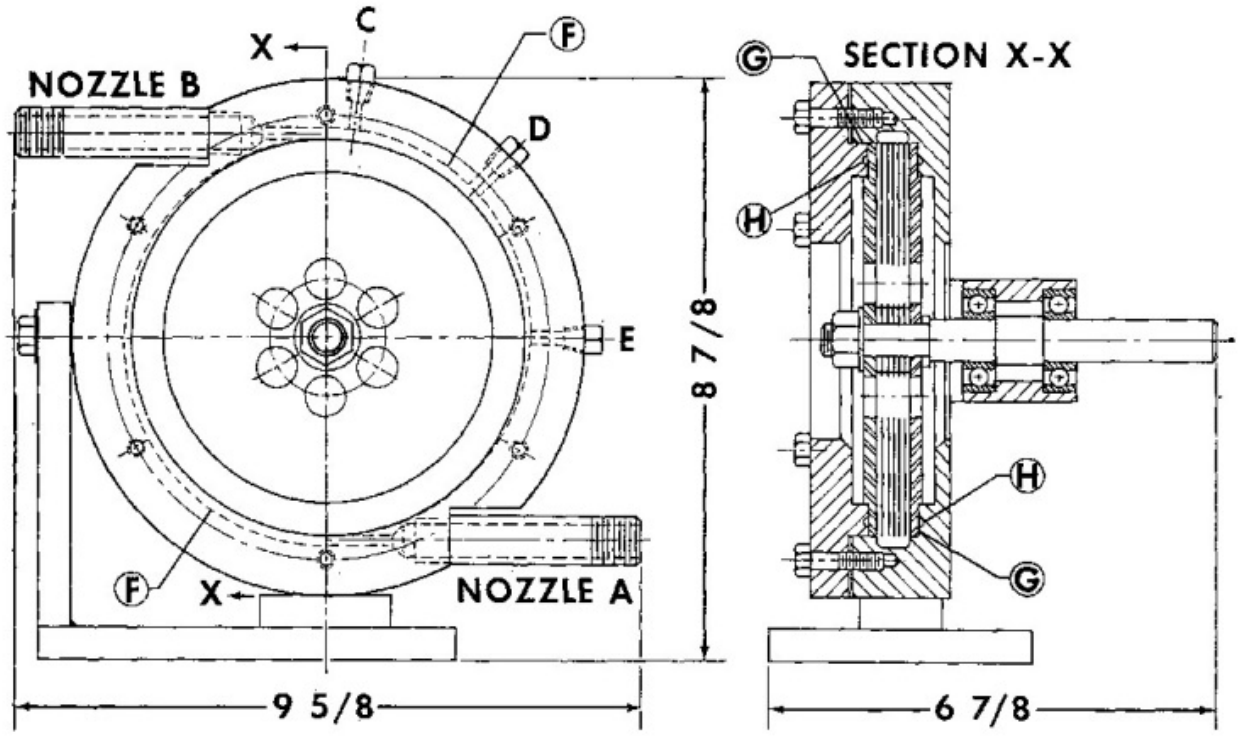

Figure 14 - Turbine design by Beans (1966)

Beans' primary investigation was on the effects of disc spacing and on the effects of inlet pressure. His design, shown in Figure 14, had two inlet nozzles, with a cantilevered bearing arrangement. Beans' design maintained a disc diameter of 6" (.152 m), operated at a pressure of 40 psig (2.76 bar), and a top speed of ~18,000 RPM. Beans (1966) determined the efficiency of his turbine, under those conditions, to be 24%.

2.8.3.1. North's Design

Finally, of these early papers, North (1969) considered a design that sought to modify the method that the fluid entered into the system. The most notable change was the creation of a 'supply chamber', a volume at pressure, to supply a relatively large number of circumferential

nozzles. The discs used in his paper were 4 7/8" in diameter (.124m), operated at an extremely low pressure of 14.5 psig (1 bar) at a maximum speed of 2,070 RPM. North calculated his maximum efficiency to be 16%. North's turbine can be seen in Figure 15.

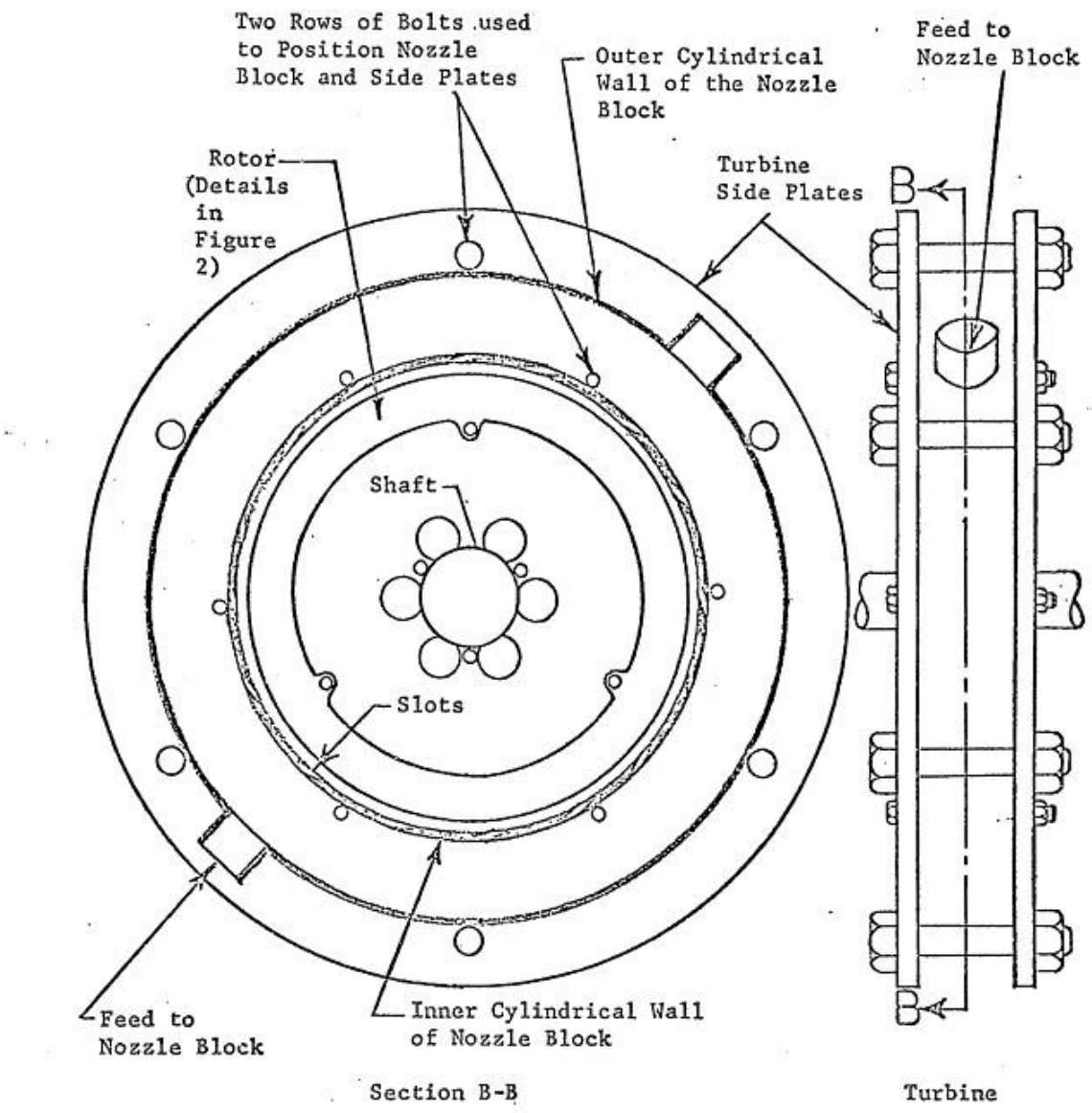

Figure 15 - Turbine design by North (1969)

2.8.4. Rice's Design

Later work was done by students under Rice, but many of those works were not available to review, including Rice's original thesis in 1963. However, one of Rice's works appeared in a Nikola Tesla Symposium in 1991, which shows an early occurrence of a hub-exhaust version, as shown in the left of Figure 16.

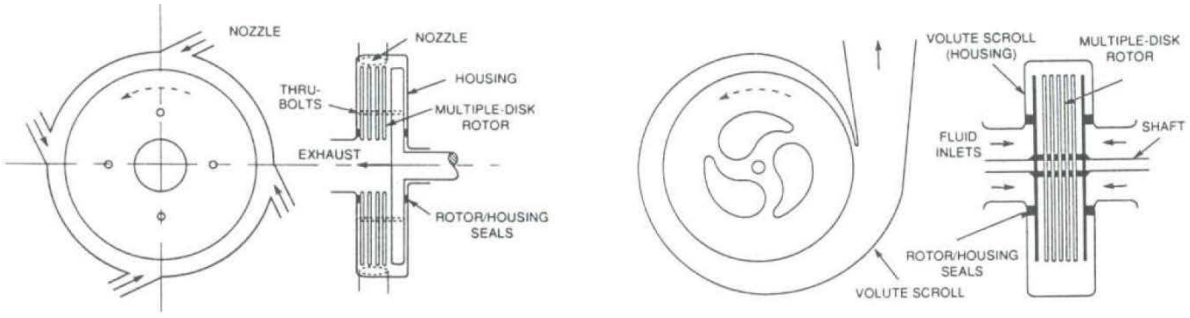

Figure 16 - Versions described by Rice (1991), with Rice's version (left) with a central exhaust, and a typical Tesla version (right) with slots in the discs, and a central shaft, configured as a pump.

2.8.5. Hoya & Guha's Design

In addition to the aforementioned theses, several papers were published based on the design presented in "The Design of a test rig and study of the performance of a Tesla disc turbine" by Hoya and Guha (2009), and "Experiment and analysis for an improved design of the inlet and nozzle in Tesla Disc Turbines" by Guha and Smiley (2009). The design used is principally the same as that of Rice, though with some subtle modifications primarily around the nozzle.

This design used discs that were 92mm in diameter, and operated at a pressure of 3.9 bar. Maximum efficiency was measured at approaching 25%, however, that value included the frictional torque within the system.

These two papers are among the most recent, and most applicable to the intended goals of this thesis, and will be discussed more in section 5.2.

2.8.6. Comparison of Various Designs.

Figure 17, below, shows a comparison of the various design features and results obtained by the authors.

Author	r_o	r_i	central(c) shaft(s) exhaust	# Discs	Disc Spacing	Steam(s) Air(a) Water(w)	Operating Pressure	max speed	max torque	max power	max efficiency
	(mm)	(mm)			(mm)		(bar)	(rpm)	(Nm)	W	%
Armstrong (1952)	88.9	47.625	s	10	variable	s	8.1	6000	0.1	530	4.26
Beans (1961)	76.2	30.5	s	6	12.7-.67	a	2.75	17000	0.9	5600	24
Rice (1963)	88.9	33.5	c	9	1.6	a	9.6	11800	n/a	1800	23.2
Leaman (1950)	63	10	c	4	3.2	a	5.8	9000	0.1	87	8.24
Lemma (2008)	25	5.95	s	6(?)	n/a	a	0.514	96000	0.04	220	20
Tesla (1913)	228.5	n/a	s	25	n/a	s	8.6	9000	n/a	150k	n/a
Emran (2011)	18.8	17	s	4	n/a	a	5.9	50000	0.345	n/a	n/a
Peshlakai (2012)	75	34.5	s	12	1.3	a	6.14	n/a	n/a	12	31
Bloudicek (2007)	100	17	c	13	n/a	a	20.5	n/a	0.7	58.3	20.45
Romanin (2012)	36.5	18	s	10	1.2	a	5.4	24170	n/a	n/a	16.3
Romanin (2012)	5	1	c	4	0.5	w	n/a	n/a	n/a	35	13.7
Hoya & Guha (2009)	46	12.5	c	8	0.2	a	3.6	25000	0.7	140	26

Figure 17 - Comparison of features from a sampling from the literature

2.9. Patents

There are a considerable number of patents that find their original prior art in Tesla's initial filing. Generally speaking, and with the caveat that most patent filings do not include very much with respect to design criteria, engineering analysis, or any results that might provide insight the viability of the design.

Given that, there are suggested developments that relate to nozzle inlets (Stocklinger, 2012) (Possell, 1978), as part of a larger generation system (Bohl, 2012), (Foulton & Taylor, 1974), including tilted rotors (Posell, 1977), staging (Ritzi, 1981), a turbine/pump arrangement (Conrad & Conrad, 2001), various modifications to the inlet edges of the discs (Fuller, 2010), and so on.

2.10. Other Sources

Outside the academic literature, there is also some significant information, though much of it is somewhat anecdotal. There are several groups, including the Tesla Universe (2015) and the Tesla Engine Builder's Association (2015) who have compiled a significant amount of this type of information. However, given the lack of scientific rigor applied, it has not been reviewed to a great extent.

2.11. Comparing Different Investigations in the Literature

Upon going through the literature, it would appear that one thing is consistent – few, if any of the researchers sought to build a platform or a testing paradigm that would provide an experimental comparison with other works found in the literature, or even Tesla's original turbine. As a result,

it is very difficult to compare any given work to another; each system contains within it many different sources of error, and flow streams. Until recently, there was not a complete theoretical description of the turbine by Sengupta & Guha (2012), and a result, it was inherently more difficult to completely define these differences.

Beyond this, much of the work has concentrated on the modeling of the flow around the discs, but most of the sources in the literature apply a diversity of approaches that have yet to be modeled, including multiple inlets, surface modifications to the discs, and exhaust configurations.

2.12. Nozzle choking

To determine if the nozzle is choked, it will be assumed that the flow is steady and one dimensional. We know the mass flow is obtained from equation 19 (Cengel & Cimbala, 2010);

$$\dot{m} = \rho_t A_t v_t \tag{19}$$

Which can be reorganized to equation 20;

$$v_t = \frac{\dot{m}}{\rho_t A_t} \tag{20}$$

The area, A_t, is the cross sectional area of the narrowest part of the nozzle, length times width. We also know the nozzle is choked if the Mach number is 1, or equal to the speed of sound in air, assuming a temperature of 303K, with a speed of sound in air at 349 m/s (Cengel & Cimbala, 2010). . This gives us equation 21;

$$M_{at} = \frac{v_t}{349} = \frac{\dot{m}}{349\rho_t A_t} \tag{21}$$

For a convergent nozzle M_{at} cannot exceed one.

2.13. Efficiencies

The literature describes many different approaches to the calculation of efficiency. For the purposes of this paper, we will follow that of Armstrong (1952), where the efficiency is defined as per equation 22;

$$n_{exp} = \frac{p_{out}}{(h_1 - h_3)'\dot{m}} \tag{22}$$

such that $h_1\dot{m} = inlet\ enthapy$ and $h_3'\dot{m} = ideal\ enthalpy\ in\ atmosphere$, which is equal to the isentropic expansion. This value is calculated using the power calculated from $p_{out} = \tau\omega$.

2.14. Expected Results from the Literature

The question remains; what is expected, for an acceleration of a Tesla Turbine, from zero to

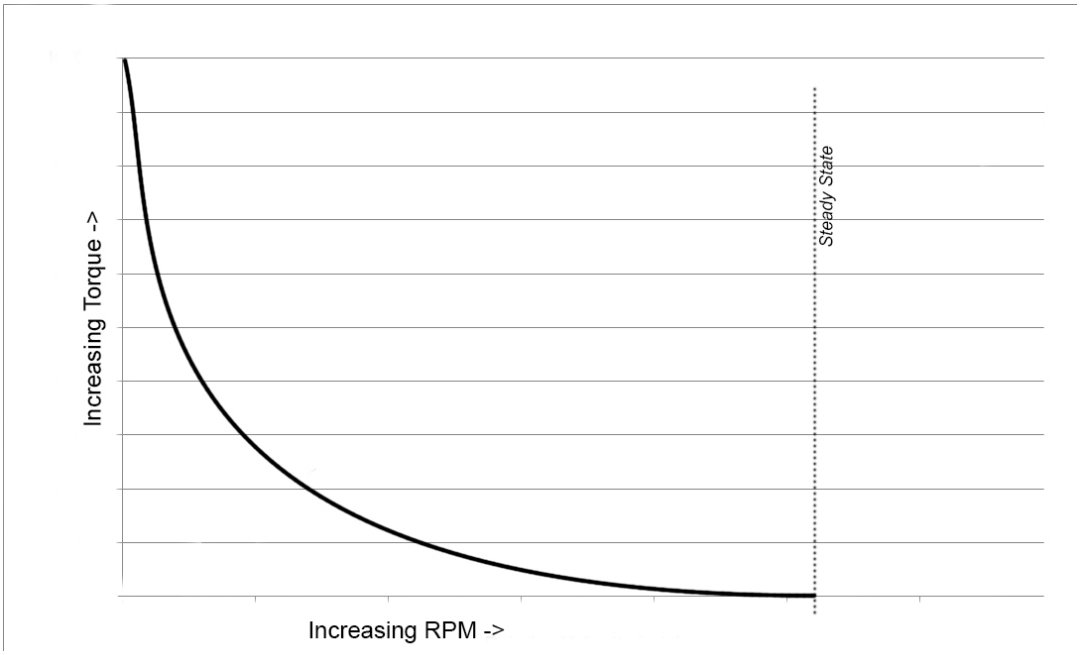

steady state? As described earlier, we expect that the maximum torque for a Tesla Turbine will be at low speed (Rice, 1965), and as the tip speed approaches the velocity in the flow, the torque will approach a steady state value, as sketched in Figure 18. This results in a turbine speed versus time variation as shown in Figure 19 , where the turbine accelerates quickly, and asymptotically approaches steady state, at some value. As the nozzle angle is changed, one would expect that the angles closest to tangential will have the greatest torque, and as the angle is changed radially inward, the torque will decrease as suggested by Romanin (2012), per Figure 20.

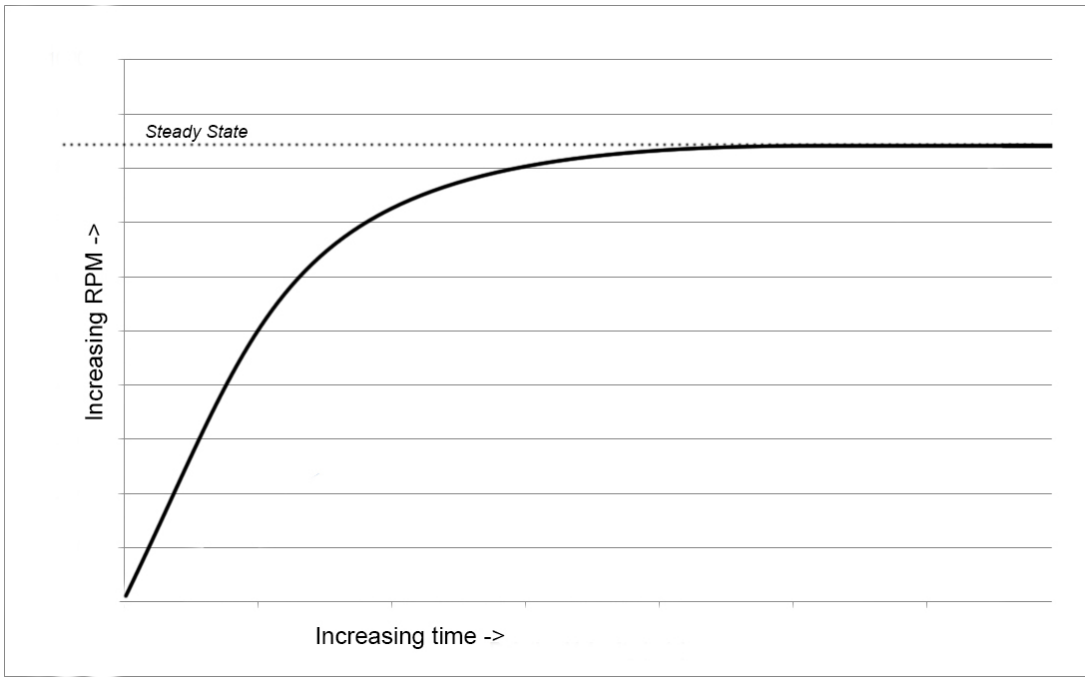

Figure 19 –Expected speed

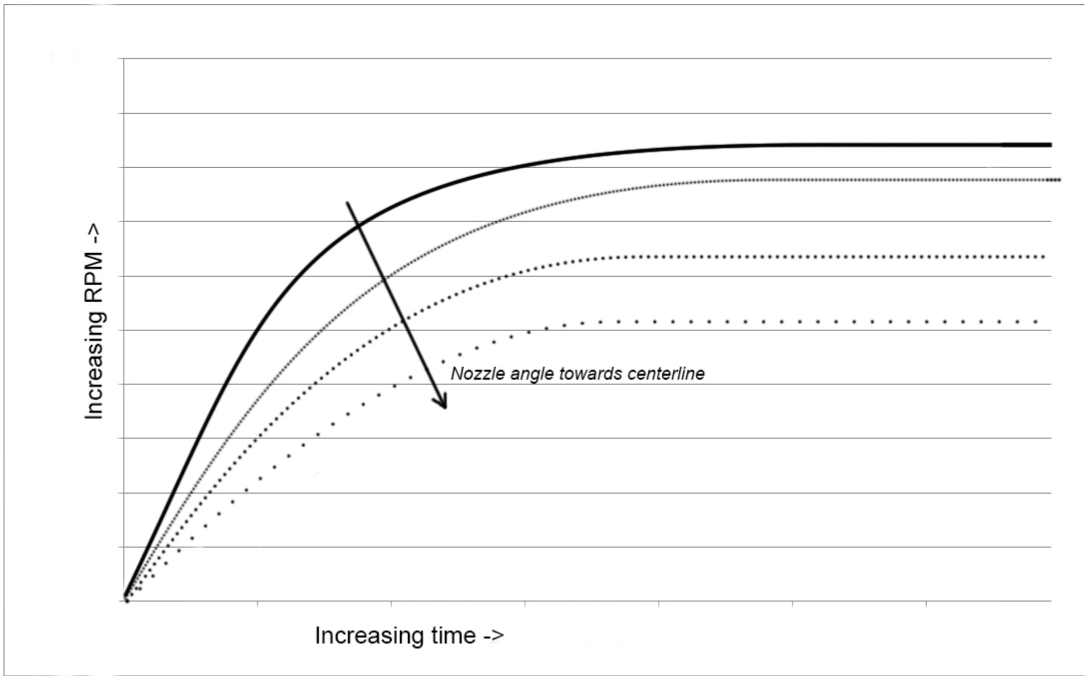

Figure 20 –Expected change in torque by changing nozzle angles

3. Turbine Design

This chapter discusses the aspects of the design of the Tesla Turbine that is the subject of this thesis, and the choices made in detail.

3.1. Turbine Overview

The fundamental advantage of this type of turbine is its simplicity; both in design, construction, and cost to build. In a high-production context, the Tesla Turbine would be able to be manufactured several orders of magnitude more cheaply than its bladed counterparts, and run in a more varied operational envelope with a greater variety of working fluids.

In the general design, one main consideration was prevalent; that is to ensure symmetry in all of the rotating components, so that there would be a good balance to the system. Because the turbine is capable of spinning at a high speed, balance issues are very important to keep in check, or there would be a risk of either catastrophic failure and/or poor data collection due to vibrations.

3.2. General Considerations of the Disc Pack

Because the disc pack is critical to the overall proportion of the system, it should be considered first. The first dimension of importance is the diameter of the discs themselves; this value can be adjusted depending on several factors, including the inlet fluid and its pressure and temperature, as well as the desired moment of inertia for the system. For example, in the case of a high pressure steam turbine, larger discs would be preferred, since the nozzle exhaust velocity would be much higher, and a larger moment would store energy in the event of a sudden load, in order

to prevent excessive deceleration. In the case of this thesis, however, relatively low pressure air is the working fluid, zero to low load requirements, and for ease of material sourcing and construction, the diameter of the disc pack was chosen to be 92mm – the diameter of a single 3.5" hard drive platter. This size also allowed for a direct comparison to the aforementioned papers of Hoya & Guha (2009) and Guha & Smiley (2009). Hard drive platters were chosen since they are extremely smooth, have extremely precise dimensions, and were readily available at no additional cost.

Figure 21 - A hard drive with its cover off, showing the platters.

Given the choice of the hard drive disc platter, there are relatively few choices for thickness of the platters themselves; they range from 0.3mm to 0.6mm. In the process of collecting hard drives, made difficult due to various privacy policies in different organizations, a relatively small number of hard drives were acquired. The original intent was to create several platter sets, and so the most common platter thickness was chosen, which was 0.8mm. The multiplicity of disc sets was intended to allow for testing of a multiplicity of disc conditions, such as surface roughness, edge sharpness, and other features. Ultimately, because of problems in manufacturing, only one disc set was used.

Lastly, the material of the disc platter is predefined by the source as aluminum. In a larger disc, where rotational speeds would dictate a higher yield strength, stronger materials such as steel or carbon fiber would be preferred (Bergen, 2009).

Hoya and Guha (2009) calculated the maximum allowable angular speed without plastic deformation or bursting by using equation 23;

$$\omega_{max}^2 = \frac{8\frac{\sigma_y}{FS}}{(3+\nu)\frac{\rho}{g}r_0}\left(\frac{1}{2+\left(\frac{r_i}{r_o}\right)^2\left[1-\frac{(1+3\nu)}{(3+\nu)}\right]}\right) \quad (23)$$

Where σ_y is the yield stress, FS is the factor of safety.

In the case of the current design (assuming aluminum 6061);

$\sigma_y = 300\ MPa$	$FS = 2$	$\nu = 0.33$	$\rho = 2.7\ g/cm^3$
$g = 9.8\ m/s^2$	$r_i = 25mm$	$r_o = 92mm$	

This results in a maximum safe rotational speed of 3616 rad/s, or ~34,500 RPM. The literature rarely speaks of a speed faster than 35,000 RPM; consequently, the platters should have no issues (Burton, 1955).

The next thing to consider in the disc pack is the exhaust methodology; that is to say how the exhaust holes are placed disc to disc, and out of the turbine. There are two approaches to this. The first was done by Tesla (1913) in his original design, where holes were placed in the discs outside the shaft, leaving three struts as a structural connection to the hub. This method has the advantage of simplifying the hub assembly, where disc spacers can be placed outside of the flow,

but decreases the duration of flow contact with the disc surface since the outlet occurs further out from the centerline.

An alternate arrangement, which was originally proposed by Rice (1991), has the exhaust being central; where the discs are mounted to a hub, and the shaft terminates prior to the disc pack itself, thereby not interfering with the flow. This has the advantage of a less complex exhaust flow, though still very turbulent, and longer time for the flow to interact with the discs. It does, however, introduce obstructions to the flow for the bolts and spacers that are introduced. Rice (1991) noted an improvement in using this method, and it was therefore chosen as part of this design. This exhaust method was also chosen by Hoya and Guha (2009).

3.3. Disc Pack, As Designed

As mentioned in the previous section, the discs were based on hard drive platters, from 3.5" hard drives. These platters can be found relatively ubiquitously, however, not all platters are identical. In the course of this initial design step, several dozen hard drives were disassembled, and then the disc platters were measured. It was discovered that there was some variance in their dimensions, especially in thickness. These variances were present in drives of the same brand, for drives of similar sizes. In any case, a large selection of discs were found that were virtually identical.

The discs chosen had the following primary dimensions;

1) OD of 95mm
2) ID of 17mm
3) Thickness of 0.80mm

The discs were then modified with the addition of a bolt circle at a radius of 20.64mm, which comprised of four 4.98mm thru holes. These would allow passage of the bolts which were used to affix the rotor assembly to the shaft hub.

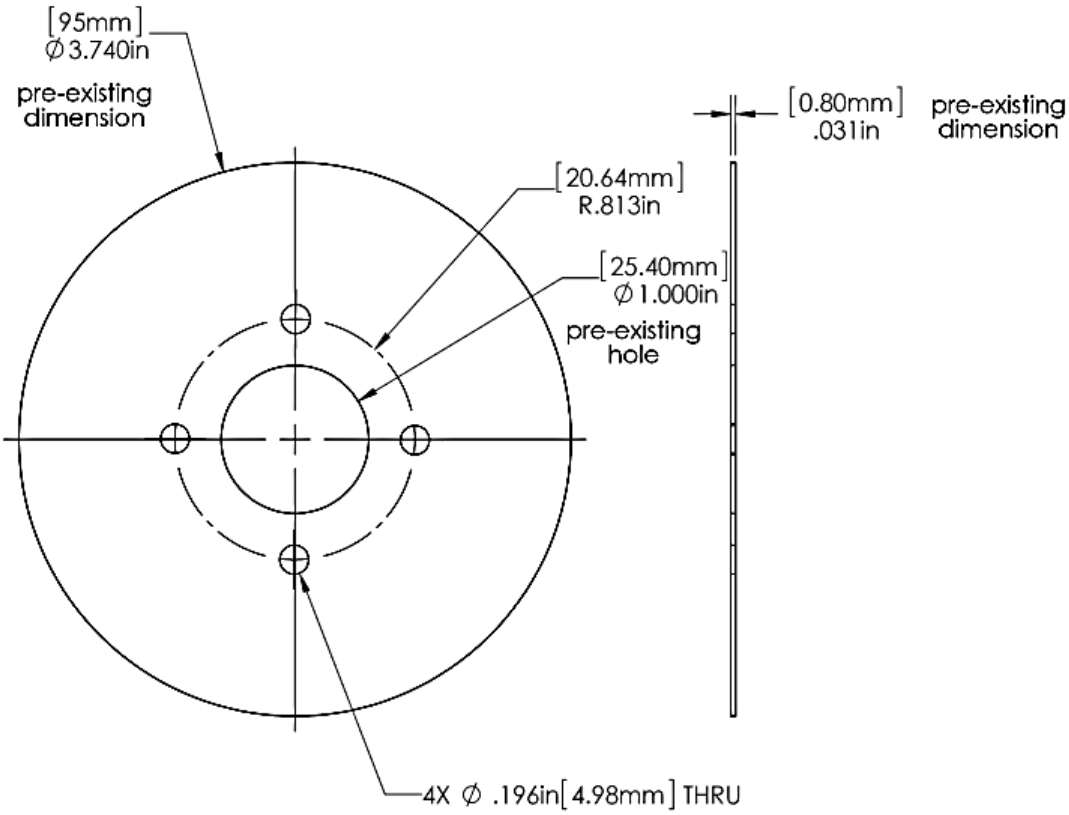

Figure 22 - Large disk

The diameter of the bolt circle was determined as a trade-off between being closer to the center of the exhaust, where flows will be relatively slower, but far enough to allow the hubs on either side to have the room to accept the bolts; consequently, the bolt circle was placed after the hubs were designed. Six large discs were made, per Figure 22, above.

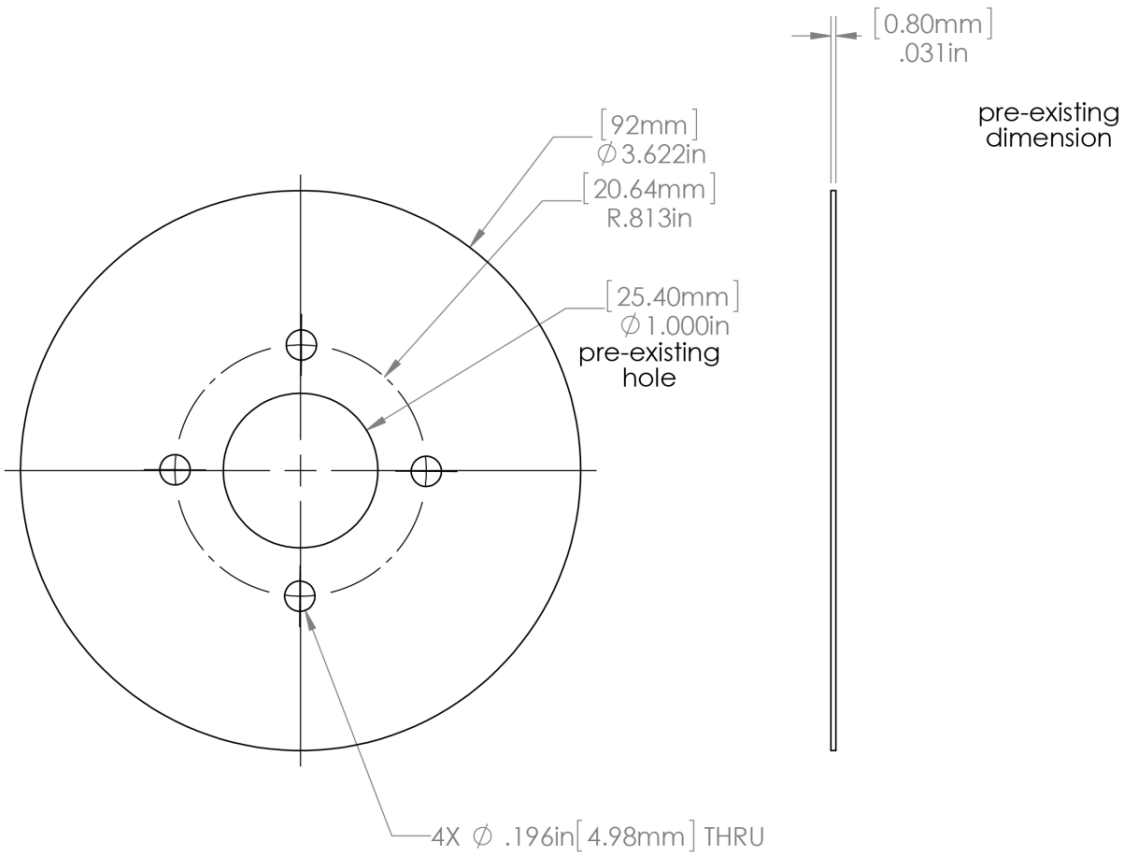

Figure 23 – Small modified disc

Several different design options were considered, including having a smaller diameter set of discs. An extra set of discs was manufactured with an additional modification; they were turned down from 95mm to 92mm, as shown in Figure 23. The goal in so doing was to have the option to create additional edge features, as well as test the effect of this larger gap. The intended goal

was to have multiple sets of discs with different features for future testing. A relatively large number of these were made, 24 in total, since it would be difficult to turn these down after the primary machining was done. The original goal was to be able to create a larger set of tests with a variety of disc configurations. Most of the extras were warped and otherwise damaged, however, and could not be used.

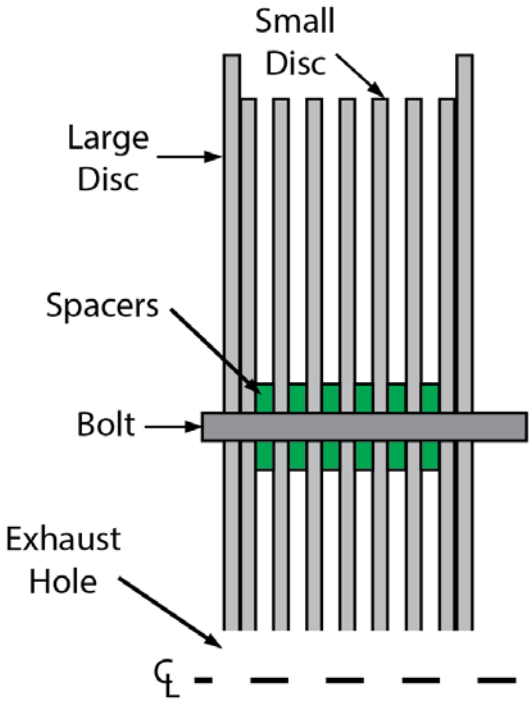

Figure 24 - Disc pack cross section with spacers

In addition, the design would include spacers between the discs, mounted on the bolts, in order to keep a consistent spacing between them. These are also noted in Figure 24, and were sourced 'off the shelf', as washers that were the desired 0.2mm thick. The overall design can be adjusted somewhat by changing the thickness of the spacers, so that one can vary the gap between the discs to test the effects of so doing.

3.4. General Considerations of the Hub Arrangement

Rice (1991) found that a centrally exhausting passageway is more desirable, insofar that it decreases the overall turbulence in the exhaust flow, thereby increasing the mass flow. Given this, and the preexisting holes in the center of a hard drive platter, several constraints are placed on the design. In order to have a central exhaust, the shaft cannot pass through. In addition,

there needed to be something to receive the disc bolts. Therefore, a hub needed to be mounted on one side with a bolt circle that matches the holes in the disc.

At this point, a decision needed to be made; did one want to have the bearings on one side of the disc pack, cantilevered, or place a bearing seat on either side? The initial plan was to build a flexible platform, where eventually the turbine could be run with diverse fluids, including steam. Given this, if there was to be a bearing seat on the exhaust side as shown in Figure 25, it would have to be a high temperature, high performance bearing. This would add significant cost, based on research, and therefore for the long term usefulness of the platform, it was decided to use a cantilevered system.

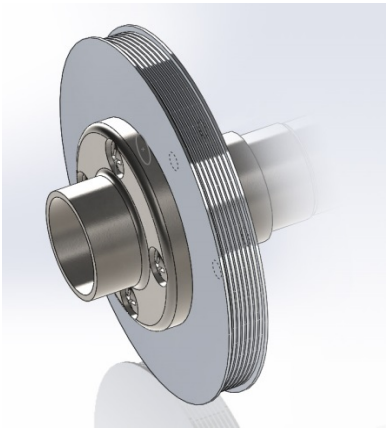

Figure 25 - Disc pack and hub assembly

Given this, the exhaust from the disc pack could be released directly from the last disc, but this would create additional backpressure at the seals that will be described later. Therefore, it was decided that an additional hub component would be added that would guide the flow outside the device. This would also provide additional surfaces for seals.

3.5. Hub Arrangement, As Designed

The primary dimension that was used to start the design of the hub was the exhaust hole, as defined by the central hole of the hard drive platters. This made this dimension 25.4mm, as seen in Figure 26.

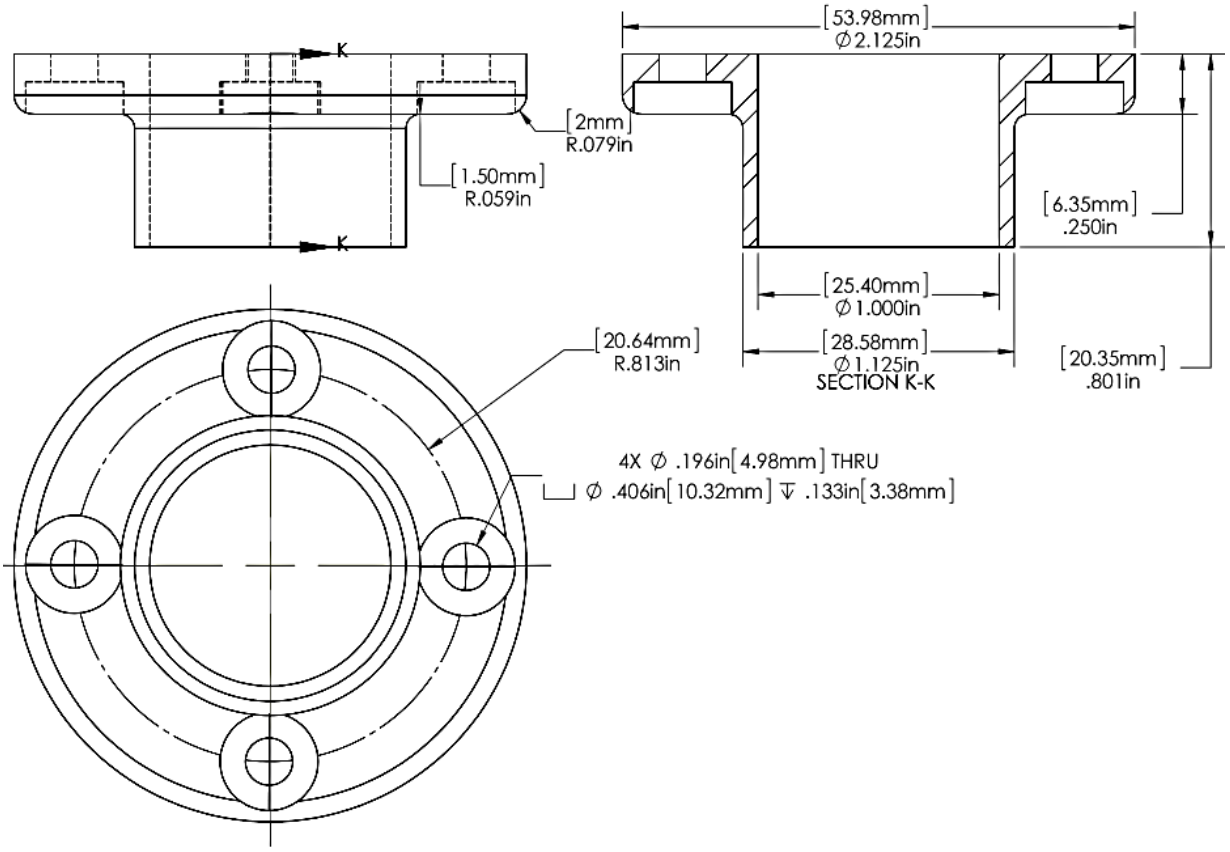

Figure 26 - Exhaust hub

The second consideration in the design was the wall of the exhaust; the goal in this case was to provide an exhaust pipe that would be able to freely rotate with the disc pack, and ensuring that there was no opportunity for the flow to interact with the non-rotating body, or interact with the potential gaps and rough surfaces located there. This feature can be seen clearly in Figure 26, in the lower part of Section K-K. This was extended 20.35mm, to provide this feature, and was given a wall thickness of 3.18mm, ensuring that it would be strong and easily machined.

The third consideration was the bolt pattern. The main consideration here was that the heads of the bolts that would be used, chosen for convenience as #10 machine head bolts, would be able to be inserted without intersecting with the exhaust pipe, and a seating surface whereby the heads

would not be protruding into the flow. Given this, the bolt circle was set to 20.66mm in radius. The bolt number was chosen to provide symmetry, with four bolts, and allow for a relatively straightforward construction process. Ideally, one wants to keep an even pressure on the discs, to prevent distortion during operation. At the same time, one needs to limit the number of bolts, as they serve as blockage to the flow. It should be noted that in some examples in the literature (Sherrer, 2008) attempt to include additional posts throughout the discs, to provide intentional blockage for the purposes of trying to improve the torque produced in the system as a reaction force. Though what effect these would have is not currently known.

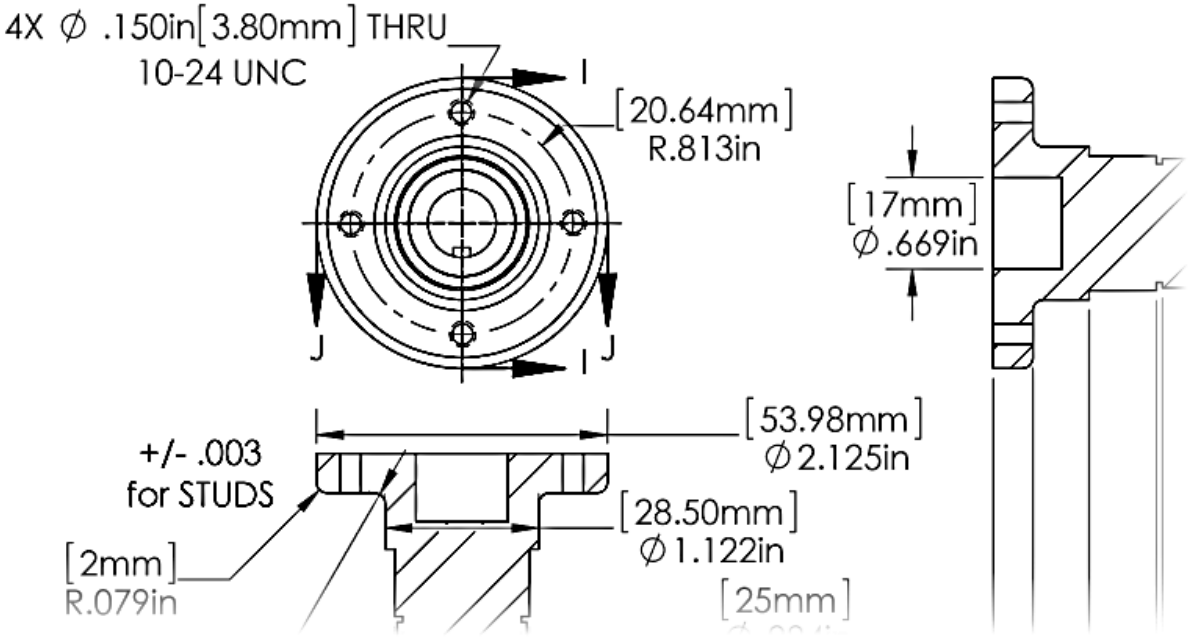

Figure 27 - Shaft hub

Lastly, the hub flange was extended slightly past the outside diameter of the bolt head seats, and given a thickness of 6.35mm, which provided sufficient thickness to both hide the bolts with a countersink and leave sufficient material below the heads for structure.

On the shaft side, the mating hub shown in Figure 27 was designed as a mirror image to the exhaust hub, though the bolt holes were tapped through with a 10-24 thread. In addition, a 17mm hole was added on the center line, in order to provide alignment for the disc pack using a plug (not shown). This plug could be inserted into this hole, the discs and hub installed with a tight fit, and the bolts torqued down to a snug fit. The plug would then be removed, leaving a perfectly centered disc pack. The balance of the shaft could not be considered until the bearings and races were considered.

3.6. General Considerations of the Bearings

Bearings are a critical component. They needed to be compact, but also able to withstand a reasonable amount of heat, and extreme speeds. Research on the turbine showed that it was reasonable to expect speeds in excess of 30,000 RPM, dependent on pressure. While it was not expected that this turbine would be run at those speeds for safety concerns, it seemed appropriate to provision bearings that were capable of reaching those speeds for the purposes of further study. SKF bearings were chosen because of the company's high quality standards, large selection, and effective online tools for determining the proper bearing based on the various criteria of the system.

There are two main factors that lead into their choice;

1) They must be capable of very high speeds. Most bearings are not designed to exceed a few thousand RPM, and it is very reasonable to expect that the Tesla Turbine can exceed 25,000RPM. Examples exist in the literature of speeds in excess of

35,000RPM (Burton, 1955). Therefore, the choice of bearings was limited to those that could easily handle these speeds, or greater.

2) They must be of high quality, and the bearings should be sealed. Since it was not desirable to include an oiler in the system, and also ensure that the disc pack and exhaust flow was not contaminated, sealed bearings were a clear choice. The tools provided by SKF indicated that the chosen bearings would have very low friction at low speed/torque. (SKF, 2015)

3.7. Bearings, As Chosen

The bearing on the disc pack side (here forward called the 'disc bearing') was set to an inner diameter (ID) of between 22 and 30mm, which was around the minimum diameter at the hub. A high speed bearing was preferred, so the minimum speed rating was set to 25,000RPM. Lastly, it was preferred the bearings not be excessively thick, for ease of installation, so a thickness between 5 and 20mm was chosen. There were relatively few available alternatives, and the bearing best suited to the criteria was the 6005-2RSLTN9/HC5C3WT, capable of speeds up to 40000RPM, 12mm thick. The ID of this bearing was 25mm, and its OD 42mm (SKF, 2015).

Next, the bearing at the opposite end of the shaft (here forward called the 'outside bearing') needed to be chosen. The only difference between the previous bearings is that the maximum ID needed to be less than the 25mm of the disc bearing. This resulted in the clear choice of 6004-2RSLTN9/HC5C3WT, capable of speeds up to 48000RPM, and a mere 12mm thick. The ID of this bearing was 20mm, and its OD 42mm (SKF, 2015).

3.8. General Considerations for the Shaft

Given the hub arrangement, the shaft is relatively straightforward to define, shown in Figure 28. It was decided to make the shaft side hub an integral component to the shaft, to simplify the setup and provide a more straightforward arrangement to ensure a balanced system.

Figure 28 - Turbine shaft

Some space needs to be provided for the inclusion of labyrinth seals, and then the shaft is designed as long as possible to increase distance between the bearings, as described by (A) in Figure 29, to maximize the stability and resistance to any bending moment. Since the shaft acts as a cantilevered beam, with the flow (and gravity) providing a radial force (B), it is preferred to

ensure the reaction force is minimized. This will therefore limit the wear on the bearing (E). Since the bearing (D) is acting a fulcrum, the force exerted by (B) is proportional to its distance from (D); likewise, the reaction force on the far side of (D). Since the bearing (E) is four times the distance from (D), the force it experiences is ¼ that of (B).

The longest practical 'bearing block' for a straightforward build was 4", which therefore defined the length of the shaft itself. The two bearing seats were placed at a maximum distance apart, given the constraints above. The two bearings were chosen with different ID and OD in order to allow for easy installation. Stress relief profiles were included at each of the various steps along the length of the shaft; either by a filleted corner, or cut grove. Profiling of the shaft minimizes stress concentrations while the shaft is under load; rounding inside corners, and stress relief grooves prevent the stress from becoming concentrated. Finally, an extension on the shaft past the last bearing, with a keyway, was provided to either mount an encoder or pulley, which could then be used for speed and torque measurements.

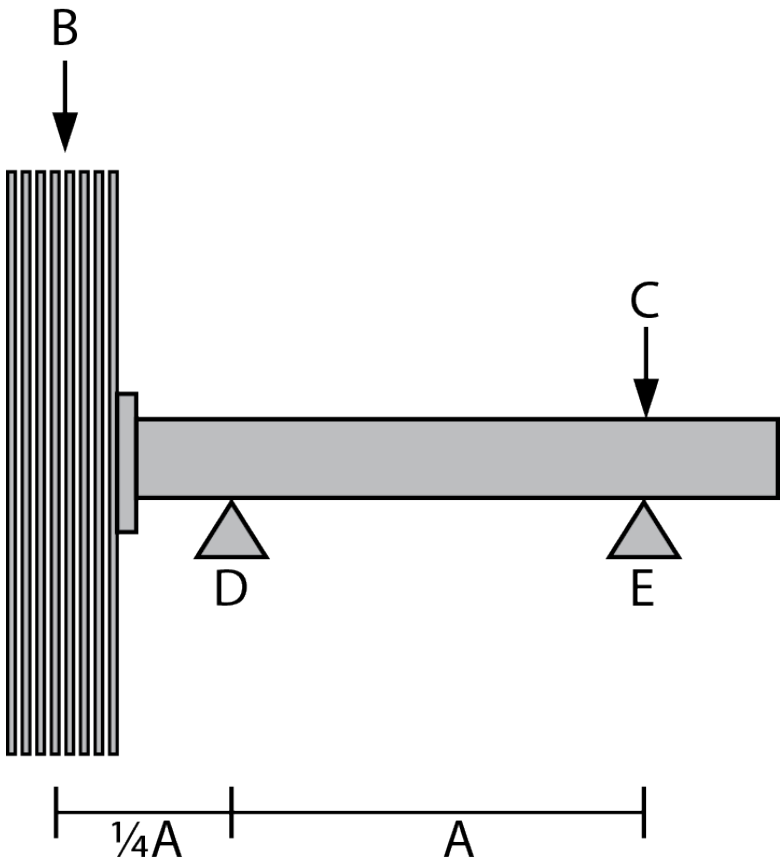

Figure 29 – Loading of the shaft

The hub section, shown on the left side of the horizontal cross section in Figure 27, was considered in the previous section. Given that, the next consideration was where the bearings would seat. Since the system would be cantilevered, it was deemed preferable to make the space between the two bearings as far apart as possible, while at the same time keeping the costs associated with the manufacture of the parts reasonable.

Consequently, upon consultation with the manufacturer, it was determined that the most practical distance between the two bearings (given the construction as described in the following sections)

would be just under 4", or 101.4mm, measured from the outside of the bearing seats. This, therefore, defined the overall length of the shaft.

Outside of the bearings, it was necessary to extend the shaft for two considerations. First was to provide a groove for a retainer clip, to keep the bearing and shaft in place. Second was to have a keyed section that would allow for the installation of the eddy brake, or other mechanism (pulley, gear) for power take off, should it be desired to do work with the system at a later date. This section was set to 12.7mm (0.5") to ensure compatibility with a large number of off-the-shelf hardware.

3.9. The Shaft, As Designed

The shaft needed to have the bearing seats manufactured into it; it was deemed necessary to step the bearing seats, such that the larger bearing could pass up the length of the shaft without interference. This meant, therefore, that the bearing closest to the disk pack would have the largest ID. This would make it considerably easier to pass the shaft through, as can be seen in Figure 30. According to this, the bearings were chosen (see 3.7), and the appropriate seats were placed such that the opposing bearing seats would be flush with what would later become the bearing block (see 3.16). Stops were placed on the disc-pack side of the bearing seats, which were simply steps to the larger diameter, as specified in the specifications of the bearings themselves. Stress relief grooves were placed on the outside of the races, which also served as the retainer clip grove. The section of the shaft extending past the outside bearing, prior to the step down for the keyed section, was a slightly smaller 18.6mm in diameter, so that it would clear the ID of the outside bearing easily.

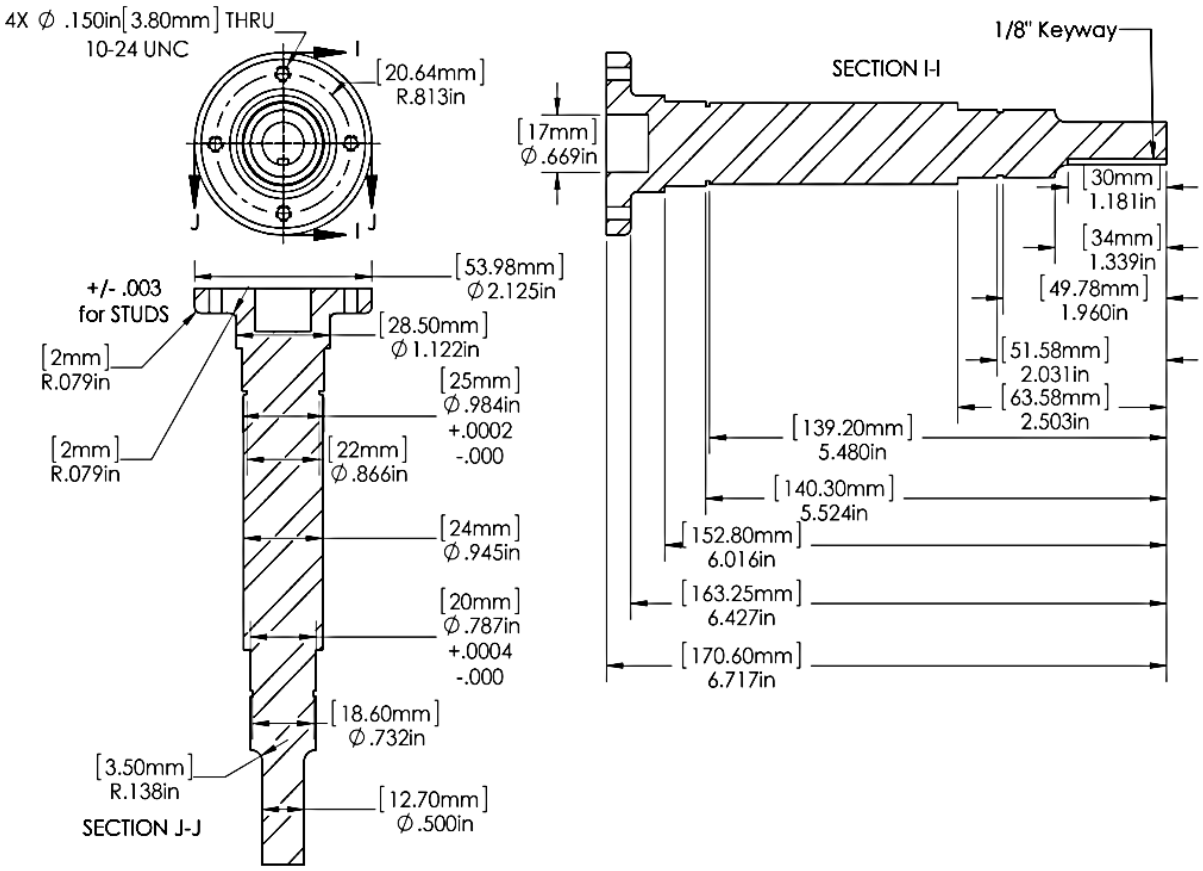

Figure 30 - The shaft

3.10. General Considerations for the Expansion Chamber

The expansion chamber's purpose is simple: surround the disc pack, and force the fluid to transit through the discs, as well as provide some protection in the event of failure. Also, the expansion chamber would serve to mount all components, including the nozzles and bearing supports.

Given that, an internal circumference slightly larger than the disc pack (to allow for stretch in the discs themselves at speed) was used as the starting dimension. This was mentioned as a potential

issue in the literature (Hoya & Guha, 2009). Then, an additional thickness of material (aluminum) was extended past this diameter, in order to receive the bolt circle.

Two rectangular pockets with filleted edges were machined in the expansion chamber on either flat side, on center, to receive the nozzles. This can be seen on the lower side of the left-hand example of the chamber, in Figure 31.

To complete the chamber, two plates were designed to be mounted on either side; one, the exhaust plate, with two bolt circles and a central hole. The outer bolt circle passed the bolts that would assemble the system as a whole, and the internal circle would hold in a labyrinth seal.

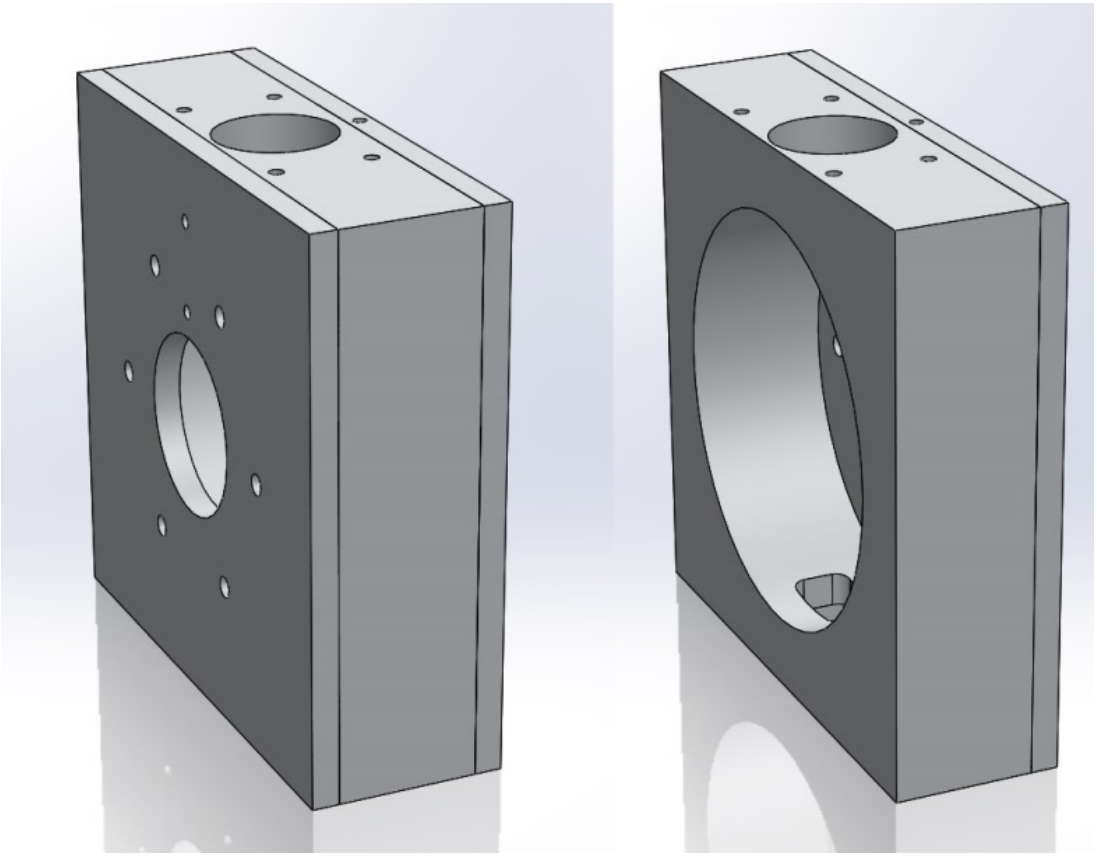

Figure 31 - Expansion chamber

The central hole was provided large enough to allow the exhaust hub free passage, as well as a second compression fit labyrinth seal.

The second plate, called the bearing plate, was mounted on the other side. It, too, needed two bolt circles and a central hole. These were similarly dimensioned to the exhaust plate, for the same reasons.

Finally, holes needed to be drilled and tapped to hold the plenum chamber, as well as holes drilled for sensors.

3.11. Expansion Chamber, As Designed

The disc pack can actually spin in free air; however, to ensure that all of the flow coming from the nozzles must pass through the disc pack, an enclosure was needed. This enclosure was called the expansion chamber', shown in Figure 32, and made by three parts, the central cavity, and two end plates, denoted by their location; the plate on the exhaust side called the 'exhaust plate', as in Figure 33, and the plate on the shaft side called the 'shaft plate', shown in Figure 34.

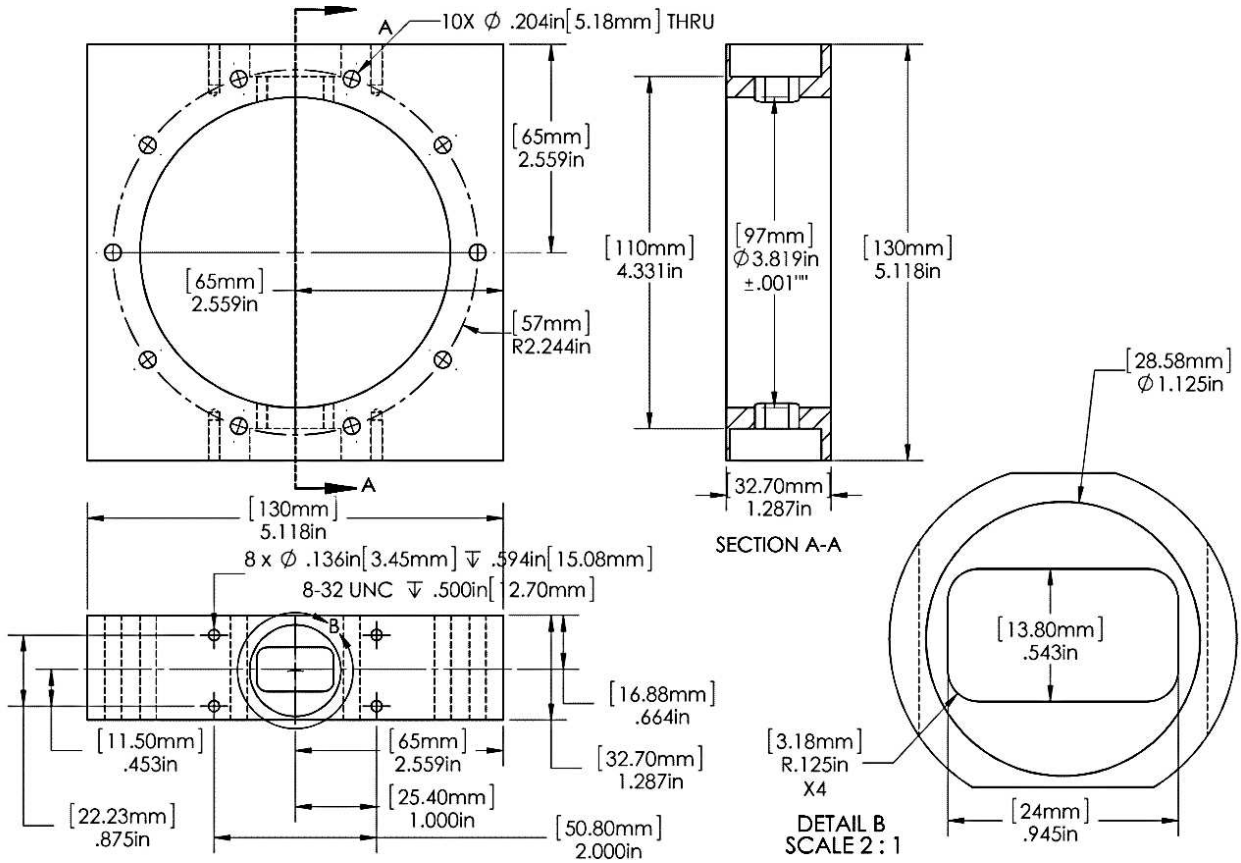

Figure 32 - Expansion chamber schematic

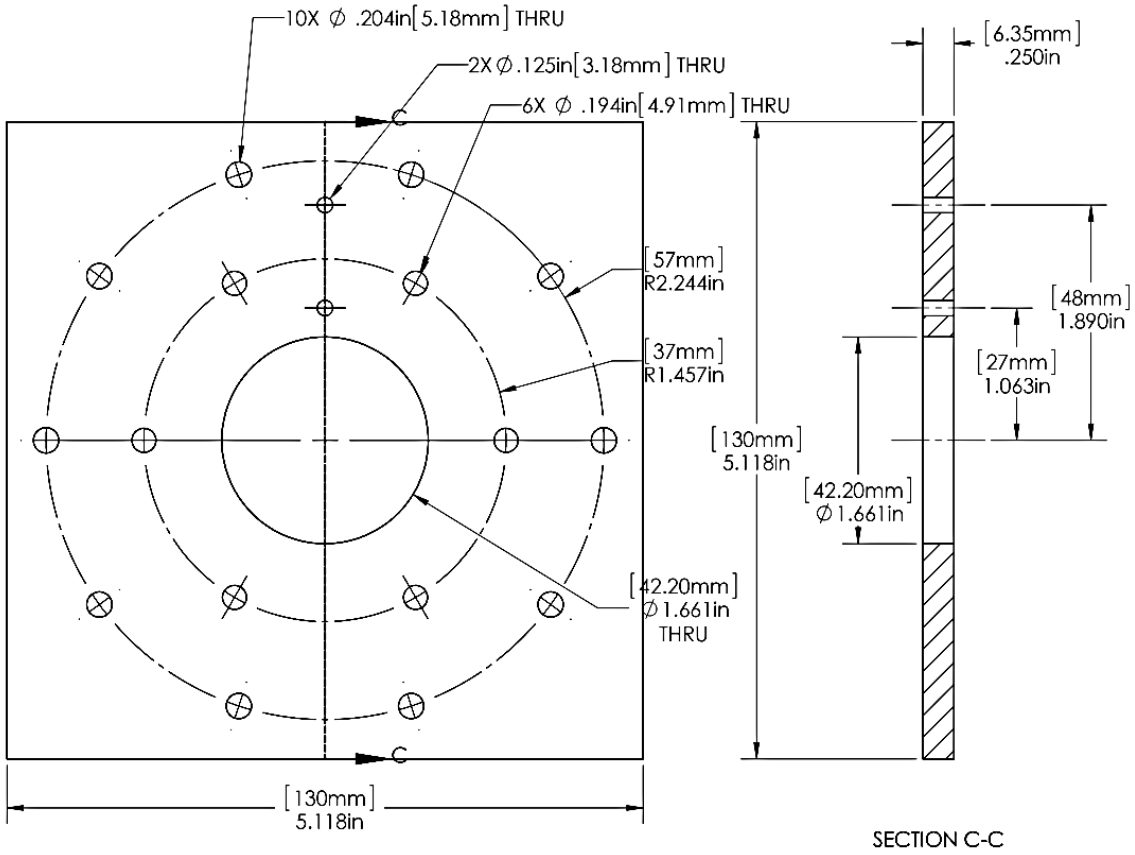

Figure 33 - Exhaust plate

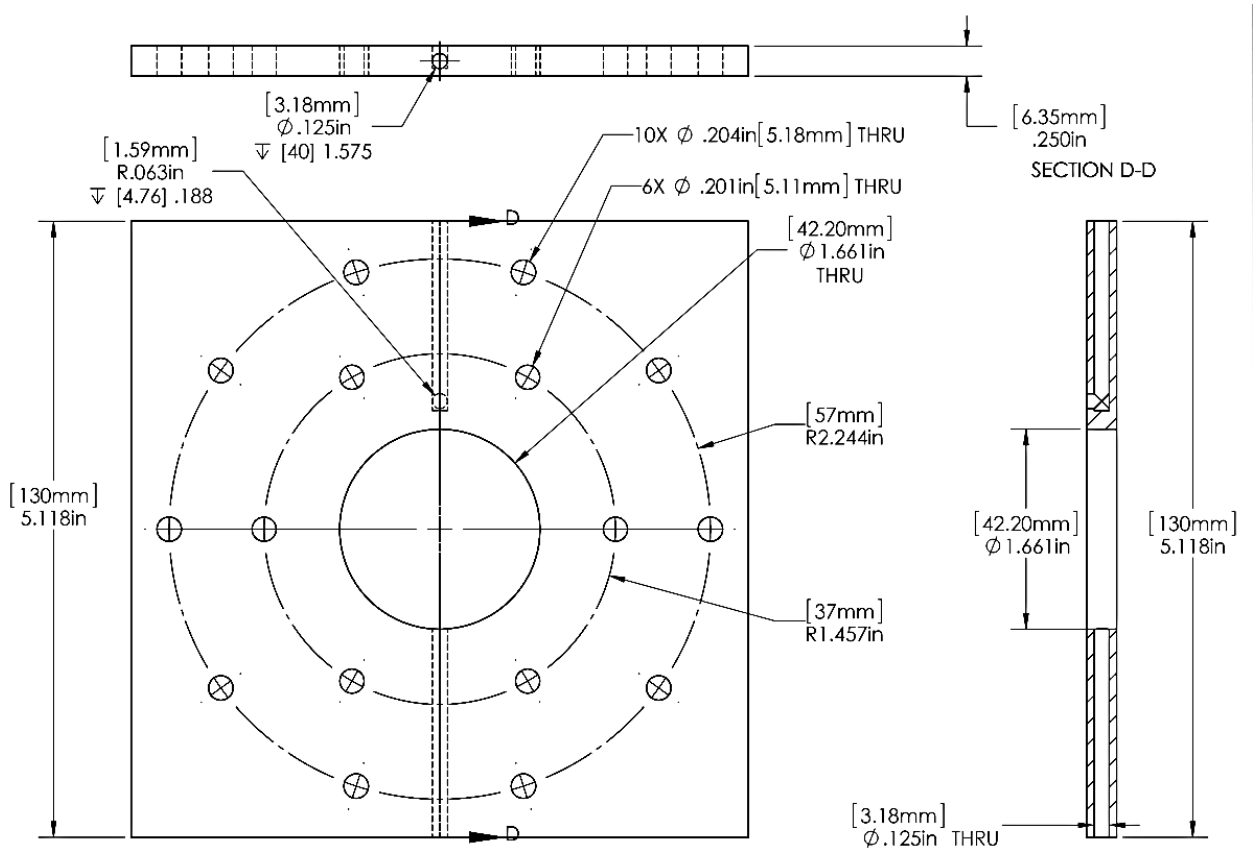

Figure 34 - Shaft plate

The dimensioning of these components was taken primarily from the disc pack, but also the layout of the shaft. The expansion chamber, shown in Figure 32, was considered first; its primary dimension is the hole that would receive the disc pack. This was set to 97mm, which provides 1mm between the largest discs and the wall, suggested by Hoya & Guha (2009). Two nozzle apertures (based on the nozzle design to be discussed later) were added opposite to each other, centered on the location of the disc pack. The outside dimensions were chosen for convenience based on standard stock sizes at 130mm for the height and width, and the thickness was set to provide just enough clearance for the labyrinth seals as described in 3.14. A bolt circle was then added at 57mm, which would pass through the entire device, holding all of its components together, as well as providing alignment. 10 bolts were used to provide a reasonably even pressure on the gasket that would eventually be placed between the expansion chamber and the side plates.

The exhaust plate, shown in Figure 33, is straightforward. It is a plate of aluminum that is 6.35mm thick, with a 42.2mm hole cut in its center to take the exhaust hub and small labyrinth seal. Two bolt circles are then added, one at 37mm in diameter with six bolts, which would hold the large labyrinth seal, and another at 57mm, for the main bolts. Two holes were placed for sensors, which will be described in greater detail in section 4.3.1.

The shaft plate, shown in Figure 34, is placed opposite to the exhaust plate. It is identical to the exhaust plate in its major features. The only difference being the holes drilled for the pressure sensors, as can be seen in 4.1.3.

3.12. General Considerations for the Nozzle

The nozzle is also a key component of the system; especially since the ability to adjust the nozzle angle was required to test the hypothesis. It was determined early on that it would be difficult to manufacture a nozzle assembly that would be easily changed on the fly, and therefore a similar approach to Hoya and Guha (2009) was taken. In the case of this thesis, a set of various angles were chosen to provide a reasonable sample from 2.5° to 45° from tangential, and individual nozzle inserts were to be 3D printed from a suitably strong material (glass impregnated nylon), that could then be changed at will.

Because of the design of the nozzles themselves, and the restriction in the overall design, it was expected that the flow path, indicated in the cross section shown in Figure 35, in the nozzle would affect the nozzle's performance to some degree; but given a similar flow path in each, it would be sufficiently indicative to provide a confirmation of the hypothesis, and possibly direct further study.

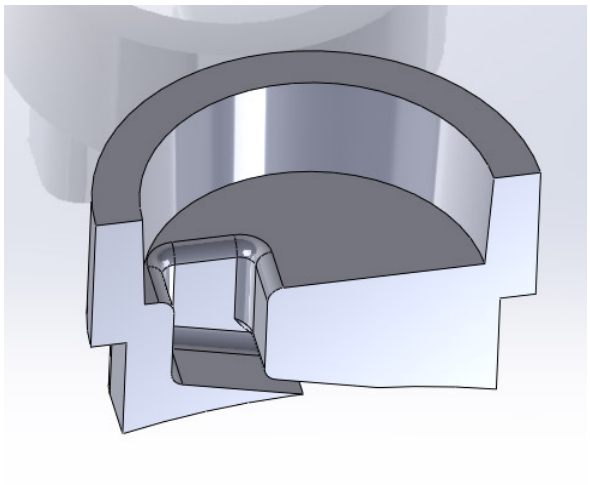

Figure 35 - Nozzle cross section

3.13. The Nozzle, As Designed

The nozzles, shown in Figure 36, were designed to be quickly interchangeable, but the machinist was concerned about the challenges of creating the holes that they would fit in, in the expansion chamber. They were, therefore, designed as a plug that could be swapped out easily, with a shoulder to prevent them from being inserted too far into the expansion chamber, and therefore

contacting the discs. Because of their relatively complex shape, they were 3D printed in glass filled nylon, which would be able to provide adequate strength.

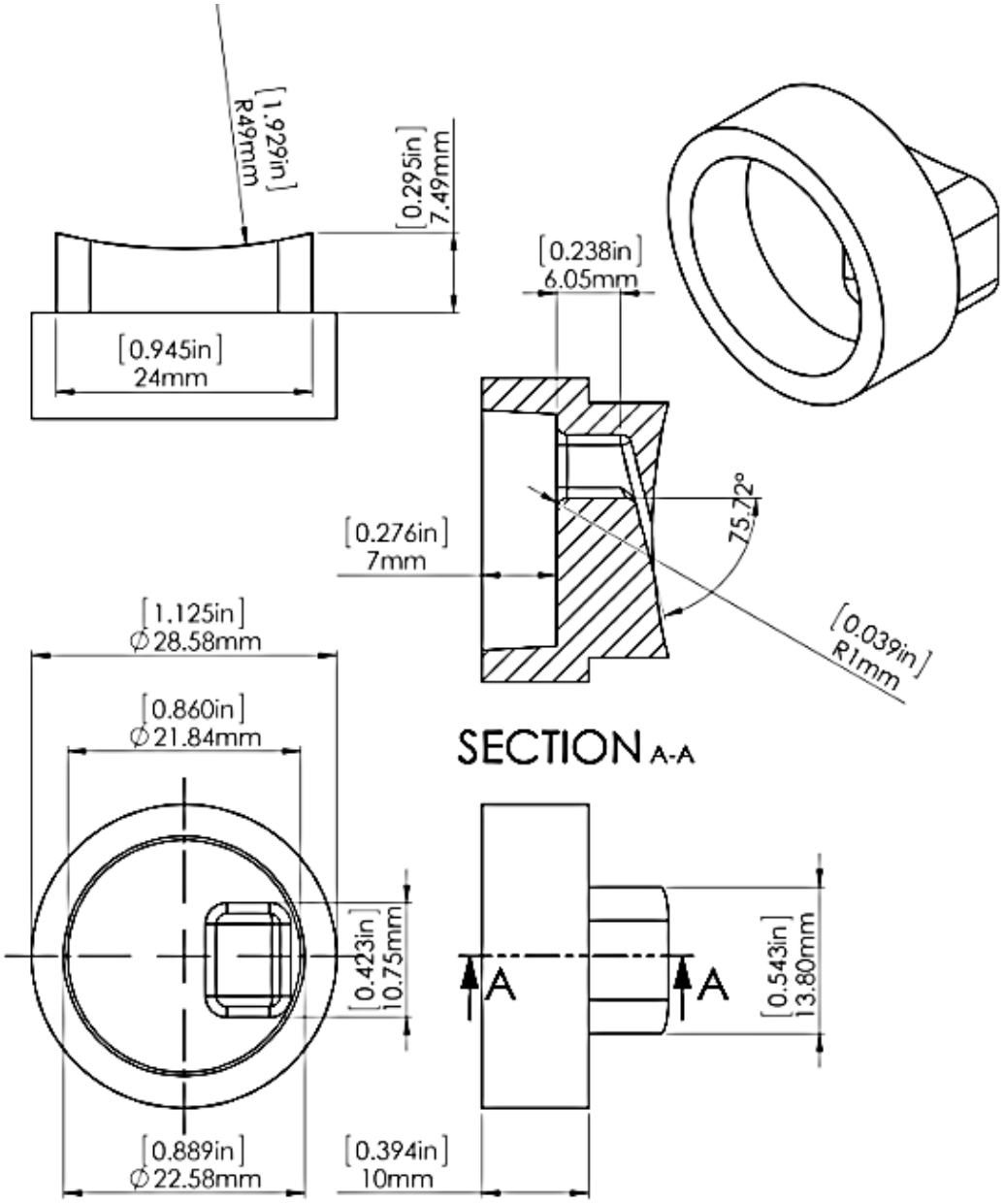

Figure 36 - Nozzle design

3.14. General Considerations for the Labyrinth Seals

Labyrinth Seals are necessary to ensure that the flow coming from the nozzles is forced to pass through the discs. In Tesla's (1913) original patent, as well traditional turbomachinery (Lieber, 2003), labyrinth seals are a typical way of providing non-contact seals that are able to provide a high degree of seal, while not requiring any lubrication or affecting the performance of the system other than through secondary windage effects. (Du, 2010)

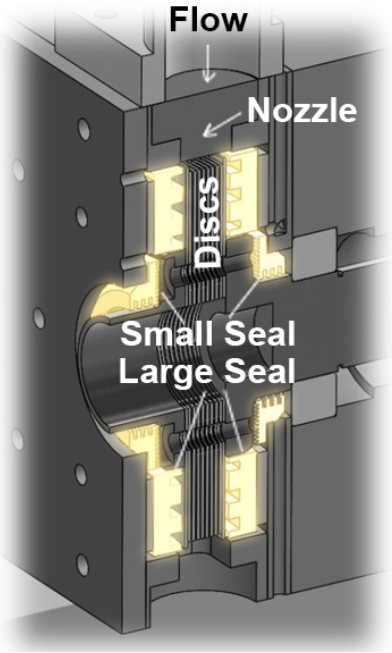

Figure 37 - Location of labyrinth seals

Tesla's original design had two sets of labyrinth seals, one coarse, and one fine (1913). It was decided to do the same with this system, shown in Figure 37, but the desire to make something a little more flexible meant that it was necessary to have seals that could be adjusted. The larger seals, seen in Figure 38, were made from brass. They are facing the discs themselves, and are adjustable by placing rubber spacers behind them. The small seals, in gray, are made from polyethylene. They interface with the hubs, and are a slip fit into the end plates of the expansion chamber, as described in 3.10.

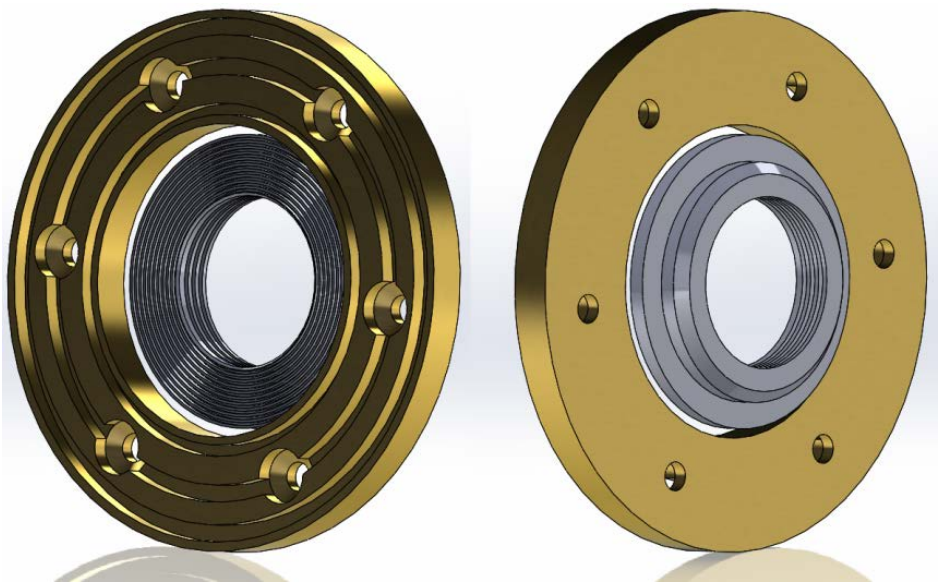

Figure 38 - Labyrinth seals, disk facing (left) and rear (right), with the coarse brass seal in yellow, and the fine plastic seal in grey.

3.15. Labyrinth Seals, As Designed

The labyrinth seals, shown in Figure 38, were designed to be both adjustable and easy to install. The coarse outer seals were made to fit on the outside of the hub assembly, and could have gaskets installed behind to bring them to fit exactly with the disc pack, providing the best seal possible. These were bolted to the assembly, but would not need to be removed if the disc pack were removed or adjusted. The inner seals were designed to have a compression fit in holes in both the shaft and exhaust plates, so that no tools were required, and they could be manually adjusted if needed.

For the larger seal, shown in Figure 39, the ID was defined as 55mm to clear the hub; the OD was chosen to be at the same diameter as the smaller disc platters, at 92mm. Six bolt holes were placed in the center of the seal, on a bolt circle at 37mm. Three teeth, each 4mm wide, with a 3mm gap were placed evenly across the disc, where each gap was 3mm deep. Two of these seals were made to match each other.

The smaller seal, shown in Figure 40, was designed with two labyrinth surfaces, one facing the disc pack in the plane of the discs themselves, and one facing centerline of the shaft, mating with the exhaust hub. The primary dimension on this seal was the ID, at 30.2mm, to clear the hub tightly. The OD that provided the compression fit was chosen arbitrarily at 42.2mm, and an outer lip beyond that at 51.57mm to act as a stop for the minimum depth of the labyrinth seal, based on the other geometry. Several 0.5mm wide/1mm deep seal elements were placed equally on disc facing side, and three 1mm wide, 2mm deep seal elements were placed on the inner diameter.

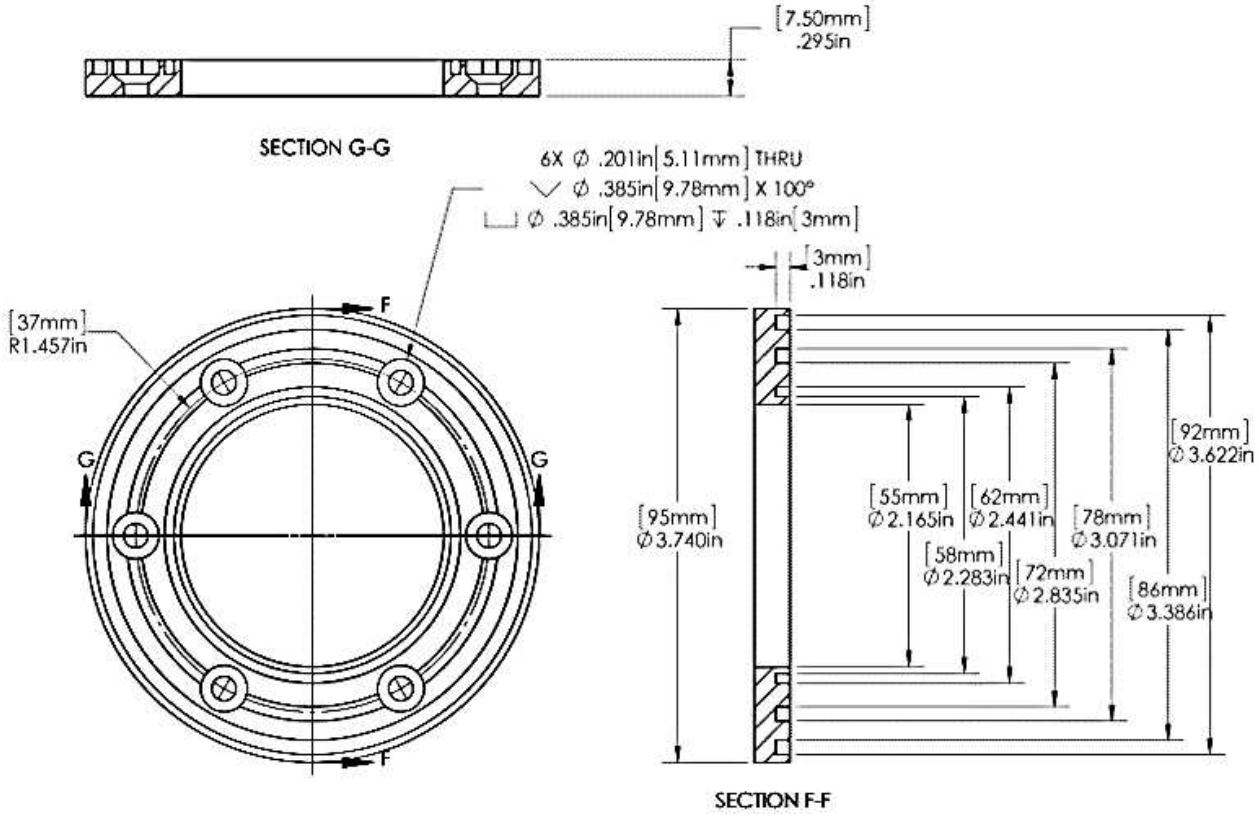

Figure 39 - Large labyrinth seal

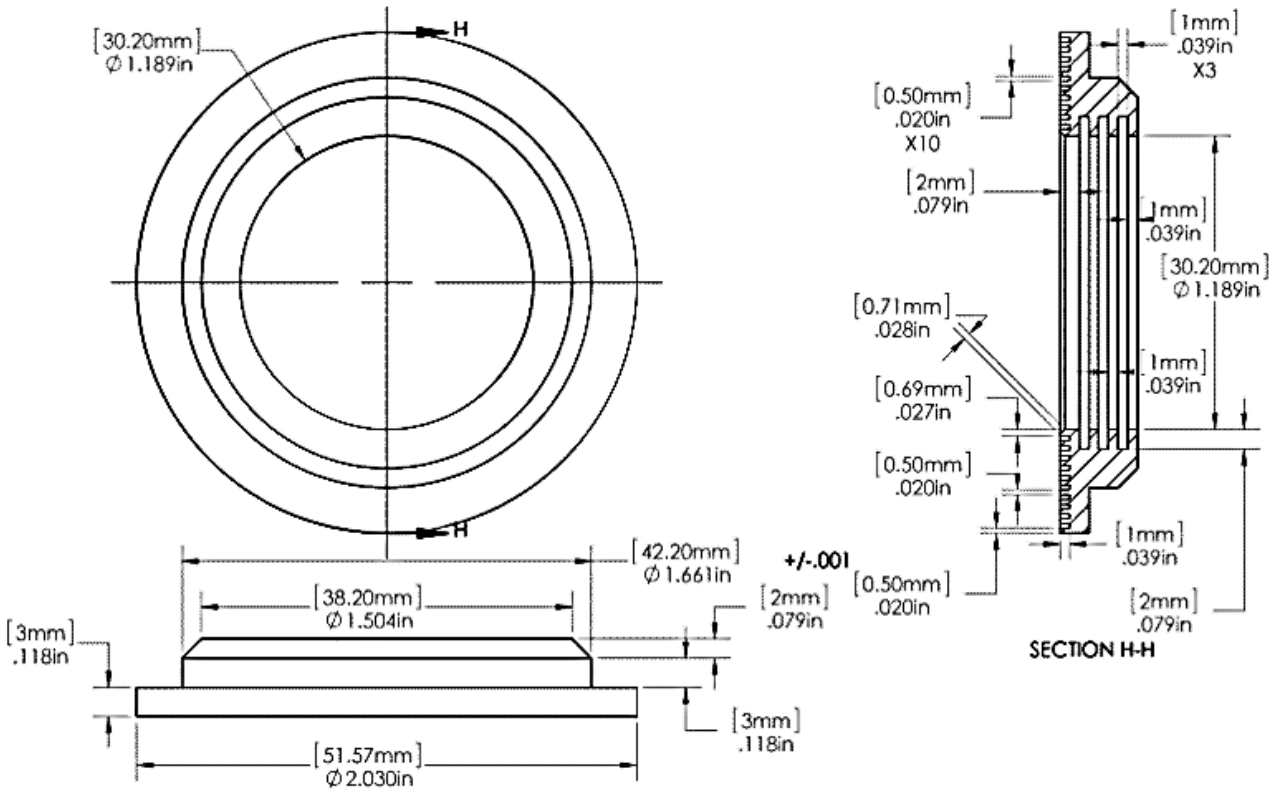

Figure 40 – Small labyrinth seal

3.16. General Considerations for the Bearing Block

In order to support the bearings and shaft, a large block was deemed to be the easiest to manufacture; the outer bearing races could be seated on both ends, and the entire structure bolted directly to the expansion chamber.

3.17. Bearing Block, As Designed

The bearing block, shown in Figure 41 was made out of a monolithic piece of steel, because it was suggested by the machinist early on that this would be preferable to many of the options available. The thickest piece of aluminum that was deemed feasible in the budget was

approximately 4" (101.6mm) thick; the final dimension was made to 101.4mm, to allow for some material to be removed ensuring the part was flat. This design does have the drawback that the two bearings need to be seated on either side of the block, and the shaft, after the two bearings are press fit into their respective seats. Consequently, it is very difficult to remove the shaft, should one want to easily make changes to it. The shaft could only be inserted with a press fit. This caused stress on the bearings, and may be responsible for some of the later issues with the bearing seals. It also made it very difficult to make fine adjustments with the labyrinth seal,

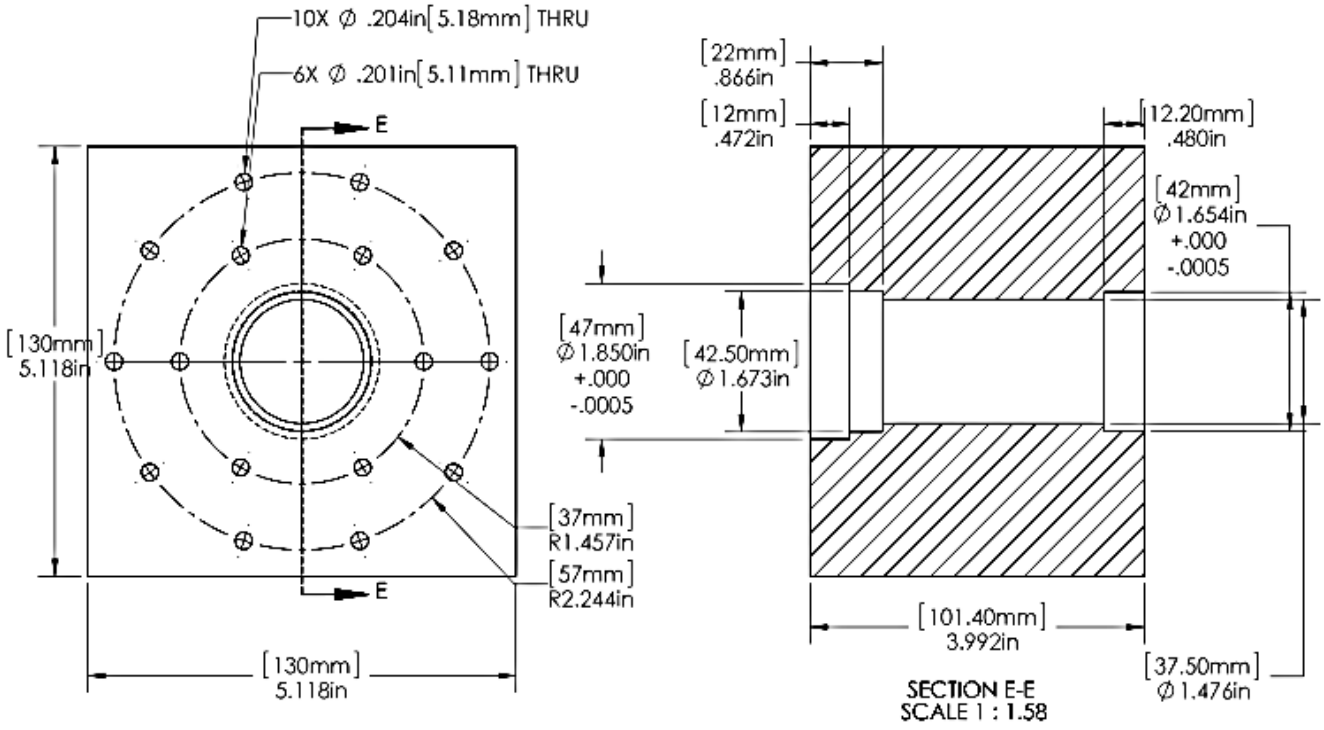

Figure 41 - Bearing block

given that with the discs being in place, one could not access the bolts in the rear labyrinth seal.

3.18. General Considerations for the Plenum Chamber

A plenum chamber was indicated as being beneficial by Guha and Smiley (2009), in order to ensure that the flow coming from the air line would reattach prior to reaching the nozzle, in order to improve the nozzle's efficiency. The dimensions were, therefore, based on their approach. An external view of the chamber can be seen in Figure 42.

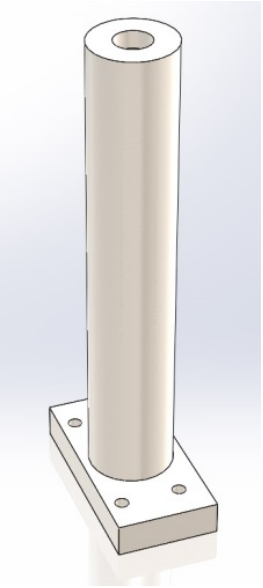

Figure 42 - Plenum chamber

The plenum chamber needed to be designed to bolt easily to the expansion chamber, and provide for a seal to ensure the pressure could only exit through the nozzle. A threaded hole at the opposite end of the plenum would receive the connection to the air line.

3.19. Plenum Chamber, As Designed

The inlet to the plenum chamber, in the current case is a 0.25" (6.35mm) hose, which therefore suggests a minimum plenum length of 159mm, based on the equations derived by Guha & Smiley (2009), shown here as equations 24 and 25:

$$H = \frac{3}{2} d_1 \tag{24}$$

$$d_2 = 4d_1 \tag{25}$$

Where H is the height of the chamber, d_1 is the inlet diameter, and d_2 is the diameter of the chamber. It was made slightly longer, for convenience. The plenum chamber itself was fabricated from a 1" pipe, four times the inlet diameter, and then welded to a base plate to allow it to be easily attached to the expansion chamber, shown in Figure 43.

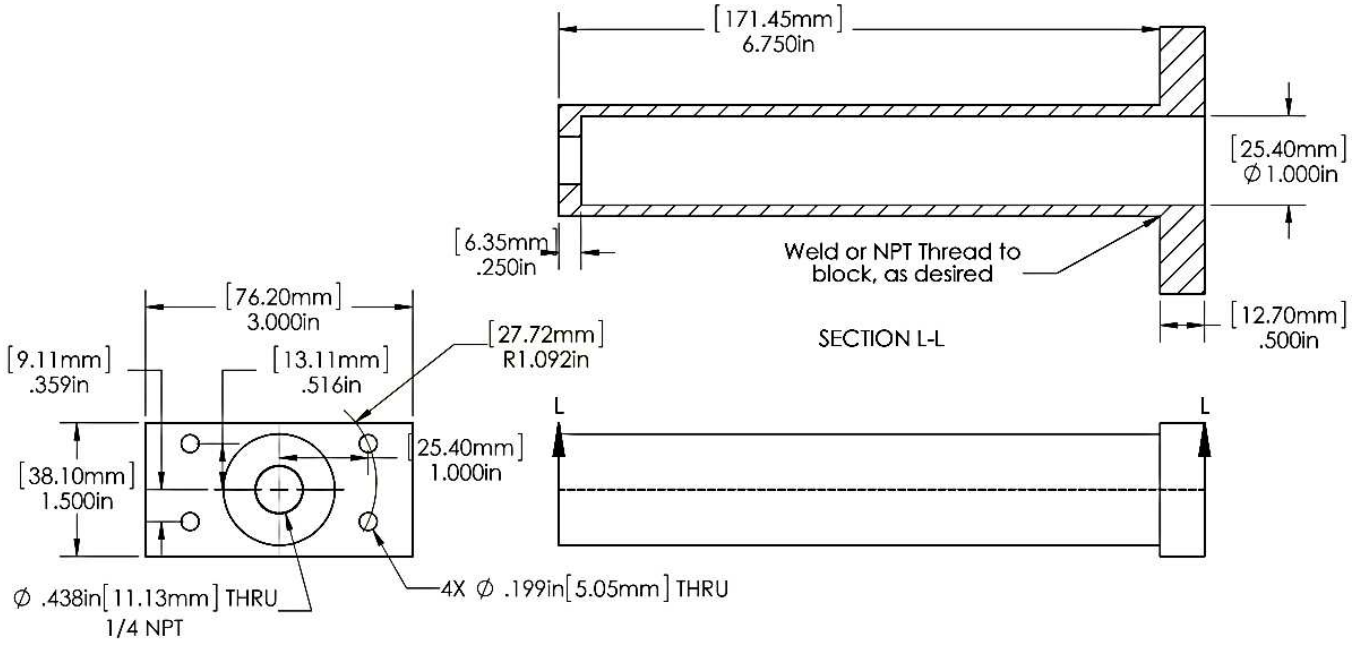

Figure 43 - Plenum chamber schematic

3.20. The Speed Monitoring System

The system for determining the speed of the turbine needed to be both simple and robust. Because the intention was to determine the torque on the system via the inertial moment of the system, it was important that no load be applied. Also, a non-contact system would allow for simplicity upon building a test rig, with some degree of forgiveness on alignment. That said, it was also important to have a reasonably high precision to be able to adequately understand the entire rotational speed range.

The speed monitoring system was designed to be as simple as possible, while at the same time being robust. Consequently, it was decided that a non-contact system would be ideal, and the easiest way to accomplish that would be with a hall effect rotation sensor, and a small diametrically magnetized magnet attached to the end of the shaft.

Very early, a hall effect rotational sensor was found that was capable of very high rotational speeds (in excess of 72,900 RPM), while providing a resolution of one degree. This sensor could, therefore, be connected to a data acquisition system, and only a magnet needed to be attached to the shaft in order to achieve a high accuracy rotational sensor (AMS, 2013).

3.21. The Dynamometer & Loading System

While the goal was to provide a high accuracy measurement of the rotation speed of the system, and therefore infer the torque being applied, it was important to be able to provide some actual torque measurements in order to corroborate the calculated torque measurements from rotational speed. To do this, a dynamometer needed to be acquired/built that would be capable of measuring very small loads. In addition, it was desirable that the dynamometer be non-contact, in order to ensure that the measurement system would not cause a stall at low speeds, which the Tesla Turbine is prone to suffering.

Building an eddy brake was determined to be the best option. The system is very simple. An aluminum disc is affixed to the shaft, via the shaft extension and keyway, and a magnet is placed at a variable distance from the disc. As the disc spins, eddy currents are created in the disc, and a force is applied to the magnet.

To measure this force, the magnet was placed on a beam, and the four corners of the beam were equipped with load cells. This allowed for a calculation of the total load applied to the magnet, and therefore the instantaneous torque. The magnet could then be placed in order to achieve a steady state (constant speed), and then be able to calculate the load based on the output of the load cells. In addition, placing the magnet sufficiently close to brake the system would allow for a full-range measurement of the torque in the system as it decelerated under this load.

3.22. Reynold's Numbers for the Given Design

In the given design, the dynamic viscosity is known, as is the characteristic length (l), which is the disc spacing. This results in a linear increase in the Reynolds number as the differential velocity of the fluid, relative to the discs, increases.

3.23. Final Design Overview

The final design of the turbine can now be inspected in Figure 44 and Figure 45, below.

To review, the overall purpose of this rig was to allow for a simple design that was adaptable, without having to completely change the design. The bearing block assembly and shaft can be used in many different variants, as one example, and the internal components to the expansion chamber are also adjustable. Indeed, given the budget, one could make a mating expansion chamber that was much larger in diameter, to accommodate larger discs, increase the number of

inlets, and vary the number of discs. The discs themselves can be modified significantly, and changed without substantive modification to the overall design.

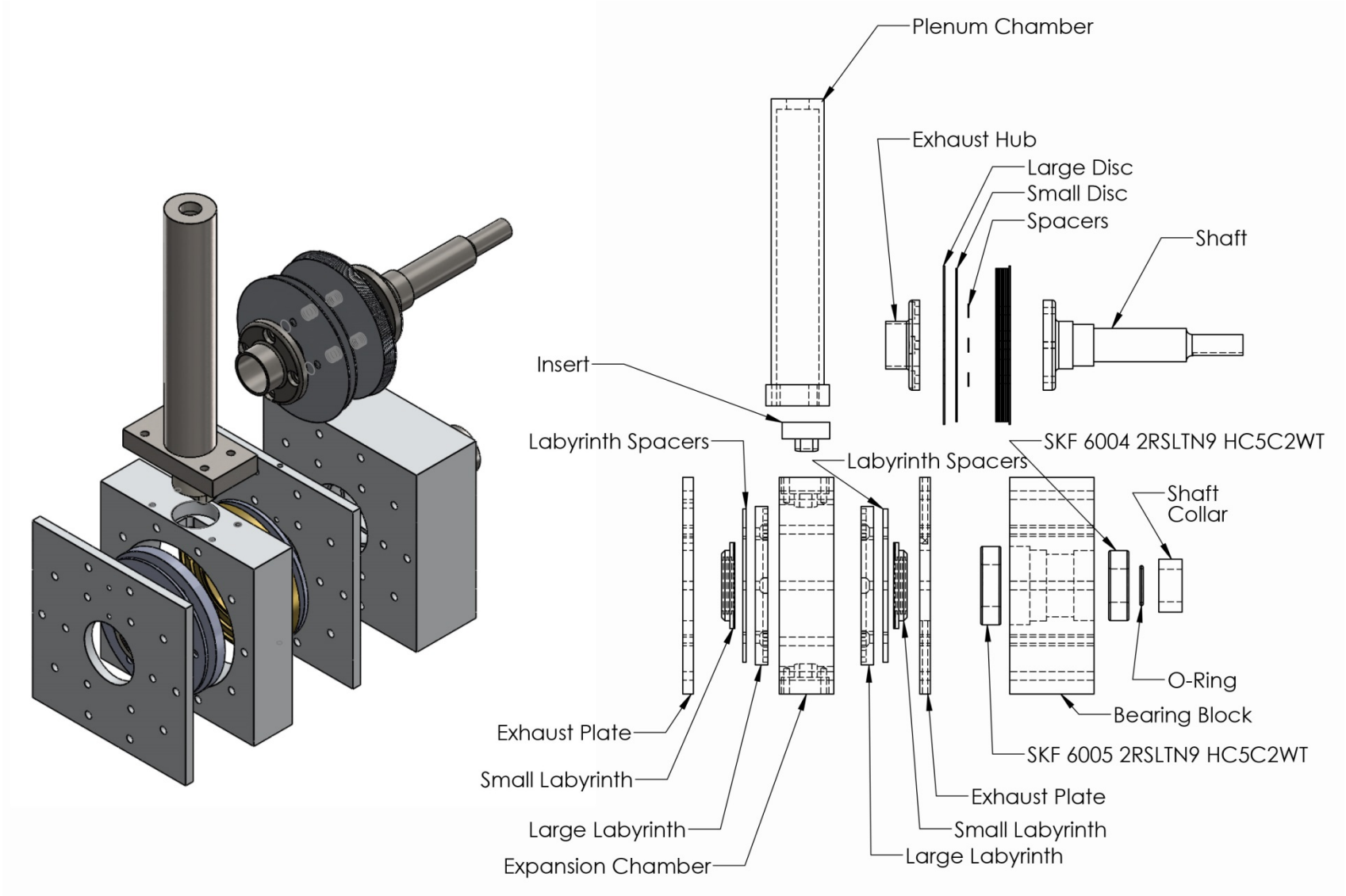

Figure 44- Final turbine design, exploded and component view

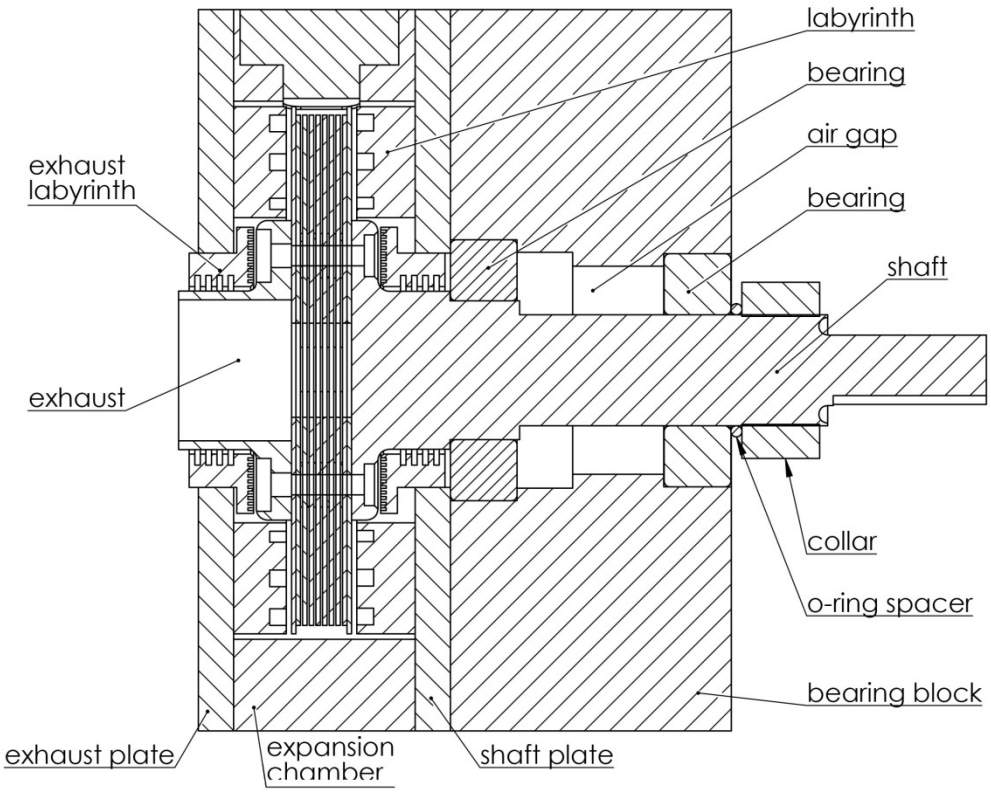

Figure 45 - Final turbine design, cross sectional view

In the process of testing with the rig, it became clear that some changes could and should be made to improve its overall usefulness, as well as increase the speed with which such changes could be made. Those will be discussed in Section 5.3.

4. Experimental Techniques and Measurement System

4.1. Variables

The Tesla Turbine has numerous variables that should be considered in order to gain an understanding of the operating conditions. For the purposes of this thesis, not all of the variables were acquired, as the scope was limited to ensuring that the rig was functional, with an eye towards further development. Prior to discussing the individual sensors used for measurements, the variables themselves should be examined.

4.1.1. Rotational Speed

One of the main variables for the Tesla Turbine is the rate of rotation of the disc pack, as this has a direct impact on the overall performance of the system. From the calculation of the torque, from equation 26;

$$\tau = I \cdot \alpha \tag{26}$$

And the rotational speed ω is recorded relative to time, t, from equation 23;The instantaneous system torque can be calculated, as equation 27;

$$\tau = I \cdot \frac{d\omega}{dt} \tag{27}$$

4.1.2. Pressure

Pressure throughout the system is important, for determining the overall efficiency of the system, as well as the mass flows. For the purposes of the experiments presented here, not all pressures were measured. The locations where the pressure can be measured as follows;

- Static pressure at the tank
- Static pressure in the plenum chamber
- Dynamic pressure in the plenum chamber
- Static pressure at the top of the disc pack
- Static pressure between the labyrinth seals on both sides of the disc pack
- Static pressure at the internal bearing
- Static pressure between bearings
- Total dynamic pressure at the exhaust
- Atmospheric pressure

There are some problems with measuring some of these values, most notably at the exhaust. This flow is extremely turbulent, unsteady and irregular, and therefore very difficult to obtain a measurement value; dynamic pressures are very variable, and would require specialized techniques. Static pressure would be variable because of this turbulence, even though it is essentially atmospheric.

4.1.3. Pressure Measurement Locations

Pressures were measured in five locations; three pressure sensors were on the turbine itself, P1 being above the disc pack (Figure 46, shown in red), P2 being behind the labyrinth seal on the bearing side (Figure 46, shown in blue) and P4 (Figure 46, shown in purple) on the hub side between the labyrinth seals. Another sensor, P3, was used for measuring

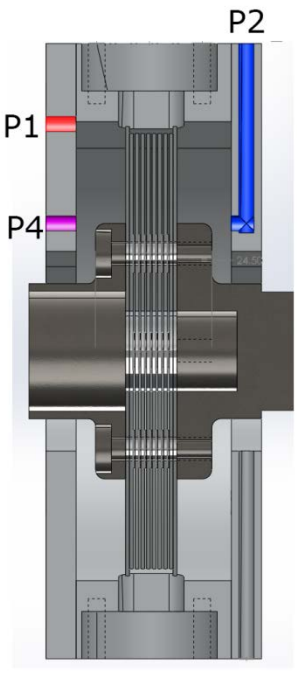

Figure 46- Pressure sensor locations

the atmospheric pressure. Lastly, an inline pressure sensor was placed in the air line at the tank to accurately set the inlet pressure. This last pressure sensor was not connected to the DAQ. An additional port exists opposite of the P2 location, which can be used to measure pressure; however, because the seals were removed from the bearings, this was left open to allow for easy lubrication of the bearings.

4.1.4. Temperature

Another relevant variable is the temperature of the fluid through the system. This provides additional information about the energy in the fluid. For the purposes of the measurements, only compressed, non-heated air was used and the main goal was to keep the inlet temperature and pressure to the turbine consistent.

Figure 47 - Temperature measurement location

4.1.5. Temperature Measurement Locations

The only place that temperature was consistently measured was on the tank, in order to ensure a reasonably consistent set of starting conditions. In order to do this, the tank was measured at the same place prior to every test; as one would expect, the tank temperature increased with each compression cycle. To keep the time between tests to a practical minimum, a fan was set up facing the compressor to cool it. A location was marked on the tank on the opposite side of the fan, noted in Figure 47; at which the

temperature was measured. Once the tank temperature reached 30°C, the test was started. It should be noted that this temperature should not be considered to be the inlet air temperature. Rather, it is only the method by which a consistent starting temperature was measured, and no other attempt was made to determine the inlet temperature. On a few tests, the temperature was taken at the exhaust, if only to get a sense of the change in temperature; this was, in reality, extremely variable, but well below room temperature.

4.1.6. Torque

In order to properly determine the actual power output of the system, torque must be measured. This indicates the delivered power potential of the system, which is directly related to the efficiency. The torque measurement of the system is the shaft torque, and no effort was made to measure reaction torque. In the context of this thesis, the torque measurement is simply to provide a check to the calculations from the acceleration.

That being said, measuring such a low torque is problematic. Many of the potential systems for measuring the torque suffer losses that would hide this low a torque, and, as such, a different method had to be used. A reaction arm with an eddy brake was used so that several small load sensors could be used to determine the total torque generated by the system.

4.2. Sensors

This section will describe the individual sensors used

4.3. Rotational Sensor

The rotational speed was determined using a Hall Effect sensor chip, the AS5132-HSST-500CT-ND. This chip is a contactless magnetic rotary encoder, capable of measuring 360 steps per rotation (8.5 bit), at a maximum rotational speed of 72,900 RPM (AMS, 2013). The chip was chosen since it was able to measure the higher rotational speeds that the Tesla Turbine is capable of, while at the same time being relatively simple to setup. In addition, being contactless meant that it was trivial to set up with the system for an accurate speed measurement. The sensor is an absolute encoder, with an error of +/- 1°, with numerous features.

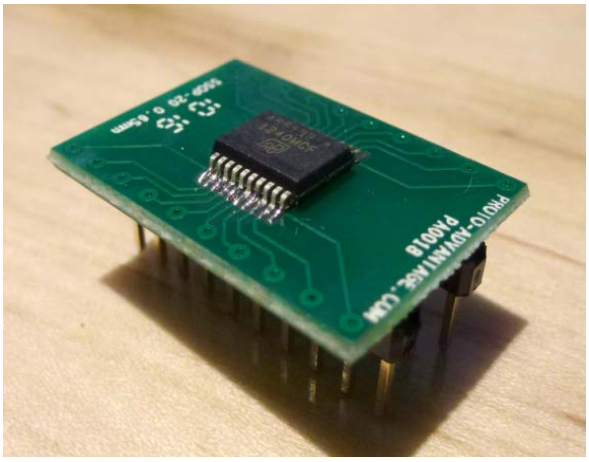

Figure 48 - Hall sensor on soldered base (courtesy of Accutron)

This encoder provided the ability to very easily align and adjust the position of the measurement, so long as an adequately strong magnet was used. The magnet itself needs to be a diametrically magnetized type, so that the magnetic field can be seen by the sensor to be alternating in a radial fashion.

Ultimately, two of these sensors were used, the first was soldered onto a 20 SSOP adapter board (Figure 48), but a wire came loose during testing and caused this chip to fail. A second chip, mounted into a spring-loaded adapter was used in its place for the actual tests presented here (Figure 49).

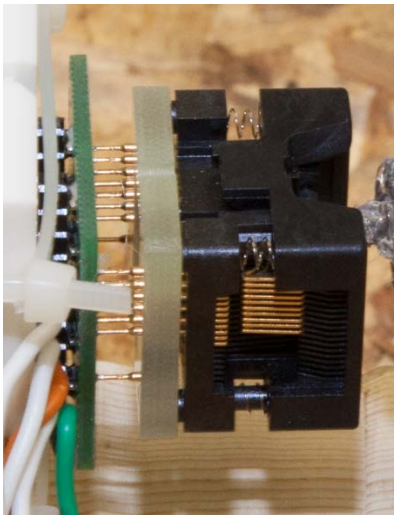

Figure 49 - Hall sensor on spring loaded base

4.3.1. Pressure Sensors

The pressure sensors chosen for the setup are two variants of the ASDX analog sensors, shown in Figure 50. The lower pressure areas (atmospheric and below) used 30psia sensors, and the high pressure areas used 100 psig sensors. These sensors have a ±2% error band, and are fully calibrated. (Honeywell, 2010)

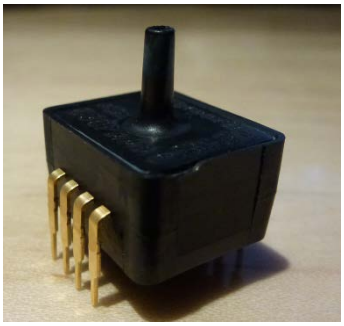

Figure 50 - Pressure sensor

4.3.2. Temperature Sensors

Only one temperature sensor was used, a K-type thermocouple, which came with a Fluke 87V, and was calibrated by the provider.

4.3.3. Loading Apparatus

A loading apparatus was built to demonstrate that torque was indeed present in the system. The setup, shown in Figure 51, consisted of a simple beam (1), with four load cells, two on each end of the beam (2-5). A magnet was placed on the beam (6), intended to interact with an aluminum disc that was shaft mounted (7), to create an eddy brake. This system could be adjusted, having been mounted on a base (8) that was in turn mounted on a set of slides (9,10), in order to adjust the load applied on the eddy brake. This therefore allowed the setting of a steady state at various speeds, to therefore validate the torque calculations derived from the acceleration of the turbine itself as measured using the RPM sensor.

Unfortunately, because the system was not adequately built, there were significant errors, as well as considerable variability. As a result, the meter would only be used as a loading device to demonstrate that torque is indeed being generated by the system.

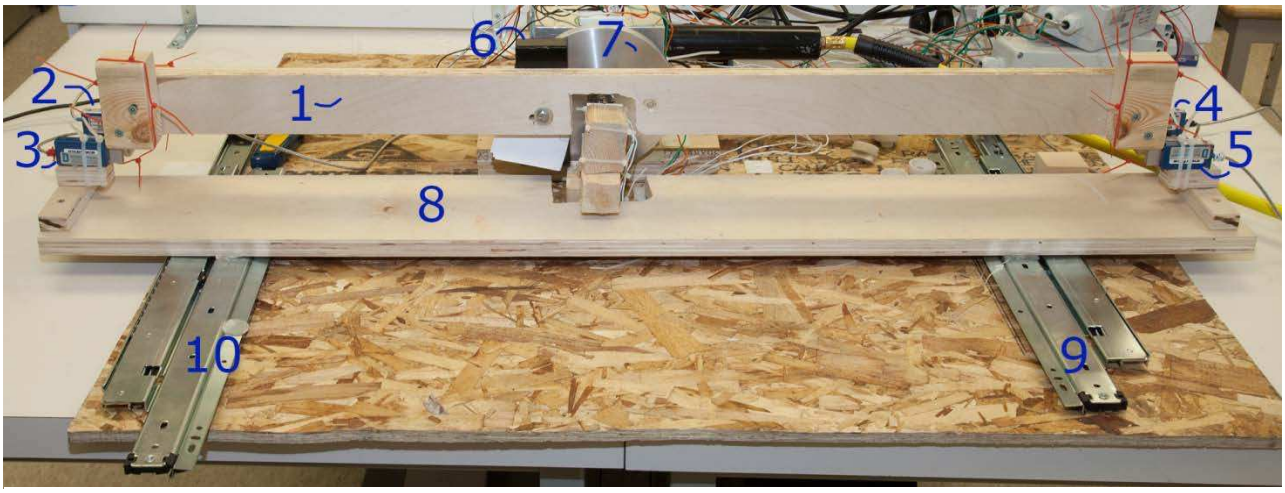

Figure 51 - Torque sensor rig

4.4. Data Acquisition System (DAQ)

The DAQ used, shown in Figure 52, for the acquisition in the sensor rig is an NI USB-6351, from National Instruments (NI). This unit was chosen because of its large number of both digital and analog inputs/outputs, as well as the ability to take a signal from a quadrature encoder.

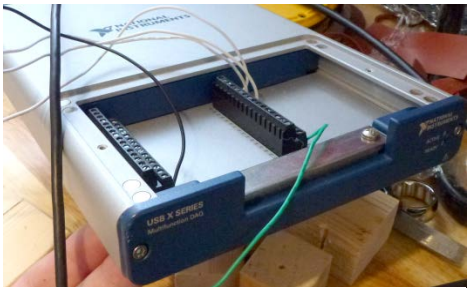

Figure 52 - NI USB-6351 DAQ

In addition, since the programming interface was designed in LabView, also from NI, the programming was significantly simplified since NI provides a premade LabView assistant.

4.5. Software

As mentioned above, LabView was the platform chosen to code the software for the data collection. It was decided early on that this would be the easiest platform on which to do so, but it had some challenges. The software itself is simple in execution; a while loop reads the values from the various sensors in the DAQ, and then appends them to an array, which is in turn written to a file for output and later analysis. In the process, several of the values have a calibration applied.

The front-end of the software shown in Figure 53 provides an interface through which the file name can be changed, calibration values can be adjusted, values can be read real-time during the run. Figure 54 shows the visual code, and data pathways.

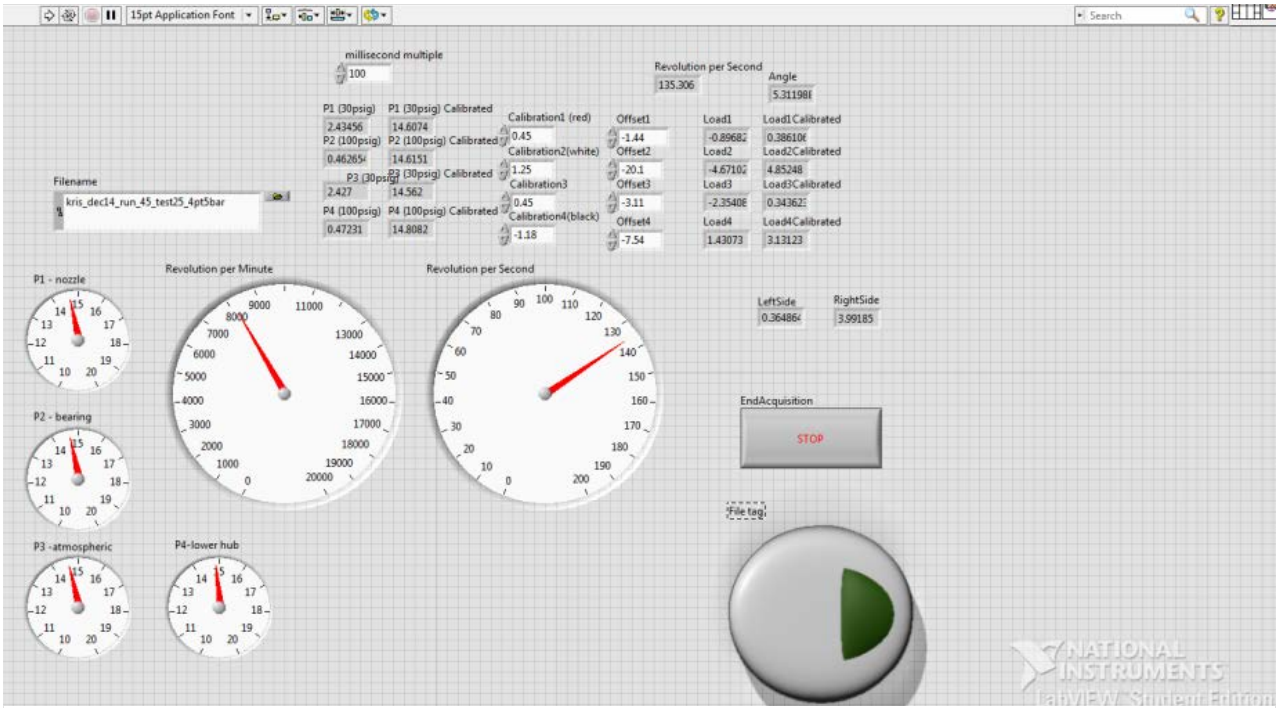

Figure 53 - LabView program front end

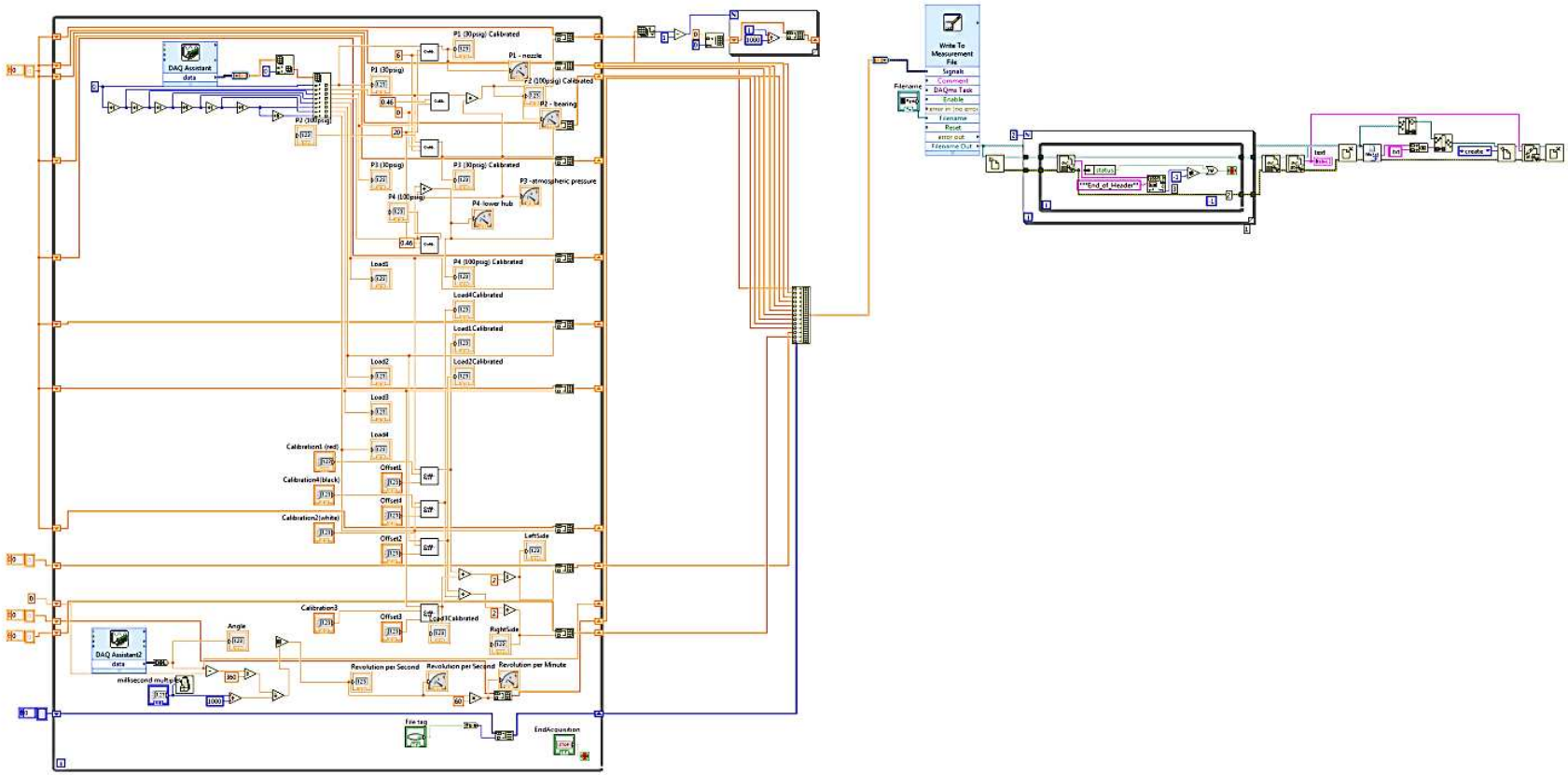

Figure 54- LabView program (Back End), courtesy Karim Omri

4.6. Calibration

The various sensors were calibrated at the beginning, and checked prior to every run. The rotational sensor is an absolute encoder, so did not require calibration.

The two pressure sensors used had slight variances; the absolute pressure sensors were adjusted to 14.7 psi, and the gage pressures were read relative to the absolute sensors. Ideally, a known pressure source should have been used to calibrate these, but only one point is required since they have a linear response between 10% and 90% (Honeywell, 2010).

The load sensors in the torque meter rig were calibrated using a known mass. These sensors, like the pressure sensors, have a linear response.

4.7. Experimental Setup

Firstly, it is important to understand the setup of the system, both conceptually and physically. The conceptual layout can be seen in Figure 55, which shows the location of the various components, sensors and gas flow. It should be noted that this is not to scale. The flow is straightforward, leaving the compressor tank, and passing through a regulator, then the precision pressure sensor, and a valve. The flow then travels down an airline where it enters the plenum chamber, passes through the nozzle, and then interacts with the discs. Lastly, it is exhausted to atmosphere. The

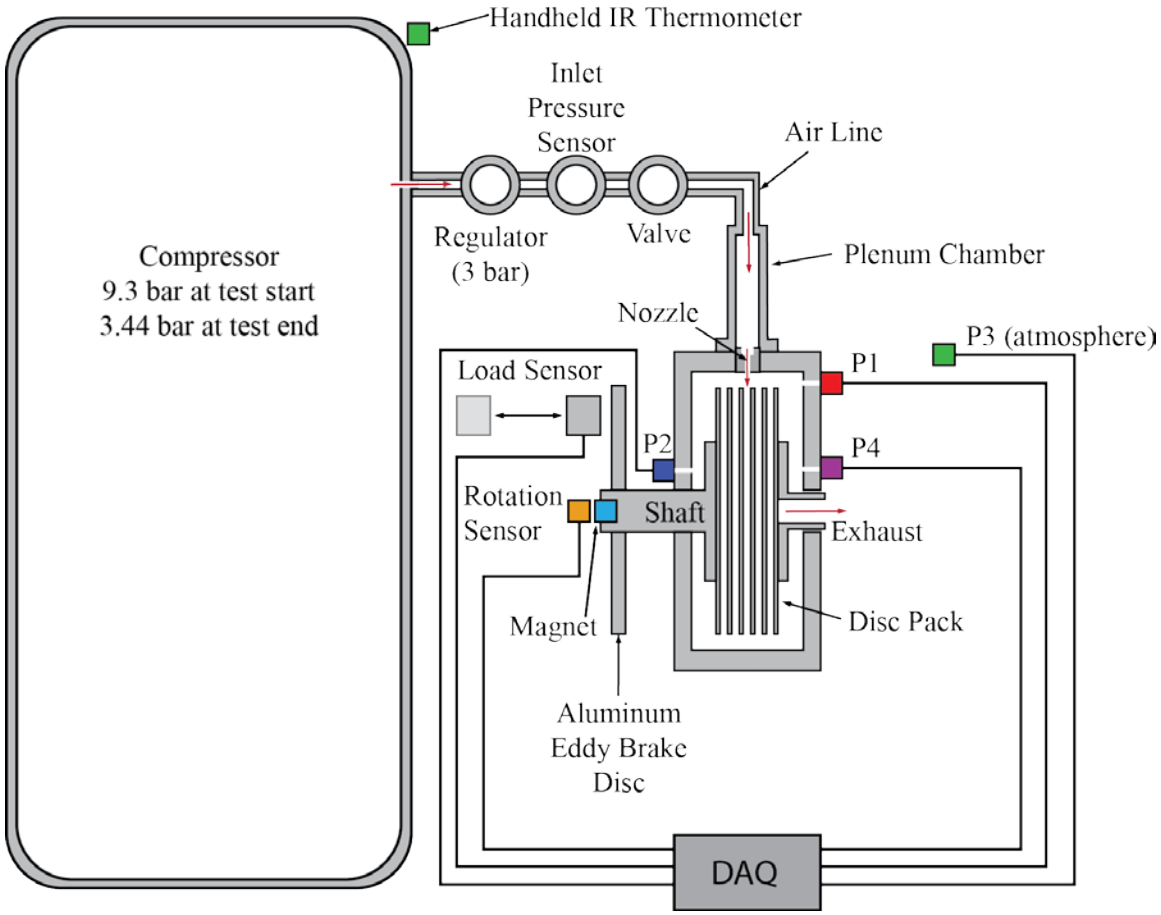

Figure 55 – Conceptual layout

Sensors are located as shown, where P2 and P4 are in between the coarse and fine labyrinth seals; P1 is in the space between the discs and nozzle, P3 is atmospheric. The initial temperature reading is taken from the compressor tank. The rotational sensor is placed at the end of the shaft, which has a diametric magnet affixed. The load sensor is setup to manually approach the eddy brake disc, which is also attached to the shaft. All the sensors, except the inlet pressure sensor and handheld temperature sensor are connected to the DAQ.

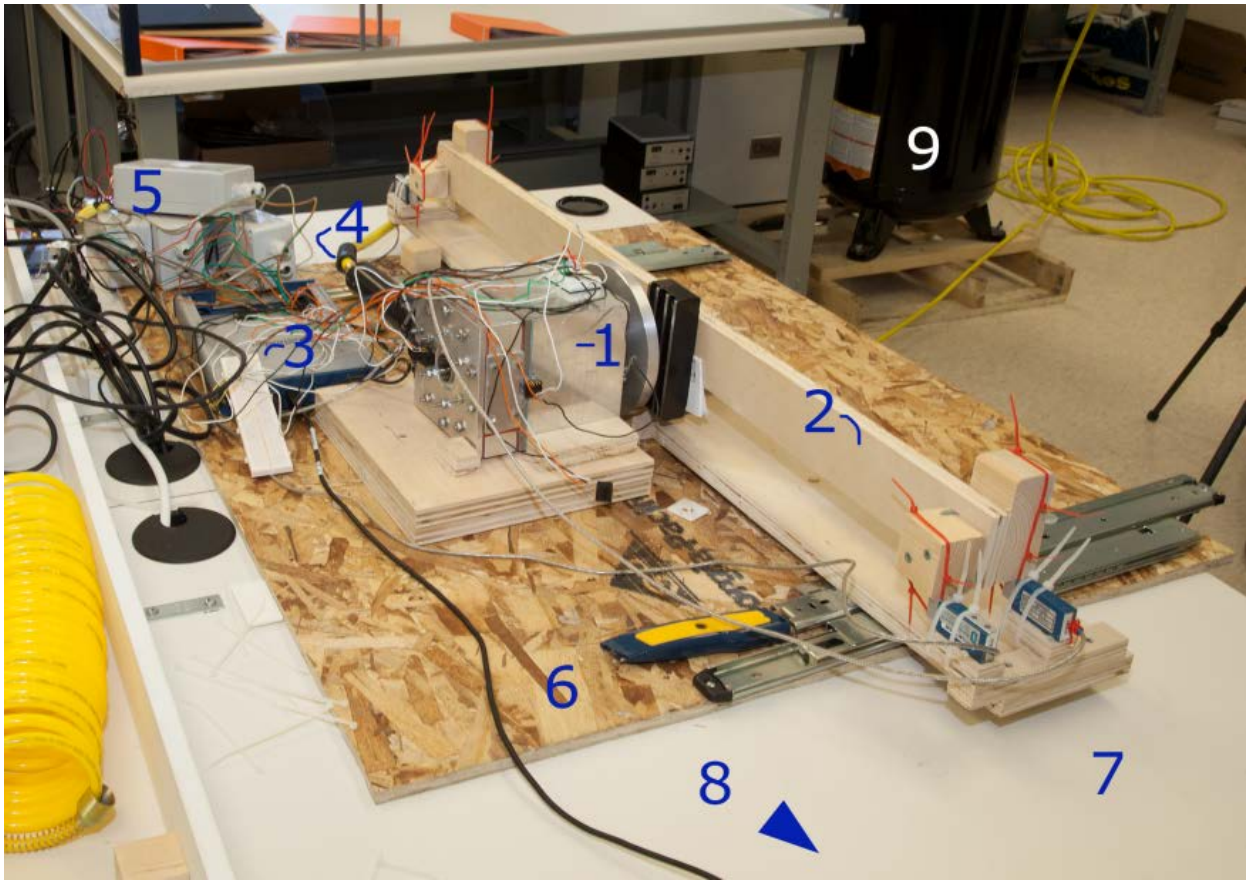

Figure 56 – Physical layout

The overall physical setup of the system is shown in Figure 56. The turbine (1), torque sensor (2), DAQ (3) and strain gauge bridges (5) were place on a piece of ½" particle board (6). This board allowed the various components to be semi permanently fixed together, using hot glue, without affecting the surfaces in the lab. This also allowed the assembly to be easily moved as needed. The compressor and tank (9) should ideally have been positioned closer to the rig, but were placed adjacent to the necessary electrical infrastructure. The airline (4), transited between them. The computer, (8, not shown) was on a desk next to the table with the setup. During testing, the monitor was placed on a stool such that it could be easily seen while the tests were being run, especially those tests where a static speed was required.

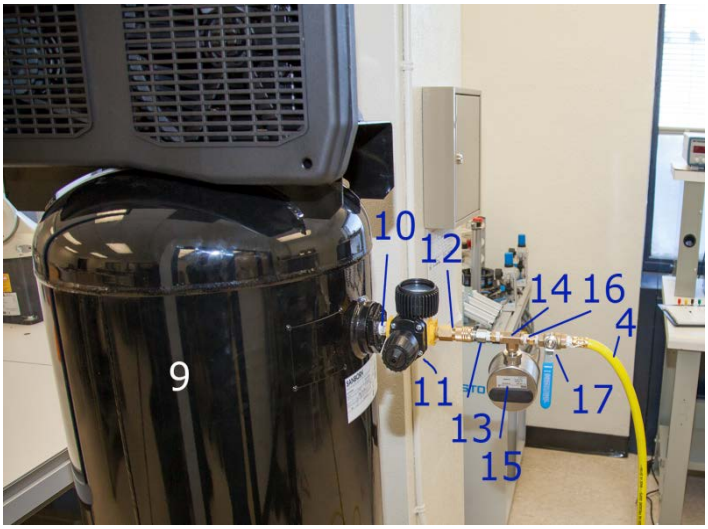

Figure 57 - Airline setup

The setup for the airline was originally done with a very short airline (1m), and the pressure gauge at the turbine inlet. However, once the setup was relocated for the purposes of the large compressor, it was not practical to do so. As a result, the assembly, as shown in Figure 57, was used for the testing, starting at the tank (9). The setup was a ¼" nipple (10), into a regulator (11), into a female quick connect (12), into a male quick connect (13), into a ¼" tee (13). To validate the pressure setting on the regulator, a high precision pressure sensor (15) was placed on the stem of the tee. Continuing on, another ¼" nipple (16), then a 14" ball valve (17), which connected to the airline to the turbine (4).

4.8. Data Acquisition Methodology

The methodology for collecting data was a straightforward series of steps. The primary goal was to ensure that the test-to-test conditions were substantively similar. To accomplish this, the initial conditions needed to be the same; i.e. the starting temperature of the compressor tank needed to be the same. The compressor was allowed to reach the same temperature before restarting, via a fan blowing across the compressor.

4.8.1. Procedure for Acquisition of the Acceleration Curves

1. Run the compressor for the first time, which takes extra time and generates additional heat. Once the compressor reaches its maximum pressure (150 psi), turn it off. Let it cool to a target temperature (30°C) at the target point, and allow the flow (through the turbine) to the low pressure point (50 psi).
2. Turn the compressor back on. Allow it to reach its maximum pressure.
3. Turn off the compressor.
4. Adjust the regulator to precisely 43.5 psi.
5. Turn on the data acquisition program.
6. Turn valve to "on" position.
7. Allow the turbine to accelerate and run until the pressure in the tank emptied to 43.5 psi.
8. Stop the data acquisition program.
9. Shut off the valve.
10. Turn on the compressor.
11. Repeat two more times with installed nozzle.
12. Switch nozzles through selection until complete.

4.8.2. Data & Errata

In the process outlined above, data was collected, and saved to sequential files, so that the values could be validated, statistical information extracted, and inconsistencies could be averaged out. Where necessary, tags were added to the data so that it would be possible to find specific areas within the data files.

The sampling interval was at 6 ms, or 166 Hz.

The raw data can be seen in *Appendix A* .

4.9. Turbine, As Built

The turbine, as it was built, had some flaws that affected the ability to fulfill the intended tests, and caused some delays in order to both completely assess and fix the issues. For example, the drive plate was thinner than expected, and slightly warped, and the spacers were inconsistent. As a result, it was difficult to get precise seals, and the discs themselves were warped in the process of machining. The end of the shaft had a slight "mushroom", which affected the fit of the eddy brake that was added on later. Lastly, the discs were, overall, very roughly machined, and had significant flaws that would ultimately affect the overall balance of the machine.

The result is that the machine is somewhat less precise and more prone to vibration than intended. These issues could be addressed through design changes, or through the machining process. In addition, the friction estimations from the bearing manufacturer proved to be inaccurate, which required the removal of three of the four seals on the bearings. This will ultimately affect the longevity of the system if the bearings are not kept properly lubricated.

That said, these flaws demonstrate the robustness of the design; with some significant vibration inherent, there was no problem achieving rotational speeds in excess of 18,000 RPM, without any apparent failure.

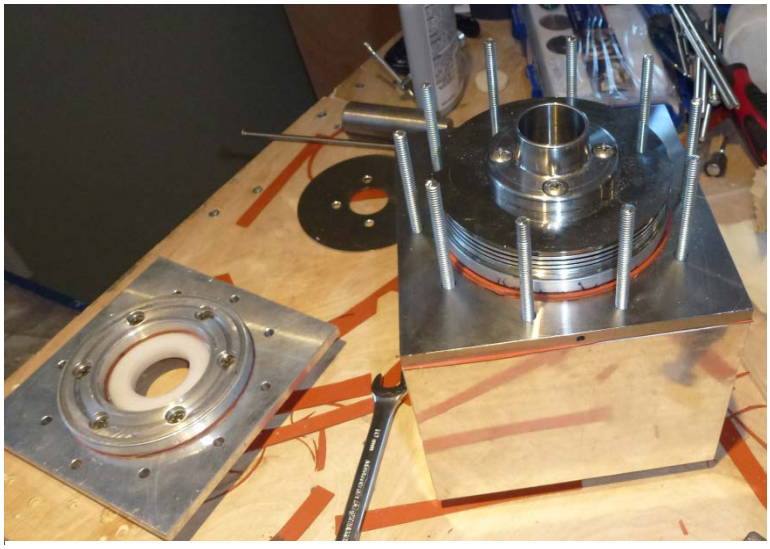

Figure 58- Tesla Turbine, as built, showing the disc pack

5. Results and Discussion

5.1. Results Overview

Data was collected in a series of runs, using the nozzles available. These were β = 2.5°, 5°, 7.5°, 12.5° and 45°. Each nozzle was run three times, as described earlier. The various runs described here are annotated by the angle used, and the run, in the order they were done. All are 3 bar tests, except those marked with "4.5" were the higher pressure tests, at 4.5 bar.

Data was collected in a time step of 0.001 minutes, or 0.06 seconds.

5.1.1. Raw Acceleration Data

Data was collected unprocessed. As a result, the data is quite noisy. In addition, there was some significant vibration, at times, and this caused some movement that occasionally caused errata spikes. This can be seen in the first primary run of the 45° nozzle, seen in Figure 59, on the deceleration component.

Runs were done sequentially per nozzle, and were differentiated by the nozzle angle (β) and the run number, in the order that they were completed in. Here forward, graphs will be denoted as β /run. Each nozzle angle was also run multiple times, to determine consistency. As can be seen in Figure 60, each run aligns extremely well, with almost no variability from test to test.

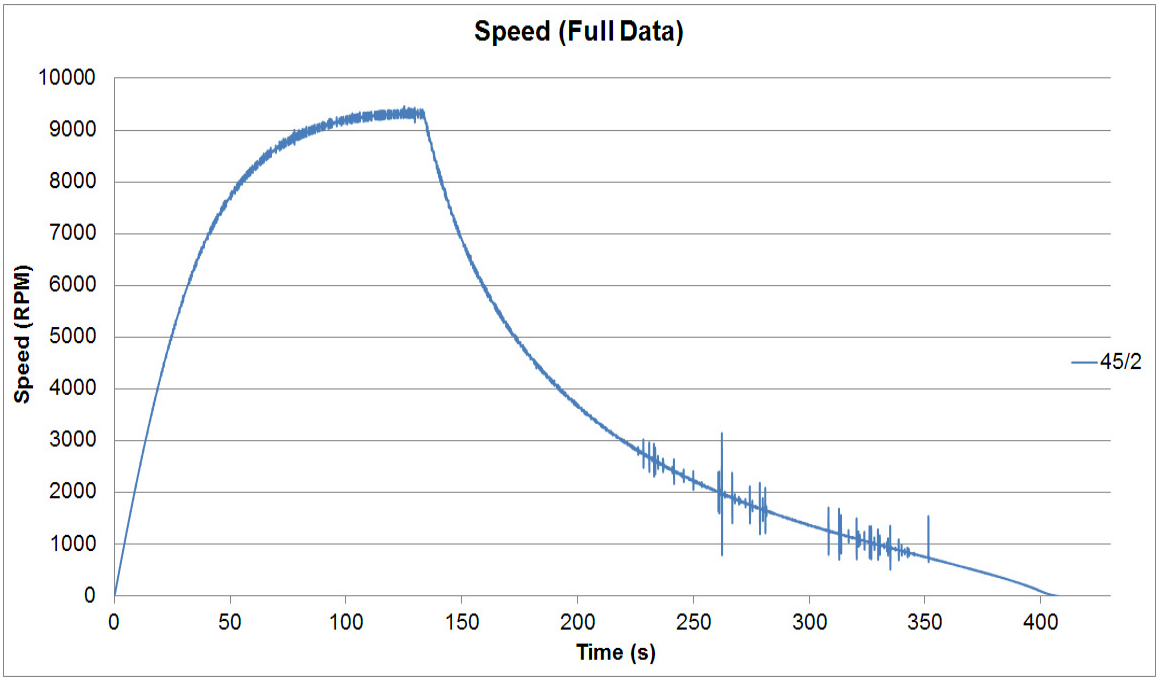

Figure 59 -Raw data for test 45/2

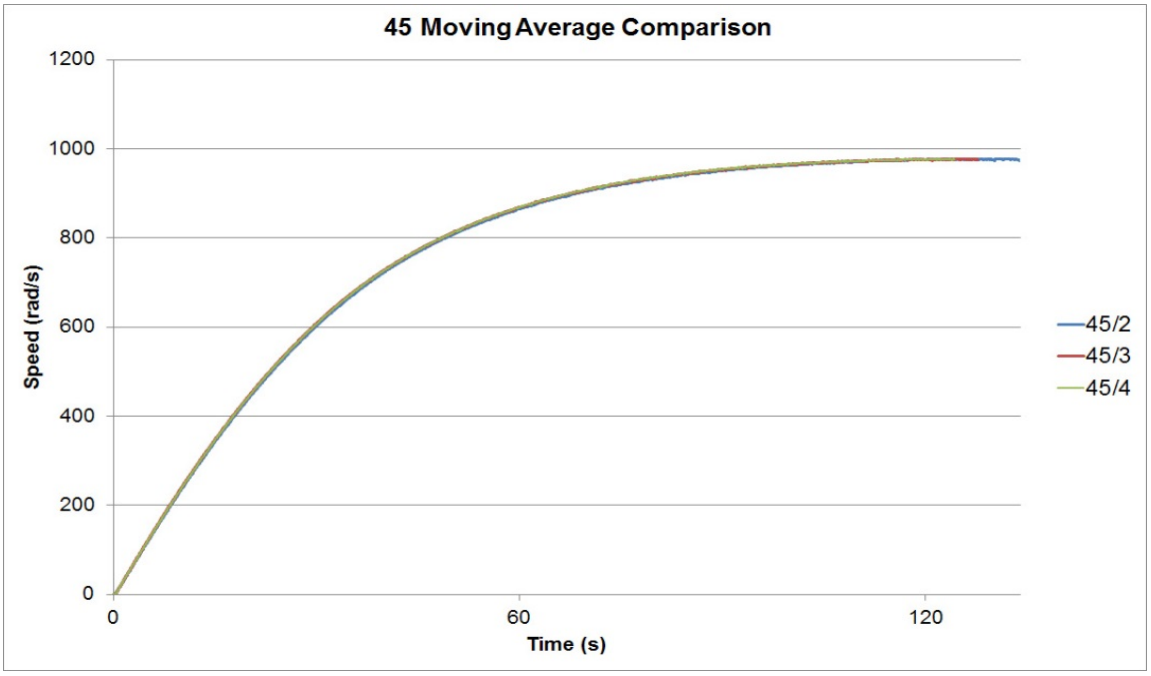

Figure 60 -Raw data for test 45/2

Only three runs collected the deceleration, as it was quickly discovered that it was very consistent run to run, as can be seen in. These are 2.5/9, 12.5/14 and 45/2. Once the nozzle flow was removed, $\tau_{friction}$ is the primary force acting on the system at that point, and should be the same regardless of α, where ω is the same. The various runs generally look the same, in raw form, and can be inspected in detail in Appendix B.

In spite of the local noisiness of the data, the runs are consistent from nozzle to nozzle, as well as run to run. The various datasets can be seen in Figure 61, which shows the various deceleration runs, as well as those which were limited to acceleration only. The 4.5 bar test, shown in orange, was cut off above 10,000 RPM due to vibration issues. It should be noted that after all data collection was completed, the 4.5 bar test was run again, but without data collection. It peaked at 18,500 RPM before it was turned off.

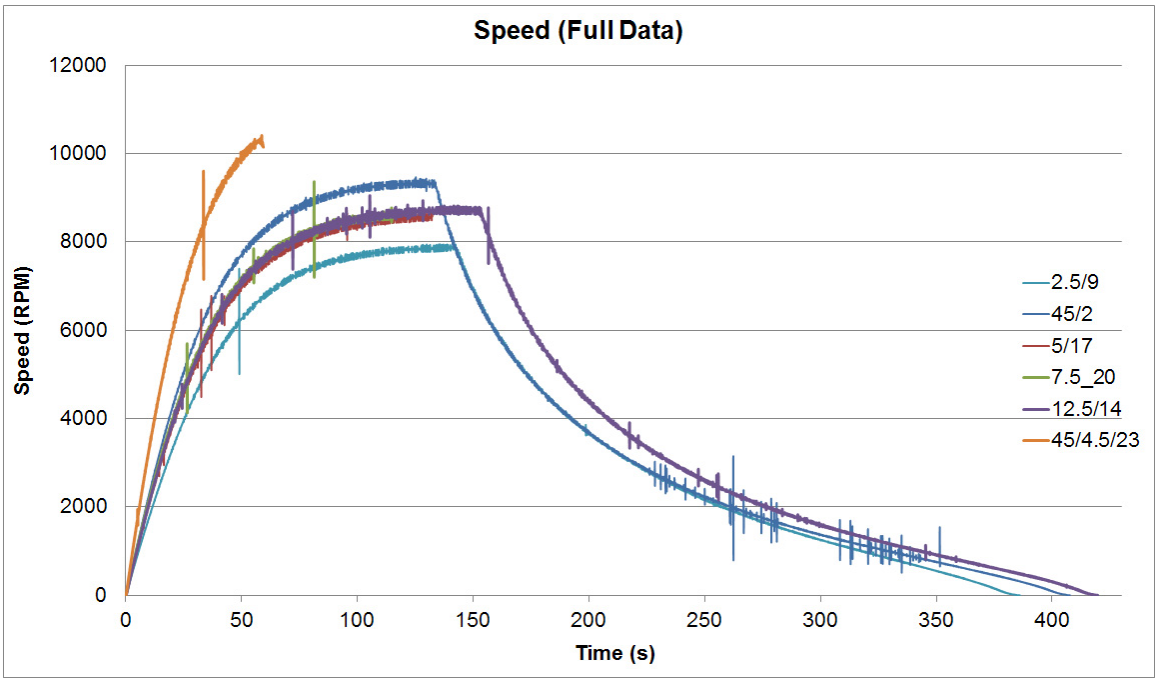

Figure 61 - Raw data v. time from all nozzles

Prior to processing the data, the individual runs were analyzed, to set up appropriate ranges for further analysis. This meant finding the start point, the cell before rotation began, and where the switch to deceleration occurred.

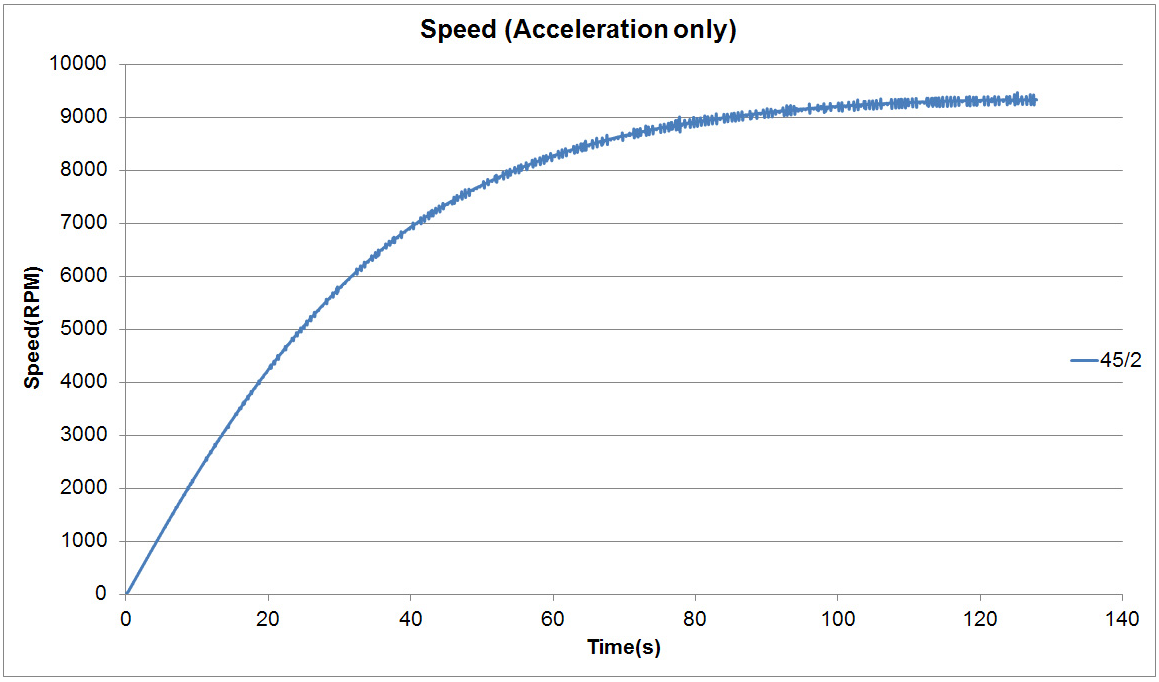

Figure 62 - Speed v time for the acceleration portion of 45/2

.

5.1.2. Smoothed Data

Once this data was isolated, further processing could be done. The first step was to take a moving average, as seen in Figure 63, below. This removes the bulk of the noise in the data. This step was likely unnecessary for most of the data, but several of the runs had additional errata that are mostly removed with this technique.

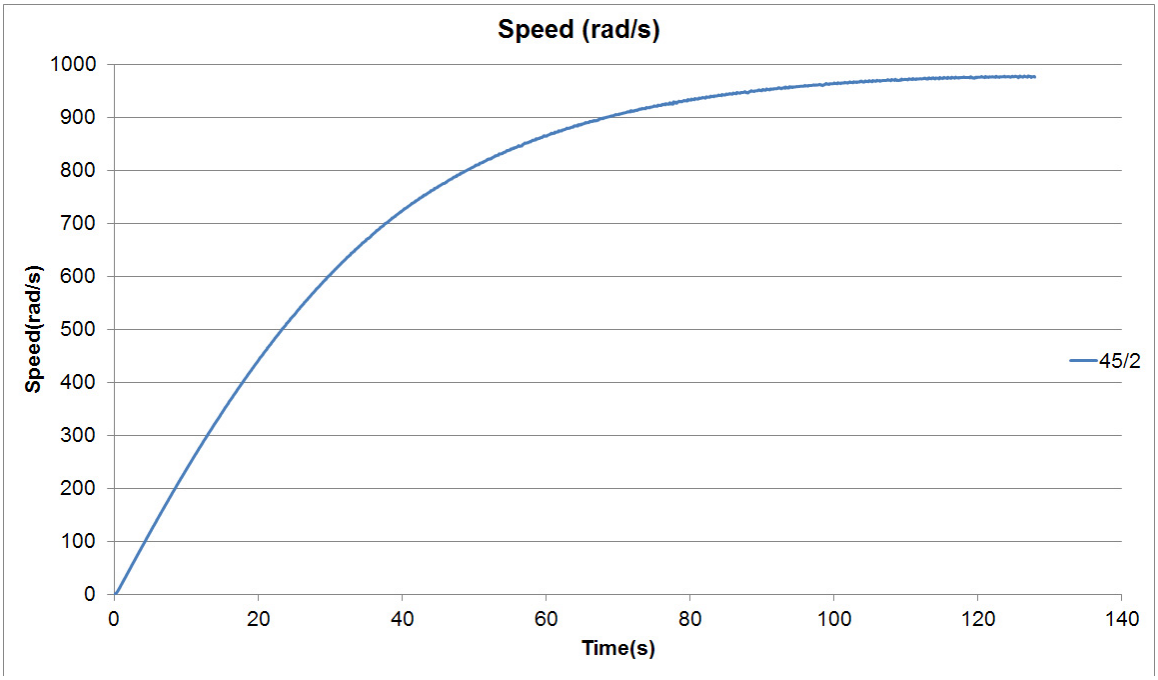

Figure 63 - Moving average, converted to rad/s

The next step was to acquire a polynomial to fit to the moving average curve, in order to take the derivative for the acceleration. From those values, a new line was created to represent the polyline in the graph, and this was combined with the moving average to ensure that the polyline was the expected match, as can be seen in Figure 64.

The resulting polyline is calculated in the form of equation 28;

$$\omega = m_6x^6 + m_5x^5 + m_4x^4 + m_3x^3 + m_2x^2 + m_1x + b \quad (28)$$

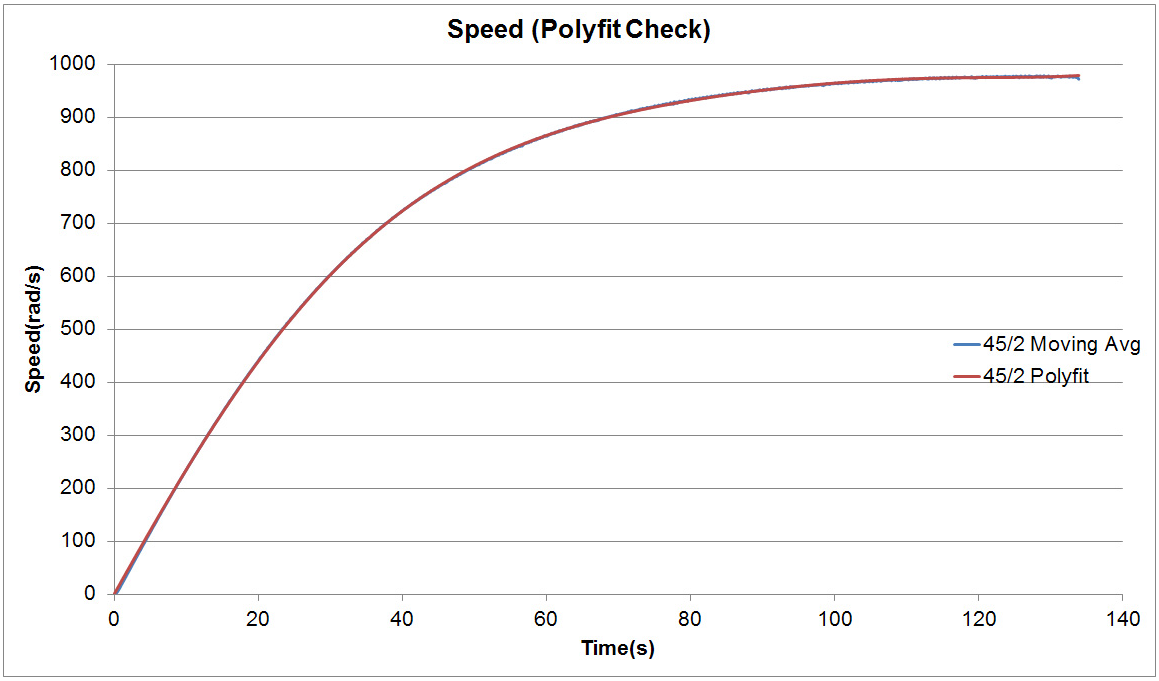

Figure 64 - Polyfit check for 45/2

5.1.3. Acceleration

One the polyline is calculated, the derivative of that polyline could be taken, which results in the acceleration curve. This results in equation 29;

$$\alpha = 6 * m_6 x^5 + 5 * m_5 x^4 + 4 * m_4 x^3 + 3 * m_3 x^2 + 2 * m_2 x + m_1 \qquad (29)$$

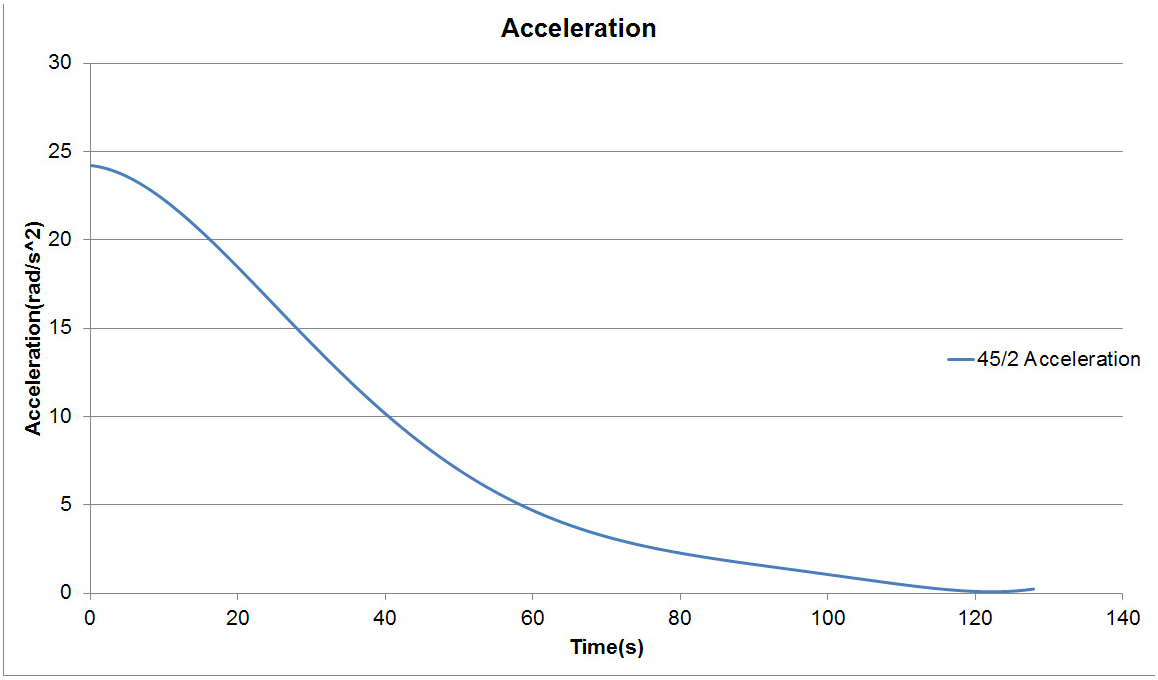

Figure 65 - Acceleration of 45/2

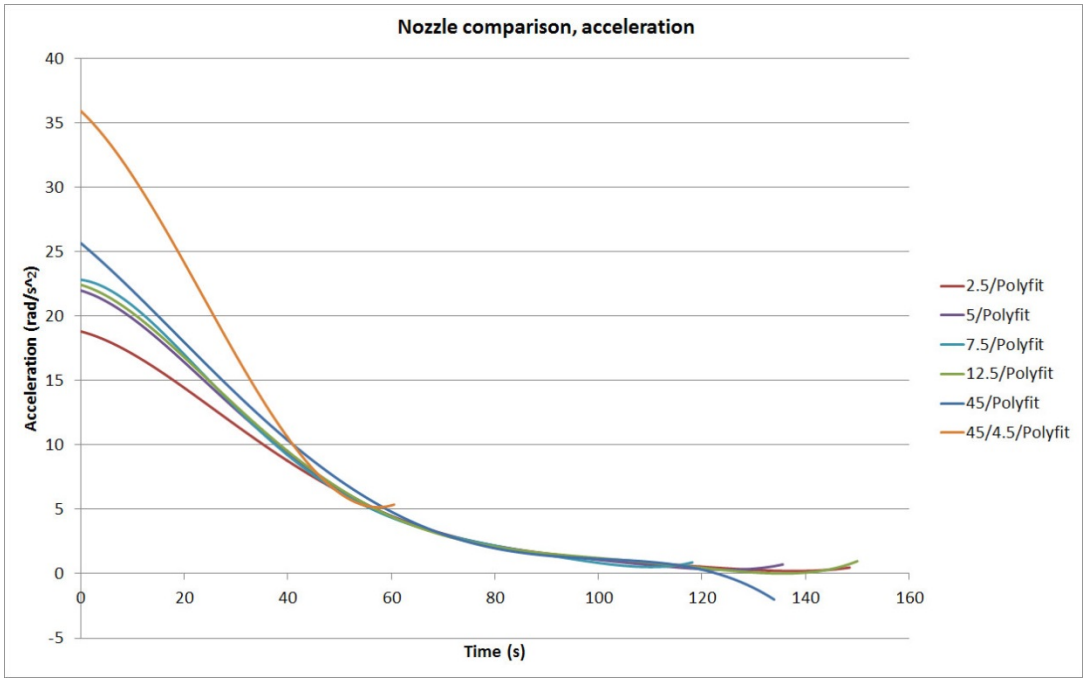

Figure 66 - Acceleration curves for the various nozzles.

The resulting curve is shown in Figure 65. This was done across all the various nozzles, and the resultant curves (with respect to time) are compared in Figure 66. These results disagree with the literature, which suggests that the highest torque, and therefore acceleration, should occur where the nozzle is tangential (Romanin, 2012). There is clearly an effect occurring here that warrants additional study.

5.1.4. Torque

In order to be able to calculate the torque of the system based on the acceleration curve above, and Equation 26, the values must be multiplied by the moment of inertia of the system. To do this, the value was calculated from the SolidWorks model. It should be understood that this will result in an approximation, given that there are many variables therein, such as the exact size/length of the fasteners, the specific alloys used, and imperfections in machining, especially in the discs. That said, the calculated value for I is .0008641 $kg*m^2$, as shown in Figure 67. The multiplication was done, and resulted in the curve shown in Figure 68.

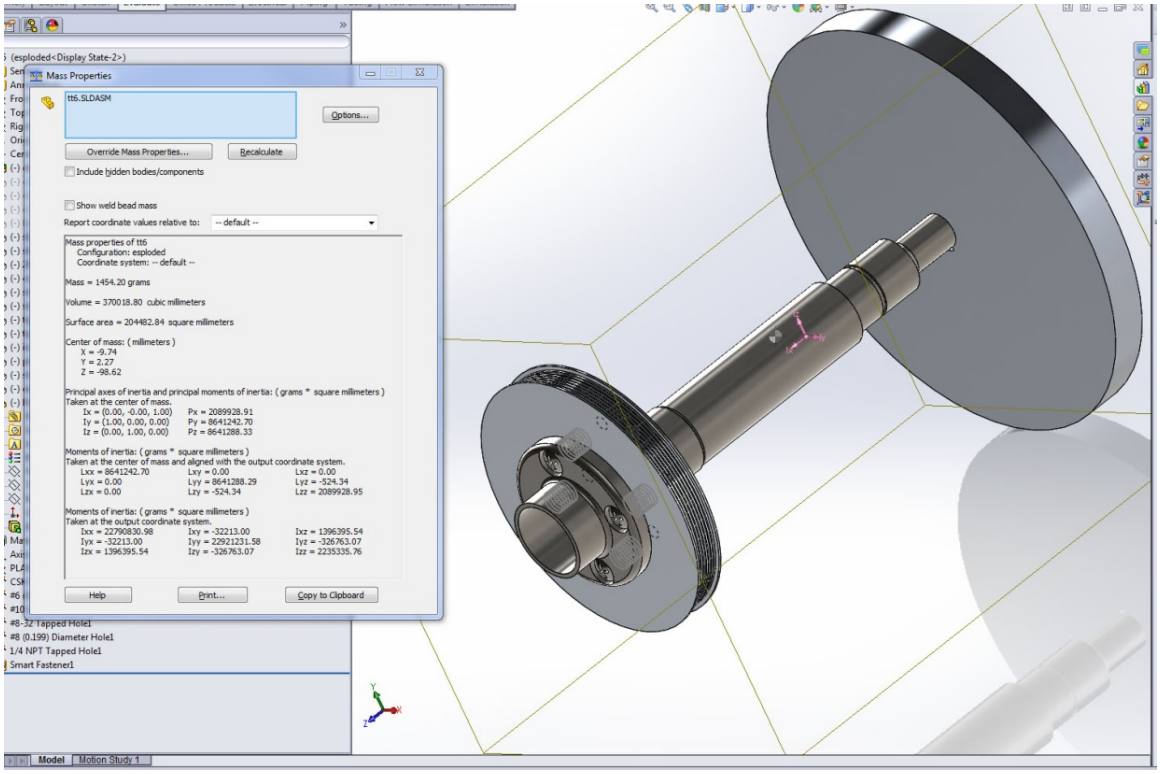

Figure 67 –SolidWorks© calculating the moment of inertia

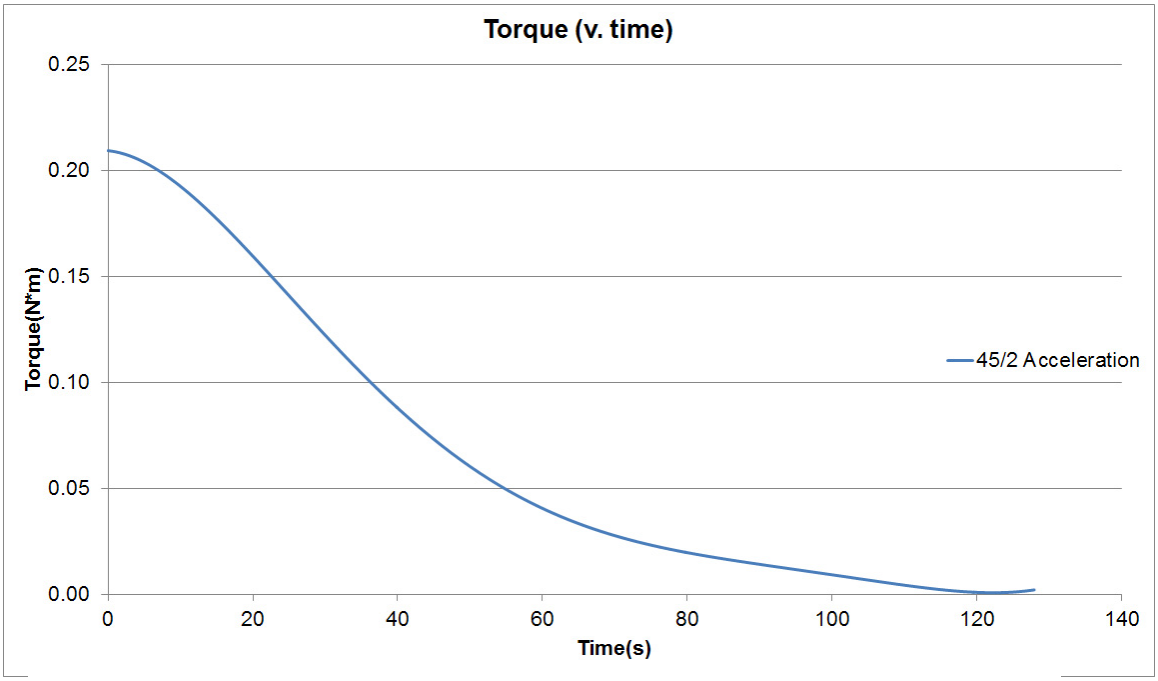

Figure 68 - Torque v time for 45/2

Comparing torque to time in this context, however, does not carry much meaning. A better reference is versus speed (ω), which is plotted in Figure 69. This is then carried across all the runs, and the runs are compared in Figure 70 and Figure 71, below. The curve uptick at the end is an artifact of the method to generate the equations.

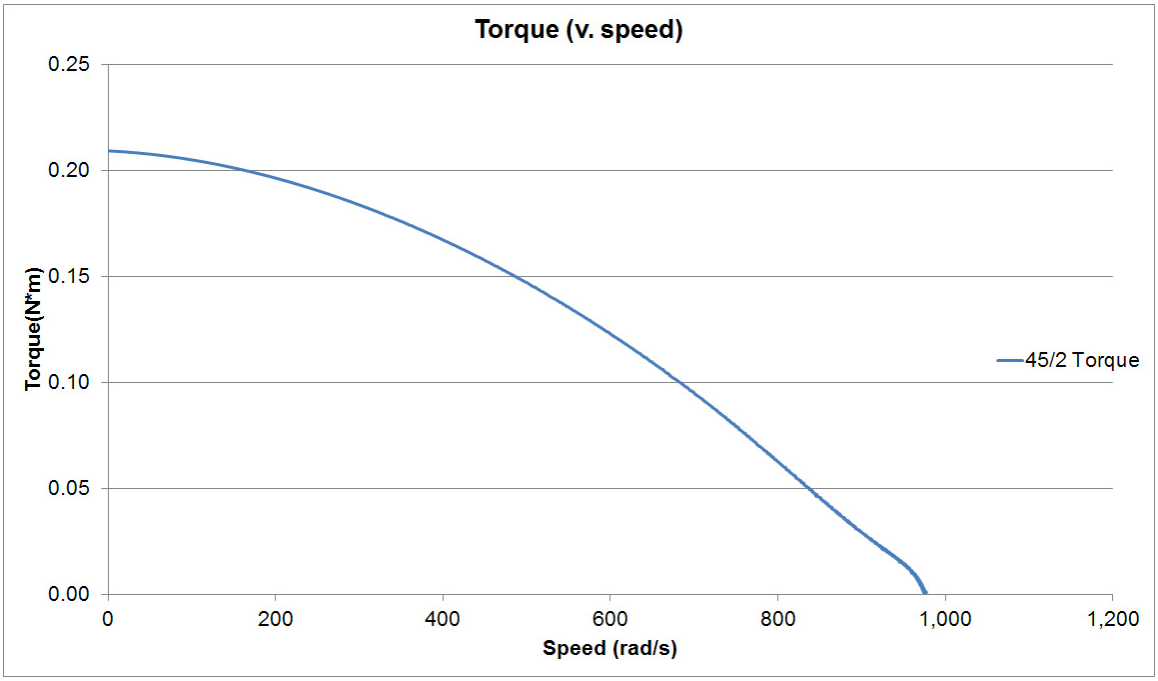

Figure 69- Torque v speed for 45/2

As expected, the higher pressure creates more torque. What is less expected is that the curves stay on the same relative path.

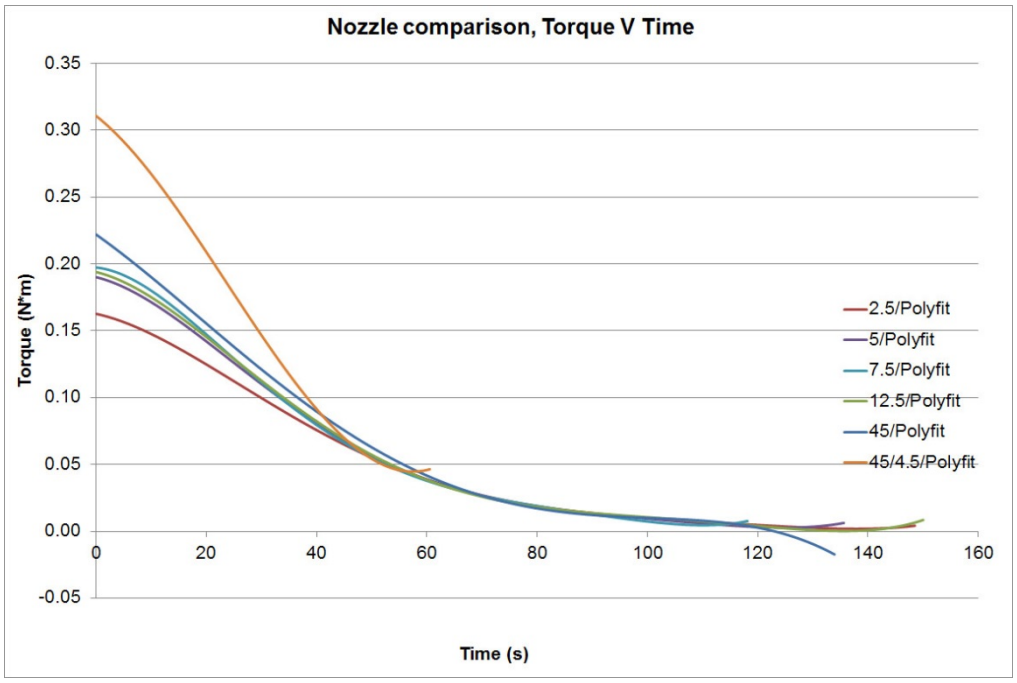

Figure 70- Torque v time, all nozzles

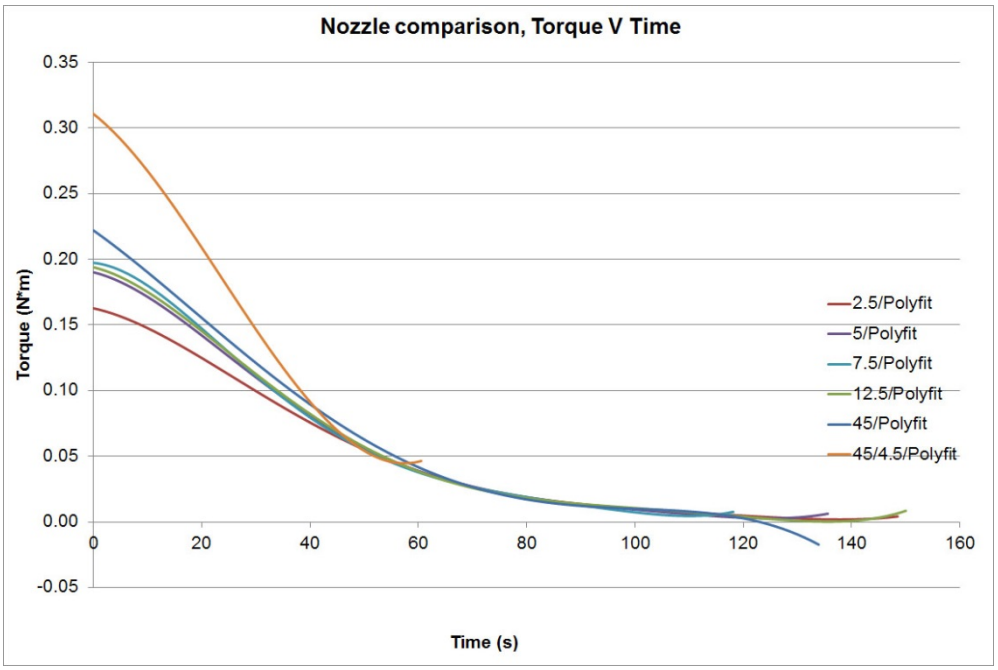

Figure 71 - Torque v speed, all nozzles

To serve as a comparison, the curves are normalized in Figure 72. Since the curves do not precisely match up, we can therefore see that there is a definite effect by changing the nozzle angles. However, because of the unknown effects caused by the geometry, discussed later in 5.2.3, further testing is required to better understand the precise effects. It should be noted that the normalized values for 45/4.5 bar are not a good representative of the state of that nozzle, since steady state was not reached.

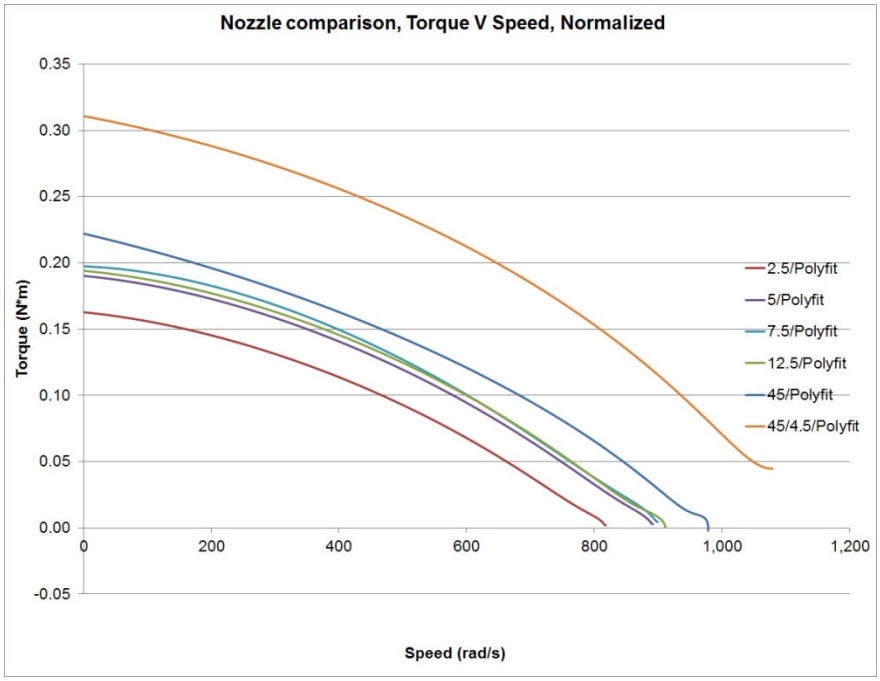

Figure 72- Torque v speed, normalized

5.1.5. Deceleration and Losses

The next piece of analysis is the losses that are incurred in the system. There are various losses occurring;

- windage losses, on the areas outside the active turbine
- centrifugal forces
- bearing losses
- vibration losses

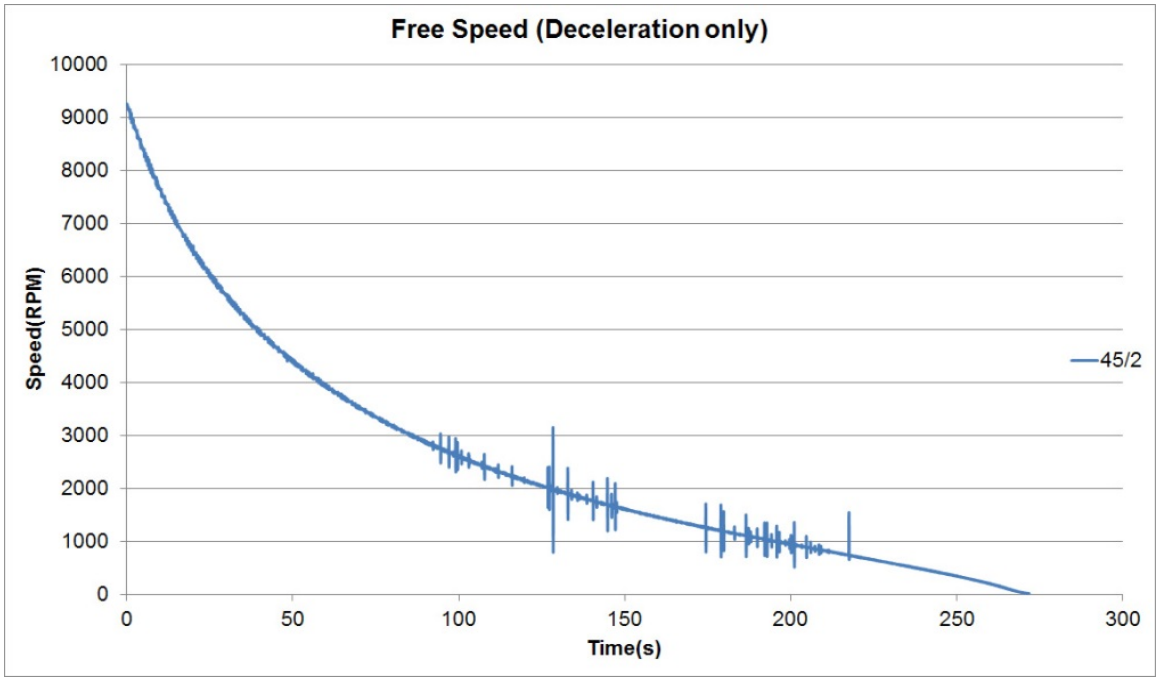

Figure 73 - Free deceleration of the turbine in 45/2

By letting the turbine decelerate completely on its own, it is possible to get an insight on the combined losses. The process for doing so is much the same as the acceleration curves. Isolating the deceleration can be seen in Figure 73.

As with the acceleration data, a moving average was taken, followed by a polyfit line, which was then use to derive the losses, as shown in Figure 74. The oscillation at the beginning of the curve is an artifact of the polyfit line used for the deceleration curve.

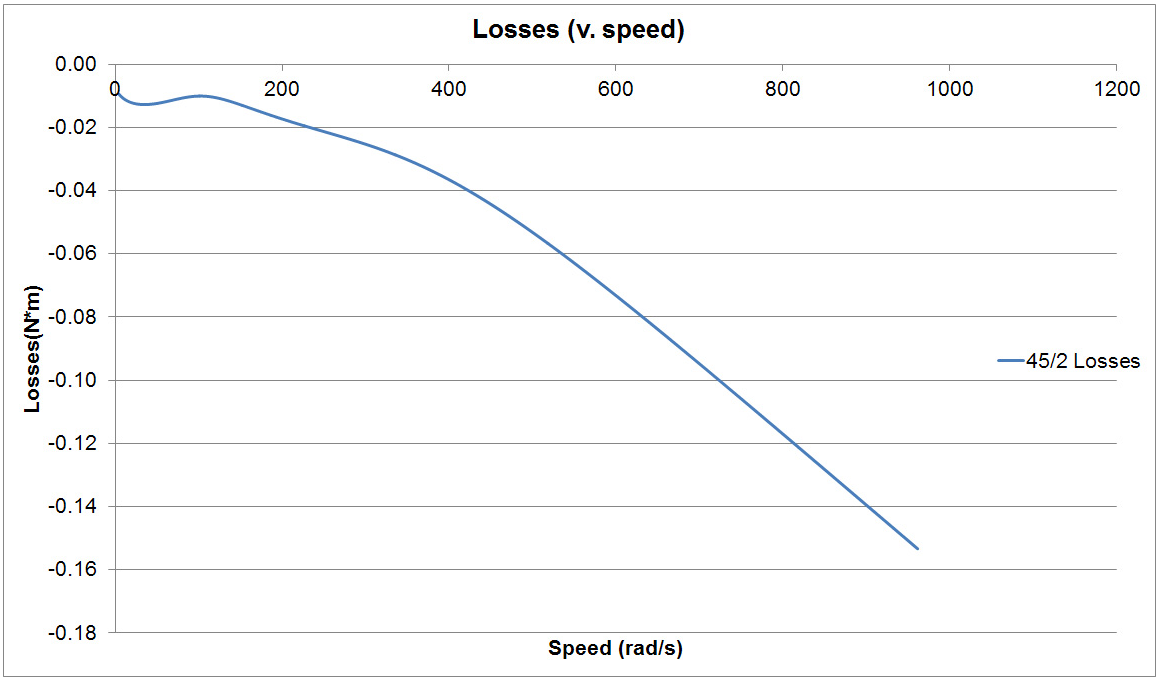

Figure 74 –Losses v. speed, 45/2

5.1.6. Steady State Loads

In order to attempt to get actual readings, a crude dynamometer was built, as described in 3.21. The goal was to be able to provide an order of magnitude comparison of the actual torque, but it would appear that there was simply inadequate sensitivity in the system to have accomplished that. The raw data is shown in Figure 75a and Figure 75b below.

It is possible to see how the author was adjusting the magnet, which caused the system to either accelerate or decelerate depending on the proximity of the magnet/eddy brake. It was possible to get very fine adjustment of the speed, but was somewhat limited only because of the ability to adjust the

relative position manually, and responding to the variation seen on the display. Certainly, this could be automated at a later date to get a very fine control of the loading system. This, in turn, can allow one to achieve very fine control over the loading of the system that may be desired for specific test conditions.

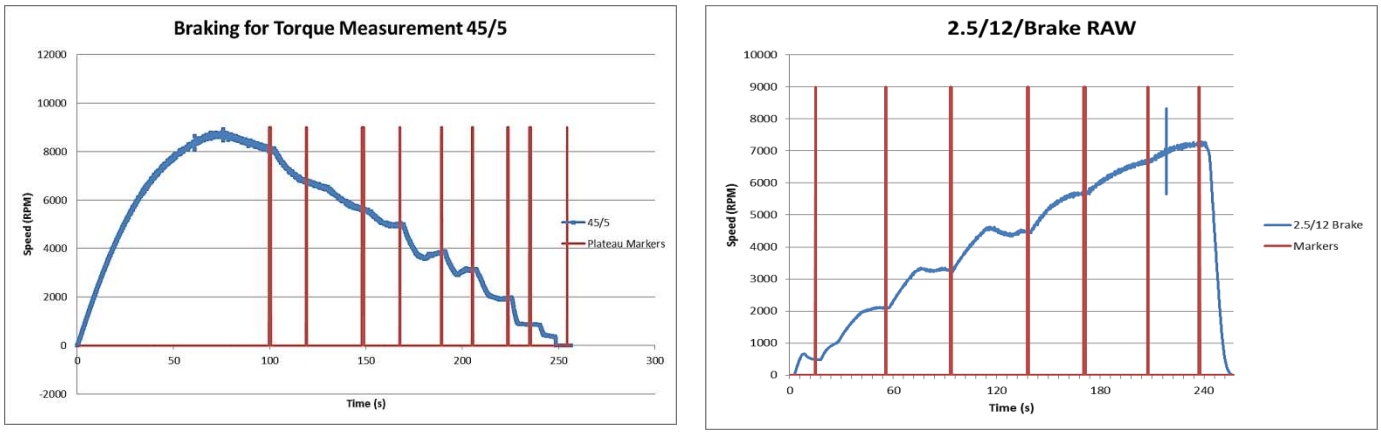

Figure 75 – a) Steady state RPM data for 45/5, b)2.5/12 steady state data

It was easier and faster to apply the brakes as the turbine accelerated, rather than letting it spin up to full speed. Given the size of the compressor tank, this also ensured there was adequate air to complete the test without the compressor engaging.

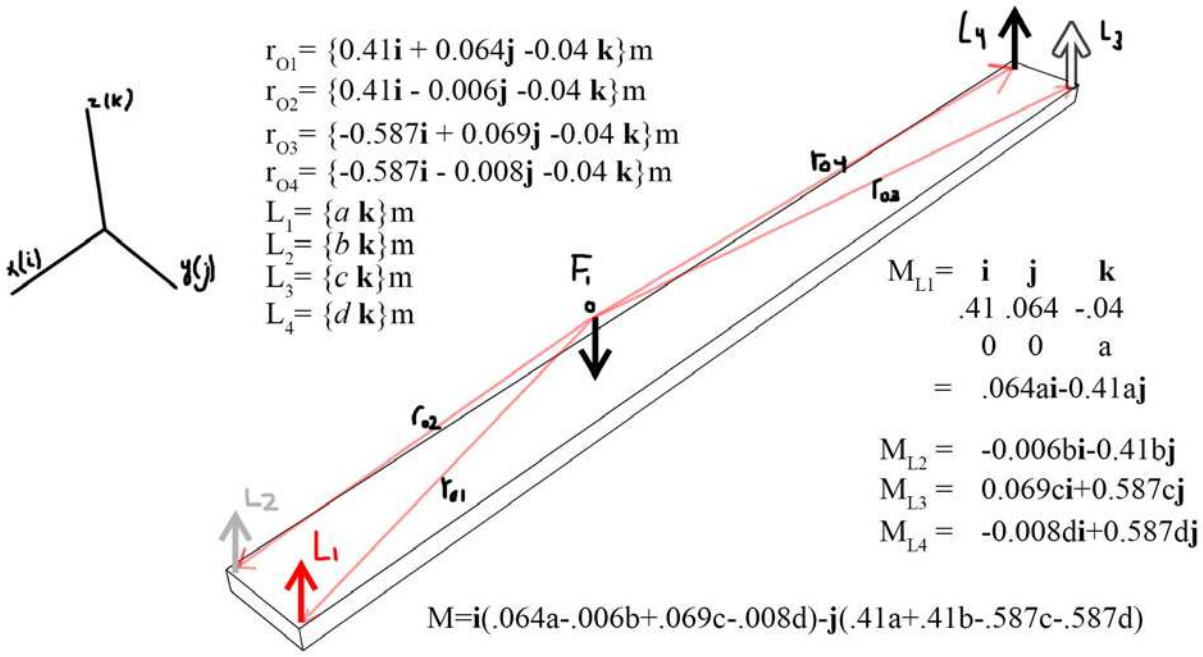

Figure 76 - Algebraic formula to calculate the resultant torque at F_1, from loads at the four sensors.

Calculation of the torque was done using the algebraic formula calculated in Figure 76.

However, as mentioned previously, the resultant values were not commensurate with the values that would be expected from the the numerical calculations based on *I* and α. They were, therefore, discarded since the instrumentation was not available to determine what the discrepancy was caused by.

5.1.7. Pressure data

The pressure data was collected with the rest of the data, and was also very noisy, relative to the atmospheric sensor P3, which was not physically connected to the device. The pressure sensors were

likely adversely affected by the significant vibration in the system, which could have included resonant frequencies, given that they are diaphragm sensors.

Figure 77 shows these results, where P1 is at the top of the disc pack, P2 is at the inner hub, P3 is atmospheric, and P4 is the front hub, per Figure 35. It should be noted that these results were not corrected in this graph from their starting offset, for visibility.

Looking at Figure 77, one can clearly see back pressure building at the top of the stack from P1, and then a sudden drop when the air supply was removed. Further, the back pressure from the discs, as they decelerate, can be seen after the air was turned off; however, there is much less since there is no new air being introduced.

This backpressure suggests that the flow is not ideal, such that not all of the mass flow was able to enter the discs and pass quickly enough. This may adversely affect the overall performance of the system. This may be due to the disc spacing relative to the mass flow, or perhaps effects relating to the radial gap, which will be discussed further in section 5.2.3.

There is a sudden pressure drop at the start, on P4. This is likely caused by the jet of air coming out of the nozzle, and entraining the local air in the volume, creating a small vacuum effect before the flow starts to back up.

P2 is less informative, as it is extremely variable. This could be due to many causes, including leakage around the bearings and other system gaps, and other issues. It is also possible that there was a minor leak around the mating surface. These things should be noted for future designs, as they represent locations for potential losses. Lastly, P3 shows atmospheric pressure, and variability in that is more likely due to the vibration of the system.

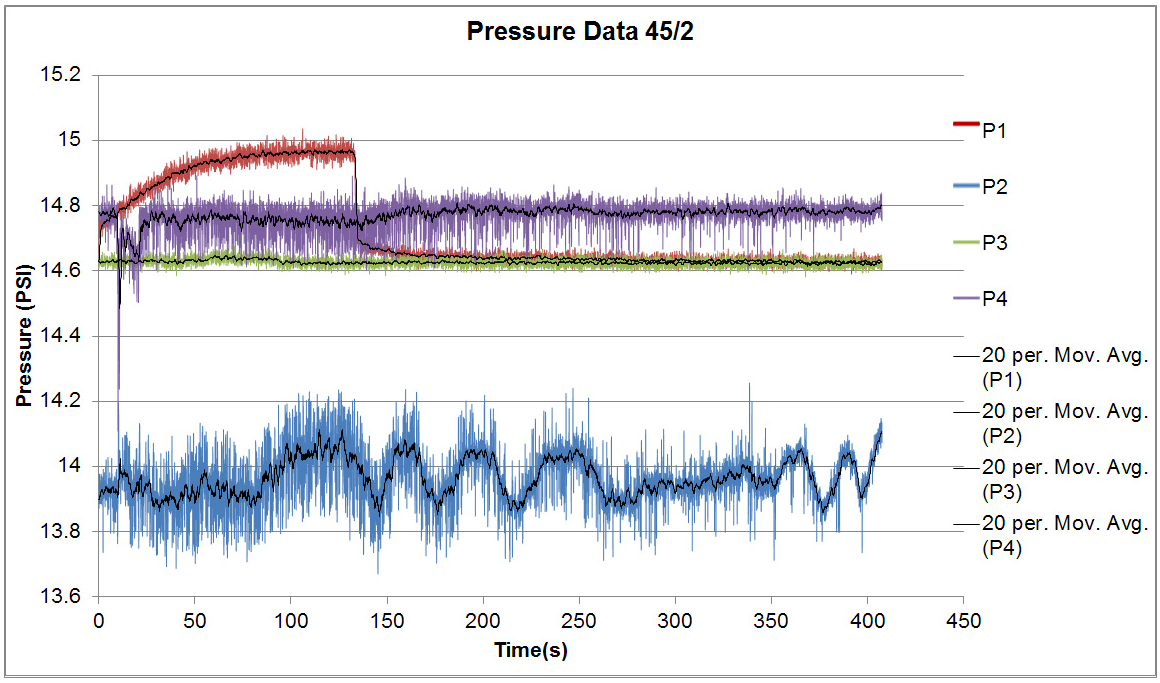

Figure 77 - Pressure data from 45/2

5.2. Discussion

This section will discuss the results described previously.

5.2.1. Overall Results

Overall, the system performed better than expected. The initial inspection of the machined parts was disappointing, and there was concern that this would affect the ability for the turbine to operate reliably. As a result the initial pressures chosen were decreased to 3 bar, which certainly made it more difficult to discern the differences between all of the nozzles.

5.2.2. Expected vs. Actual Results.

The literature suggests that as the nozzle angle approaches the centerline, torque will decrease (Romanin, 2012). This is not what was observed. Looking at the curves in Figure 71, the individual nozzles seem have a relative offset, with very little crossover in the respective curves. However, there may be additional reasons for this, which could be corrected in further investigations.

5.2.3. Possible Cause of Unexpected Results

Certainly, with much more testing, it would have become easier to determine where issues in these tests could be found, but the primary area that this particular turbine diverged from that of Tesla's original design is in the fact that the discs in this test had a step, such that there was a gap between the exterior wall of the expansion chamber, and the leading edge of the discs.

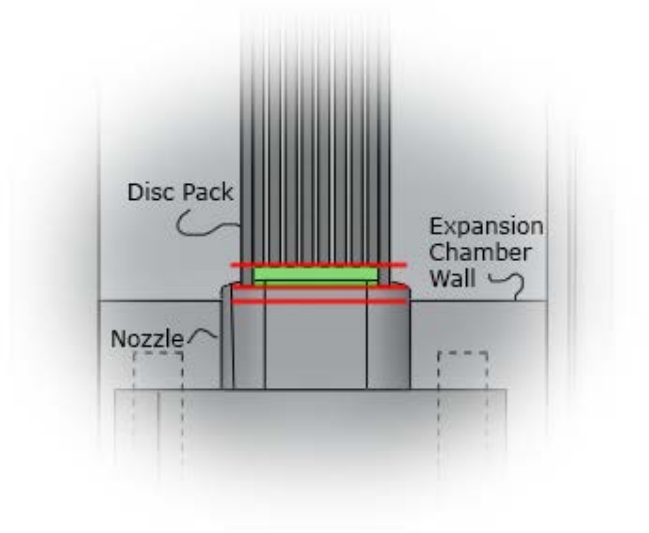

Figure 78 - Possible Problem area.

This can be seen in Figure 78, in the area in green. As the working fluid leaves the nozzle, it is not immediately entrained between the discs, and therefore has the opportunity to experience additional losses. The edges of the discs were not very smooth in this area, which may have made the problem worse. Conversely, the gap may have been acting as a total inlet nozzle, which would also confuse the data. The original intention of this thesis was to try

several versions of the disc pack, and this would have verified if this was the problem or not. It would also be possible to make an insert, and or other control measures, but these were beyond the scope of this thesis.

5.2.4. Efficiency

In the setup, there was not a proper pressure sensor by which one could measure the static and dynamic pressures prior to the nozzle, which is an oversight in this design that can easily be rectified. In the case of the setup to be discussed later in this thesis, the pressure to the turbine was set at the compressor, via a regulator. Instead, it is necessary to calculate an estimation, which can be done from the source compressor. The compressor is 60 gallons. Its starting pressure is 135 psi @ 30°C, and the tank pressure switch kicks on at 50 psi, when the valve was closed to end that portion of the test.

5.2.5. Diagram

Because the tank itself is only decreasing from 135 psi to 50 psi, we must break down the analysis of the flow into steps. To denote these, we will use the following nomenclature, as described in Figure 79;

Subscript i will be the initial tank conditions

Subscript f will be the final tank conditions

Subscript 1 will be the change in tank conditions that result in $\dot{m}$

Subscript 2 will be the conditions after the regulator, but before the turbine

Subscript 3 will be the ideal isentropic conditions after the turbine

Subscript 3' will be the actual conditions after the turbine

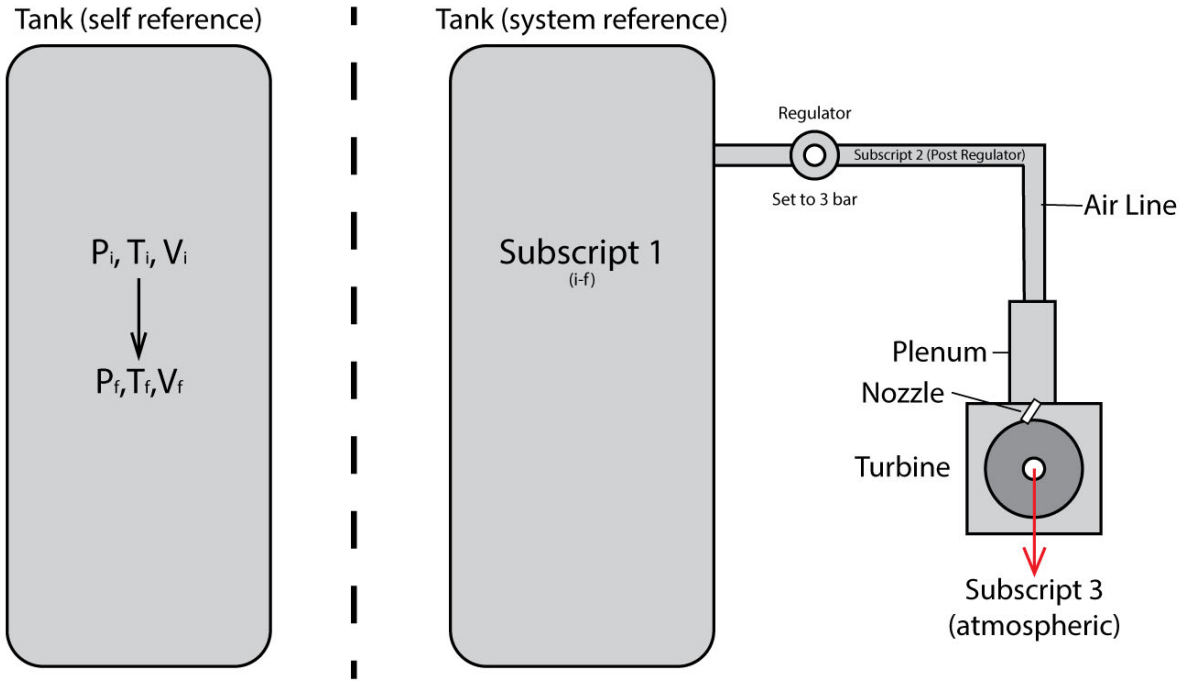

Figure 79 - Diagram to note the nomenclature of the sections of flow, for calculating the mass flow (left) and change

5.2.6. Assumptions

The conditions from start to end of the test (with respect to the frame of the tank) are;

$V_i = V_f = 60gal$	$P_i = 135psi$	$T_i = 30°C$	$P_f = 50psi$
$V_i = V_f = .227\ m^3$	$P_i = 930.8kPa$	$T_i = 303\ K$	$P_f = 344kPa$

Given that it is qualitatively known, from touching the tank during testing, it did not get cold to the touch. Therefore, it will be assumed that the temperature of the tank did not go below ambient $T_3 = 293\ K$.

From this, we are able to get an approximation of $\dot{m}$, which is then assumed to be constant across the test. It is known that as the turbine accelerates, a backpressure is formed, which would, in turn, affect this value. However, in absence of chronological data, we must assume an average.

By using REFPROP (Lemmon, et al., 2013), we are then able to calculate the properties of the air as it passes through the system. To do so, we must make one further assumption as to the temperature at the regulator (subscript 2). There was no temperature sensor here, either; however, by manually adjusting values for T_2, we can see that the salient properties of the air in the system are not dramatically affected by small changes in temperature. At best, there is a slight change at the third or fourth significant digit across the expected range. Based on the aforementioned qualitative measurements, we can assume that the temperature at this change did not decrease significantly, as it was likely that there was additional heat transfer in the area of the regulator, and certainly in the plenum chamber. Thereafter, we can use REFPROP (Lemmon, et al., 2013) to determine the system enthalpy and entropy, which then results in the calculation of efficiency based on the calculated power output.

Lastly, from above, the path from the regulator to the turbine is assumed to be isentropic, even though there would be losses due to the air line, fittings, plenum chamber, and nozzle.

5.2.7. Calculations of Properties

By using REFPROP (Lemmon, et al., 2013), and the values of P_i and T_i we can determine the initial density in the tank; $\rho_i = 10.73\ kg/m^3$. From that, the mass of the air in the tank is described in equation 30;

$$m_i = \rho_i * V_i \tag{30}$$

Which results in $m_i = 2.43\ kg$.

Next, we must calculate the final tank air mass. We know:

$V_f = V_i$	$P_f = 50psi$
$V_f = .227\ m^3$	$P_f = 344.7kPa$

If we assume $T_f = 293K$ and the value of P_f, REFPROP (Lemmon, et al., 2013) gives a density of $\rho_f = 4.1\ kg/m^3$, and $m_f = .93\ kg$. Given that the time of the 45/2 test was $\Delta t = 134s$, and if we assume a constant flow rate as assured by the regulator, equation 31 is derived;

$$\dot{m} = \left(m_i - m_f\right)/\Delta t \tag{31}$$

Which results in $\dot{m} = 0.0123\frac{kg}{s}$.

From this, we know that at the regulator that the mass flow will be constant, and;

$P_3 = 43.5psi$
$P_3 = 300kPa$

From this, REFPROP (Lemmon, et al., 2013) and the values of P_3 and T_3,then calculates;

$\rho'_3 = 3.6\frac{kg}{m^3}$ and $\dot{V}'_3 = 0.00314\ \frac{m^3}{s}$, $h'_3 = 292.8\ \frac{kJ}{kg}$ and $s'_3 = 6.53\ \frac{kJ}{kgK}$.

Finally, we know that the ambient pressure is;

$$P_4 = 14.6psi$$

$$P_4 = 100.7kPa$$

From this, REFPROP (Lemmon, et al., 2013) and the values of P_3 and s'_4, where $s'_4 = s_3$;

$\rho'_4 = 1.64 \frac{kg}{m^3}$ and $\dot{V}'_4 = 0.0068 \frac{m^3}{s}$, $h'_4 = 214.1 \frac{kJ}{kg}$.

Then, as described in section 2.13, efficiency is described as equation 32;

$$n_{exp} = \frac{P_{out}}{(h_1 - h_3')\dot{m}} \tag{32}$$

Where $P_{out=}\tau\omega$, and is calculated from the data, $h_1 = h_3\dot{m}$ and $h_3' = h'_4\dot{m}$. Therefore;

$$h_3\dot{m} - h'_4\dot{m} = .88\,{}^{kJ}/_{S}$$

This value is calculated for each run, and results in the curves represented in Figure 81 and Figure 80.

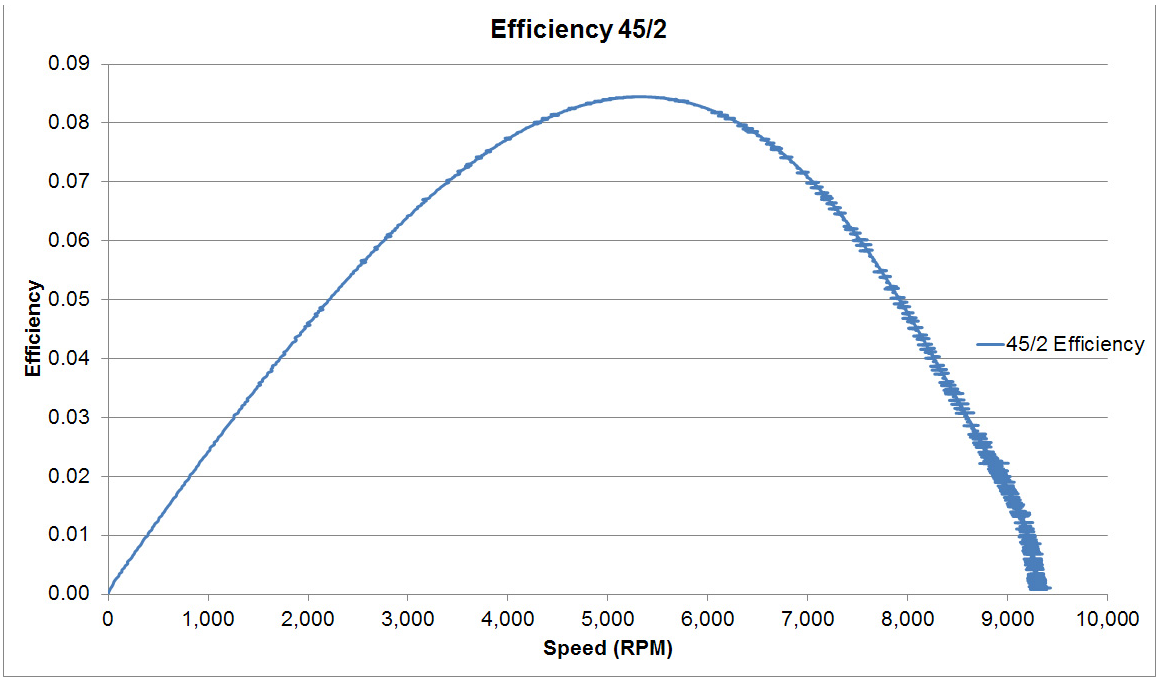

Figure 80 - Turbine efficiency for a nozzle at 45°

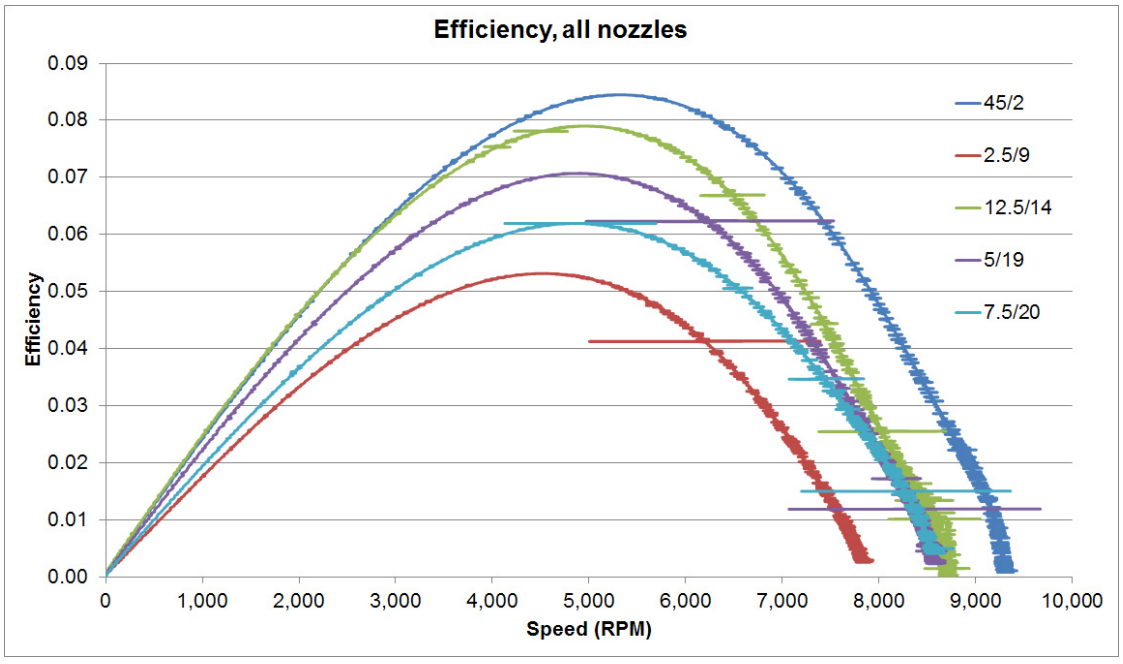

Figure 81- Turbine efficiency for all nozzles

5.2.8. Nozzle choking

From equation 21, we know

$$M_{at} = \frac{v_t}{349} = \frac{\dot{m}}{349\rho_t A_t}$$

Where $\rho_t = 1.63\ {}^{kg}/_{m^3}$, and $A_t = 1mm\ x\ 10.75mm = 1.075 \times 10^{-5}\ m^2$, and $\dot{m} =$ $0.0123\ kg/s$.

This provides the result that $M_{at} = 2.01$. Therfore, the flow should be choked. However, it is possible that the actual resultant shape of the nozzle, due to the curvatures, post processing, and other effects, resulted in a divergent nozzle. In this case, it would allow for a supersonic flow.

Figure 82 shows a macro image of the 12.5° nozzle aperture, which shows an overall curvature on the various surfaces, which result in an increase in the size of the exit aperture that would create a divergent profile. Consequently, this would create a convergent/divergent nozzle, and

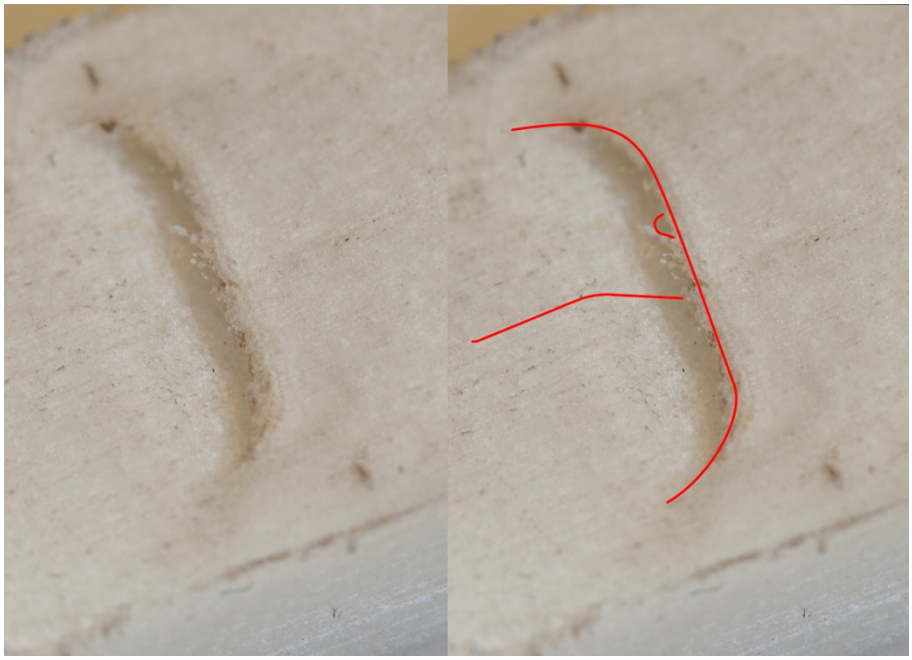

Figure 82- Nozzle apertures\ close up (12.5°)

allow for supersonic flow. The other nozzles show similar openings.

5.2.9. Comparison to Hoya & Guha

To begin the comparison, it should be noted that due to the restrictions imposed by the safety concerns caused by the construction, the author did not run the turbine beyond 11,000 RPM, which makes the comparison difficult, as the turbine's entire performance profile happens within the first 40% of that of Hoya & Guha (2009). That said, one can infer some information, as well as find discrepancies that would be worth testing.

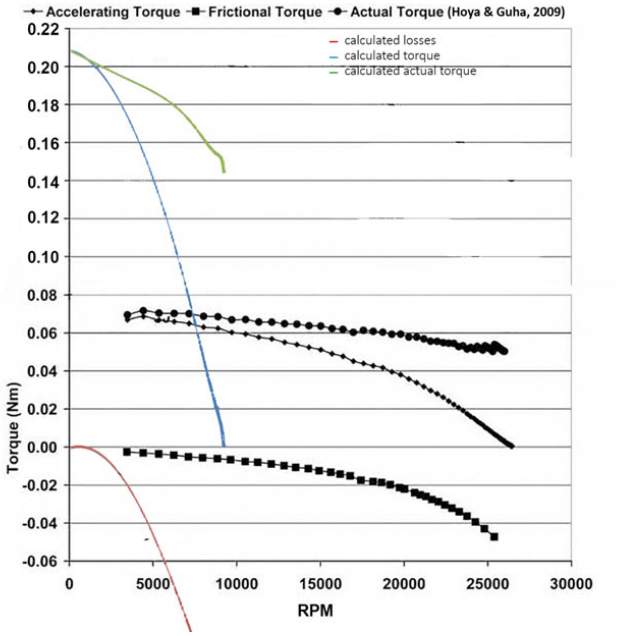

Figure 83- Comparison of the 45/2 and 45/6 data, calculated and measured respectively, to Hoya & Guha (2009)

While the measured data is off of the calculated acceleration with the data presented herein, it is interesting to note that it fits in relatively well with that of Hoya and Guha (2009), and their rig, as can be seen in Figure 82. Their data was run at 3.8 bar at the nozzle, and therefore would be expected to be higher overall that than present data, run at 3 bar from the tank. That said, the calculated values suggest the opposite. This could be due to many factors, including slight differences between the calculated value of I, differences in the nozzle, and due to the fact that the above values were in a system that did not include a plenum chamber, a later addition to their setup.

In the case of efficiency, the curves clearly do not match, but this is due in large part to the fact that the present turbine was run to steady state by 10,000 RPM. In addition, Hoya & Guha (2009)

calculated their efficiency based on the combined value of accelerating torque and frictional torque, shown in Figure 83, which is why the graph does not have the same shape. That said, Hoya & Guha clearly did not reach a steady state, as the steady state for a Tesla Turbine is $\tau = 0$, when the flow exiting the nozzle is $\approx$ the tangential speed of the discs. It is interesting to note the relatively higher efficiency at low RPM, which is no doubt a function of the aforementioned compressed power band. Since the present turbine took advantage of a plenum chamber, and had a different nozzle, this could play a part. Not having had measured values for mass flow and exit temperatures would certainly impact the curve as well, and therefore it would be recommended to acquire these values in future tests to ensure that the overall efficiency is accurate. An overall comparison to various turbines from the literature is presented in Figure 84.

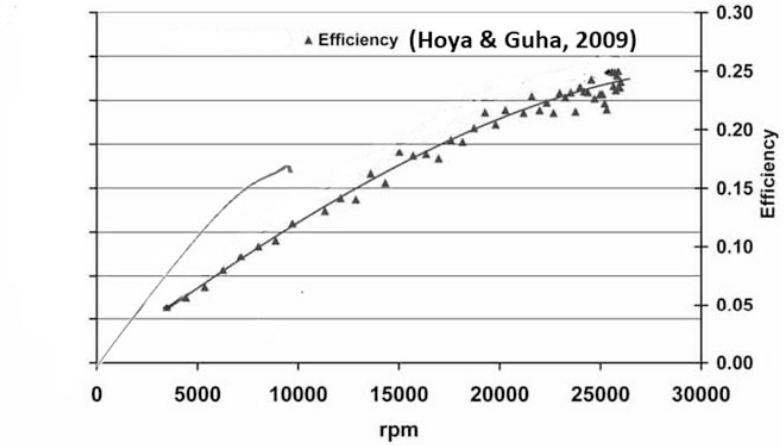

Figure 84 - Comparison of the efficiency of the 45° nozzle to Hoya & Guha's (2009) results, in a relative pressure operation

Author	r_o	r_i	central(c) shaft(s) exhaust	# Discs	Disc Spacing	Steam(s) Air(a) Water(w)	Operating Pressure	max speed	max torque	max power	max efficiency
	(mm)	(mm)			(mm)		(bar)	(rpm)	(Nm)	W	%
Armstrong (1952)	88.9	47.625	s	10	variable	s	8.1	6000	0.1	530	4.26
Beans (1961)	76.2	30.5	s	6	12.7-.67	a	2.75	17000	0.9	5600	24
Rice (1963)	88.9	33.5	c	9	1.6	a	9.6	11800	n/a	1800	23.2
Leaman (1950)	63	10	c	4	3.2	a	5.8	9000	0.1	87	8.24
Lemma (2008)	25	5.95	s	6(?)	n/a	a	0.514	96000	0.04	220	20
Tesla (1913)	228.5	n/a	s	25	n/a	s	8.6	9000	n/a	150k	n/a
Emran (2011)	18.8	17	s	4	n/a	a	5.9	50000	0.345	n/a	n/a
Peshlakai (2012)	75	34.5	s	12	1.3	a	6.14	n/a	n/a	12	31
Bloudicek (2007)	100	17	c	13	n/a	a	20.5	n/a	0.7	58.3	20.45
Romanin (2012)	36.5	18	s	10	1.2	a	5.4	24170	n/a	n/a	16.3
Romanin (2012)	5	1	c	4	0.5	w	n/a	n/a	n/a	35	13.7
Hoya & Guha (2009)	46	12.5	c	8	0.2	a	3.6	25000	0.7	140	26
This Thesis	46	12.7	c	8	0.2	a	3	9100	0.21	74	8.5

Figure 85 - Comparison of features of the turbine built in this thesis, versus a sampling from the literature

5.3. Recommendations for a Future Design of a Test Rig

After having gone through the design, assembly, disassembly and measurement, it became apparent that there are lessons to be learned. The following are recommendations to that effect:

- Easier disassembly
- As few bolts/screws as possible for components that need to be removed regularly
- Spring clamps or knobs preferred
- Easier alignment
- Components should all have some sort of key or alignment post to ensure quick and easy alignment
- Includes sensors, at least the rotational sensor into the base
- Easy sensor adjustment and sealing

- Proper base; ability to quickly install and place turbine, and other components (torque sensor), so that the parts are securely fastened and vibrations can be dampened
- Torque measurement system must be developed further, and be more sensitive. Ideally, the torque sensor should not be moved to be engaged, and should be fine-tuned via a rheostat or computer control. This would suggest the use of an electromagnet
- Full sensor suite – flow meter; static/dynamic pressure and pressure in plenum, anemometer and temperature at exhaust, pressure at four locations inside housing, RPM, torque, vibration.
- Complete modularity
- Ability to mount a transparent panel/disc to see flow
- Ability to mount variable pitch nozzle with consistent flow conditions
- Ability to quickly and easily change nozzle type (i.e. straight thru, different profiles including expansion nozzles
- Ability to easily add additional nozzles around circumference
- Ability to change expansion chamber out to be able to create a full admission turbine
- Ability to make a version that is identical to Tesla's patent to provide relative benchmarks
- Ability to change the depth of the chamber so that one can have a single disc up to some number, while being able to have the chamber/nozzle configuration be ideal for that configuration
- Bearing mounts should allow for easy change of bearings, and/or lubrication for uncaged bearings; additional labyrinth seals on shaft so sealed bearings are not required

- Bearing structure should be independently adjustable from the overall system so that minor adjustments can be easily made without having to make new parts.
- Bearing seats should be compression fit, not press fit
- Bearings should be completely isolated from the turbine chamber, from a pressure and temperature perspective
- The use of magnetic bearings would be an improvement
- All wiring should be incorporated into wiring harnesses, for easy installation and removal
- Seals should be more consistent (grooved), as well as proper seals for pressure sensors
- Nozzles should be adjustable to cause choked or full passthru flows
- Ability to change/adjust nozzles without dismantling system.
- Inlet airflow should be 3/8", or ½", to limit line losses from compressor
- Regulator should be at the plenum
- Reaction torque sensor should be included in the base mount

6. Conclusions

In the current setup, it is clear that the 45° nozzle performs better than all other nozzles. However, this is not expected, as the 2.5° nozzle should eventually overtake it. Therefore, there is another mechanism at work, likely issues caused by divergence and/or flow separation due to the shape of the nozzle and the gap into which the fluid is injected. Consequently, more work needs to be done to determine if this is the case. Implementing additional disc sets in the current model, without any modification, would undoubtedly serve to clarify this point.

That said the process was extremely informative, even with the challenges presented along the way. In spite of the fact that the machine suffered vibration issues, it was still capable of reliably running over 10,000 RPM, with an extremely repeatable acceleration curve across all tests, at only 3 bar, and an efficiency of 8.5%. With proper machining of the discs, with some additional effort at balancing, the machine will undoubtedly be able to perform very well at higher pressures.

Furthermore, while crude, the torque sensor performed better than expected. Clearly, with a more careful assembly and choice of materials (and associated budget), a very sensitive torque sensor could be fashioned to accommodate the relatively low torques seen in the system at these low pressures.

With some changes and additional instrumentation, the author believes that the turbine as designed could serve as a test bed for future work.

Works Cited

Allen, J. (1990). *A Model for Fluid Flow Between Parallel, Co-Rotating Annular Disks.* Masters Thesis, University of Dayton, Mechanical Engineering, Dayton, OH. Retrieved 2015

AMS. (2013). AS5132, 360 Step (8.5 bit) Programmable High Speed Magnetic Rotary Encoder.

Armstrong, J. H. (1952). *An Investigation of the Performance of Modified Tesla Turbine.* Georgia Institute of Technology, Mechanical Engineering. Atlanta, GA: Georgia Institute of Technology.

Beans, E. (1966). Investigation into the Performance Characteristics of a Friction Turbine. *Journal of Spacecraft, 3*(1), 131-134.

Beans, E. W. (1961). *Performance cs of a Friction Disc Trubine.* Pennsylvania State University, Mechanical Engieering. College, PA: Pennsylvania State University.

Bergen, E. (2009, 10 29). *Patent No. WO2010.* USA.

Bloudicek, P., & Palousek, D. (2007). Design of a Tesla Turbine. *Konference diplomovych praci 2007.* Brno: KDP 2007.

Bohl, G. (2012). *Patent No. WO2012/003508A2.* US.

Burton, W. E. (1955, September). Cardboard Blower Works. *PopularScience, 167, 3*, 230-232.

Cairns, W. (2003). *The Tesla Disc Turbine.* Somerset, UK: Camden Minature Steam Services.

Cengel, Y., & Cimbala, J. (2010). *Fluid Mechanics, Fundamentals And Applications* (2nd ed.). New York, NY, USA: McGraw-Hill.

Conrad, W., & Conrad, H. (2001). *Patent No. 6174127B1.* USA.

Crawford, M., & Rice, W. (1974, July). Calculated Design Dta for the Multiple-Disk Pump Using Incomressible Fluid. *Journal of Engineering for Power, Transactions of the ASME*, 276-282.

Du, Y. (2010, 12 17). Numerical Simulation of Mechanical and Thermal Fluid Structur Interaction in Labyrinth Seals. Darmstadt, Germany: Technishchen Universitat Darmstadt.

Eastop, T., & McConkey, A. (2009). *Applied Thermodynamics for Engineering Technologists, 5th Ed.* Delhi, India: Pearson Education, Ltd.

Emran, T. (2011). *Tesla Turbine Torque Modeling For Construction of a Dynamometer and Turbine.* University of North Texas.

Foulton, G., & Taylor, D. (1974). *Patent No. 3978657.* USA.

Fuller, H. (2010). *Patent No. 7695242.* USA.

Guha, A., & Sengupta, S. (2013). The fluid dynamics of the rotating flow in a Tesla disc turbine. *European Journal of Mechanics B/Fluids, 37*, 112-123.

Guha, A., & Smiley, B. (2009, September 4). Experiment and analysis for an improved Design of the inlet and nozzle in Tesla disc turbines. *Journal of Power and Energy, 223*, 261-277.

Honeywell. (2010, July). ASDX SEries Silicon Pressure Sensors. Golden Valley, MN.

Hoya, G., & Guha, A. (2009, December 18). The design of a test rig and study of the performance and efficiency of a Tesla disc turbine. *Journal of Power and Energy, 224*, 451-465.

Ladino, A. (2004). *Numerical Simulation of the Flow Field in a Friction-Type Turbine (Tesla Turbine).* Vienna University of Technology, Engineering. Vienna: Technische Universitat Wien.

Lapart, P., & Jedrzejewsky, L. (2011). Investigation of Aerodynamics of Tesla Bladeless Microturbines. *Journal of Theoretical and Applied Mechanics, 49*(2), 477-499.

Leaman, A. B. (1950). *The Design, Construction and Investigation of a Tesla Turbine.* University of Maryland. Maryland: University of Maryland.

Lemma, e. a. (2008). Characterisation of a small viscous flow turbine. *Experimental Thermal and Fluid Science, 33*, 96-105.

Lemmon, E. W., Huber, M. L., & McLinden, M. O. (2013). NIST Standard Reference Database: Refrence Fluid Thermodynamic and Transport Properties-REFPROP, Version 9.1. Gaithersburg, MA, USA: National Institute of Standards and Technology, Standard Reference Data Program.

Lieber, L. (2003). Fluid Dynamics of Turbomachinery. In J. E. Logan, & R. Roy (Eds.), *Handbook of Turbomachinery, Second Ed.* (pp. 43-94). New York, NY, USA: Marcel Dekker, Inc.

McCloskey, T. (2003). Steam Turbines. In J. E. Logan, & R. Roy (Eds.), *Handbook of Turbomachinery, Second Ed.* (pp. 427-564). New York, NY, USA: Marcel Dekker, Inc.

Mrfixitrick. (2007, Oct 14). *Running the Tesla CD Turbine Prototype With Saw Attachment.* Retrieved Oct 14, 2012, from YouTube: https://www.youtube.com/watch?v=Dn6MR0Wslf8

North, R. (1969). *An Investigation of the Tesla Turbine.* University of Maryland, Mechanical Engineering. Ann Arbor, Michigan: University Microfilms, Inc.

O'Neill, J. J. (1944). *Prodigal Genius: The Life of Nikola Tesla.* Ives Washburn.

Parodi, R. (1981, January-February). The Shear Torque Turbine. *Turbomachinery International*, 30-32.

Peshlakai, A. (2012). *Challenging the Versatility of the Tesla Turbine: Working Fluid Variations and Turbine Performance.* Arizona State University.

Posell, C. (1977). *Patent No. 4186554.* USA.

Possell, C. (1978). *Patent No. 4232992.* USA.

Rice, W. (1965, January). An Analytical and Experimental Investigation of Multiple Disk Turbines. *Journal of Engineering for Power*, 29-36.

Rice, W. (1991, September 23-25). Tesla Turbomachinery. *Proc. IV International Nickola Tesla Symposium*.

Ritzi, E. (1981). *Patent No. 4441322.* USA.

Romanin, V. (2012). *Theory and Peformance of Tesla Turbines.* PhD Thesis, UC Berkeley, Mechanical Engineering, Berkeley, CA.

Sengupta, & Guha. (2013). Analytical and computational solutions for three-dimentional flow field and relative pathlines for the rotating flow in a Tesla disc turbine. *Computers & Fluids*, 344-353.

Sengupta, S., & Guha, A. (2012). A theory of Tesla disc Turbines. *Journal of Power and Energy, 226*(5), 650-663.

Sherrer, G. D. (2008, 05 5). *Patent No. WO2008/134868A1.* WIPO.

SKF. (2015, 08 31). *SKF Bearing Calculator*. Retrieved 08 31, 2015, from http://www.skf.com/ca/en/knowledge-centre/engineering-tools/skfbearingcalculator.html

Stearns, E. (1911, December). The Tesla Turbine. *Popular Mechanics*.

Stocklinger, R. (2012). *Patent No. WO2012/004127A1.* Germany.

Tesla Engine Builders Association. (2015). Retrieved 01 10, 2015, from http://www.teslaengine.org/

Tesla Universe. (2015). Retrieved 01 11, 2015, from http://www.teslauniverse.com/

Tesla, N. (1911, September 18). Dr. Tesla Talks of Gas Turbines. *Motor World*.

Tesla, N. (1913, May 6). *Patent No. 1061206.* USA.

Appendix A Design Drawings

The following pages are the drawings used for the construction of the turbine.

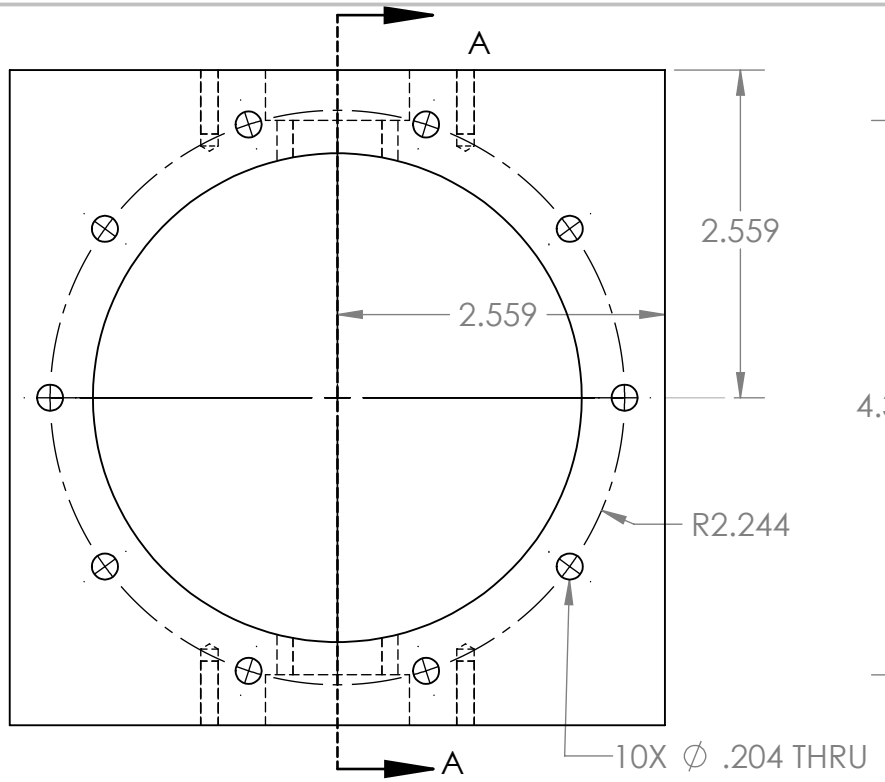

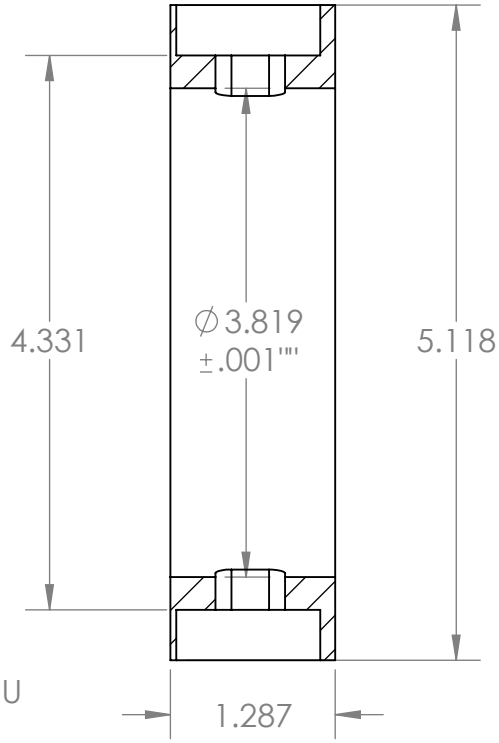

SECTION A-A

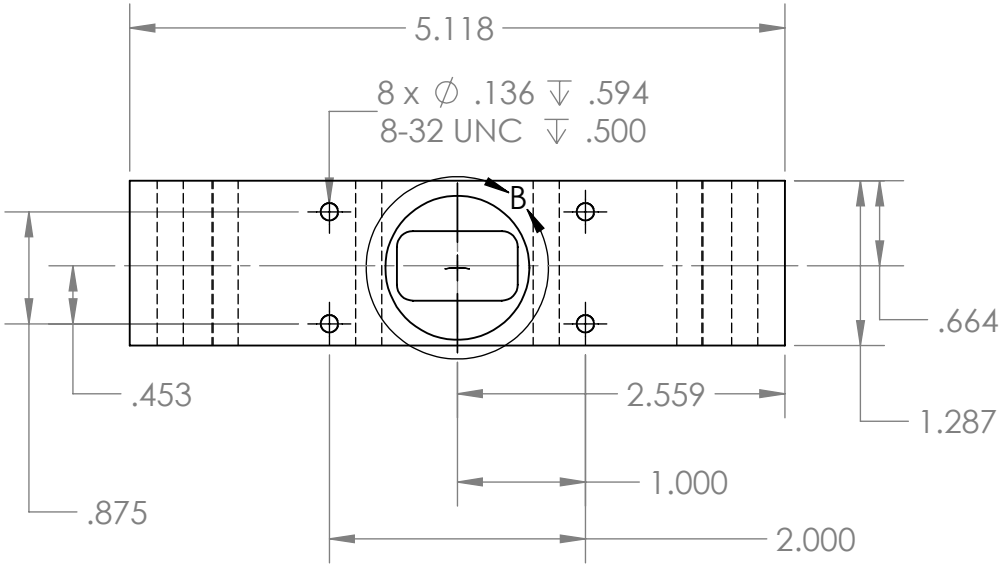

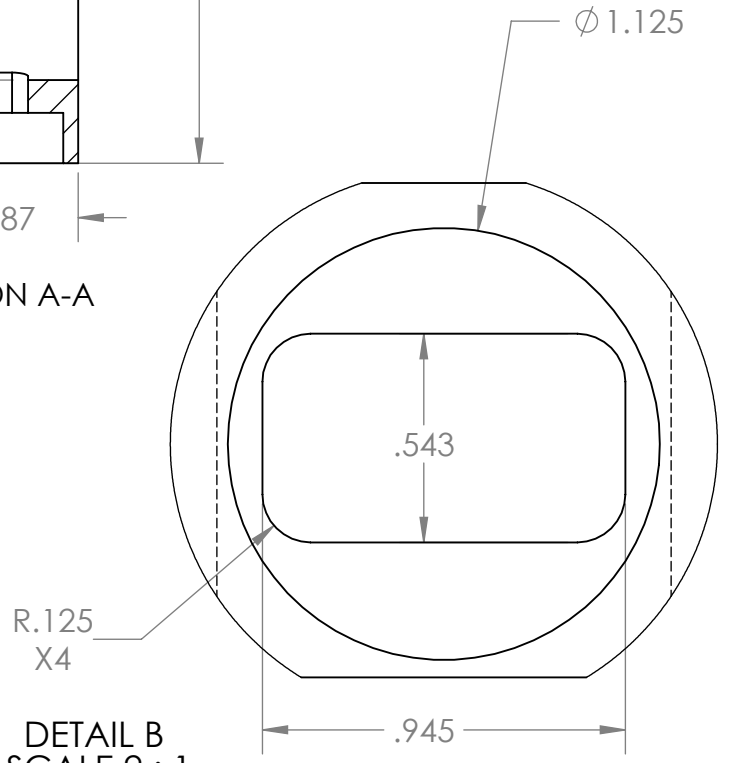

DETAIL B
SCALE 2 : 1

DIMENSIONS ARE IN [MILLIMETERS] and INCHES. TOLERANCES: +/-.003 UNLESS OTHERWISE NOTED	MATERIAL: Aluminum	DEBUR AND BREAK SHARP EDGES	TITLE: Expansion Chamber	Rev 3	A4
					SCALE:2:3
DATE September 18th, 2012			DO NOT SCALE DRAWING		SHEET 1 OF 15

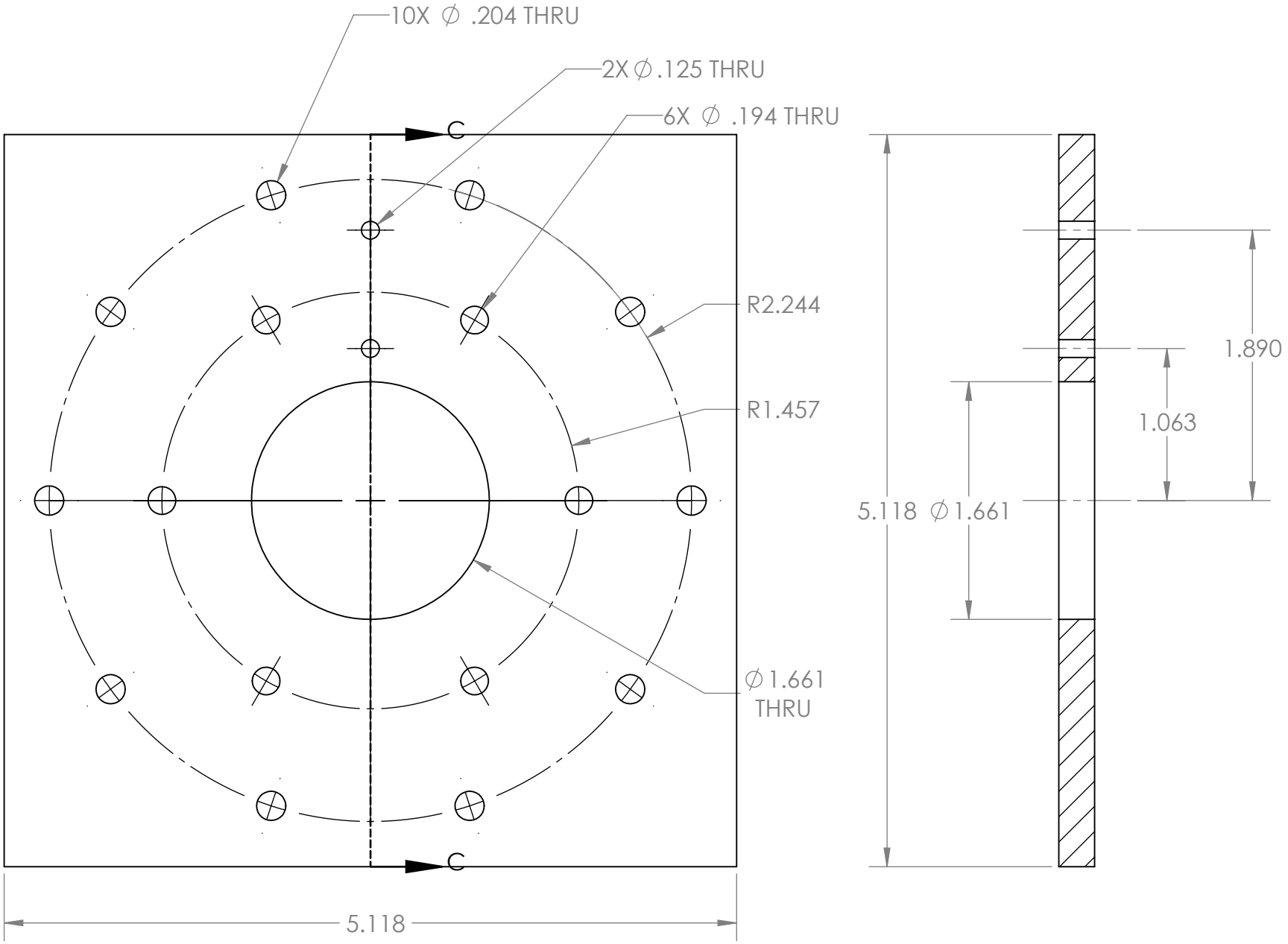

SECTION C-C

DIMENSIONS ARE IN [MILLIMETERS] and INCHES. TOLERANCES: +/-.003 UNLESS OTHERWISE NOTED	MATERIAL: Aluminum	DEBUR AND BREAK SHARP EDGES	TITLE: Exhaust Plate	Rev 3	A4
					SCALE:1:1
DATE September 18th, 2012			DO NOT SCALE DRAWING		SHEET 2 OF 15

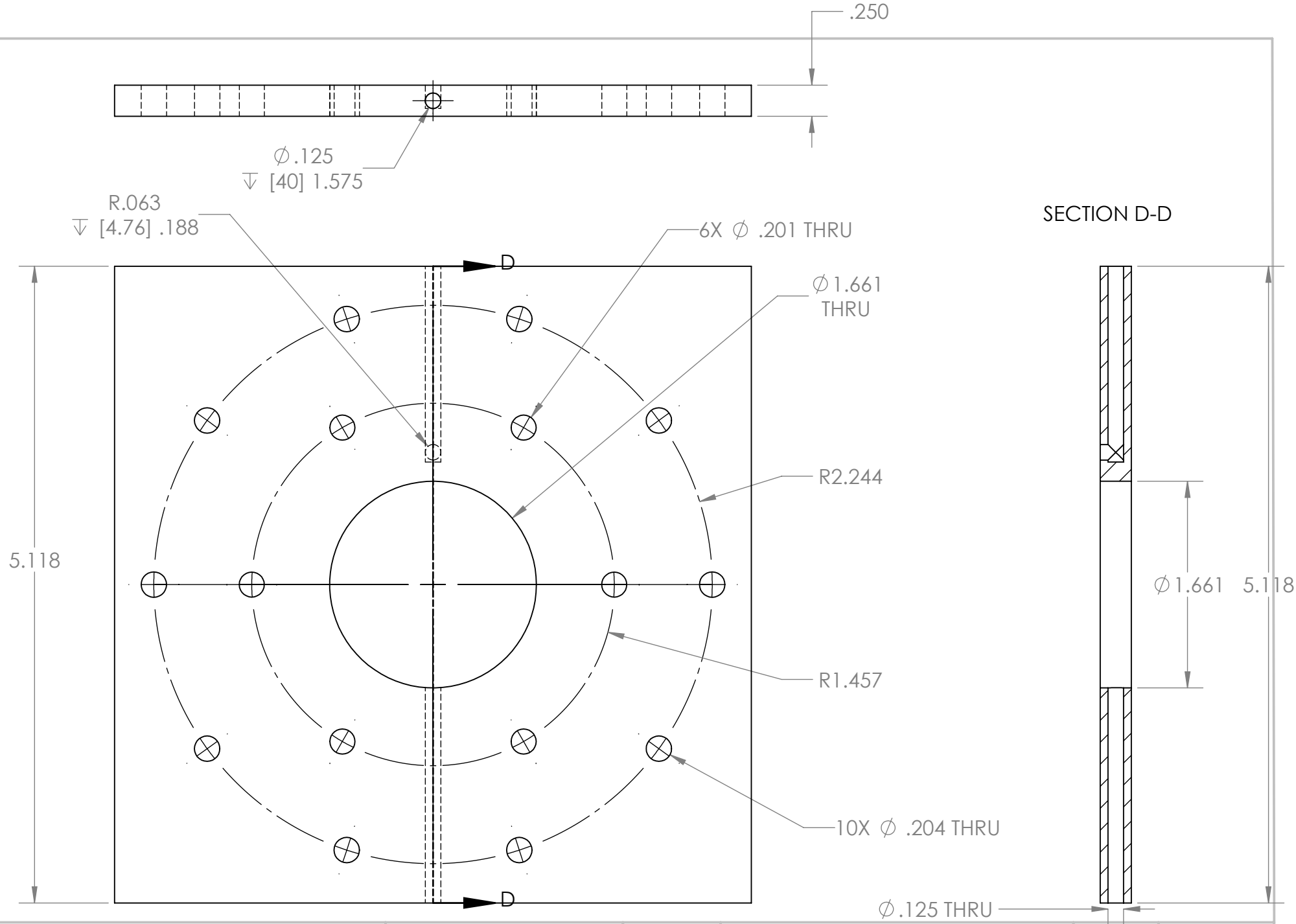

DIMENSIONS ARE IN [MILLIMETERS] and INCHES. TOLERANCES: +/-.003 UNLESS OTHERWISE NOTED	MATERIAL: Aluminum	DEBUR AND BREAK SHARP EDGES	TITLE: Drive Plate	Rev 3	A4
DATE September 18th, 2012			DO NOT SCALE DRAWING		SCALE:1:1
					SHEET 3 OF 15

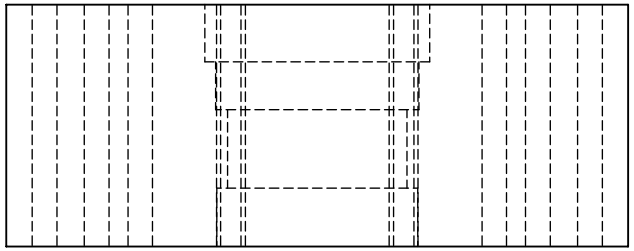

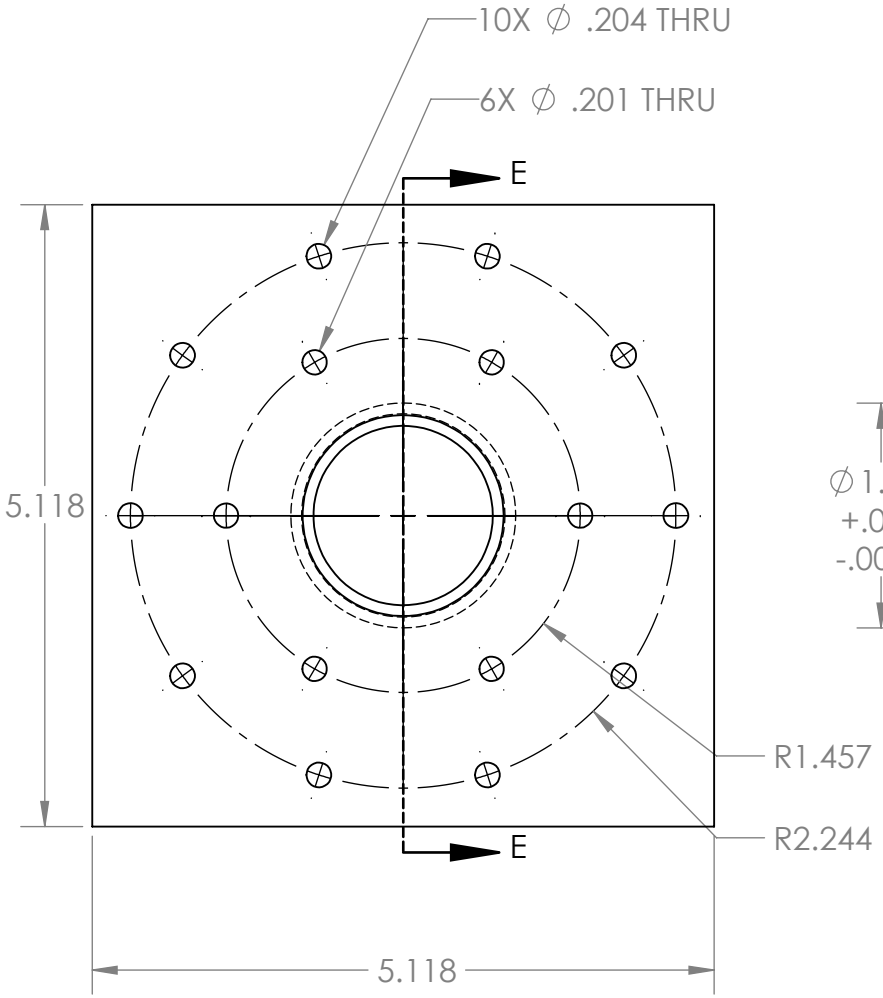

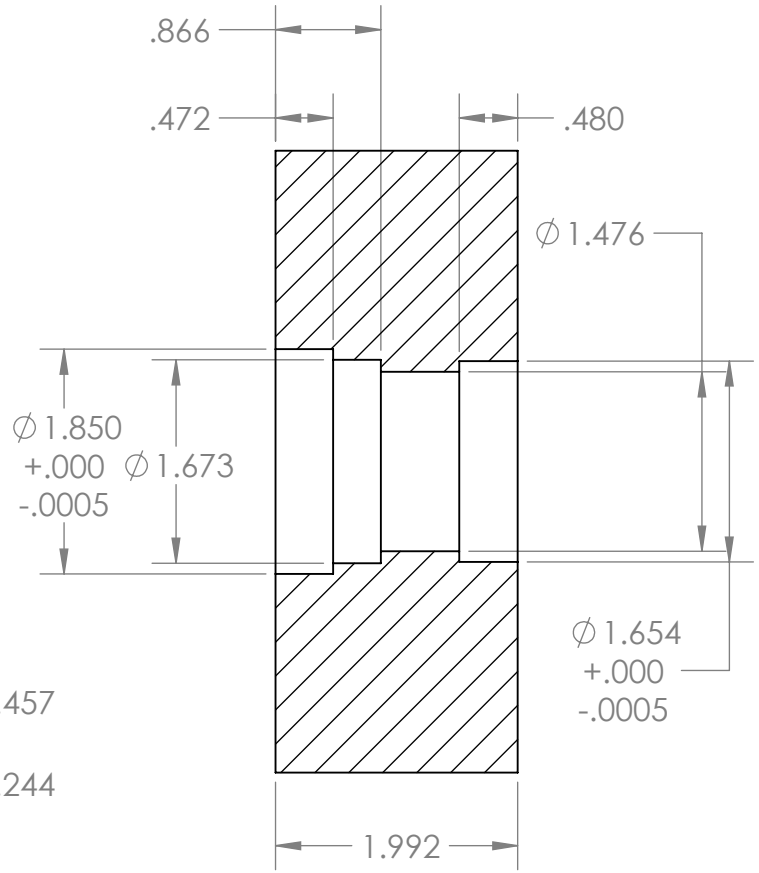

SECTION E-E
SCALE 1 : 1.58

DIMENSIONS ARE IN [MILLIMETERS] and INCHES. TOLERANCES: +/-.003 UNLESS OTHERWISE NOTED	MATERIAL: Aluminum	DEBUR AND BREAK SHARP EDGES	TITLE: Bearing Block	Rev 3	A4
DATE September 18th, 2012			DO NOT SCALE DRAWING		SCALE:1:1
					SHEET 4 OF 15

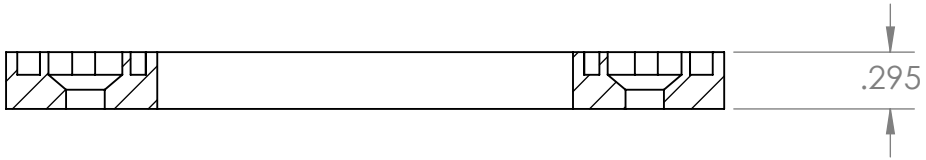

SECTION G-G

QUANTITY 2

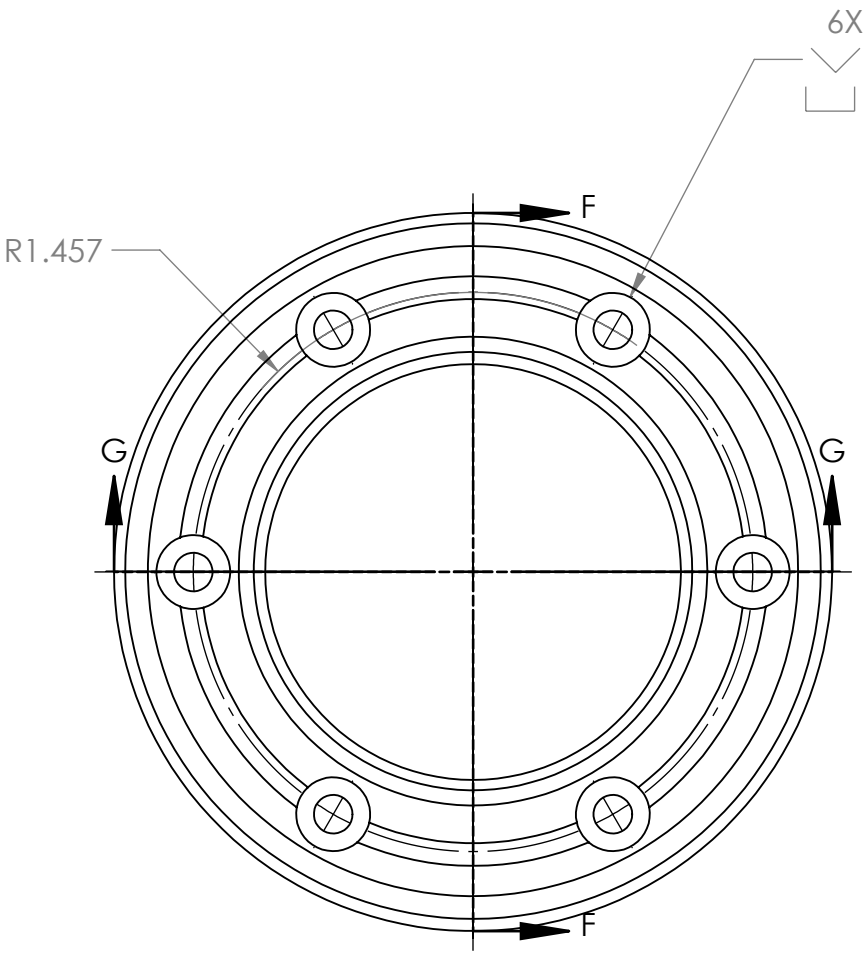

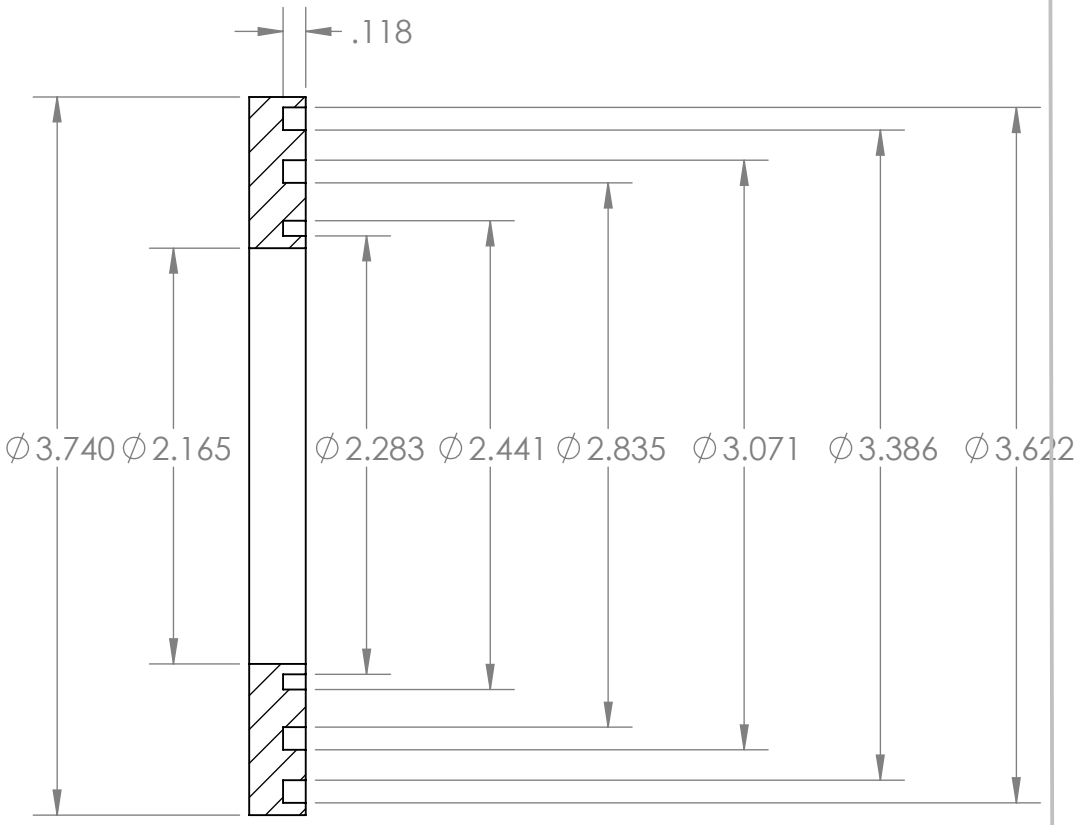

SECTION F-F

DIMENSIONS ARE IN [MILLIMETERS] and INCHES. TOLERANCES: +/-.003 UNLESS OTHERWISE NOTED	MATERIAL: Aluminum or Brass	DEBUR AND BREAK SHARP EDGES	TITLE: Large Labyrinth	Rev 3	A4
DATE September 18th, 2012			DO NOT SCALE DRAWING		SCALE:1:1
					SHEET 5 OF 15

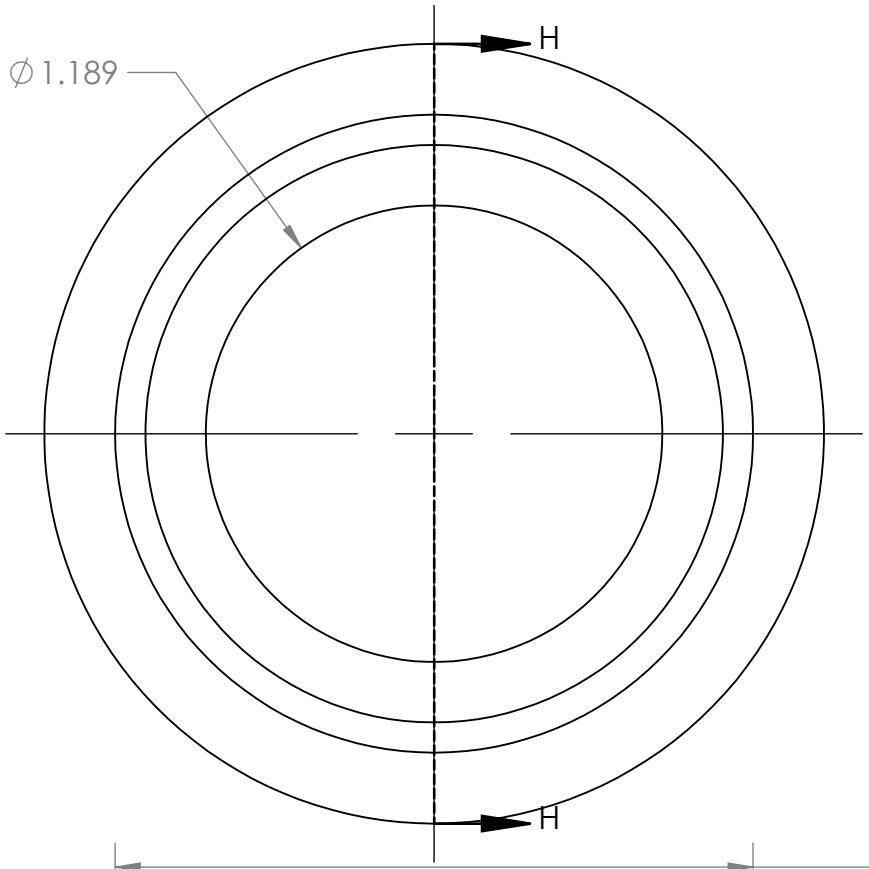

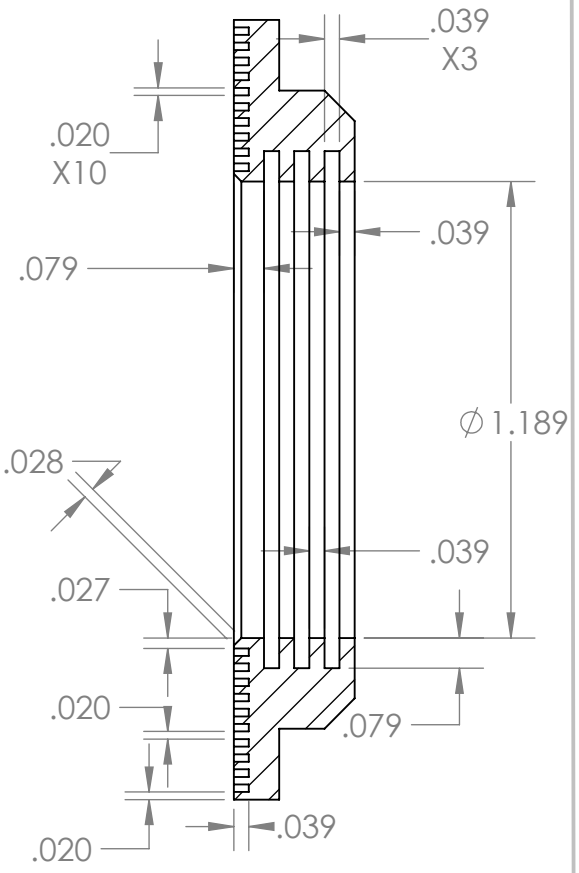

SECTION H-H

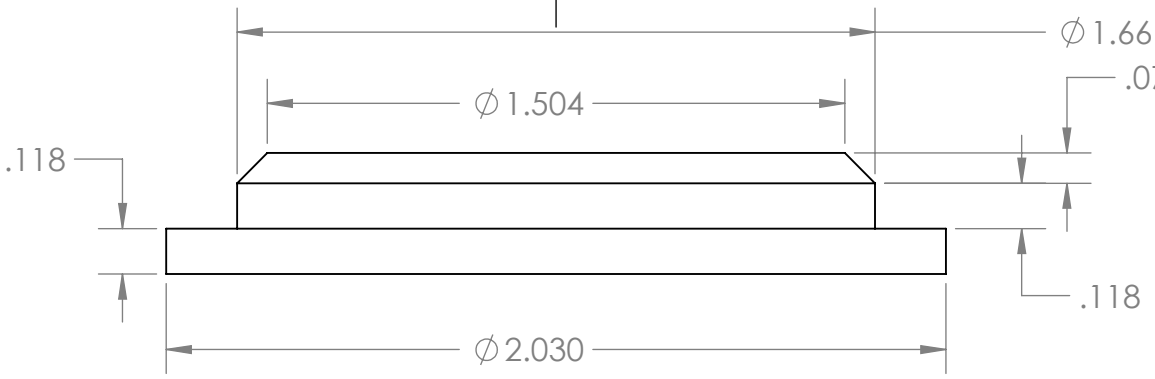

QUANTITY
2

DIMENSIONS ARE IN [MILLIMETERS] and INCHES. TOLERANCES: +/-.003 UNLESS OTHERWISE NOTED	MATERIAL: PTFE or Delerin	DEBUR AND BREAK SHARP EDGES	TITLE: Small Labyrinth	Rev 3	A4
DATE September 18th, 2012			DO NOT SCALE DRAWING		SCALE:2:1

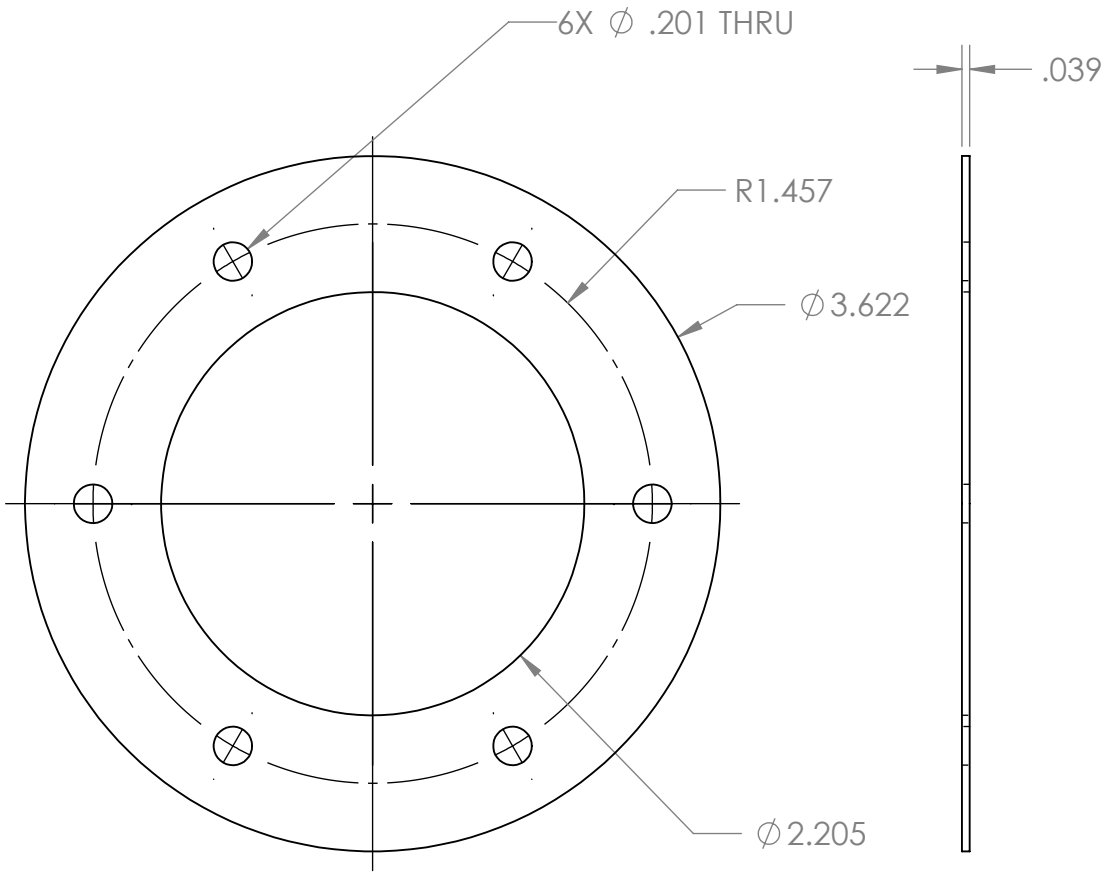

QUANTITY 12

DIMENSIONS ARE IN [MILLIMETERS] and INCHES. TOLERANCES: +/-.1 UNLESS OTHERWISE NOTED	MATERIAL: Silicone Rubber	DEBUR AND BREAK SHARP EDGES	TITLE: Labyrinth Spacer	Rev 3	A4
					SCALE:1:1
DATE September 18th, 2012			DO NOT SCALE DRAWING		SHEET 7 OF 15

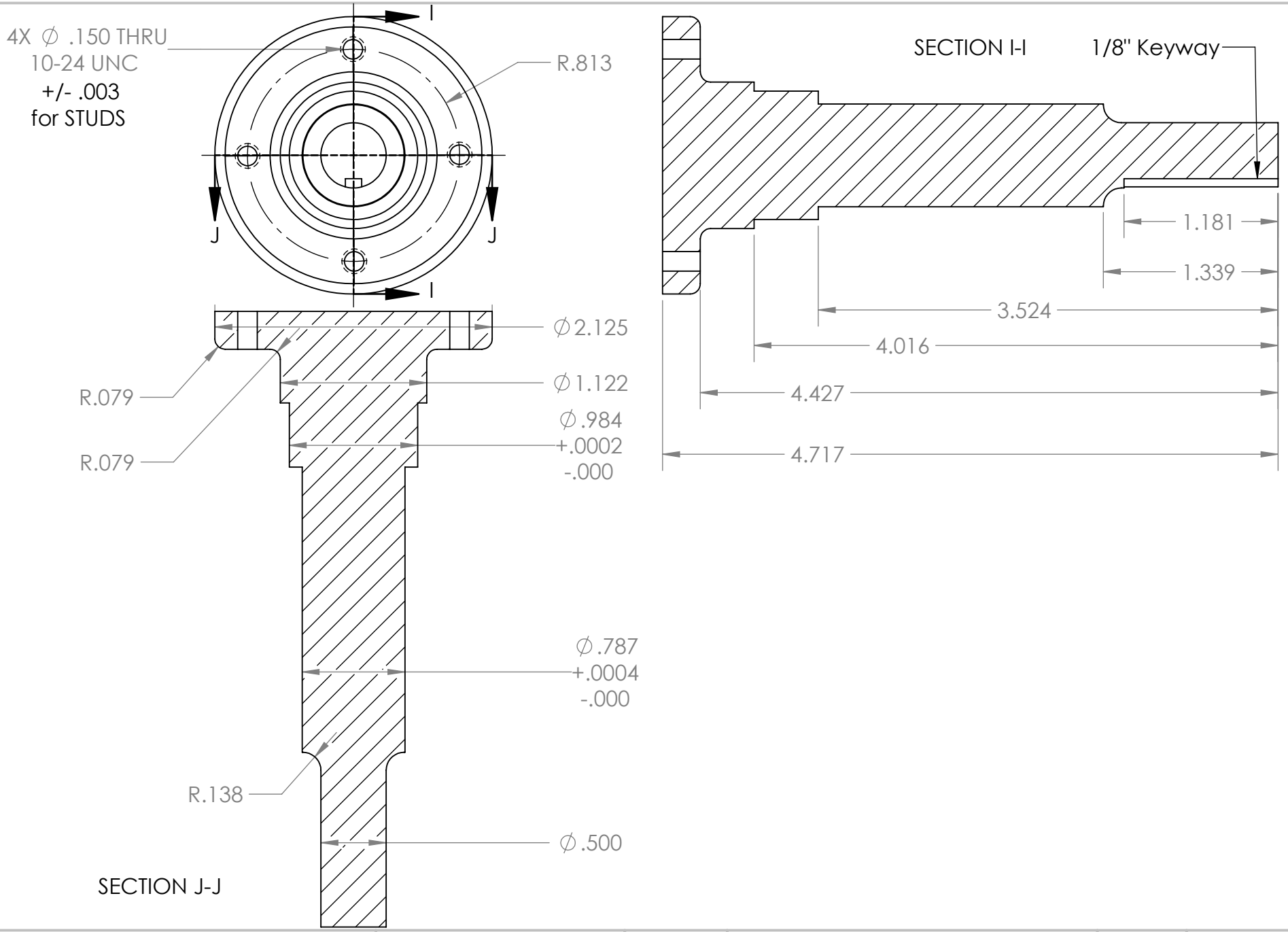

DIMENSIONS ARE IN [MILLIMETERS] and INCHES. TOLERANCES: -.000" +.001" UNLESS OTHERWISE NOTED	MATERIAL: Stainless Steel	DEBUR AND BREAK SHARP EDGES	TITLE: Shaft	Rev 3	A4
DATE September 18th, 2012			DO NOT SCALE DRAWING		SCALE:1:1
					SHEET 8 OF 15

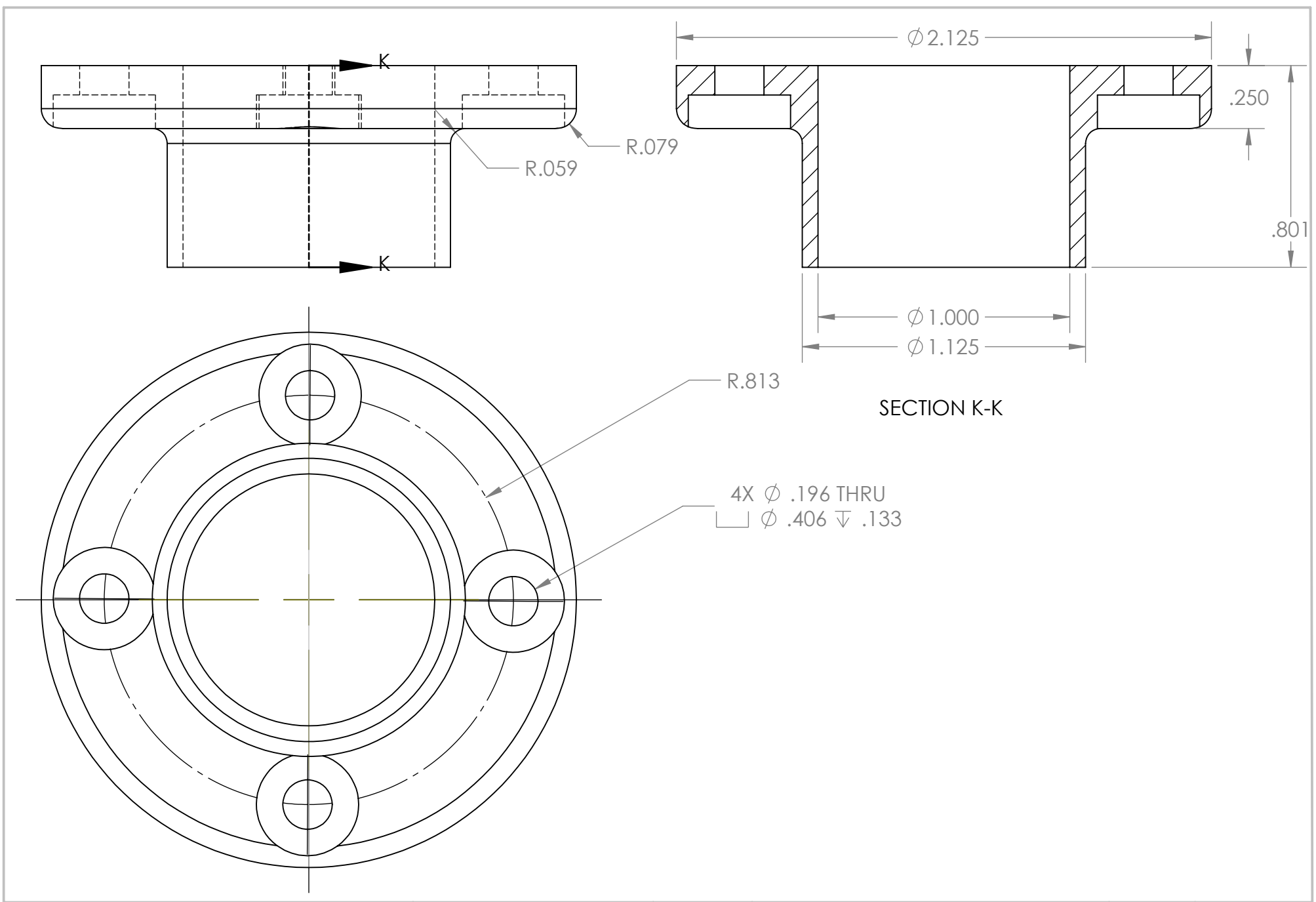

SECTION K-K

DIMENSIONS ARE IN [MILLIMETERS] and INCHES. TOLERANCES: +/-.003 UNLESS OTHERWISE NOTED	MATERIAL: Stainless Steel	DEBUR AND BREAK SHARP EDGES	TITLE: Exhaust Hub	Rev 3	A4
					SCALE:2:1
DATE September 18th, 2012			DO NOT SCALE DRAWING		SHEET 9 OF 15

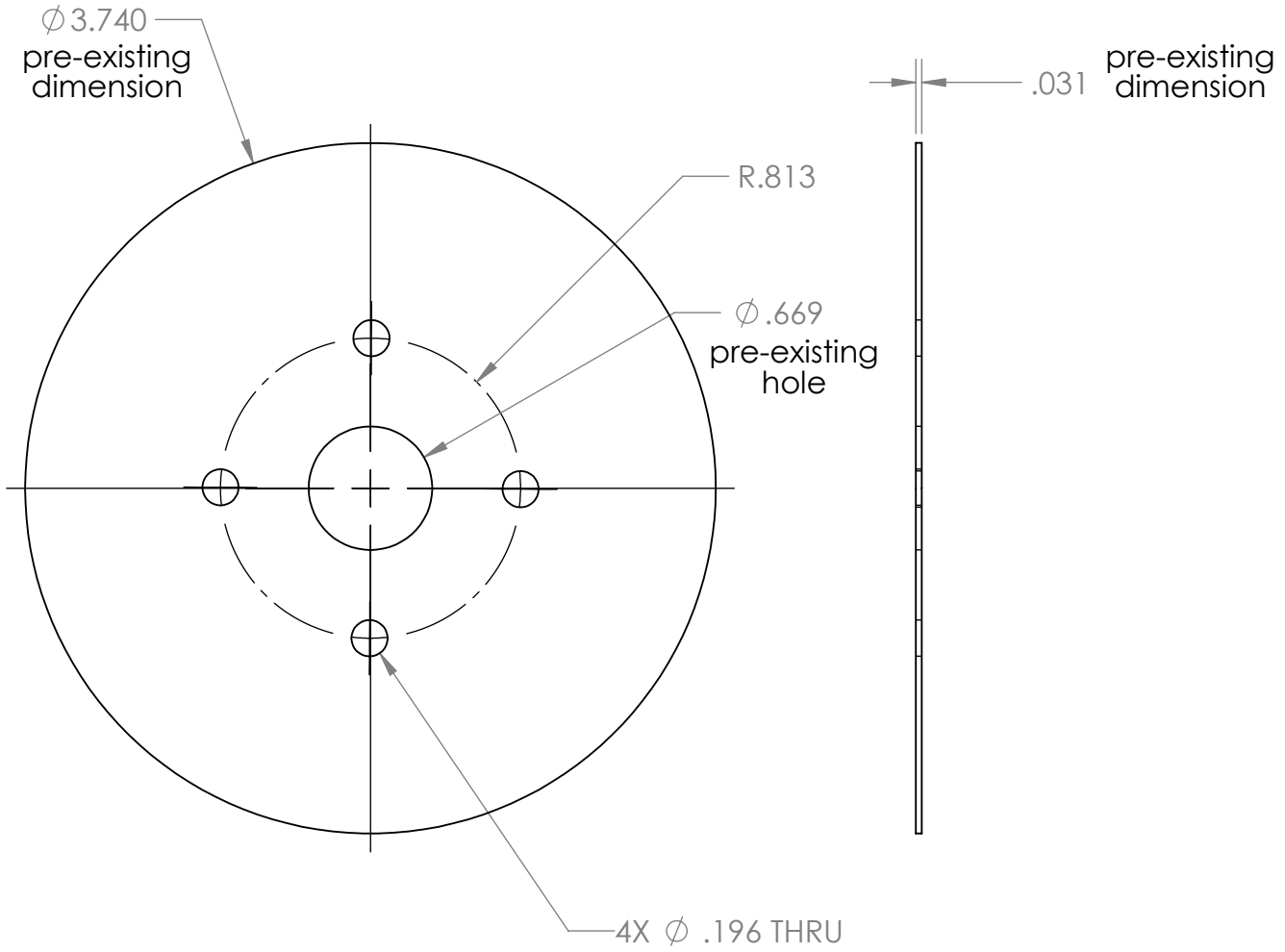

QUANTITY
6

Will provide HD platters

DIMENSIONS ARE IN [MILLIMETERS] and INCHES. TOLERANCES:+/-.003 UNLESS OTHERWISE NOTED	MATERIAL: Aluminum - HD Platter	DEBUR AND BREAK SHARP EDGES	TITLE: Large Disc	Rev 3	A4
DATE September 18th, 2012			DO NOT SCALE DRAWING		SCALE:1:1
					SHEET 10 OF 15

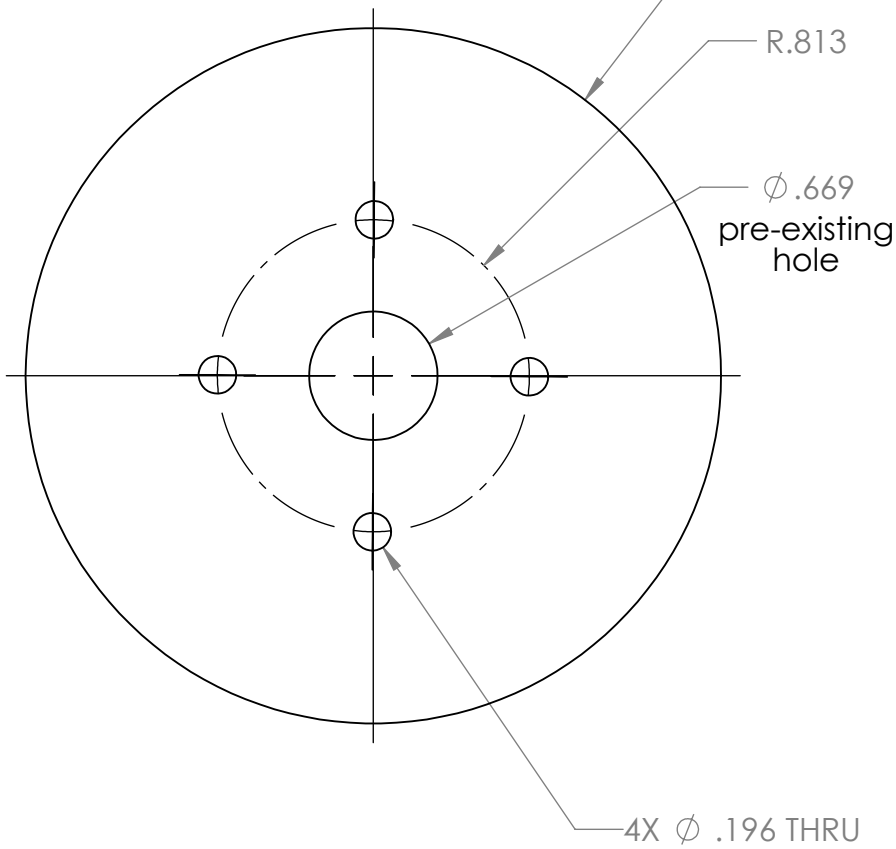

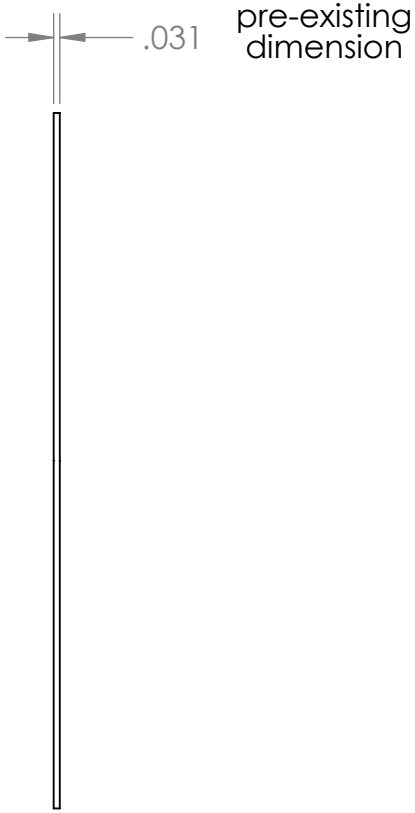

QUANTITY
24

Will provide HD platters

DIMENSIONS ARE IN [MILLIMETERS] and INCHES. TOLERANCES:+/-.003 UNLESS OTHERWISE NOTED	MATERIAL: Aluminum - HD Platter	DEBUR AND BREAK SHARP EDGES	TITLE: Small Disc	Rev 3	A4
DATE September 18th, 2012			DO NOT SCALE DRAWING		SCALE:1:1
					SHEET 11 OF 15

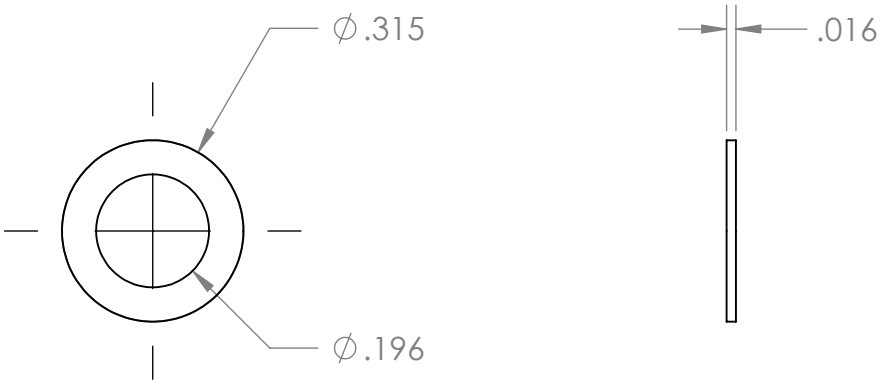

QUANTITY
36

DIMENSIONS ARE IN [MILLIMETERS] and INCHES. TOLERANCES: +/-.003 UNLESS OTHERWISE NOTED	MATERIAL: Any material	DEBUR AND BREAK SHARP EDGES	TITLE: Spacer	Rev 3	A4
					SCALE:3:1
DATE September 18th, 2012			DO NOT SCALE DRAWING		SHEET 12 OF 15

QUANTITY
2

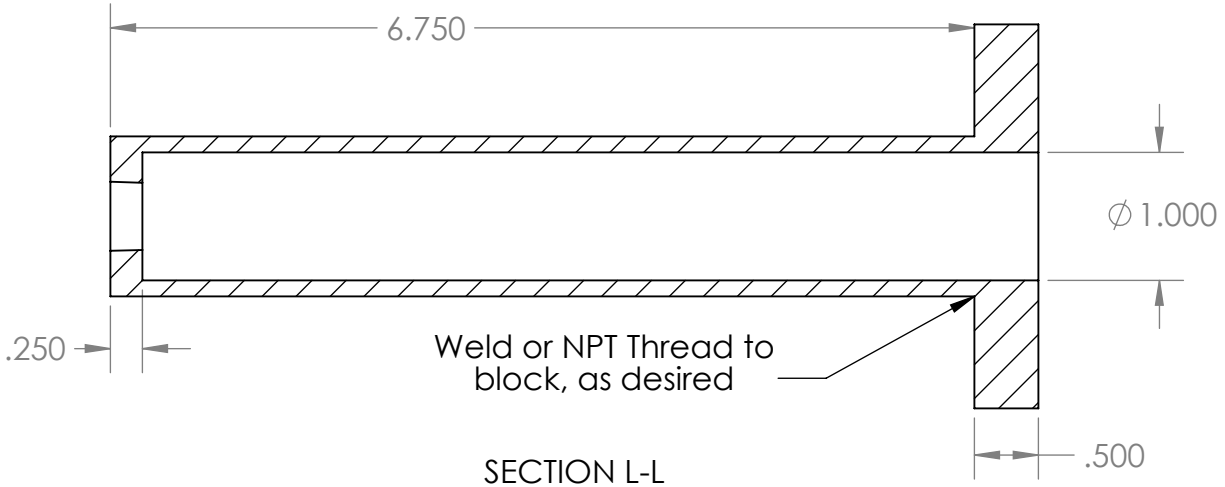

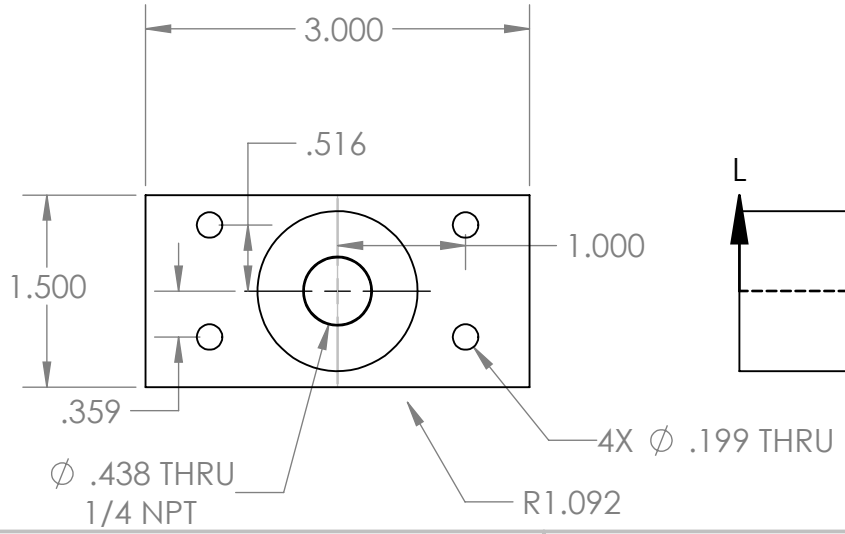

DIMENSIONS ARE IN [MILLIMETERS] and INCHES. TOLERANCES:+/-.003 UNLESS OTHERWISE NOTED	MATERIAL: Steel	DEBUR AND BREAK SHARP EDGES	TITLE: Plenum Chamber	Rev 3	A4
DATE September 18th, 2012			DO NOT SCALE DRAWING		SCALE:2:3
					SHEET 13 OF 15

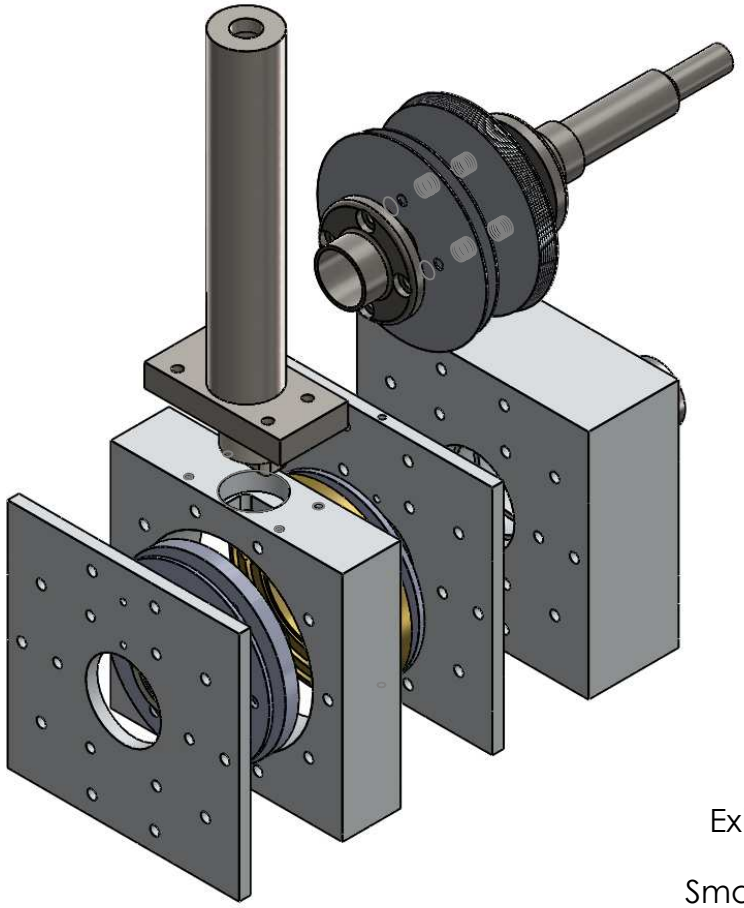

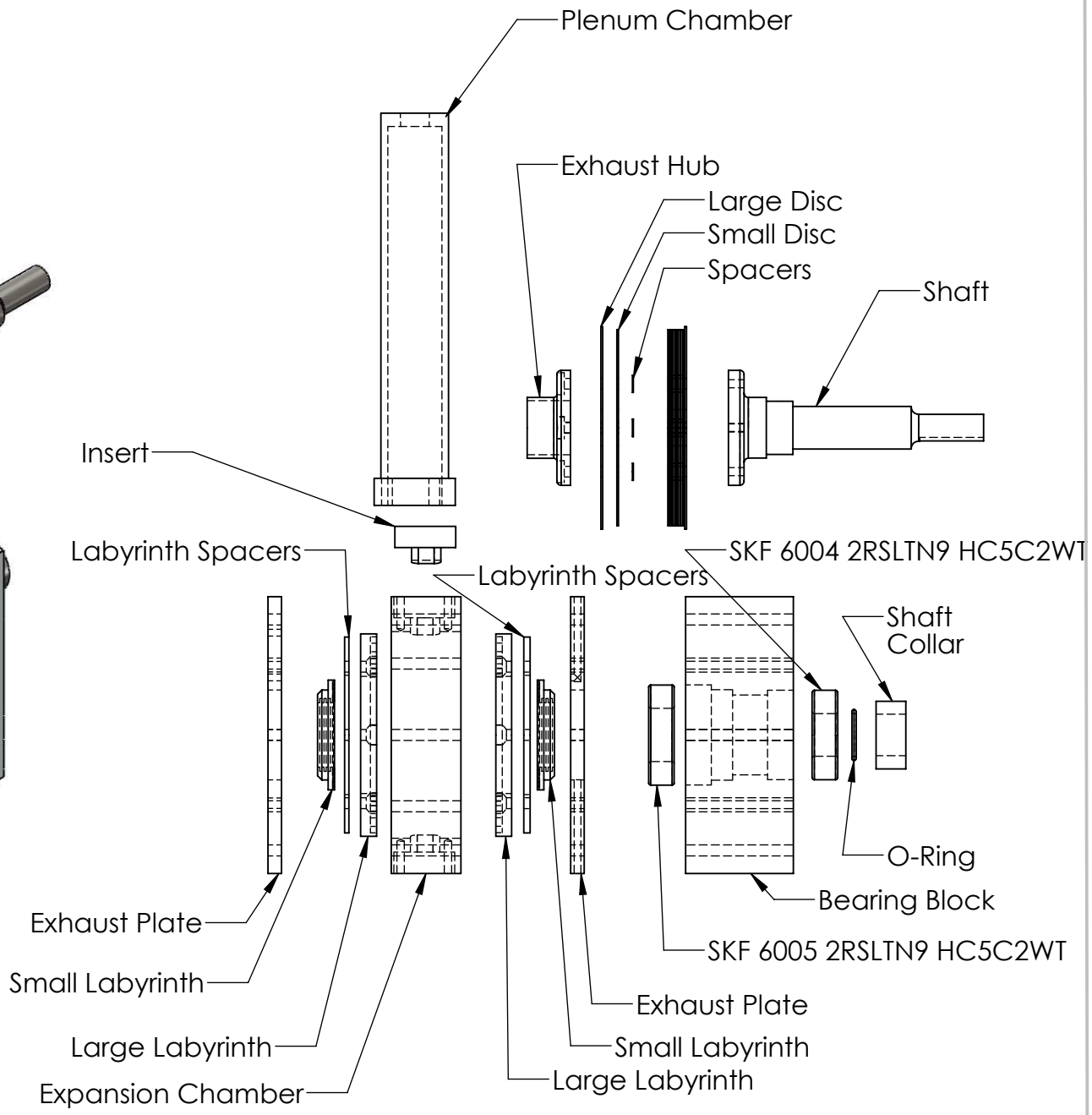

DIMENSIONS ARE IN [MILLIMETERS] and INCHES. TOLERANCES: +/-.003 UNLESS OTHERWISE NOTED	MATERIAL: N/A	DEBUR AND BREAK SHARP EDGES	TITLE: Assembly	Rev 3 / A4 / SCALE:1:3
DATE September 18th, 2012			DO NOT SCALE DRAWING	SHEET 14 OF 15

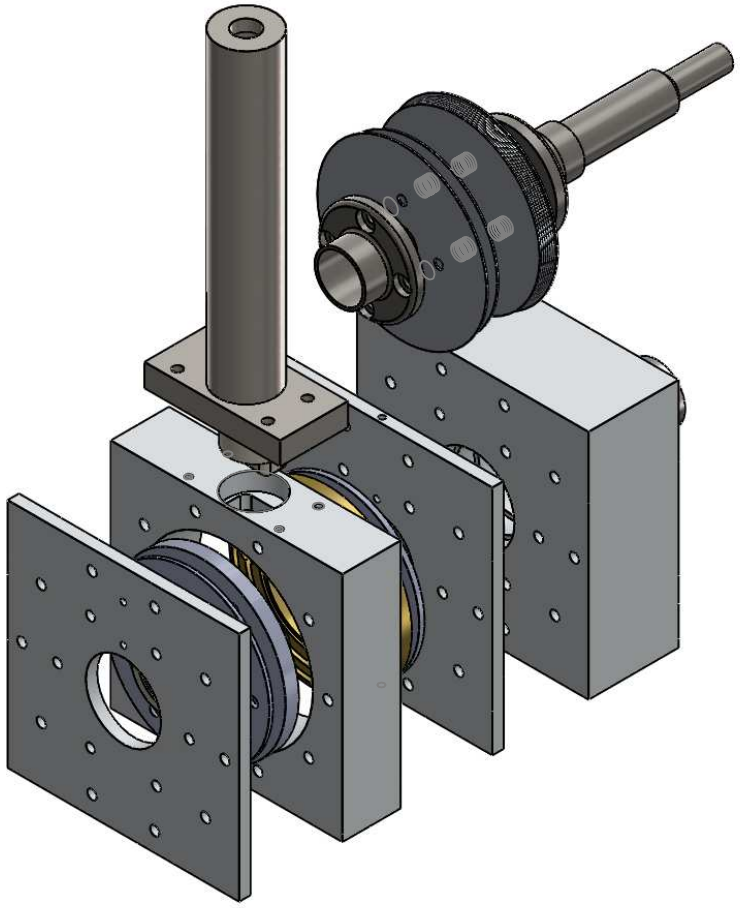

ITEM NO.	DESCRIPTION	QTY.
1	Large Disc	6
2	Spacer	36
3	Exhaust Hub	1
4	Shaft	1
5	Small Disc	24
6	Disc Chamber	1
7	Shaft Plate	1
8	Exhaust Plate	1
9	Bearing Block	1
10	Bearing	1
11	Bearing	1
12	O-Ring	1
13	Collar	1
14	Large Labyrinth	2
15	Small Labyrinth	2
17	Plenum Chamber	2
18	Labyrinth Spacer	12

DIMENSIONS ARE IN [MILLIMETERS] and INCHES.

TOLERANCES: +/-.003 UNLESS OTHERWISE NOTED

MATERIAL: N/A

DEBUR AND BREAK SHARP EDGES

TITLE: Assembly

Rev 3

A4

SCALE:1:3

DATE September 18th, 2012

DO NOT SCALE DRAWING

Appendix C - Results

45/2

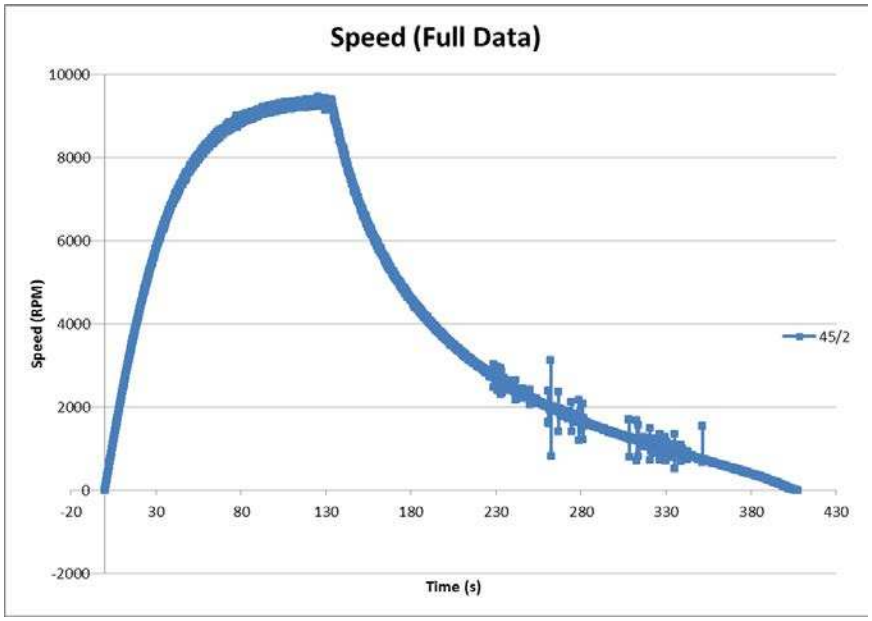

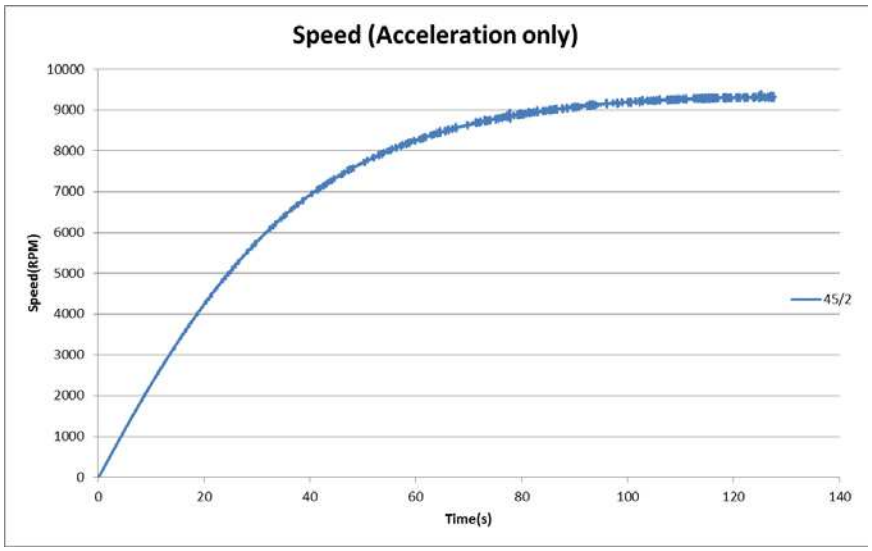

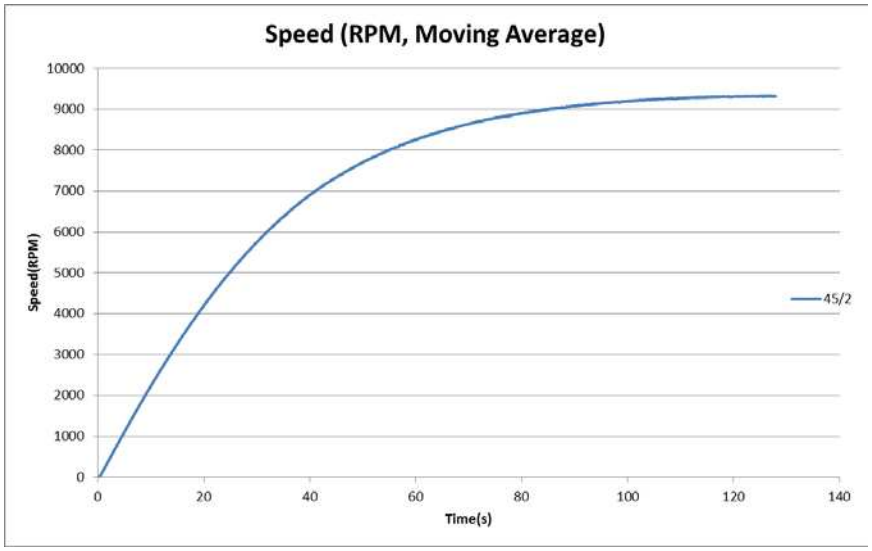
Speed (RPM, Moving Average)
Speed(RPM)
Time(s)
45/2

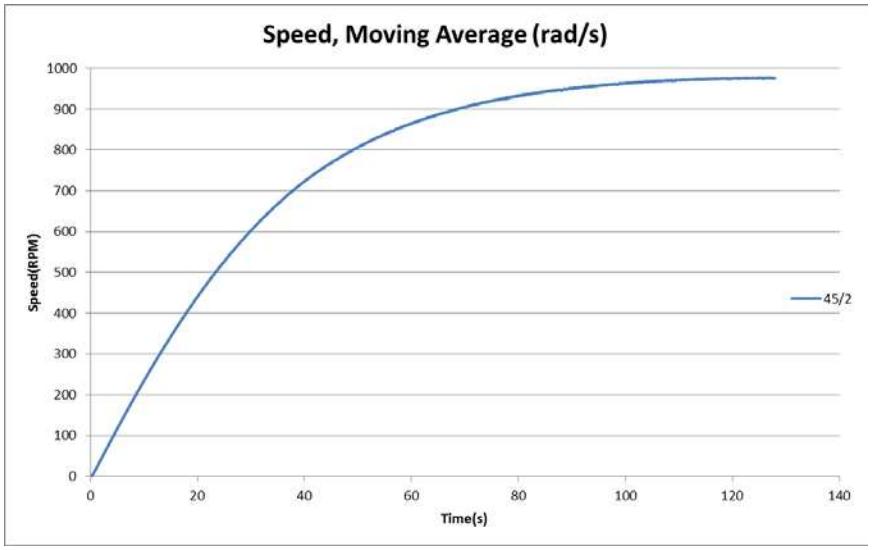
Speed, Moving Average (rad/s)
Speed(RPM)
Time(s)
45/2

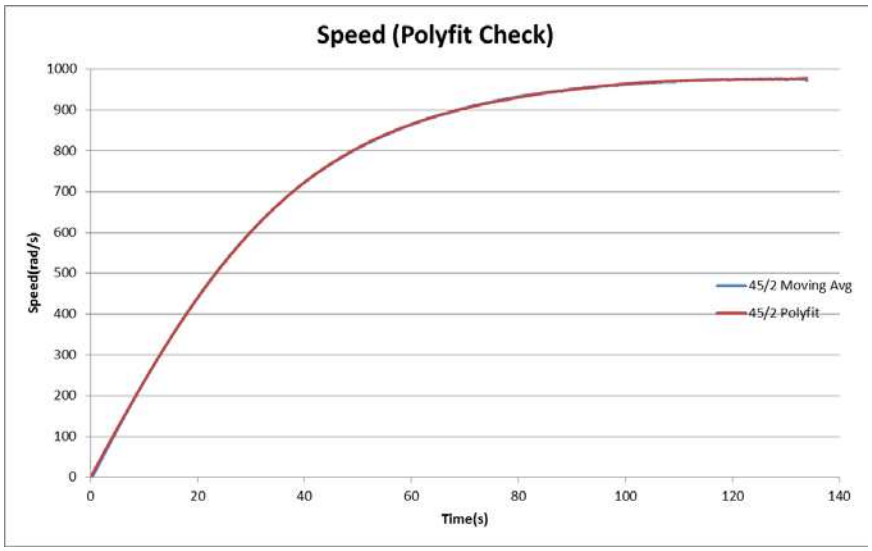
Speed (Polyfit Check)
Speed(rad/s)
Time(s)
45/2 Moving Avg
45/2 Polyfit

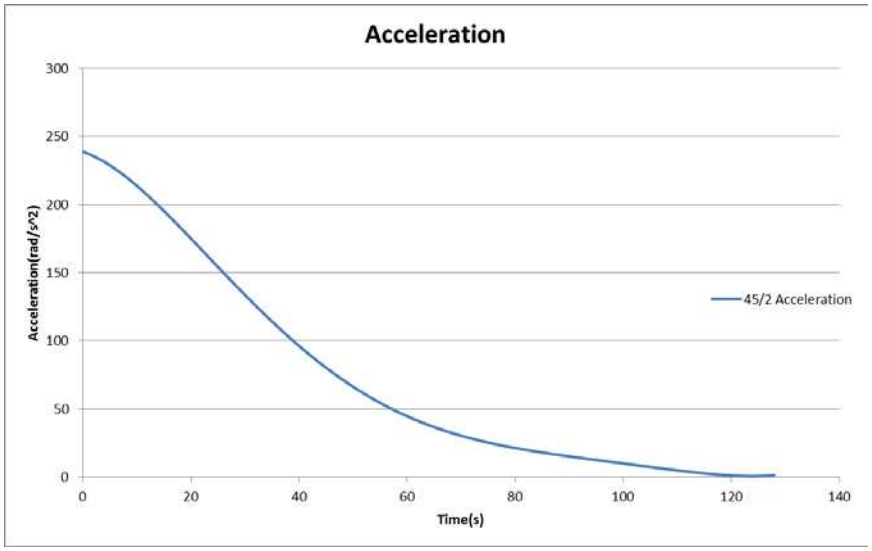
Acceleration
300
250
200
150
100
50
0
Acceleration(rad/s^2)
0
20
40
60
80
100
120
140
Time(s)
45/2 Acceleration

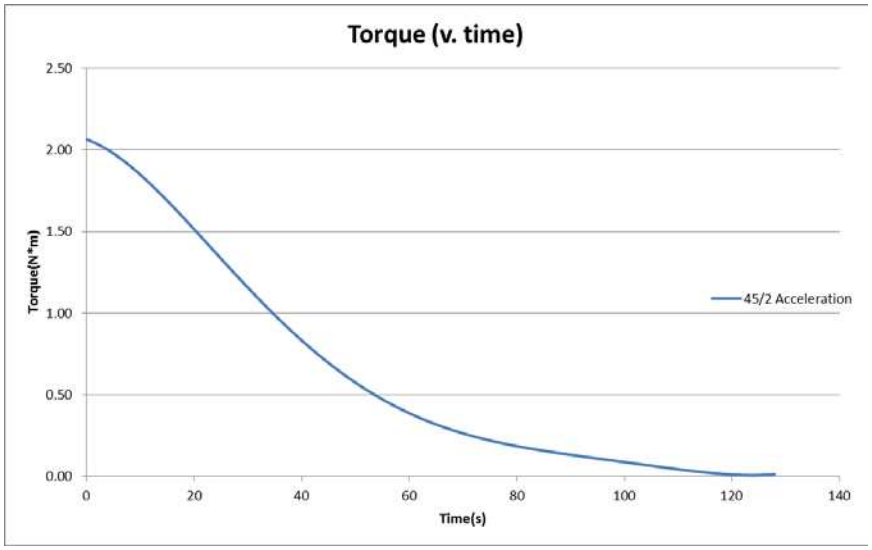
Torque (v. time)
2.50
2.00
1.50
1.00
0.50
0.00
Torque(N*m)
0
20
40
60
80
100
120
140
Time(s)
45/2 Acceleration

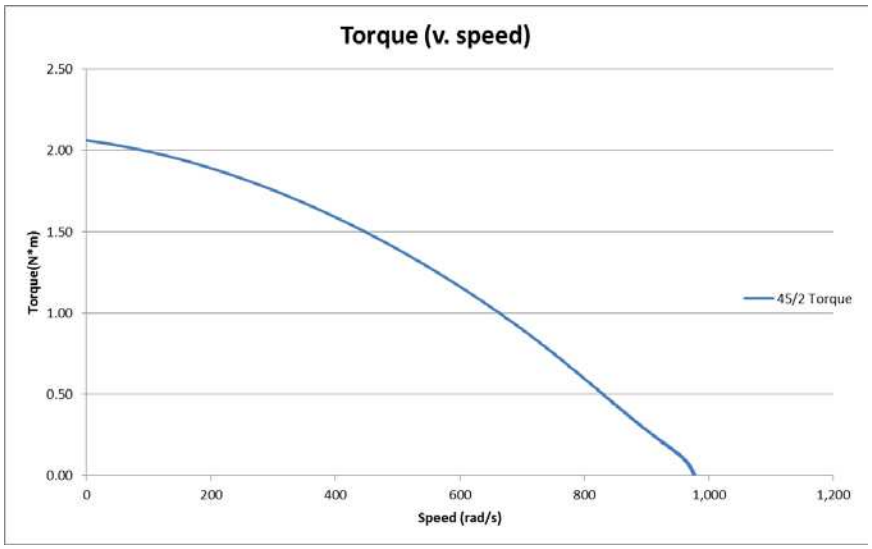
Torque (v. speed)
2.50
2.00
1.50
1.00
0.50
0.00
Torque(N*m)
0
200
400
600
800
1,000
1,200
Speed (rad/s)
45/2 Torque

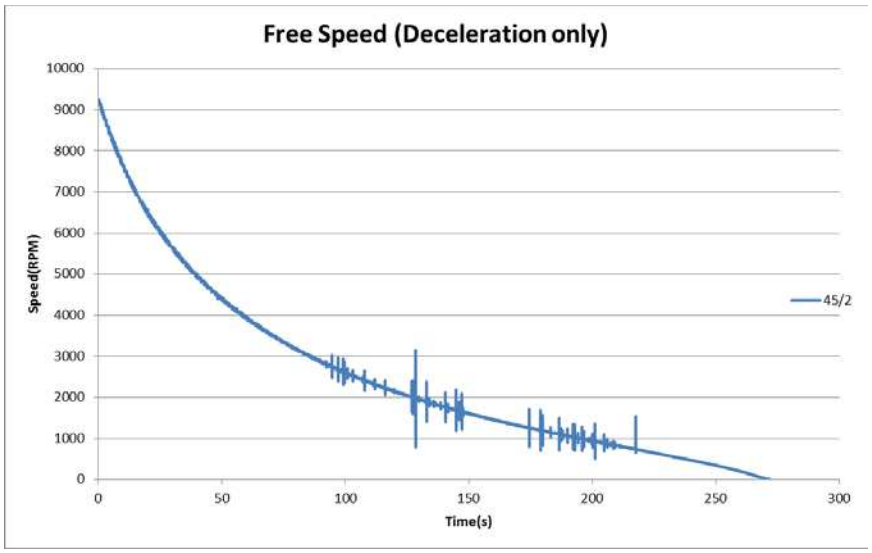
Free Speed (Deceleration only)
Speed(RPM)
Time(s)
45/2

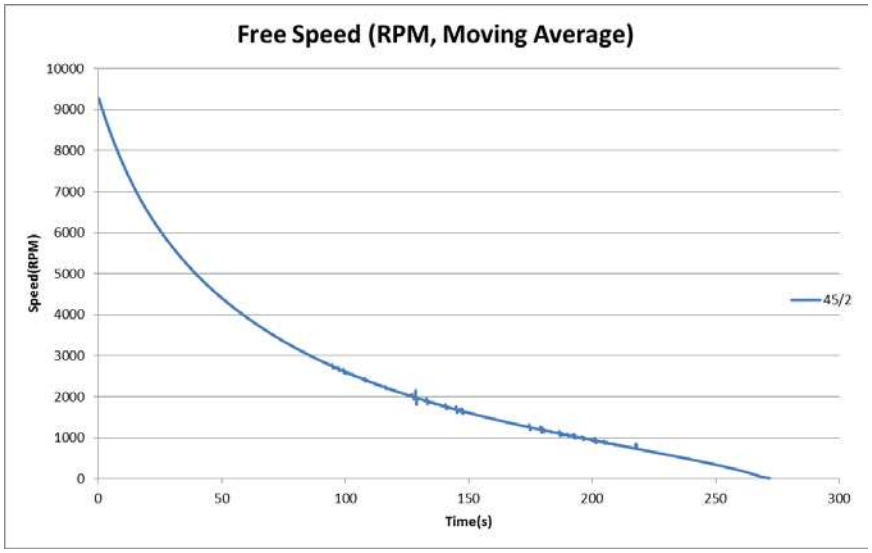
Free Speed (RPM, Moving Average)
Speed(RPM)
Time(s)
45/2

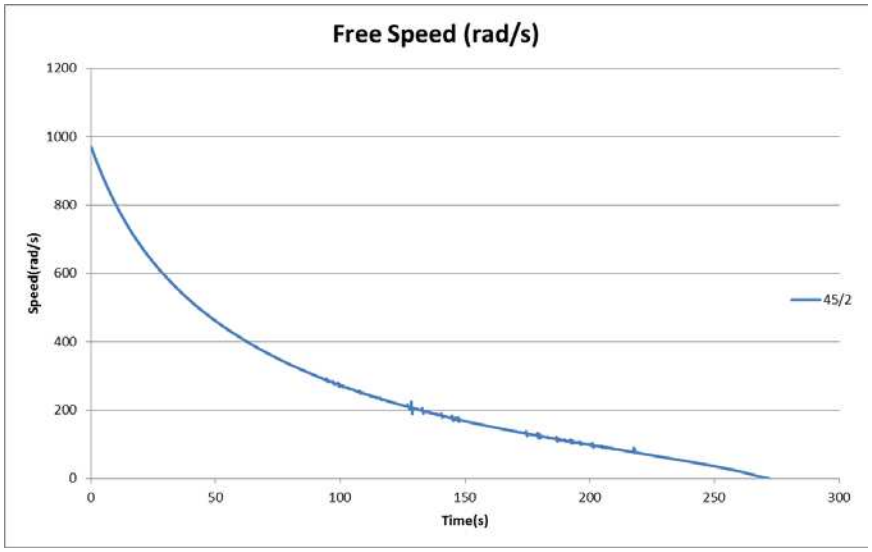
Free Speed (rad/s)
Speed(rad/s)
Time(s)
45/2

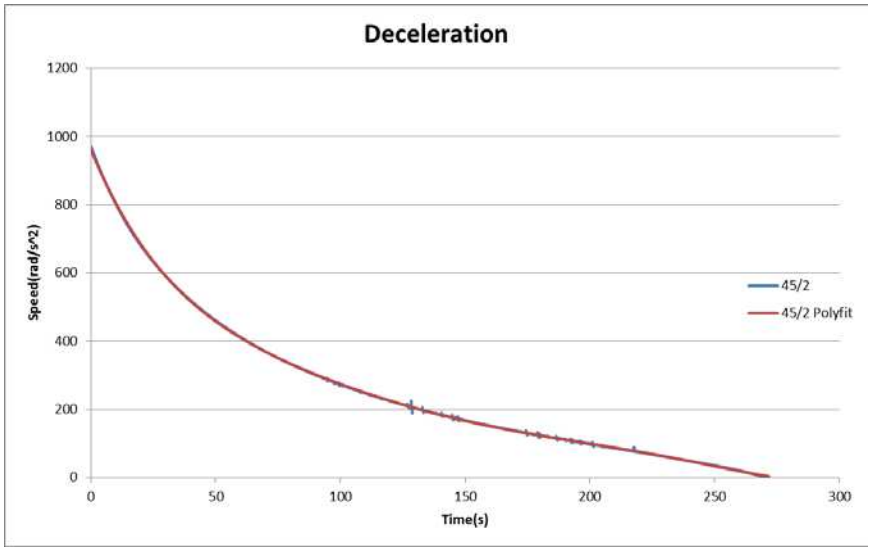
Deceleration
1200
1000
800
600
400
200
0
Speed(rad/s^2)
0
50
100
150
200
250
300
Time(s)
45/2
45/2 Polyfit

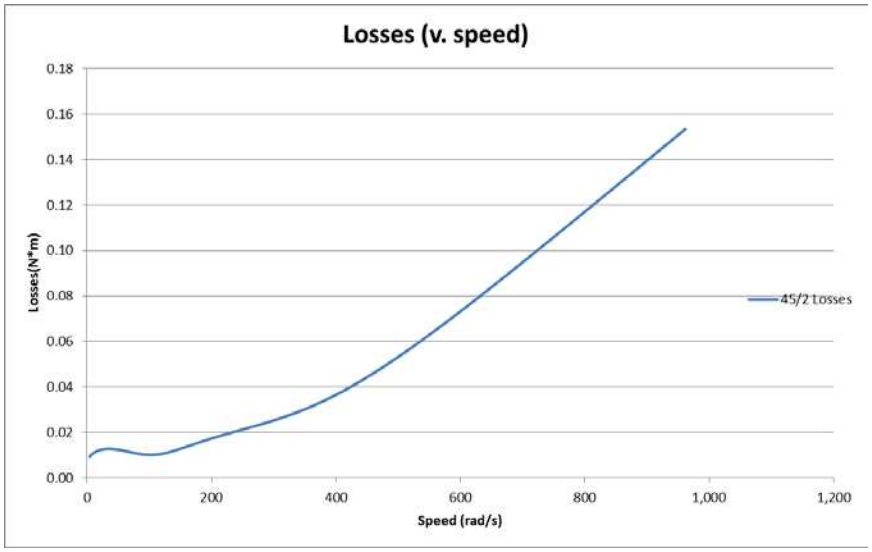
Losses (v. speed)
0.18
0.16
0.14
0.12
0.10
0.08
0.06
0.04
0.02
0.00
Losses(N*m)
0
200
400
600
800
1,000
1,200
Speed (rad/s)
45/2 Losses

45/3

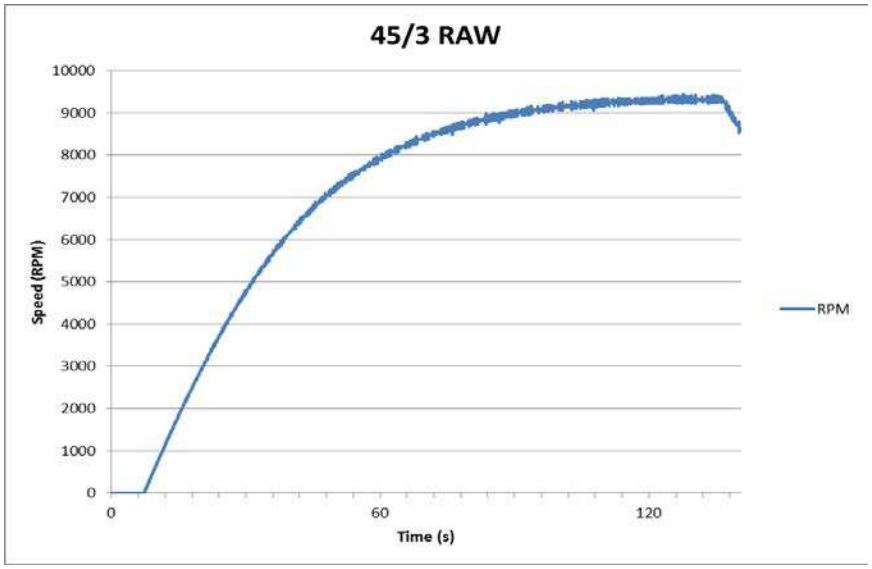
45/3 RAW
10000
9000
8000
7000
6000
5000
4000
3000
2000
1000
0
Speed (RPM)
0
60
120
Time (s)
RPM

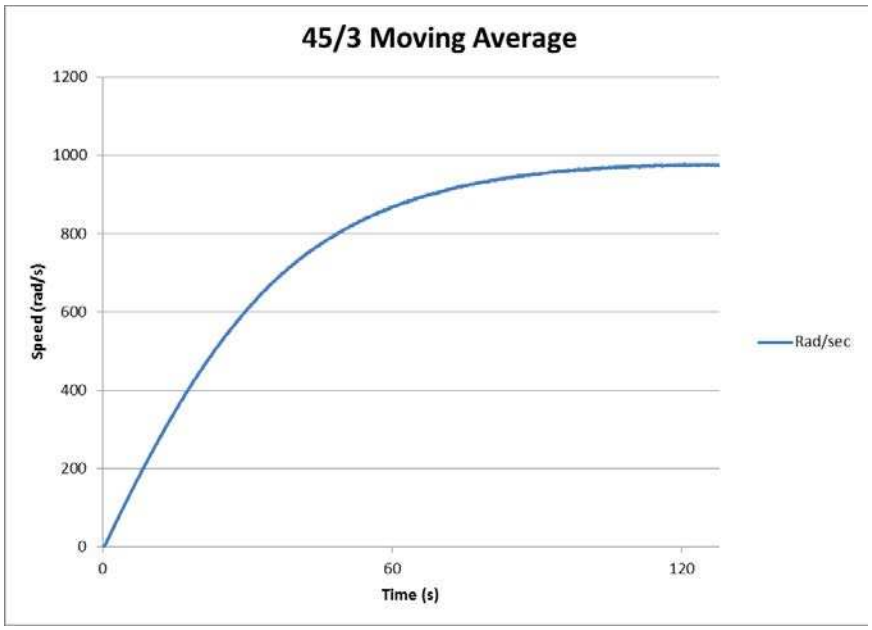
45/3 Moving Average
1200
1000
800
600
400
200
0
Speed (rad/s)
0
60
120
Time (s)
Rad/sec

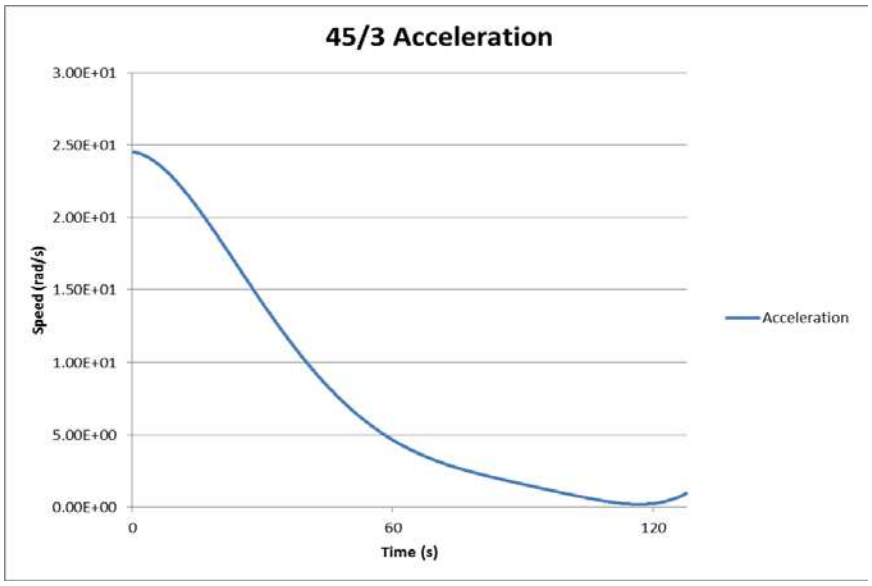
45/3 Acceleration
3.00E+01
2.50E+01
2.00E+01
1.50E+01
1.00E+01
5.00E+00
0.00E+00
Speed (rad/s)
0
60
120
Time (s)
Acceleration

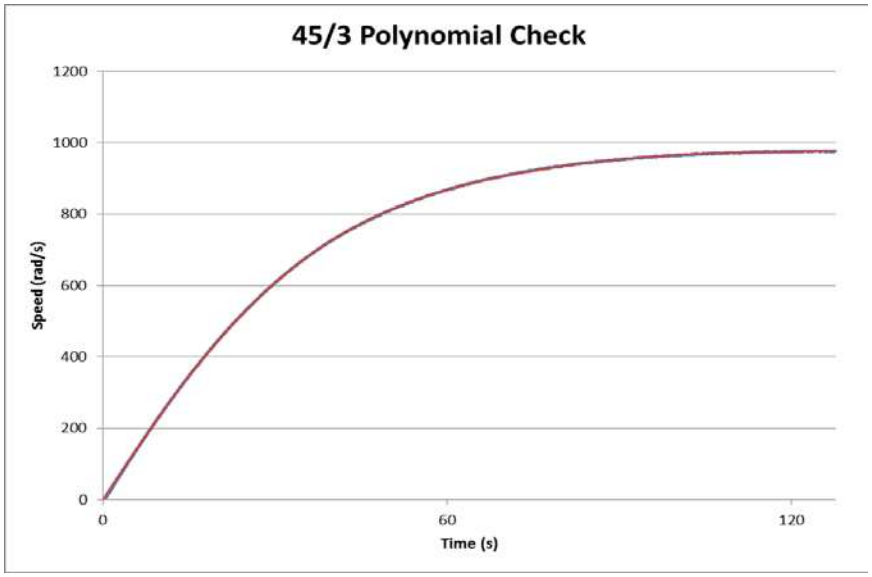
45/3 Polynomial Check
1200
1000
800
600
400
200
0
Speed (rad/s)
0
60
120
Time (s)

45/4

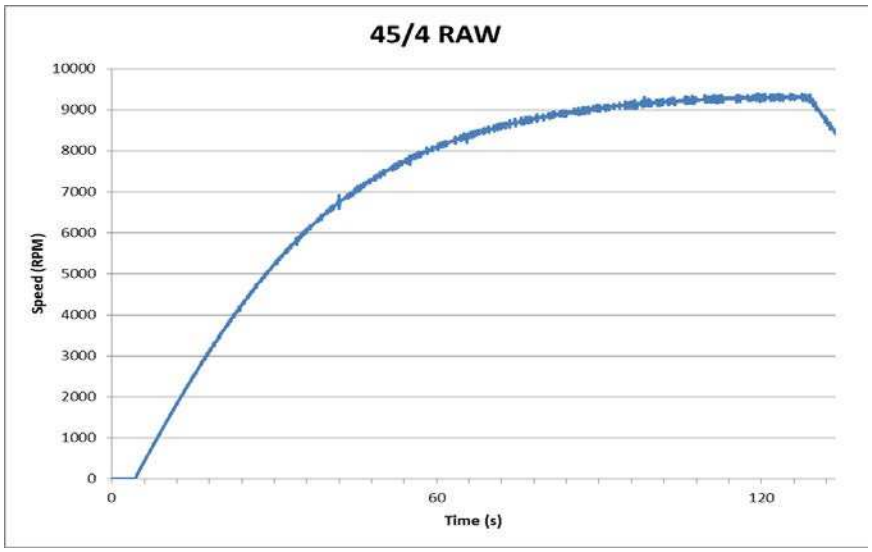
45/4 RAW
10000
9000
8000
7000
6000
5000
4000
3000
2000
1000
0
Speed (RPM)
0
60
120
Time (s)

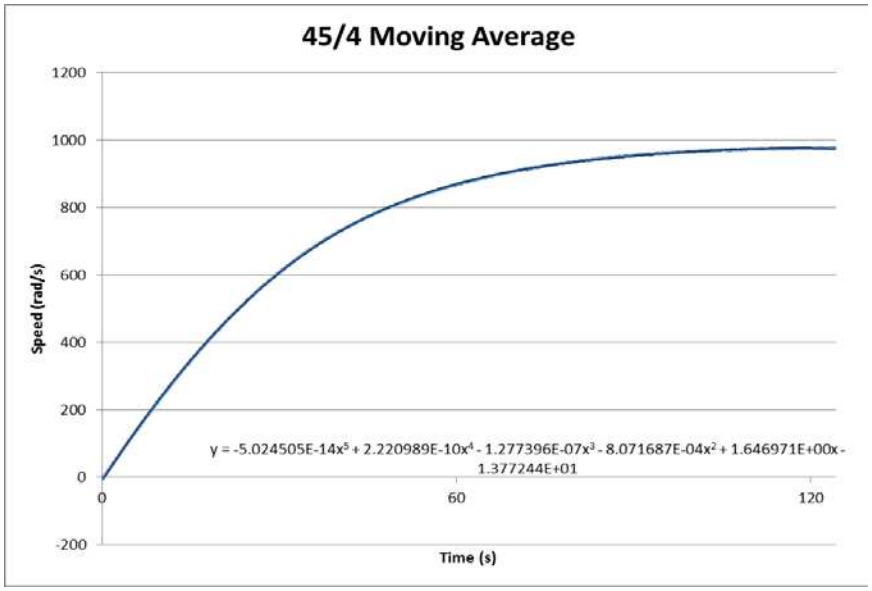
45/4 Moving Average
1200
1000
800
600
400
200
0
-200
Speed (rad/s)
y = -5.024505E-14x5 + 2.220989E-10x4 - 1.277396E-07x3 - 8.071687E-04x2 + 1.646971E+00x - 1.377244E+01
0
60
120
Time (s)

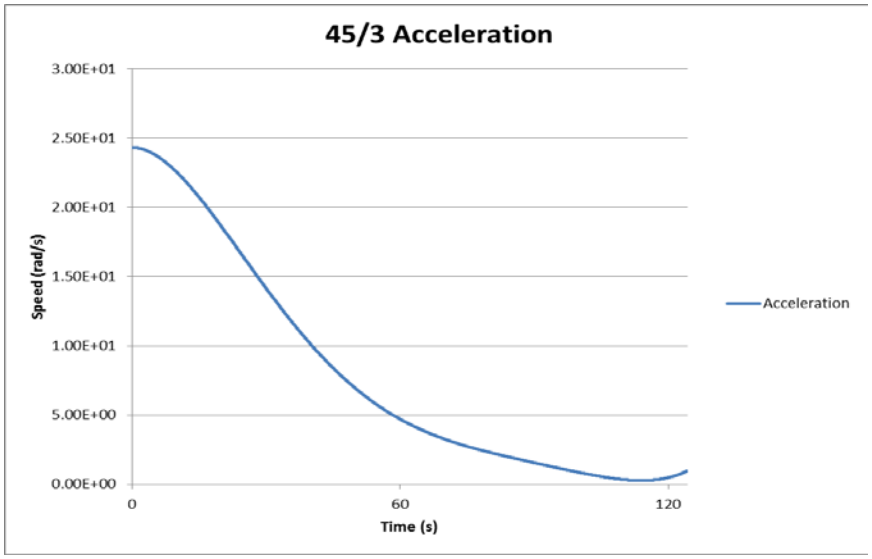
45/3 Acceleration
3.00E+01
2.50E+01
2.00E+01
1.50E+01
1.00E+01
5.00E+00
0.00E+00
Speed (rad/s)
0
60
120
Time (s)
Acceleration

2.5/9

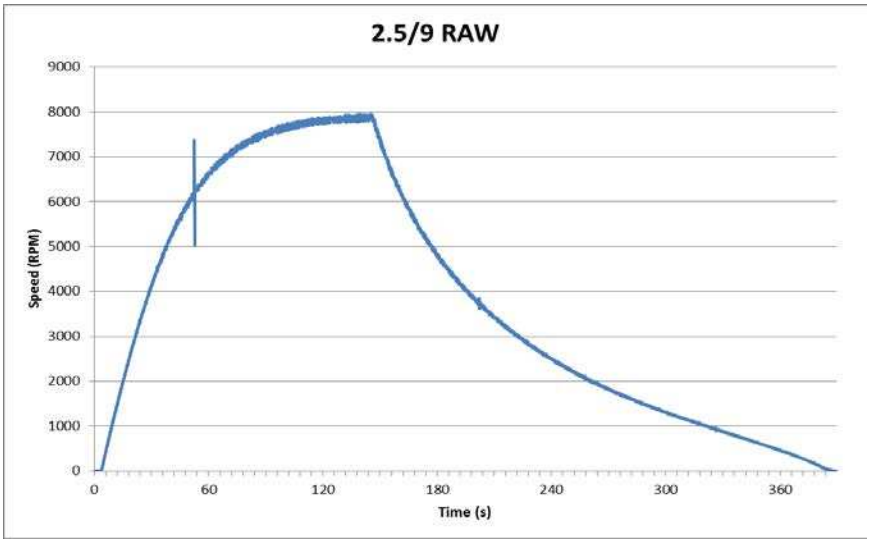
2.5/9 RAW
Speed (RPM)
9000
8000
7000
6000
5000
4000
3000
2000
1000
0
0
60
120
180
240
300
360
Time (s)


2.5/9 Moving Average
Speed (rad/s)
900
800
700
600
500
400
300
200
100
0
-100
y = -3.484709E-14x⁵ + 1.813388E-10x⁴ - 2.061557E-07x³ - 4.317365E-04x² + 1.208891E+00x - 7.561020E+00
0
60
120
Time (s)

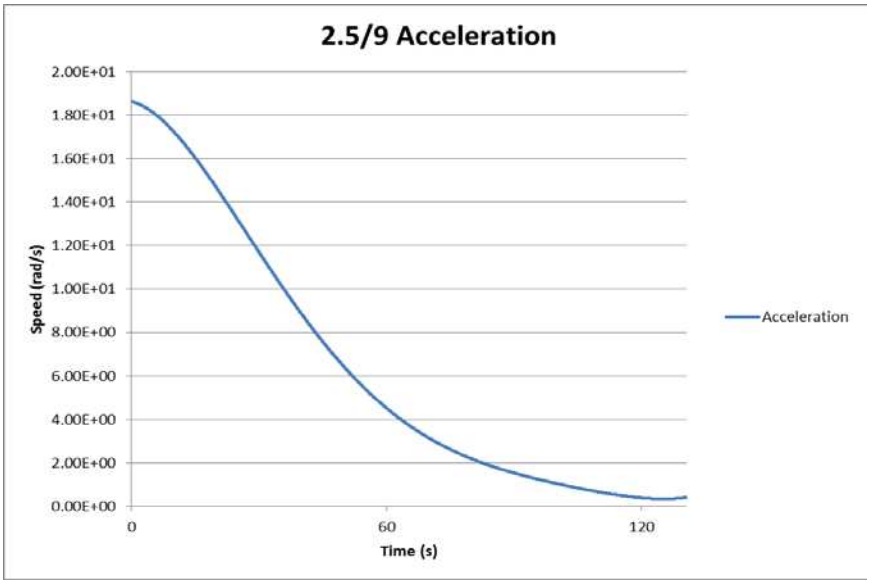
2.5/9 Acceleration
2.00E+01
1.80E+01
1.60E+01
1.40E+01
1.20E+01
1.00E+01
8.00E+00
6.00E+00
4.00E+00
2.00E+00
0.00E+00
Speed (rad/s)
0
60
120
Time (s)
Acceleration

2.5/10

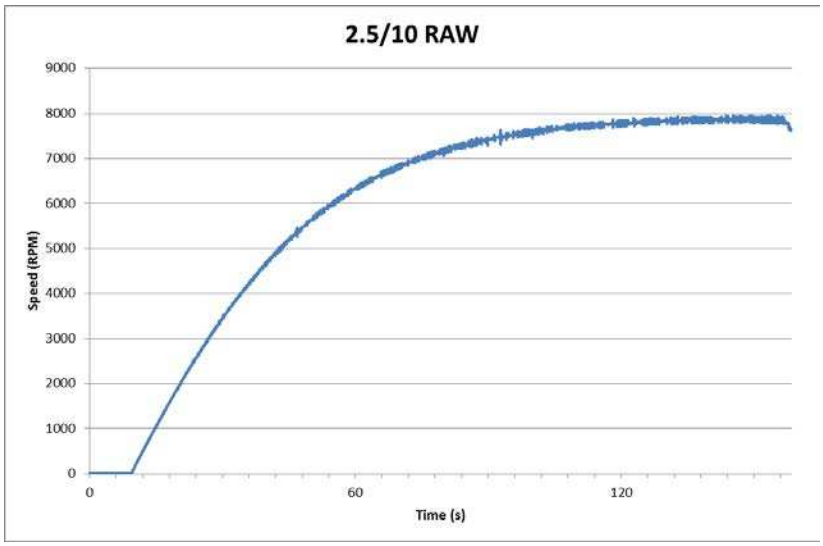
2.5/10 RAW
9000
8000
7000
6000
5000
4000
3000
2000
1000
0
Speed (RPM)
0
60
120
Time (s)


2.5/10 Moving Average
900
800
700
600
500
400
300
200
100
0
-100
Speed (rad/s)
y = -1.758933E-14x⁵ + 8.271028E-11x⁴ + 1.427045E-09x³ - 6.265927E-04x² + 1.282680E+00x - 1.093944E+01
0
60
120
Time (s)

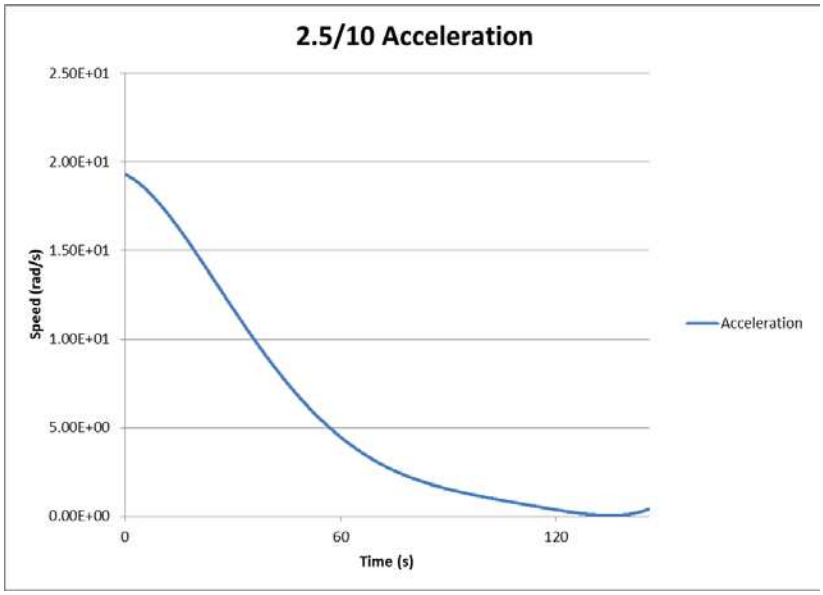
2.5/10 Acceleration
2.50E+01
2.00E+01
1.50E+01
1.00E+01
5.00E+00
0.00E+00
Speed (rad/s)
0
60
120
Time (s)
Acceleration

2.5/11

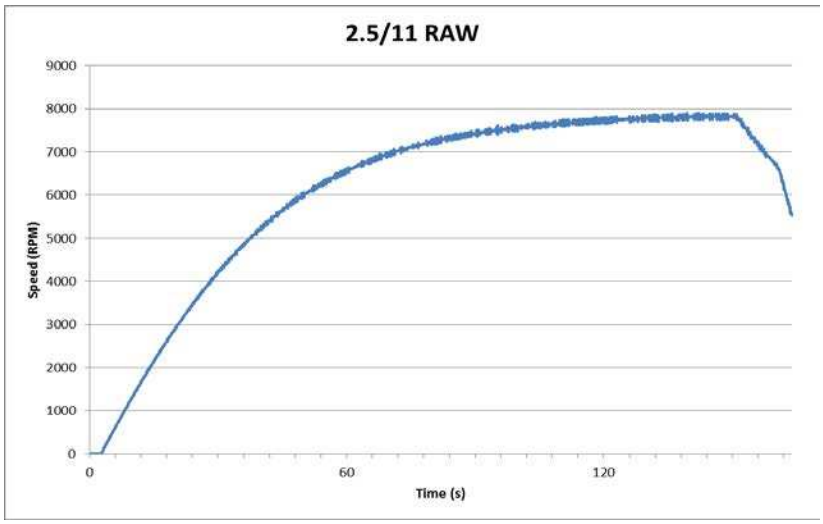
2.5/11 RAW
9000
8000
7000
6000
5000
4000
3000
2000
1000
0
Speed (RPM)
0
60
120
Time (s)

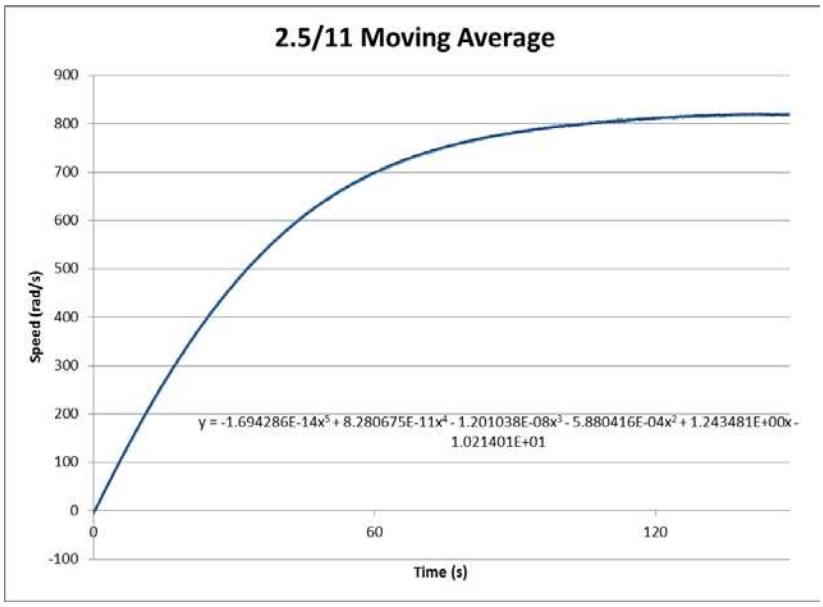
2.5/11 Moving Average
900
800
700
600
500
400
300
200
100
0
-100
Speed (rad/s)
y = -1.694286E-14x⁵ + 8.280675E-11x⁴ - 1.201038E-08x³ - 5.880416E-04x² + 1.243481E+00x - 1.021401E+01
0
60
120
Time (s)

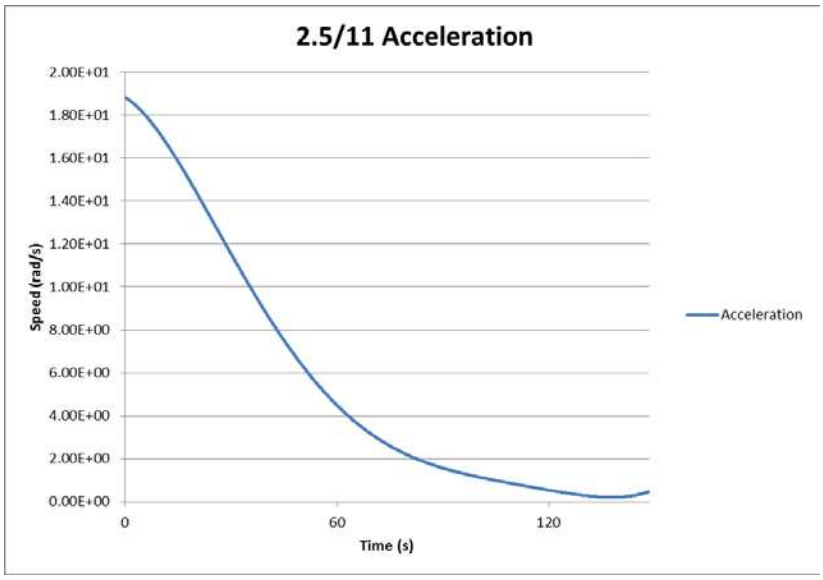
2.5/11 Acceleration
2.00E+01
1.80E+01
1.60E+01
1.40E+01
1.20E+01
1.00E+01
8.00E+00
6.00E+00
4.00E+00
2.00E+00
0.00E+00
Speed (rad/s)
0
60
120
Time (s)
Acceleration

12.5/14

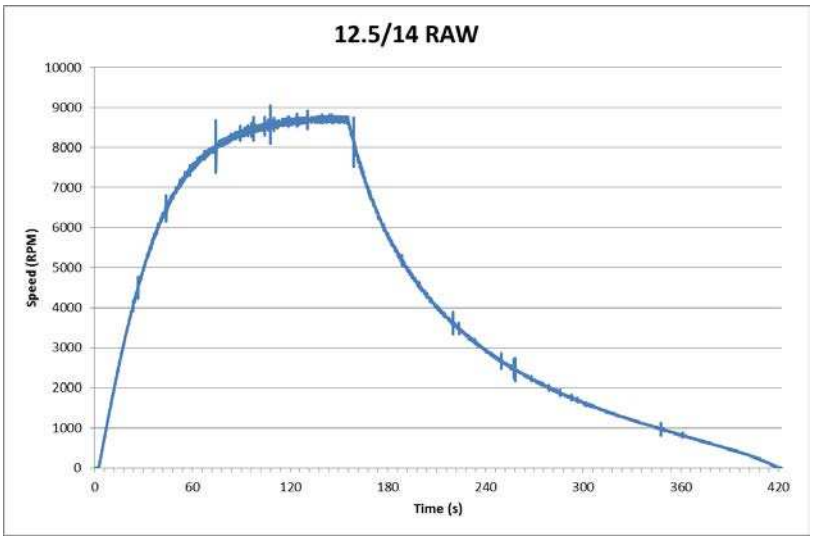
12.5/14 RAW
Speed (RPM)
10000
9000
8000
7000
6000
5000
4000
3000
2000
1000
0
0
60
120
180
240
300
360
420
Time (s)

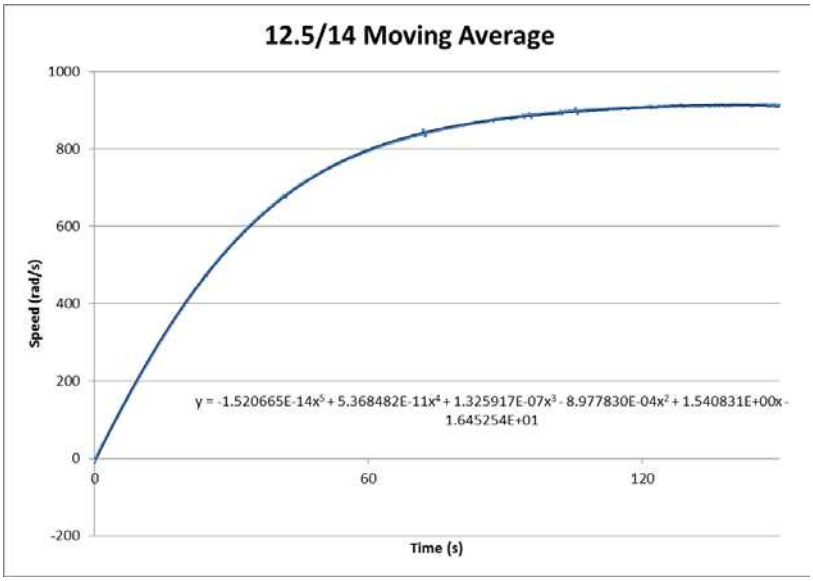
12.5/14 Moving Average
Speed (rad/s)
1000
800
600
400
200
0
-200
y = -1.520665E-14x⁵ + 5.368482E-11x⁴ + 1.325917E-07x³ - 8.977830E-04x² + 1.540831E+00x - 1.645254E+01
0
60
120
Time (s)

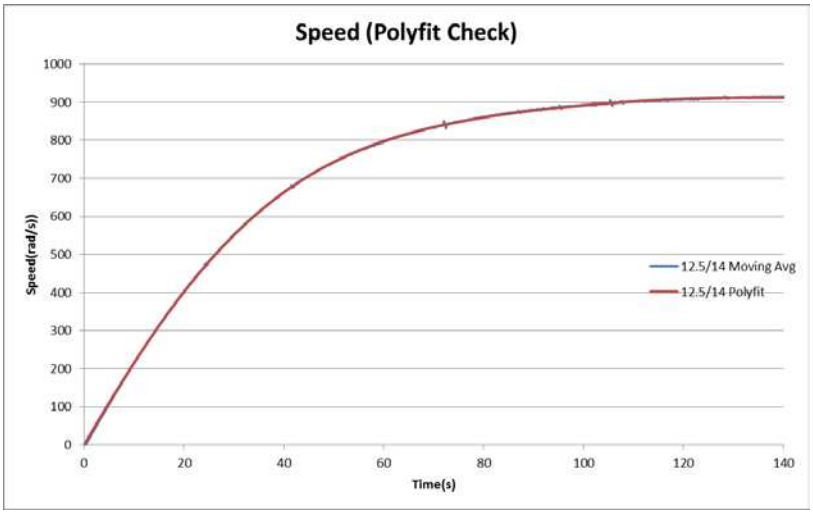
Speed (Polyfit Check)
Speed(rad/s)
Time(s)
12.5/14 Moving Avg
12.5/14 Polyfit

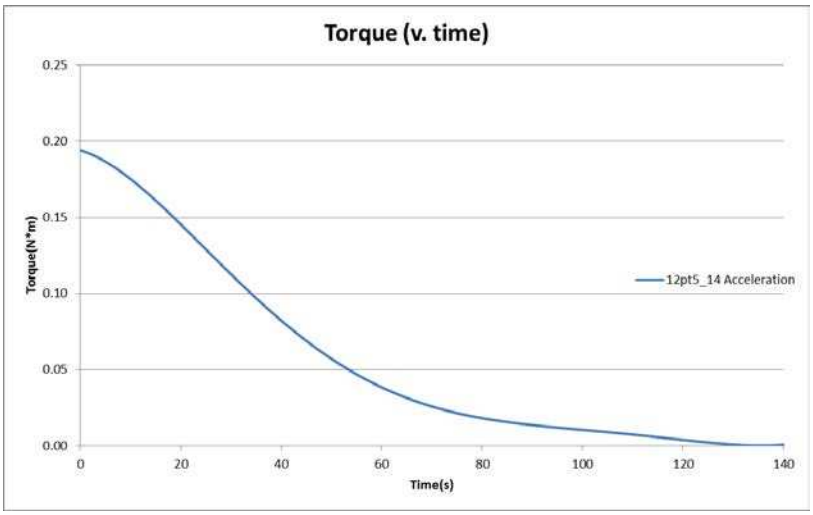
Torque (v. time)
Torque(N*m)
Time(s)
12pt5_14 Acceleration

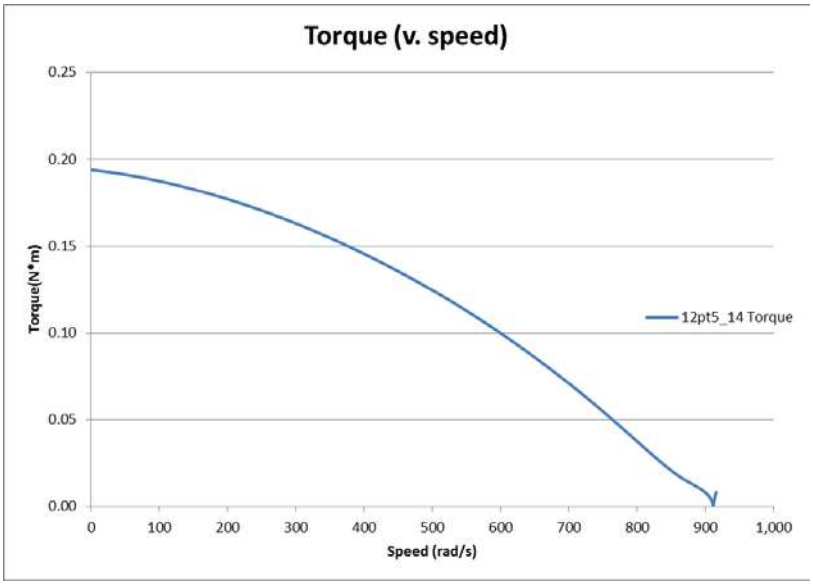
Torque (v. speed)
Torque(N*m)
Speed (rad/s)
12pt5_14 Torque

12.5/15

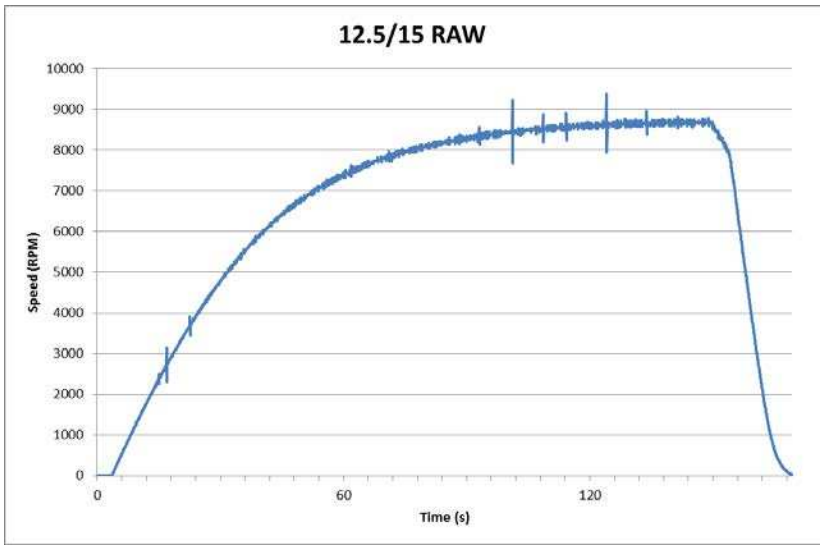
12.5/15 RAW
Speed (RPM)
10000
9000
8000
7000
6000
5000
4000
3000
2000
1000
0
0
60
120
Time (s)

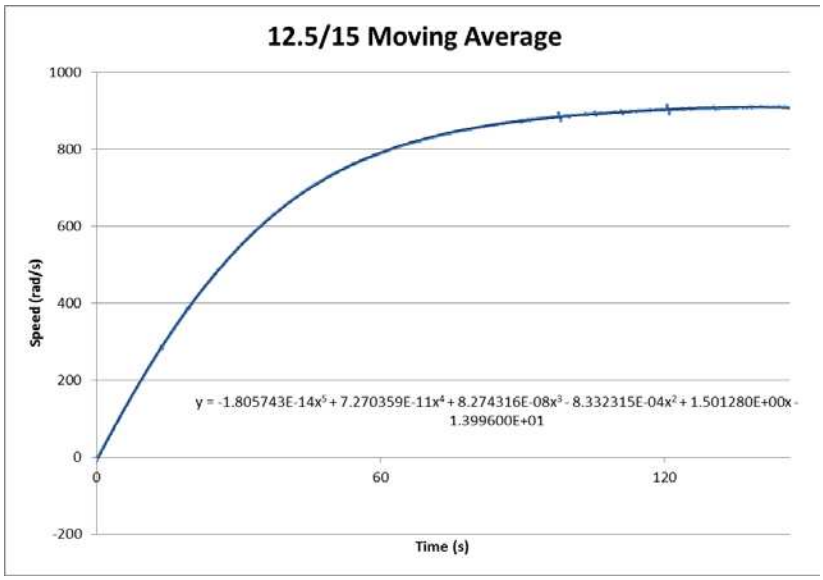
12.5/15 Moving Average
Speed (rad/s)
1000
800
600
400
200
0
-200
y = -1.805743E-14x⁵ + 7.270359E-11x⁴ + 8.274316E-08x³ - 8.332315E-04x² + 1.501280E+00x - 1.399600E+01
0
60
120
Time (s)

12.5/16

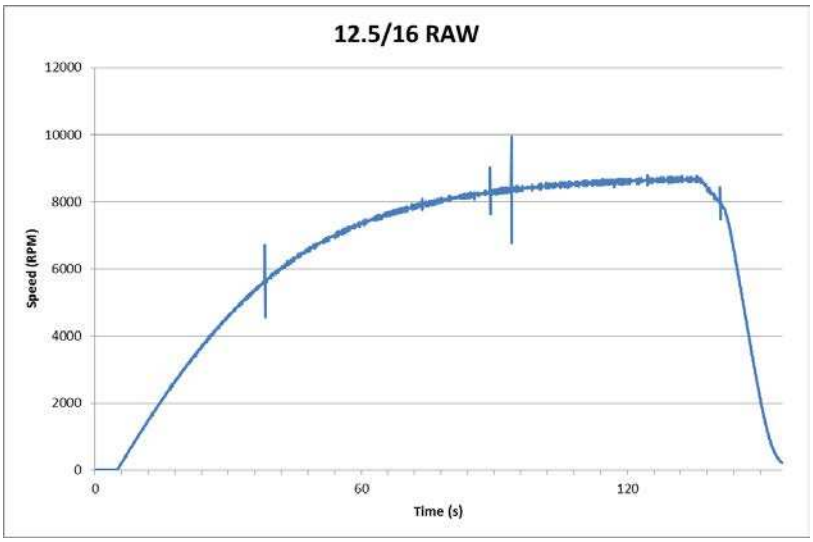
12.5/16 RAW
12000
10000
8000
6000
4000
2000
0
Speed (RPM)
0
60
120
Time (s)


12.5/16 Moving Average
1000
800
600
400
200
0
-200
Speed (rad/s)
y = -3.731565E-14x⁵ + 1.770325E-10x⁴ - 1.201305E-07x³ - 6.666958E-04x² + 1.454465E+00x - 1.228459E+01
0
60
120
Time (s)

5/17

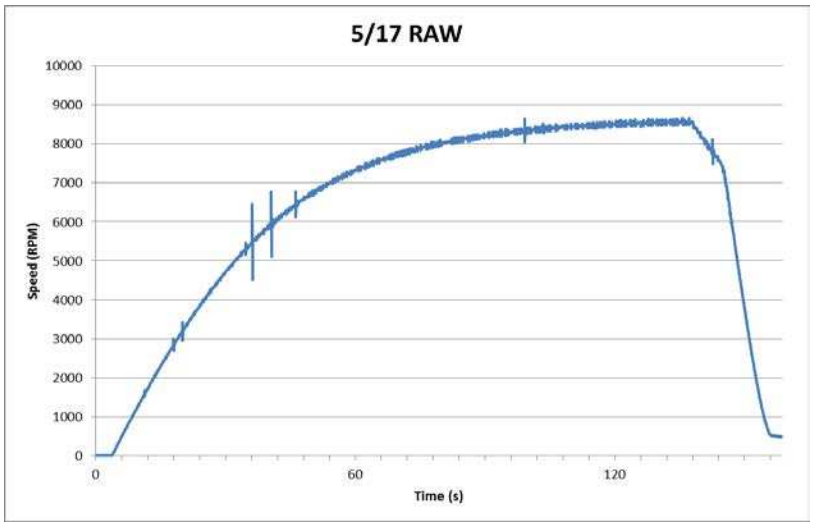
5/17 RAW
Speed (RPM)
10000
9000
8000
7000
6000
5000
4000
3000
2000
1000
0
0
60
120
Time (s)

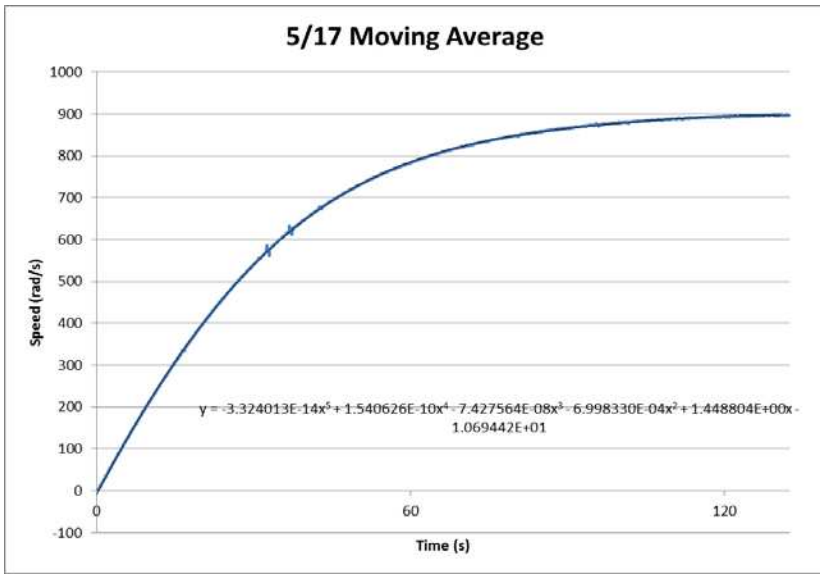
5/17 Moving Average
Speed (rad/s)
1000
900
800
700
600
500
400
300
200
100
0
-100
y = -3.324013E-14x⁵ + 1.540626E-10x⁴ - 7.427564E-08x³ - 6.998330E-04x² + 1.448804E+00x - 1.069442E+01
0
60
120
Time (s)

5/18

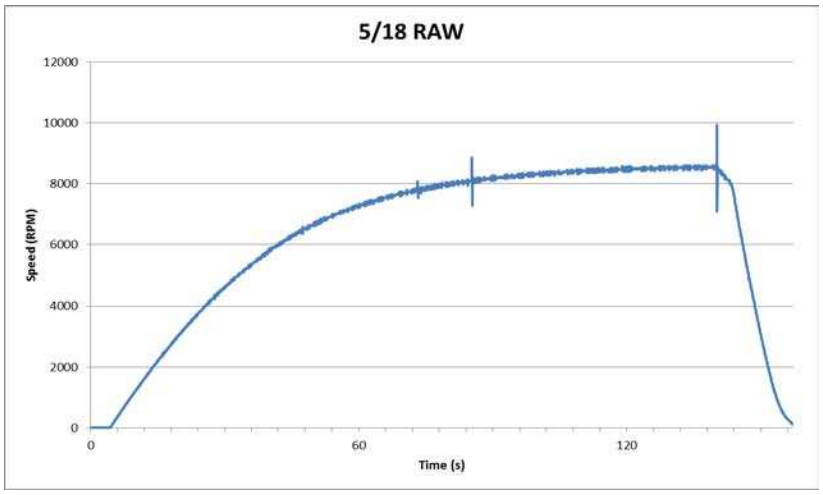
5/18 RAW
12000
10000
8000
6000
4000
2000
0
Speed (RPM)
0
60
120
Time (s)

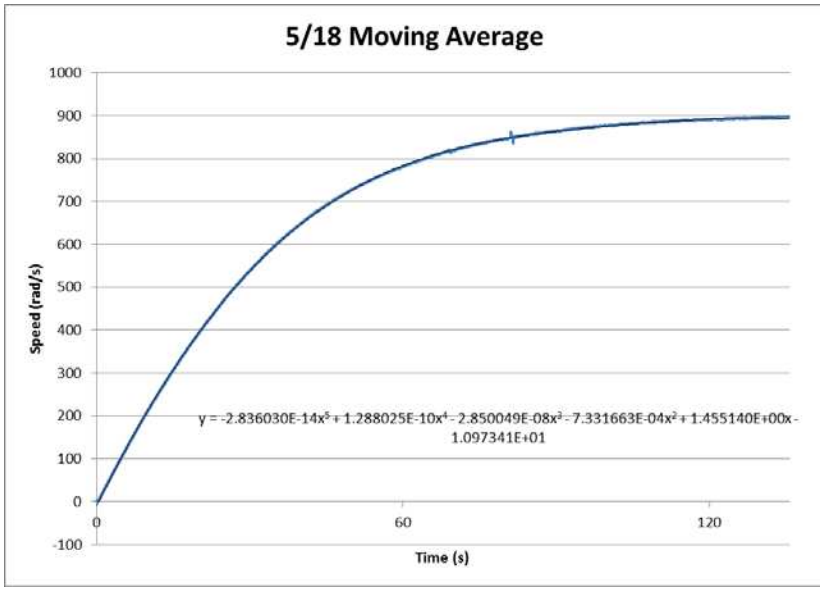
5/18 Moving Average
1000
900
800
700
600
500
400
300
200
100
0
-100
Speed (rad/s)
y = -2.836030E-14x⁵ + 1.288025E-10x⁴ - 2.850049E-08x³ - 7.331663E-04x² + 1.455140E+00x - 1.097341E+01
0
60
120
Time (s)

5/19

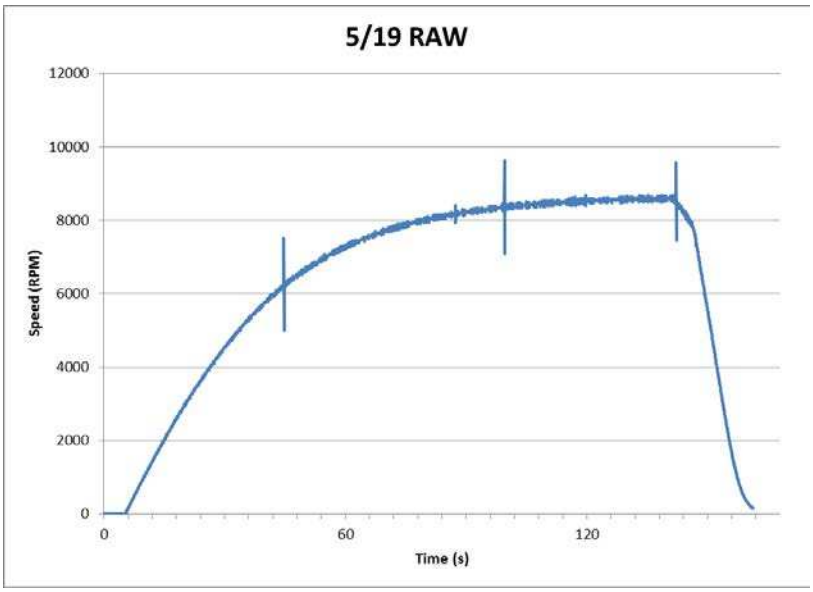
5/19 RAW
12000
10000
8000
6000
4000
2000
0
Speed (RPM)
0
60
120
Time (s)

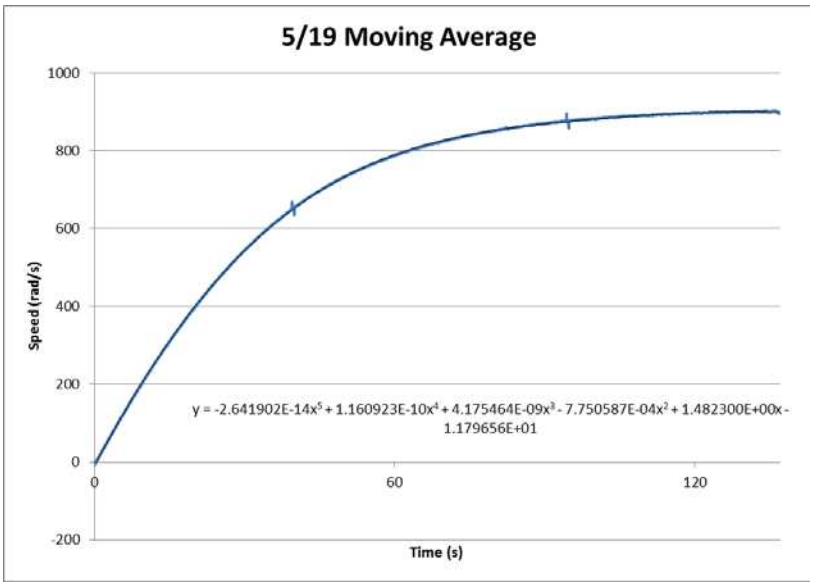
5/19 Moving Average
1000
800
600
400
200
0
-200
Speed (rad/s)
y = -2.641902E-14x^5 + 1.160923E-10x^4 + 4.175464E-09x^3 - 7.750587E-04x^2 + 1.482300E+00x - 1.179656E+01
0
60
120
Time (s)

7.5/20

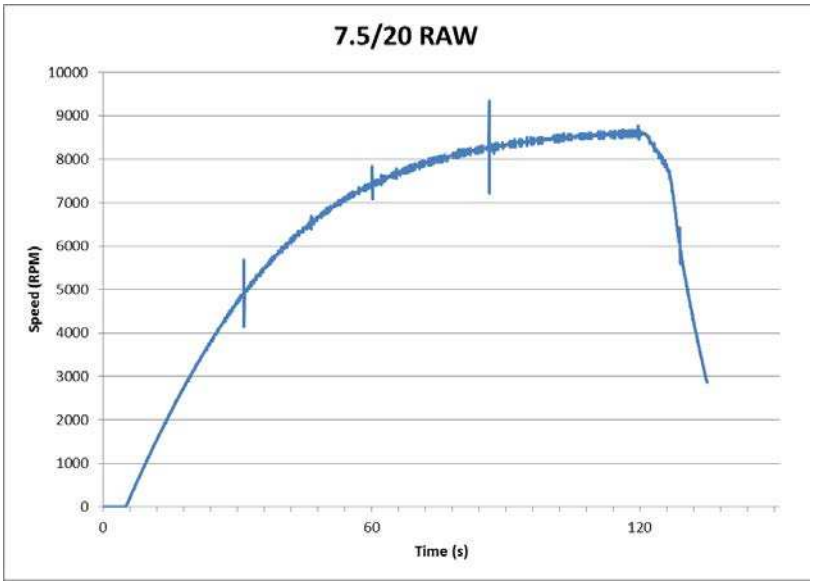
7.5/20 RAW
10000
9000
8000
7000
6000
5000
4000
3000
2000
1000
0
Speed (RPM)
0
60
120
Time (s)

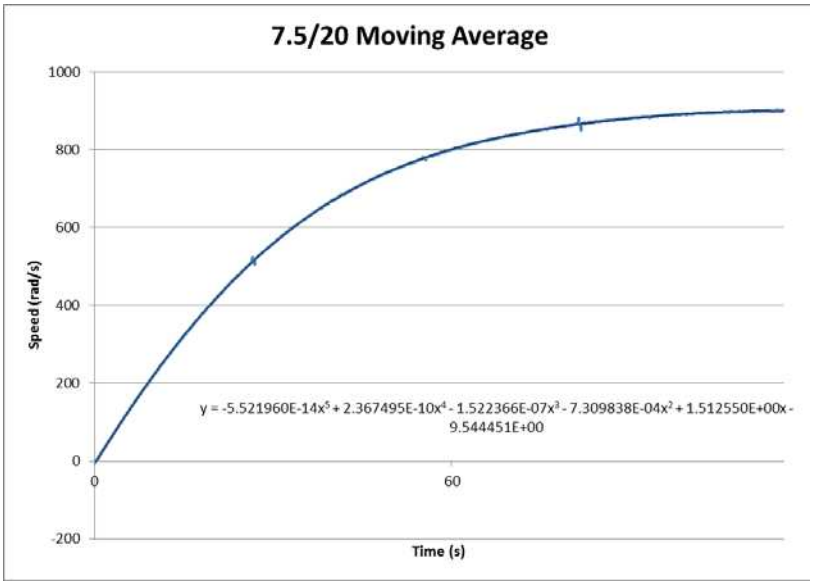
7.5/20 Moving Average
1000
800
600
400
200
0
-200
Speed (rad/s)
y = -5.521960E-14x5 + 2.367495E-10x4 - 1.522366E-07x3 - 7.309838E-04x2 + 1.512550E+00x - 9.544451E+00
0
60
Time (s)

7.5/21

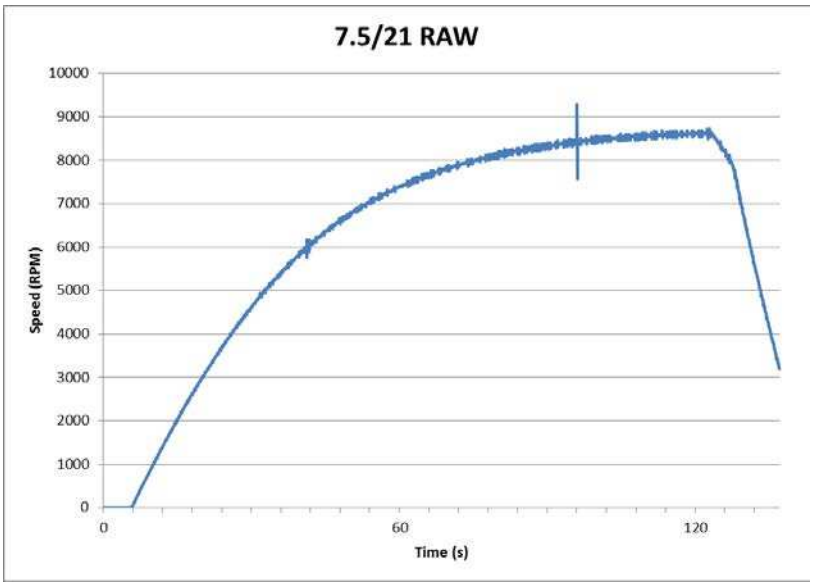
7.5/21 RAW
10000
9000
8000
7000
6000
5000
4000
3000
2000
1000
0
Speed (RPM)
0
60
120
Time (s)

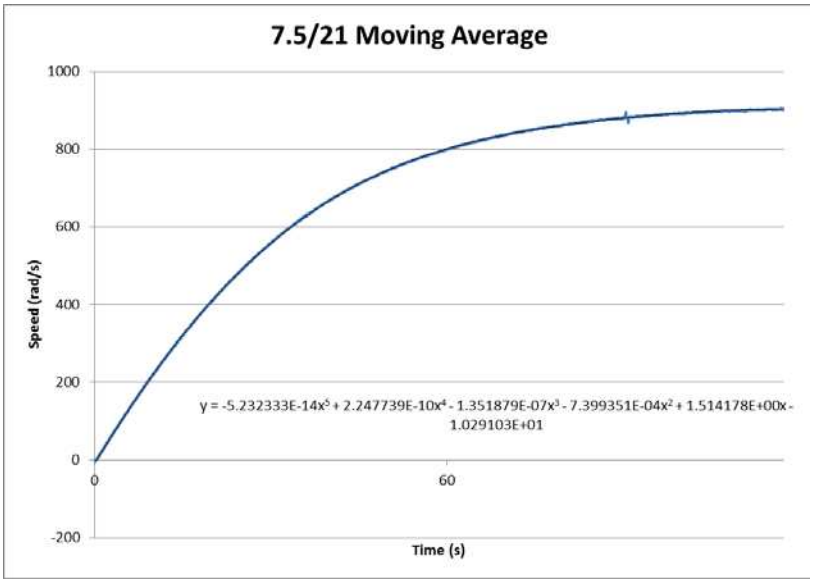
7.5/21 Moving Average
1000
800
600
400
200
0
-200
Speed (rad/s)
y = -5.232333E-14x⁵ + 2.247739E-10x⁴ - 1.351879E-07x³ - 7.399351E-04x² + 1.514178E+00x - 1.029103E+01
0
60
Time (s)

7.5/22

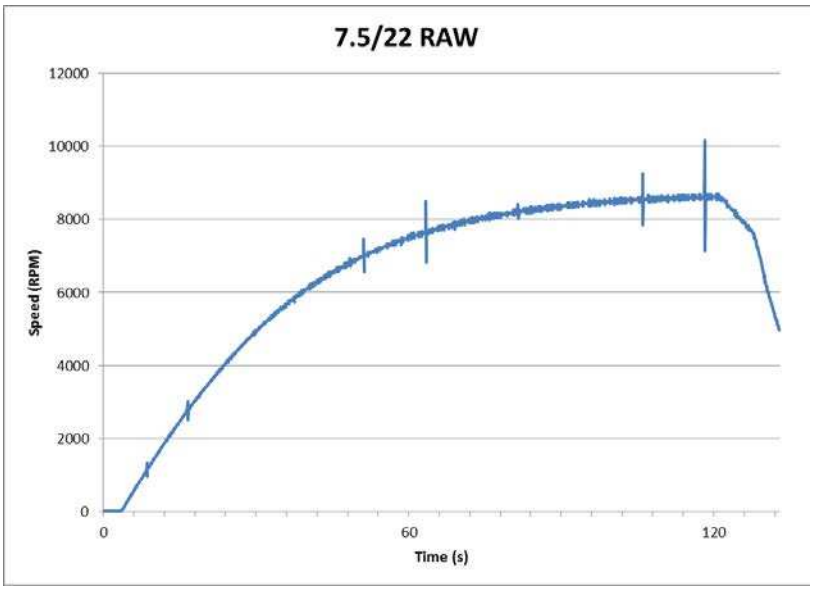
7.5/22 RAW
12000
10000
8000
6000
4000
2000
0
Speed (RPM)
0
60
120
Time (s)


7.5/22 Moving Average
1000
800
600
400
200
0
-200
Speed (rad/s)
y = -5.293349E-14x⁵ + 2.266771E-10x⁴ - 1.333480E-07x³ - 7.504969E-04x² + 1.523022E+00x - 1.141820E+01
0
60
Time (s)

45/4.5/23

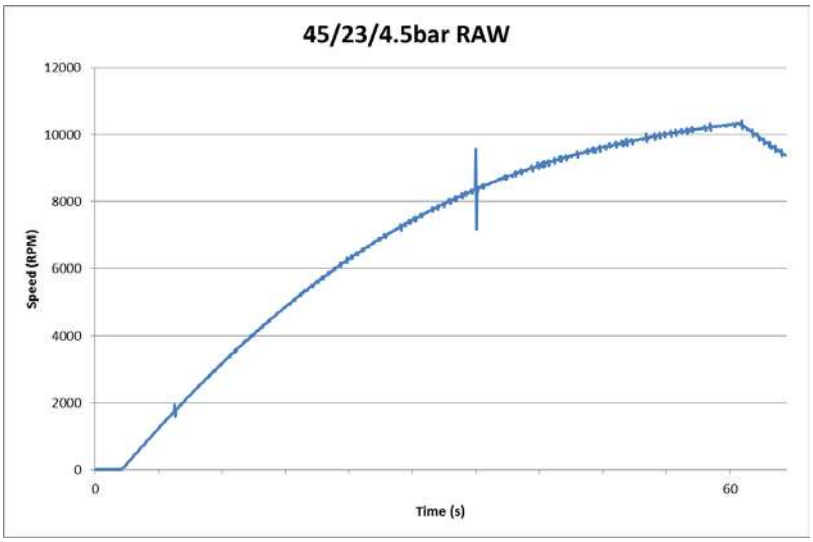
45/23/4.5bar RAW
12000
10000
8000
6000
4000
2000
0
Speed (RPM)
0
60
Time (s)


45/2 Moving Average
1200
1000
800
600
400
200
0
-200
Speed (rad/s)
y = 3.762424E-07x³ - 1.704784E-03x² + 2.427725E+00x - 1.815554E+01
0
Time (s)

45/4.5/24

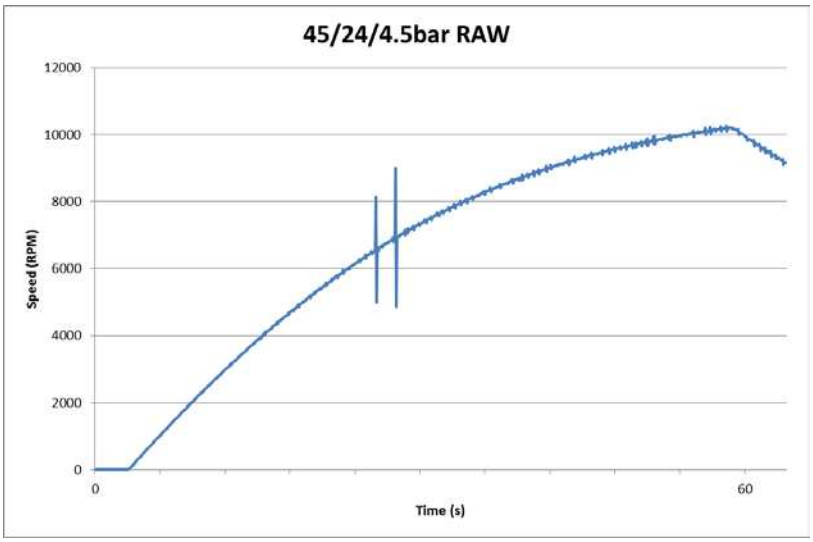
45/24/4.5bar RAW
12000
10000
8000
6000
4000
2000
0
Speed (RPM)
0
60
Time (s)

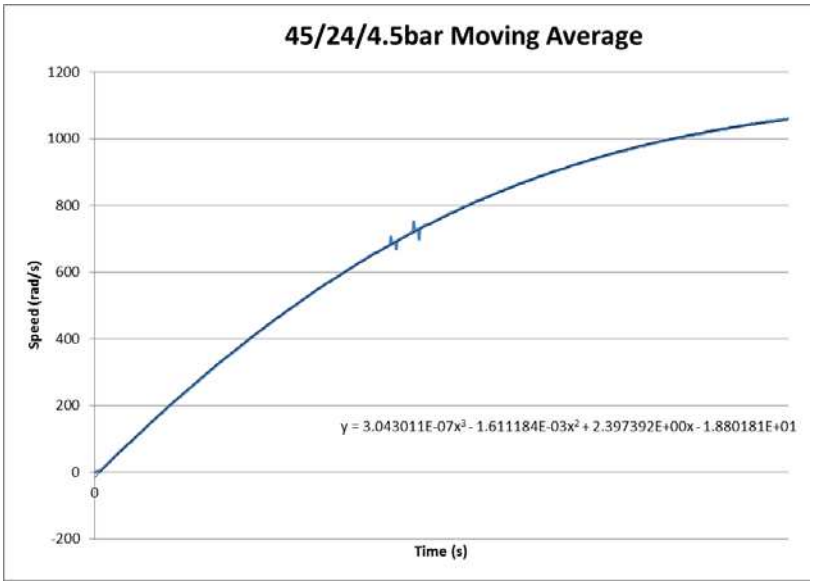
45/24/4.5bar Moving Average
1200
1000
800
600
400
200
0
-200
Speed (rad/s)
y = 3.043011E-07x³ - 1.611184E-03x² + 2.397392E+00x - 1.880181E+01
0
Time (s)